Astrophysics and Space Science Library 449

Toshifumi Shimizu
Shinsuke Imada
Masahito Kubo *Editors*

First Ten Years of Hinode Solar On-Orbit Observatory

ASSL

Springer

First Ten Years of Hinode Solar On-Orbit Observatory

Astrophysics and Space Science Library

Toshifumi Shimizu • Shinsuke Imada
Masahito Kubo
Editors

First Ten Years of Hinode Solar On-Orbit Observatory

Springer

Editors
Toshifumi Shimizu
Institute of Space and Astronautical Science
Japan Aerospace Exploration Agency
Sagamihara, Kanagawa, Japan

Shinsuke Imada
Institute for Space-Earth Environmental Research (ISEE)
Nagoya University
Nagoya, Aichi, Japan

Masahito Kubo
SOLAR-C Project Office
National Astronomical Observatory of Japan
Mitaka, Tokyo, Japan

ISSN 0067-0057 ISSN 2214-7985 (electronic)
Astrophysics and Space Science Library
ISBN 978-981-10-7741-8 ISBN 978-981-10-7742-5 (eBook)
https://doi.org/10.1007/978-981-10-7742-5

Library of Congress Control Number: 2018934850

Cover illustration: The solar limb, imaged with a broadband filter covering the Ca II H line at 397 nm by the Solar Optical Telescope onboard the Hinode satellite. A large sunspot is visible in the telescope's field of view. The Hinode observations have revealed that the chromosphere, part of the Sun's outer atmosphere formed above the solar surface and below the corona, is much more dynamic than previously thought. (C) JAXA/NAOJ/Hinode.

Printed on acid-free paper

This Springer imprint is published by the registered company Springer Nature Singapore Pte Ltd.
The registered company address is: 152 Beach Road, #21-01/04 Gateway East, Singapore 189721, Singapore

Preface

Following *Hinotori* and *Yohkoh*, *Hinode* is the third solar physics satellite in Japan and is equipped with three state-of-the-art telescopes for observing the Sun with three different wavelength bands, i.e., visible light, extreme UV, and soft X-ray. These telescopes were developed with substantial international collaboration and have been operated in orbit since the launch of Hinode in September 2006. The main scientific objective of the mission is to understand the magnetic origins of the dynamically changing corona. Using data from the three telescopes, we have investigated how magnetic fields evolve and change dynamically at the solar surface, how their variations are linked to the corona, how the corona is heated, and how dynamical nature is created in the corona. Remarkable progress and discoveries have been reported in various areas of research, such as the occurrence of solar flares, the origins of solar wind, and magneto-convection at the surface. This book describes the scientific achievements and insights gained from observations made by *Hinode* during its first 10 years of operation by compiling 23 articles by scientists in the *Hinode* team. Most of the articles were originally written in Japanese for the *Hinode* special issues of *The Astronomical Herald*, a monthly magazine by the Astronomical Society of Japan (Volume 109, August, September, and October 2016). They have been translated into English and their contents enhanced with further detail for the purposes of writing this book, Other articles have been added by our colleagues in the USA and the UK, covering current solar research more broadly. A collection of impressive photographs acquired by *Hinode* is appended to this book.

The Sun is the most important astronomical object for human beings and all life on the Earth. It is the only star that can be observed in detail by resolving the surface spatially. Spatially resolved observations may lead to discoveries that are not predicted theoretically. With such discoveries, we realize that physical processes and plasma conditions that were not focused on may be of great importance to our understanding of the magnetic dynamism in astrophysical plasma. *Hinode* has provided observations with high spatial resolution and high accuracy and has been at the forefront of solar physics research over these 10 years, especially in Japan. The *Hinode* observations were actively coordinated with space-based and ground-

based observations, providing unique datasets. This can improve our understanding of certain phenomena that are poorly understood with solely *Hinode* observations. Based on *Hinode* observations, many young researchers have been exposed to various aspects of solar physics, including data analysis, numerical simulations, and instrumental development. We believe that the perception and experience acquired with *Hinode* will contribute to the future of space science.

Tokyo, Japan
May 2017

Toshifumi Shimizu
Shinsuke Imada
Masahito Kubo

Acknowledgements

Hinode is a Japanese mission developed and launched by the Institute of Space and Astronautical Science, Japan Aerospace Exploration Agency (ISAS/JAXA), collaborating with National Astronomical Observatory of Japan (NAOJ) as a domestic partner, the National Aeronautics and Space Administration (NASA) and the United Kingdom's Science and Technology Facilities Council (STFC) as international partners. Scientific operation of the *Hinode* mission is conducted by the *Hinode* science team, organized at ISAS/JAXA. This team mainly consists of scientists from institutes in the partner countries. Support for the post-launch operation is provided by JAXA and NAOJ (Japan), STFC (UK), NASA (USA), European Space Agency (ESA), and Norwegian Space Center (NSC). The editors would like to thank all individuals involved for their contributions to the *Hinode* mission. They are also grateful to the Astronomical Society of Japan for publishing the original special issue in the *Astronomical Herald*. The publication of this book was realized with the help of Akiyuki Tokuno, Taeko Sato, and Kazumi Nishihara at Springer and Keiko Daiguji at ISAS/JAXA, to whom the authors are grateful.

Contents

Acronyms

1D	one-dimensional
2D	two-dimensional
2.5D	two-and-half-dimensional
3D	three-dimensional
AAS	American Astronomical Society
ACE	Advanced Composition Explorer
ADC	Astronomy Data Center
ADS	Astrophysics Data System
AIA	Atmospheric Imaging Assembly
ALMA	Atacama Large Millimeter/submillimeter Array
AR	Active Region
ASJ	Astronomical Society of Japan
AU	Astronomical Unit
BCS	Bragg Crystal Spectrometer
BFI	Broad-band Filter Imager
CCD	Charge-Coupled Device
CDS	Coronal Diagnostic Spectrometer
CH	Coronal Hole
CLASP	Chromospheric Lyman-Alpha Spectro-Polarimeter
CLASP2	Chromospheric Layer Spectro-Polarimeter 2
CLV	Center-to-Limb Variation
CME	Coronal Mass Ejection
CMOS	Complementary Metal Oxide Semiconductor
CO	Chief Observer
COSMO	The Coronal Solar Magnetism Observatory
CP	Chief Planner
CPU	Central Processing Unit
CSHKP	Carmichael, Sturrock, Hirayama, Kopp, and Pneuman
C-SODA	Center for Science Satellite Operation and Data Archive
DARTS	Data Archive and Transmission System
DEM	Differential Emission Measure

DKIST	Daniel K. Inouye Solar Telescope
DST	Domeless Solar Telescope
DVD	Digital Versatile Disc
EB	Ellerman Bomb
EIS	EUV Imaging Spectrometer
EIT	Extreme Ultraviolet Imaging Telescope
EPO	Education and Public Outreach
ESA	European Space Agency
EST	European Solar Telescope
EUV	Extreme Ultraviolet
EUVST	Extreme Ultraviolet Spectroscopic Telescope
FG	Filtergram
FIP	First Ionization Potential
FOXSI	Focusing Optics X-ray Solar Imager
FPGA	Field-programmable Gate Array
FPP	Focal Plane Package
GFSC	Goddard Space Flight Center
GIS	Grazing Incidence Spectrometer
GOES	Geostationary Operational Environmental Satellite
GONG	Global Oscillation Network Group
HAZEL	Hale and Zeeman Light
HCI	High-resolution Coronal Imager
Hi-C	High-resolution Coronal Imager
HMI	Helioseismic and Magnetic Imager
HOP	Hinode Operation Plan
HSC	Hinode Science Center
HTML	Hypertext Markup Language
IBIS	Interferometric Bidimensional Spectropolarimeter
IDL	Interactive Data Language
IPS	Interplanetary Scintillation
IR	Infrared
IRIS	Interface Region Imaging Spectrograph
ISAS	Institute of Space and Astronautical Science
ISEE	Institute for Space-Earth Environment Research
JAXA	Japan Aerospace Exploration Agency
JpGU	Japan Geoscience Union
JST	Japan Science and Technology Agency
LCT	Local Correlation Tracking
LEST	Large European Solar Telescope
LFFF	Linear Force-Free Field
LOS	Line-of-Sight
MDI	Michelson Doppler Imager
MDP	Mission Data Processor
MEXT	Ministry of Education, Culture, Sports, Science, and Technology
MHD	Magnetohydrodynamic

MK	Million Kelvin
Mm	Megameter
MMF	Moving Magnetic Feature
MSFC	Marshall Space Flight Center
NAL	National Aerospace Laboratory of Japan
NAOJ	National Astronomical Observatory of Japan
NASA	National Aeronautics and Space Administration
NASDA	National Space Development Agency of Japan
NFI	Narrow-band Filter Imager
NICT	National Institute of Information and Communications Technology
NIS	Normal Incidence Spectrometer
NLFFF	Non-Linear Force-Free Field
NOAA	National Oceanic and Atmospheric Administration
NSC	Norwegian Space Centre
NSO	National Solar Observatory
NuSTAR	Nuclear Spectroscopic Telescope Array
OP	Opposite Polarity
OSO	Orbiting Solar Observatory
OTA	Optical Telescope Assembly
PAONET	Public Astronomical Observatory Network
PASJ	Publications of the Astronomical Society of Japan
PIL	Polarity Inversion Line
PSTEP	Project for SolarâĂŞTerrestrial Environment Prediction
QS	Quiet Sun
RHESSI	Reuven Ramaty High-Energy Solar Spectroscopic Imager
RS	Reversed Shear
SAA	South Atlantic Anomaly
SAD	Supra-Arcade Downflow
SAO	Smithsonian Astrophysical Observatory
SCIP	Sunrise Chromospheric Infrared Spectropolarimeter
SDO	Solar Dynamics Observatory
SIRIUS	Scientific Information Retrieval Integrated Utilization System
SMART	Solar Magnetic Activity Research Telescope
SMEX	Small Explorer Program
SMM	Solar Maximum Mission
SoHO	Solar and Heliospheric Observatory
SOT	Solar Optical Telescope
SP	Spectro-Polarimeter
SSC	Science Schedule Coordinators
SSW	Solar Software
STFC	Science and Technology Facilities Council
STEREO	Solar Terrestrial Relations Observatory
SUMER	Solar Ultraviolet Measurements of Emitted Radiation
SUVIT	Solar Ultraviolet-Visible-IR Telescope
SWAMIS	Southwest Automatic Magnetic Identification Suite

SXT	Soft X-ray Telescope
TR	Transition Region
TRACE	Transition Region and Coronal Explorer
TRENDY	Transition Region Energetics and Dynamics
UFSS	Ultra-Fine Sun Sensor
UK	United Kingdom
USA	United States of America
USC	Uchinoura Space Center
UV	Ultraviolet
UVCS	Ultraviolet Coronograph Spectrometer
VALC	Vernazza, Avrett, and Loeser C
XBP	X-ray Bright Point
XRT	X-ray Telescope

Part I
Reviews on 10 Years of Hinode

Chapter 1
A Brief History of *Hinode*: Toward the Success in Orbit

Toshifumi Shimizu

Abstract The 7th M-V rocket carrying the solar-observing satellite *Hinode* was launched at Uchinoura Space Center at 6:36 JST on 23 September 2006. In the 10 years that have passed, *Hinode* has been active in the global front line of solar researches, although there have been some difficulties in the operation of the spacecraft. All the onboard telescopes have achieved a high standard of performance as expected, providing unique scientific data that had not previously been acquired by other facilities. *Hinode* is an orbiting solar observatory that carries out observations proposed by any researchers in the world, and the mission data is fully open to the rest of the world. We, the *Hinode* team, are proud of the scientific achievement by *Hinode*.

Keywords Sun · Hinode · Solar observatory · Spacecraft operations · History

1.1 Birth of *Hinode*

1.1.1 A Long Way Toward the Launch

The solar-observing satellite *Hinode* was called SOLAR-B during the development of the spacecraft (Kosugi et al. 2007). Following the Japanese tradition regarding the naming of science satellites, the satellite was named *Hinode* after the successful installation into its orbit.

After a mission idea was proposed in a domestic symposium around 1992, some scientists with graduate students began studying the specific concepts of the mission around 1993. The *Yohkoh* satellite (Ogawara et al. 1991), which began

T. Shimizu (✉)
Institute of Space and Astronautical Science, Japan Aerospace Exploration Agency, Sagamihara, Kanagawa, Japan
e-mail: shimizu@solar.isas.jaxa.jp

T. Shimizu et al. (eds.), *First Ten Years of Hinode Solar On-Orbit Observatory*,
Astrophysics and Space Science Library 449,
https://doi.org/10.1007/978-981-10-7742-5_1

observations in 1991, revealed a dynamically changing X-ray corona that was considerably more dynamic than we had thought, leading to the basic concept behind the *Hinode* mission. There was a common scientific motivation among the researchers involved, namely, the desire to understand the magnetic origin of the coronal dynamics. In order to gain an understanding, the main requirement of the mission was that the properties of magnetic fields would be measured precisely with high spatial resolution at the solar surface (photosphere), where the magnetic origins of the coronal dynamics lie. These measurements would be carried out with simultaneous imaging observations of the corona either using soft X-rays or with extreme ultraviolet (EUV) and EUV spectroscopic measurements of the coronal plasma. Japanese scientists continued to keep this basic concept in mind, and finally the SOLAR-B project officially started in 1998.

It was nearly another 8 years before the launch took place. To achieve high spatial resolution and fulfill various key performance criteria, we concentrated on the development of onboard telescopes and spacecraft. Each scientist had a different experience and made a unique contribution, and thus each has his/her own memories from the development phase. Due to the limited scope of this article, I will save the story of this development for another occasion.

1.1.2 Launch and Early Operations

The spacecraft was launched at 6:36 JST on 23 September 2006 (21:36 UT on 22 September 2006), by the 7th in the series of the M-V rocket, which is world's biggest three-stage solid-fuel vehicle, developed by ISAS (Institute of Space and Astronautical Science) of JAXA (Japan Aerospace Exploration Agency). This launch was perfect (Fig. 1.1), ending the course of the M-V rocket on a high note.

After it had been placed in a low Earth orbit, it was named *Hinode*, which means sunrise in Japanese. The committee led by Prof. Kosugi, the first project manager for the *Hinode* project, chose this new name from a list of names proposed by engineers and scientists working on the project. Prof. Kosugi linked the following objectives to the name *Hinode*: the desire to greatly advance our understanding of the Sun, resulting in a new era (i.e., sunrise) in solar physics; JAXA's leadership role in *Hinode*'s international collaboration, which would result in a new era (i.e., sunrise) in space science; and the desire for a new beginning (i.e., sunrise) for Japanese space development. As well as being motivated by these objectives when selecting the name, he also took into consideration the fact that *Hinode* is a simple and popular word in Japan and it can be understood by the international community.

The series of orbital maneuver operations in the period from 25 September to 1 October adjusted the spacecraft to a sun-synchronous polar orbit with an altitude of about 680 km, allowing the telescopes to view the Sun continuously for more than 8 months per year. After various kinds of functional checks were performed in the spacecraft (Fig. 1.2), especially in the attitude control system,

Fig. 1.1 The launch of the 7th vehicle in the M-V rocket series carrying the *Hinode* satellite. 6:36 JST on 23 September 2006. At Uchinoura Space Center. (C) JAXA

each telescope was turned on and started its observations from late October. At the time of the launch of *Hinode*, about 6 years had already passed since the maximum (1999–2000) phase of the solar cycle 23, and the solar activity was approaching its minimum phase. Fortunately, however, an active region (NOAA 10930) was developed on the solar surface in December 2006, producing a series of three X-class flares. The Solar Optical Telescope (SOT) successfully recorded the temporal evolution of the spatial distribution of vector magnetic fields at the photospheric level in this active region (Fig. 1.3) (Kubo et al. 2007). The X-ray telescope (XRT) and EUV Imaging Spectrometer (EIS) captured unique coronal data, which allowed scientists to investigate the hot plasma and dynamics associated with the occurrence of flares. These observations, carried out during the initial period of the mission, made a great contribution to the numerical modeling of coronal magnetic field structures (Schrijver et al. 2008) and coronal dynamics responsible for flares and coronal mass ejections (Harra et al. 2007). Since then, the Sun has shown a low level of activity, including a long continuous period, in 2008–2010, during which there were no sunspot on the solar surface. During this period, *Hinode* was concentrated on observations of the quiet Sun, where small-scale, but ubiquitous occurrences of dynamical, magnetohydrodynamic (MHD) phenomena

Fig. 1.2 A group photo with spacecraft engineers in an operation room at Uchinoura Space Center (USC)

were revealed, including ubiquitous horizontal magnetic flux (Lites et al. 2008; Ishikawa et al. 2008), the dynamics of magnetic flux tubes in the convective surface (Nagata et al. 2008; Shimizu et al. 2008a), ubiquitous jets (Shibata et al. 2007), and the internal dynamics of prominences (Berger et al. 2008).

1.1.3 Prof. Kosugi's Passing

It was just after verifying the good performance of the telescopes onboard *Hinode* that Prof. Takeo Kosugi (Fig. 1.4) suddenly passed away on 26 November 2006. He had led the project team since the project started in 1998, and the *Hinode* mission would not have been conceived without him. At the time of his passing, the daily operations of the spacecraft and onboard telescopes were already being conducted by a team led by scientists from the younger generation. In addition, his passing left young scientists with no option other than to manage the international project on their own. In ISAS, Drs. Taro Sakao and Toshifumi Shimizu have led the *Hinode* project as the 3rd and 4th project managers. Note that Prof. Ichiro Nakatani, an

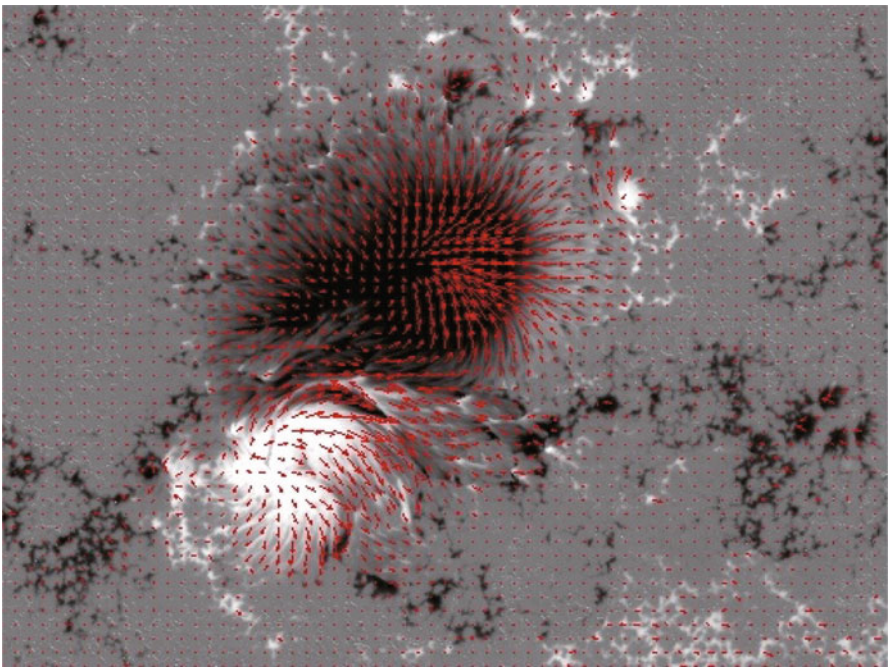

Fig. 1.3 The magnetic field distribution of active region NOAA 10930 which produced three large-scale flares. The map was taken with a spectropolarimeter (SP) of the Solar Optical Telescope on 13 December 2006. The background grayscale shows the spatial distribution of the magnetic polarity of the line-of-sight component of the magnetic flux. Red arrows indicate the transversal component of the magnetic flux. (C) NAOJ/JAXA/NASA/Hinode

Fig. 1.4 Late Prof. Takeo Kosugi, the first project manager for the *Hinode* mission. (C) JAXA

engineering professor, acted as project manager during 2006–2007. We hope that Kosugi-san has given us a pass mark if he has been watching our activities, and *Hinode*'s great success, from the heavens.

It should also be noted that scientists and graduate students from the National Astronomical Observatory of Japan (NAOJ), which is the domestic partner, and from Japanese universities have been participating in daily scientific operations at ISAS. As described later, the *Hinode* mission is a Japanese-led mission, and all the telescopes onboard were developed under international collaboration with NASA (USA) and United Kingdom (UK)'s Science and Technology Facilities Council (STFC). Therefore, scientists from the foreign institutes and universities involved in the development have also been participating in the daily scientific operations. These domestic and foreign scientists have been working hard, not only in operations but also in the data analysis, providing new discoveries and proliferating knowledge. These academic activities contribute most to the *Hinode* project.

1.2 Instrument Overview

The *Hinode* mission (Fig. 1.5) is equipped with three state-of-the-art telescopes, which observe the Sun using three different wavelength channels. The SOT (Tsuneta et al. 2008) is a Gregorian solar telescope with a primary mirror of 50 cm diameter, which is the largest aperture for observing the Sun on orbit (as of 2017). This telescope achieved the diffraction-limited performance associated with this diameter in the visible light range, allowing high spatial resolution observations in the range of 0.2–0.3 arcsec (corresponding to a range of 150–200 km on the Sun's surface) (Suematsu et al. 2008; Shimizu et al. 2008b). Moreover, continuous observations from the stable environment on orbit, i.e., the seeing-free condition, permitted scientists to reliably identify MHD waves excited along magnetic fields in the solar atmosphere for the first time (Okamoto et al. 2007; De Pontieu et al. 2007). The focal plane package (FPP) of the SOT has the capability to measure vector magnetic fields (Lites et al. 2013), spatially distributed as magnetic flux tubes on the solar surface, with high accuracy (Ichimoto et al. 2008). Our knowledge about the dynamical behaviors of magnetic fields distributed on the solar surface has been much improved by the SOT measurements. The XRT (Golub et al. 2007; Kano et al. 2008) is a grazing incidence X-ray telescope and observes soft X-ray flux emitted by hot coronal plasma in the range of 1 million Kelvin (MK) to tens of MK of the spatial distribution, i.e., images with a spatial resolution of about 1 arcsec, which is about three times higher than that of *Yohkoh* soft X-ray images. From the time series of the XRT images, scientists have identified the existence of plasma flows streaming out from beside an active region, which is now considered as one of the sources for slow solar winds (Sakao et al. 2007). High-cadence imaging observations allow us to study dynamical behaviors of the corona using high-resolution imaging. The EIS (Culhane et al. 2007) is a high-dispersion spectrometer for measuring EUV emission in the 17–21 nm and 25–29 nm ranges, where several emission lines originating

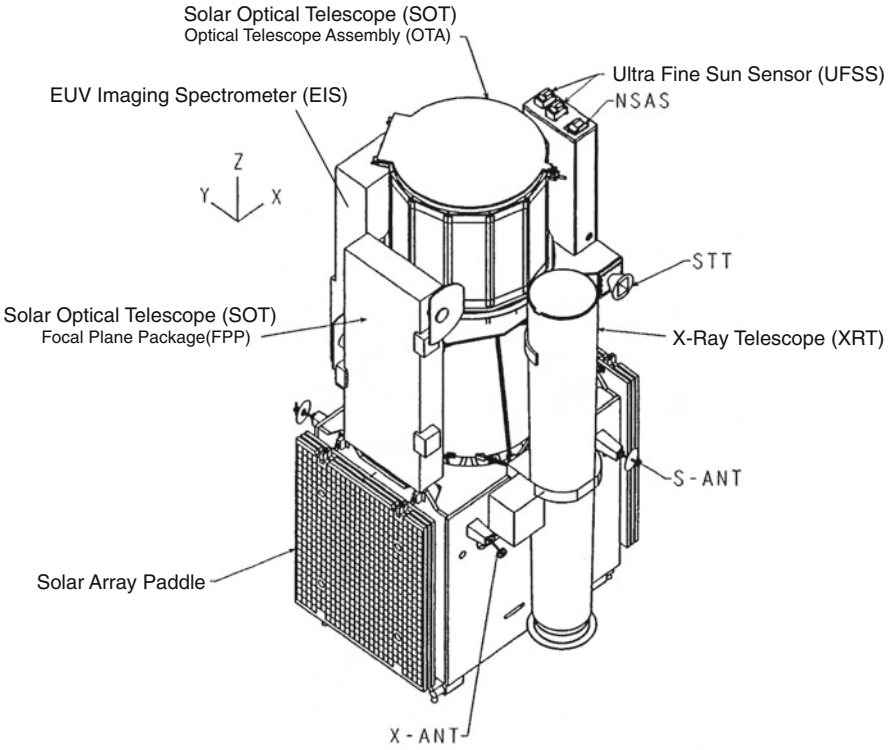

Fig. 1.5 The external view of the *Hinode* satellite at the launch configuration. The solar array paddles attached at the both sides of the spacecraft bus were deployed after the orbital installation. (C) JAXA

from the coronal plasma exist. This spectrometer has a slit scanning mechanism for mapping various sizes of field of view. The intensity, the spectral position in wavelength, and the shapes of large-dispersion emission lines are used to diagnose the plasma conditions, such as temperature, density, and line-of-sight motions, helping us to make progress in understanding the heating and dynamical behaviors of the corona.

One of the key performance features of the *Hinode* telescopes is high spatial resolution at a level that had not previously been achieved. The spacecraft is also required to guarantee high pointing accuracy at a level that has never been realized in Japanese spacecrafts. In order to achieve this challenging standard of performance, new technical developments were necessary in the spacecraft attitude and telescope pointing control (Shimizu et al. 2008b), as well as in its thermal-structural design (Minesugi et al. 2013). As can be seen in the *Hinode* images and movies, the cultivation of new high-precision spacecraft technology was a consequence of *Hinode*'s development. For instance, the pre-launch testing and evaluation of micro-vibration has been applied to subsequent observation satellites in Japan.

1.3 Science Achievements

The data acquired by the three telescopes has been of the highest quality and has provided various new discoveries and insights, many of which have already been published in peer-reviewed journals. Special issues covering *Hinode* results were released by several peer-reviewed journals, including *Science* in 2007, *Publications of the Astronomical Society of Japan (PASJ)* in 2007 and 2014, *Astronomy & Astrophysics* in 2008, and *Solar Physics* (instrument papers) in 2007 and 2008. Some of these special issues can be seen in Fig. 1.6.

Figure 1.7 (left) shows the annual evolution of the number of peer-reviewed papers that contain research based on data obtained by *Hinode*'s telescopes, published from 2007 to 2015. In the space of a few years following the launch, the number of papers was increased to over 120 publications per year (2009–2012), simply because a great deal of progress was made, by many scientists, in analyzing the data and interpreting the results. The number of publications has been maintained at around 90–100 per year in the last few years (2013–present). The total number of refereed papers published by 2016 exceeded 1,000, and the papers are still being published, although the frequency of the publications may recently

Fig. 1.6 Some peer-review journals featuring *Hinode*

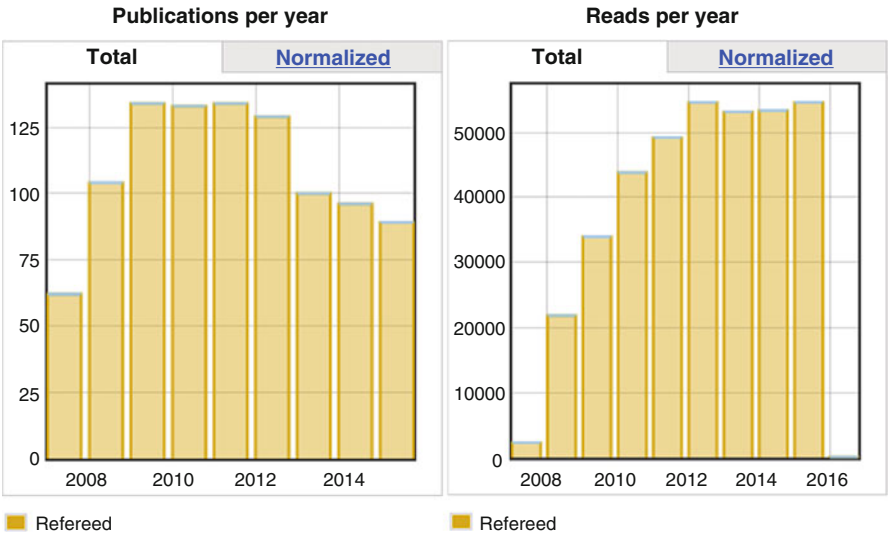

Fig. 1.7 The number of peer-review papers published in each year (left) and the number of paper downloads (right). The statistics are recorded with support by the Astrophysics Data System (ADS) funded by NASA

have decreased slightly. Figure 1.7 (right) shows the statistics derived by using the Astrophysics Data System (ADS) funded by NASA, revealing how frequently the published *Hinode* papers have been read. This bar chart clearly indicates that *Hinode*'s popularity gradually increased after publications started. After 2012, the number of paper downloads exceeded 50,000 times every year, and the researchers have had constant access to the published papers.

All of the data acquired by *Hinode* have been open to the public immediately after the observations (Matsuzaki et al. 2007), and therefore, any researchers may utilize the data if interested. Note that this did not apply during the performance verification and the calibration of the data, which took place during the initial 6 months following the launch. The regional distribution of the publications is in an almost equal ratio (i.e., 1:1:1) for the Asian, American region, and European regions. As regards the number of publications by country, the USA has produced the most, followed by Japan and the UK. These three countries made hardware contribution to the telescopes onboard *Hinode*. Moreover, Germany and Spain, which have a good history of spectropolarimetric observations in visible light at ground-based observatories, have also produced many publications in this regard. More recently, the numbers of publications from China and India have been increasing. Scientists and graduate students working in Japan, the UK, and the USA have been able to carry out their research activities with the knowledge that the other countries are catching up, which is a favorable environment for research.

1.4 International Collaboration

All three of the telescopes onboard were developed under international collaboration. As well as the spacecraft and launch vehicle, Japan took responsibility for developing the following key portions of the telescopes and, in doing so, preserved Japan's role as the principal contributor: (1) the main telescope (Optical Telescope Assembly, OTA) and a portion of the image stabilization system including the tip-tilt mirror mechanism and servo control for the SOT, (2) the charge-coupled device (CCD) camera for the XRT, and (3) the Mission Data Processor (MDP) for controlling the observation sequence for the SOT and the XRT and for compression of the data from all the three telescopes. However, the following parts of the telescopes were developed under international collaboration with NASA (USA) and STFC (UK): (1) for the SOT, the FPP including filter imager, spectropolarimeter (SP), and correlation tracker as a part of the image stabilization system, (2) the XRT excluding the CCD camera, and (3) the entire portion of the EIS.

Many institutes and universities in the USA and the UK were extensively involved, with support from NASA and STFC, in the development of the *Hinode* mission. Such a large-scale international collaboration was challenging for an ISAS mission. Our guiding principle was to eliminate any black boxes as much as possible, not only for the Japanese part of the collaboration but also for the USA and the UK. We held a series of design meetings at regular intervals, where discussions took place and explanations were given, until both development teams understood and accepted the design- and performance-related ideas of one another. During the testing phase, Japanese scientists participated in performance testing in the USA; scientists and engineers from the USA and the UK also took part in various kinds of testings, not only at the telescope level but also at the system level, including the end-to-end optical performance, and electrical functional, vibration, thermal vacuum, and micro-vibration tests. For me, these technical meetings and tests were the unique opportunities for gaining valuable experience and knowledge about the development of spacecraft and space-borne instruments.

Another important international collaboration is that involving the European Space Agency (ESA) and the Norwegian Space Center (NSC), which have been offering 15 passes every day at ground stations located near the North Pole and in the Antarctica for the mission data downlinks. This post-launch support has strengthened *Hinode*'s scientific activities, because the continuous acquisition of time-lapsed high-cadence images is one of the key performance criteria specified for many solar research projects.

1.5 As On-Orbit Solar Observatory

Scientific daily operations have been carried out daily at ISAS/JAXA in Japan, with the participation of scientists from the institutes and universities in the USA, the UK, and Norway who were involved in the instrument development (Fig. 1.8). The

Fig. 1.8 One scene from daily planning meetings at ISAS/JAXA. Taken in January 2009. (C) JAXA

Chief Observer (CO) takes the role of the observation planning and quick data checking for each telescope. At the early phase of the operations, scientists and graduate students, not only from Japan but also from the USA, the UK, and Norway, visited ISAS and worked on observation planning. As the daily operations were running smoothly a few years after the launch, the daily planning was gradually shifted to remote operations. For example, the US CO working on the SOT would remotely participate in the daily meeting and discuss the observation plans with the other COs in the meeting. They would then prepare the timeline and parameters for SOT observations, according to the agreed observations plans. The participation of scientists and students in scientific daily operations is a type of volunteer work, but they gain benefits from it, because they can check the acquired data and identify good data and interesting phenomena immediately after the data are downlinked. Each telescope team has a shift schedule for the role of CO, according to which each scientist/student may work as the CO for a few weeks per year. Since each scientist/student should also have a plenty of working time available for data analysis equally, we have arranged the shift schedule in which one can make the equal contribution to daily operations. In daily meetings from 10:30 JST every day except on Sunday, the Chief Planner (CP) leads discussions between the three COs regarding observation coordinates for the three telescopes as well as for other facilities, such as *Interface Region Imaging Spectrograph (IRIS)* and ground-based observatories, and eventually defines the observation (satellite pointing) schedule. The daily meetings are also a good place for Japanese graduate students to improve their proficiency of the English language.

Observations consist of standard observations defined by each instrument team and proposed observations (HOP; *Hinode* Operation Plan). The *Hinode* spacecraft

has been operated as an international on-orbit solar observatory fully open to all scientists. The *Hinode* team has been accepting proposals from scientists all over the world. The team, or, to be precise, the Science Schedule Coordinators (SSCs) group in the team, reviews the proposed observations every month and schedules them after reviewing them with the proposers so as to improve each observation's definition.

The Ca II H movies from the SOT show that the chromosphere is more dynamic than had ever been thought. With the SOT data, scientists have recognized the importance of studying the chromosphere connecting the solar surface to the corona in order to make progress in our understanding of the coronal heating and dynamics. In 2013, NASA launched a Small Explorer Program (SMEX) satellite called IRIS, which performs ultraviolet (UV) spectroscopy of the chromosphere. The *IRIS* observations are regularly coordinated with observations made by *Hinode*, as both satellites have a fairly narrow field of view.

1.6 Ups and Downs in Operations

It may appear that *Hinode*'s daily operations have been smooth sailing, but these operations have experienced ups and downs during the past 10 years. The biggest difficulty was the malfunction of the X-band modulator on board. The X-band channel has a 4 Mbps bandwidth, and it is important for downloading huge amounts of scientific data on Earth. From the last week of December in 2007, the X-band signals from the spacecraft started to show anomalous wave patterns in the latter portion of some downlink passes. The situation was steadily getting worse, until finally the X-band signals showed anomalies all the time. It should be pointed out that further investigations suggest a malfunction in the field-programmable gate array (FPGA) used in the X-band modulator. After various trials of the spacecraft configuration and the technical supports at ground stations, the science data downlink was finally switched from the X-band to an S-band backup channel. The S-band transmitter has a considerably lower transmission rate, i.e., about one sixteenth of that of the X-band transmitter. To compensate for this lower rate, we have increased the level of data compression without significantly affecting the quality of the data and have improved our operational efficiency, by, for example, reducing the field of view and/or the number of wavelengths (filters) and/or the summation of pixels, depending on the objectives for each observation. Another initiative has been to increase the number of ground stations and downlinks. JAXA has explored new ground stations with strong supports from the government as well as from various other organizations and has increased the number of downlink stations to 40–55 passes per day. As a result, the amount of data received from *Hinode* recovered to a level equivalent to roughly 60% or more of the original capability.

Another difficulty was related to the Great East Japan Earthquake on 11 March 2011 and the subsequent Fukushima Daiichi nuclear disaster. Because of insufficient electric power being available in the Tokyo metropolitan area, rolling blackouts began across Tokyo and surrounding areas. The announcement of possible rolling blackouts had a significant impact on daily operations. Computers and other equipments in the *Hinode* operation room were forced to shutdown when a rolling blackout was scheduled for the area where the ISAS campus is located. The scheduled blackouts affected the daily schedule of the COs' activities, reducing the frequency of command uploads in March 2011.

Space debris is currently a concern for *Hinode*, which has a polar orbit at an altitude of about 680 km. The density of debris is relatively high at this altitude, and we have sometimes been warned that we should consider debris avoidance maneuvers when close approaches are predicted. In 2010, JAXA determined the criteria and operational procedure for avoidance for *Hinode*, which can adjust its orbit using the thruster engine if a critically close approach is predicted. In the case of a close approach by a foreign-owned small satellite in March 2012, we decided to perform an emergency orbital maneuver to avoid a possible collision. This was the first case of debris-avoidance maneuvers by the ISAS satellites.

1.7 Future Prospects

The *Hinode* mission celebrated its 10th anniversary on 23 September 2016. Scientists all over the world hope very much that the *Hinode* observations will continue. The functions and performance of the spacecraft and the three telescopes remain functional, although a slight degradation can be observed in the trend history. Soon after the launch, solar activity went to the deep solar minimum. The Sun has shown a low level of activity in cycle 24 (2009–), leading some scientists to predict a decline in solar activity in the coming years. In view of this situation, it is extremely important for *Hinode* to continue to record the photospheric magnetic fields and corona as we approach the solar minimum around 2020. Furthermore, the continuation of observations beyond 2020, and switching to the next generation of solar mission, would be important for solar physics research. Fortunately, all the space agencies have offered high praise for the scientific activities of *Hinode* so far. For example, the NASA senior review of heliophysics missions in 2015 rated *Hinode* the third highest among 14 missions involved in the heliophysics system observations. In December 2016, the ISAS science steering committee confirmed its strong recommendation to extend the *Hinode* mission until March 2021; ISAS confirmed that this mission extension is reasonable and passed approval for the extension plan. For the further continuation of *Hinode* observations beyond 2020, the most important driver would be the continuation of high-quality research, using the *Hinode* data, by the scientific community.

Acknowledgements This article was written with partial support from JSPS KAKENHI Grant Number JP15H05814. *Hinode* is a Japanese mission developed and launched by ISAS/JAXA, with NAOJ as domestic partner and NASA and STFC (UK) as international partners. Scientific operation of the *Hinode* mission is conducted by the *Hinode* science team organized at ISAS/JAXA. This team mainly consists of scientists from institutes in the partner countries. Support for the postlaunch operation is provided by JAXA and NAOJ (Japan), STFC (UK), NASA, ESA, and NSC (Norway). *Hinode*'s success is based on participations, contributions, and support by various kinds of people (not only scientists but also engineers and administrative people) and organizations. It is impossible to acknowledge all the contributors by describing all the contributions and names in the limited space of this article, but I would like to use this opportunity to express our thanks to all the contributors. I appreciate your continuous support.

References

Berger, T.E., Shine, R.A., Slater, G.L., Tarbell, T.D., Title, A.M., Okamoto, T.J., Ichimoto, K., Katsukawa, Y., Suematsu, Y., Tsuneta, S., Lites, B.W., Shimizu, T.: Hinode SOT observations of solar quiescent prominence dynamics. Astrophys. J. Lett. **676**, L89 (2008)

Culhane, J.L., Harra, L.K., James, A.M., Al-Janabi, K., Bradley, L.J., Chaudry, R.A., Rees, K., Tandy, J.A., Thomas, P., Whillock, M.C.R., Winter, B., Doschek, G.A., Korendyke, C.M., Brown, C.M., Myers, S., Mariska, J., Seely, J., Lang, J., Kent, B.J., Shaughnessy, B.M., Young, P.R., Simnett, G.M., Castelli, C.M., Mahmoud, S., Mapson-Menard, H., Probyn, B.J., Thomas, R.J., Davila, J., Dere, K., Windt, D., Shea, J., Hagood, R., Moye, R., Hara, H., Watanabe, T., Matsuzaki, K., Kosugi, T., Hansteen, V., Wikstol, Ø.: The EUV imaging spectrometer for Hinode. Sol. Phys. **243**, 19 (2007)

De Pontieu, B., McIntosh, S.W., Carlsson, M., Hansteen, V.H., Tarbell, T.D., Schrijver, C.J., Title, A.M., Shine, R.A., Tsuneta, S., Katsukawa, Y., Ichimoto, K., Suematsu, Y., Shimizu, T., Nagata, S.: Chromospheric Alfvenic waves strong enough to power the solar wind. Science **318**, 1574 (2007)

Golub, L., Deluca, E., Austin, G., Bookbinder, J., Caldwell, D., Cheimets, P., Cirtain, J., Cosmo, M., Reid, P., Sette, A., Weber, M., Sakao, T., Kano, R., Shibasaki, K., Hara, H., Tsuneta, S., Kumagai, K., Tamura, T., Shimojo, M., McCracken, J., Carpenter, J., Haight, H., Siler, R., Wright, E., Tucker, J., Rutledge, H., Barbera, M., Peres, G., Varisco, S.: The X-ray telescope (XRT) for the Hinode mission. Sol. Phys. **243**, 63 (2007)

Harra, L.K., Hara, H., Imada, S., Young, P.R., Williams, D.R., Sterling, A.C., Korendyke, C., Attrill, G.D.R.: Coronal dimming observed with Hinode: outflows related to a coronal mass ejection. Publ. Astron. Soc. Jpn. **59**. S801 (2007)

Ichimoto, K., Lites, B., Elmore, D., Suematsu, Y., Tsuneta, S., Katsukawa, Y., Shimizu, T., Shine, R., Tarbell, T., Title, A., Kiyohara, J., Shinoda, K., Card, G., Lecinski, A., Streander, K., Nakagiri, M., Miyashita, M., Noguchi, M., Hoffmann, C., Cruz, T.: Polarization calibration of the solar optical telescope onboard Hinode. Sol. Phys. **249**, 233 (2008)

Ishikawa, R., Tsuneta, S., Ichimoto, K., Isobe, H., Katsukawa, Y., Lites, B.W., Nagata, S., Shimizu, T., Shine, R.A., Suematsu, Y., Tarbell, T.D., Title, A.M.: Transient horizontal magnetic fields in solar plage regions. Astron. Astrophys. **481**, L25 (2008)

Kano, R., Sakao, T., Hara, H., Tsuneta, S., Matsuzaki, K., Kumagai, K., Shimojo, M., Minesugi, K., Shibasaki, K., Deluca, E.E., Golub, L., Bookbinder, J., Caldwell, D., Cheimets, P., Cirtain, J., Dennis, E., Kent, T., Weber, M.: The Hinode X-ray telescope (XRT): camera design, performance and operations. Sol. Phys. **249**, 263 (2008)

Kosugi, T., Matsuzaki, K., Sakao, T., Shimizu, T., Sone, Y., Tachikawa, S., Hashimoto, T., Minesugi, K., Ohnishi, A., Yamada, T., Tsuneta, S., Hara, H., Ichimoto, K., Suematsu, Y., Shimojo, M., Watanabe, T., Shimada, S., Davis, J.M., Hill, L.D., Owens, J.K., Title, A.M., Culhane, J.L., Harra, L.K., Doschek, G.A., Golub, L.: The Hinode (Solar-B) mission: an overview. Sol. Phys. **243**, 3 (2007)

Kubo, M., Yokoyama, T., Katsukawa, Y., Lites, B., Tsuneta, S., Suematsu, Y., Ichimoto, K., Shimizu, T., Nagata, S., Tarbell, T.D., Shine, R.A., Title, A.M., Elmore, D.: Hinode observations of a vector magnetic field change associated with a flare on 2006 December 13, Publ. Astron. Soc. Jpn. **59**, S779 (2007)

Lites, B.W., Kubo, M., Socas-Navarro, H., Berger, T., Frank, Z., Shine, R., Tarbell, T., Title, A., Ichimoto, K., Katsukawa, Y., Tsuneta, S., Suematsu, Y., Shimizu, T., Nagata, S.: The horizontal magnetic flux of the quiet-sun internetwork as observed with the Hinode spectro-polarimeter. Astrophys. J. **672**, 1237 (2008)

Lites, B.W., Akin, D.L., Card, G., Cruz, T., Duncan, D.W., Edwards, C.G., Elmore, D.F., Hoffmann, C., Katsukawa, Y., Katz, N., Kubo, M., Ichimoto, K., Shimizu, T., Shine, R.A., Streander, K.V., Suematsu, Y., Tarbell, T.D., Title, A.M., Tsuneta, S.: The Hinode spectro-polarimeter. Sol. Phys. **283**, 579 (2013)

Matsuzaki, K., Shimojo, M., Tarbell, T.D., Harra, L.K., Deluca, E.E.: Data archive of the Hinode mission. Sol. Phys. **243**, 87 (2007)

Minesugi, K., Inoue, T., Tabata, M., Shimizu, T., Sakao, T., Katsukawa, Y.: Telescope co-alignment design and its performance on-orbit of solar observational satellite "Hinode". Trans. Jpn. Soc. Aeronaut. Space Sci. **56**, 104 (2013)

Nagata, S., Tsuneta, S., Suematsu, Y., Ichimoto, K., Katsukawa, Y., Shimizu, T., Yokoyama, T., Tarbell, T.D., Lites, B.W., Shine, R.A., Berger, T.E., Title, A.M., Bellot Rubio, L.R., Orozco Suárez, D.: Formation of solar magnetic flux tubes with kilogauss field strength induced by convective instability. Astrophys. J. Lett. **677**, L145 (2008)

Ogawara, Y., Takano, T., Kato, T., Kosugi, T., Tsuneta, S., Watanabe, T., Kondo, I., Uchida, Y.: The solar-A mission – an overview. Sol. Phys. **136**, 1 (1991)

Okamoto, T.J., Tsuneta, S., Berger, T.E., Ichimoto, K., Katsukawa, Y., Lites, B.W., Nagata, S., Shibata, K., Shimizu, T., Shine, R.A., Suematsu, Y., Tarbell, T.D., Title, A.M.: Coronal transverse magnetohydrodynamic waves in a solar prominence. Science **318**, 1577 (2007)

Sakao, T., Kano, R., Narukage, N., Kotoku, J., Bando, T., DeLuca, E.E., Lundquist, L.L., Tsuneta, S., Harra, L.K., Katsukawa, Y., Kubo, M., Hara, H., Matsuzaki, K., Shimojo, M., Bookbinder, J.A., Golub, L., Korreck, K.E., Su, Y., Shibasaki, K., Shimizu, T., Nakatani, I.: Continuous plasma outflows from the edge of a solar active region as a possible source of solar wind. Science **318**, 1585 (2007)

Schrijver, C.J., DeRosa, M.L., Metcalf, T., Barnes, G., Lites, B., Tarbell, T., McTiernan, J., Valori, G., Wiegelmann, T., Wheatland, M.S., Amari, T., Aulanier, G., Démoulin, P., Fuhrmann, M., Kusano, K., Régnier, S., Thalmann, J.K.: Nonlinear force-free field modeling of a solar active region around the time of a major flare and coronal mass ejection. Astrophys. J. **675**, 1637 (2008)

Shibata, K., Nakamura, T., Matsumoto, T., Otsuji, K., Okamoto, T.J., Nishizuka, N., Kawate, T., Watanabe, H., Nagata, S., UeNo, S., Kitai, R., Nozawa, S., Tsuneta, S., Suematsu, Y., Ichimoto, K., Shimizu, T., Katsukawa, Y., Tarbell, T.D., Berger, T.E., Lites, B.W., Shine, R.A., Title, A.M.: Chromospheric anemone jets as evidence of ubiquitous reconnection. Science **318**, 1591 (2007)

Shimizu, T., Lites, B.W., Katsukawa, Y., Ichimoto, K., Suematsu, Y., Tsuneta, S., Nagata, S., Kubo, M., Shine, R.A., Tarbell, T. D.: Frequent occurrence of high-speed local mass downflows on the solar surface. Astrophys. J. **680**, 1467 (2008a)

Shimizu, T., Nagata, S., Tsuneta, S., Tarbell, T., Edwards, C., Shine, R., Hoffmann, C., Thomas, E., Sour, S., Rehse, R., Ito, O., Kashiwagi, Y., Tabata, M., Kodeki, K., Nagase, M., Matsuzaki, K., Kobayashi, K., Ichimoto, K., Suematsu, Y.: Image stabilization system for Hinode (solar-B) solar optical telescope. Sol. Phys. **249**, 221 (2008b)

Suematsu, Y., Tsuneta, S., Ichimoto, K., Shimizu, T., Otsubo, M., Katsukawa, Y., Nakagiri, M., Noguchi, M., Tamura, T., Kato, Y., Hara, H., Kubo, M., Mikami, I., Saito, H., Matsushita, T., Kawaguchi, N., Nakaoji, T., Nagae, K., Shimada, S., Takeyama, N., Yamamuro, T.: the solar optical telescope of solar-B (Hinode): the optical telescope assembly. Sol. Phys. **249**, 197 (2008)

Tsuneta, S., Ichimoto, K., Katsukawa, Y., Nagata, S., Otsubo, M., Shimizu, T., Suematsu, Y., Nakagiri, M., Noguchi, M., Tarbell, T., Title, A., Shine, R., Rosenberg, W., Hoffmann, C., Jurcevich, B., Kushner, G., Levay, M., Lites, B., Elmore, D., Matsushita, T., Kawaguchi, N., Saito, H., Mikami, I., Hill, L.D., Owens, J.K.: The solar optical telescope for the Hinode mission: an overview. Sol. Phys. **249**, 167 (2008)

Chapter 2
Hinode's Contributions to Solar Physics

Takashi Sakurai

Abstract High-resolution optical observations of the Sun in the pre-*Hinode* era, typically at spatial resolutions of 1–2 arcsec, are reviewed, and the new findings of *Hinode* with 0.2 arcsec resolution for magnetic flux tubes, polar fields, canopy structure, and horizontal magnetic fields are presented. In combination with the X-ray and extreme ultraviolet instruments on *Hinode*, I present observations of coronal waves in the context of coronal heating and the acceleration of the solar wind from active regions.

Keywords Sun: corona · Magnetic fields: measurements · Sun: magnetic field · Solar activity cycle · Solar wind

2.1 High-Resolution Observation of the Sun in the Visible Wavelengths

The largest instrument onboard *Hinode* is the Solar Optical Telescope (SOT), an optical telescope with a main mirror aperture of 50 cm. In the observational studies of the Sun, high-resolution imaging has always been a central issue. Why is that so?

The resolving power (the so-called diffraction limit in optics) of a telescope is given by the formula: (observing wavelength)/(telescope aperture). For example, at a wavelength of 500 nm (green light), a 10 cm aperture telescope gives a resolving power of about 1 arcsec. (Hence, a 50 cm telescope like SOT provides a resolving power of 0.2 arcsec.) The Sun's apparent diameter is about 2000 arcsec; therefore, with a resolution of 1 arcsec, the entire solar image is divided into 2000 × 2000 pixels. In actuality, however, turbulence in the atmosphere causes image distortions (called "seeing" in astronomy). A larger aperture does not automatically guarantee

T. Sakurai (✉)
National Astronomical Observatory of Japan, Mitaka, Tokyo, Japan
e-mail: sakurai@solar.mtk.nao.ac.jp

T. Shimizu et al. (eds.), *First Ten Years of Hinode Solar On-Orbit Observatory*,
Astrophysics and Space Science Library 449,
https://doi.org/10.1007/978-981-10-7742-5_2

an increase in resolving power in proportion to the aperture. The situation is particularly problematic when observing the Sun, because of turbulent air from the heated ground or inside the warmed telescope tube. During the 1960s, solar astronomers recognized that the resolution could be improved consistently beyond 1 arcsec by choosing an observing site in high mountains or by the side of a lake or ocean (isolated islands) or by evacuating the telescope tube. A benchmark for a good image resolution is to clearly see granules, which are convective cells on the solar surface with a size of 1–2 arcsec (about 1000 km). However, it was still not possible to detect any structure smaller than the granules (e.g., the flux tubes described later).

An attempt to get rid of the atmospheric seeing effect by observing from outside the atmosphere also started in the early days with balloon experiments. The most famous one is the Stratoscope experiment (a 30 cm aperture telescope) led by M. Schwarzschild of Princeton University in 1957 (Schwarzschild 1959). It may be said, though, that the balloon floats because there actually is an atmosphere thin it is. The first "real" observation of the Sun from outside the atmosphere was the Spacelab-2 experiment (July 29–August 5, 1985) carried on the Space Shuttle Challenger (Title et al. 1989). (Among the crew was Loren Acton, who later became the US principal investigator of the X-ray telescope onboard *Yohkoh*.) The aperture of the telescope was 30 cm, and they planned magnetic field observations as well, but the instrument did not work until the last day due to troubles with the power supply. Consequently, they were able to obtain an image sequence that lasted only for 16 h. (The tragic accident of Challenger was the second flight after this one.) American solar astronomers then proceeded to propose a more full-scale space-borne optical solar telescope with an aperture of 1 m (interestingly it was also called SOT), but the plan never materialized. In Europe, a large ground-based solar telescope LEST (Large European Solar Telescope) with an aperture of 2.4 m was planned, but this was not approved either by the funding agencies. Thus, the *Hinode* SOT was a long-waited telescope for all solar researchers.

2.1.1 Magnetic Flux Tubes

When observing from the ground, the images are degraded due to atmospheric seeing even in simple imaging observations, but the effect of seeing is more serious for magnetic field observations. To measure the magnetic field, it is necessary to measure the polarization of spectral lines, which means that we have to combine multiple images. In addition, the optical system becomes complicated for polarimetry.

The instruments used to measure solar magnetic fields (called magnetographs) had only a resolution of 2–3 arcsec in the 1970s, but an indication of an unresolved small structure below the resolution limit was obtained (Harvey and Livingston 1969). The degree of polarization due to the Zeeman effect, if the magnetic field is not too strong (less than several hundred gauss), is proportional to the magnetic field strength and the Landé factor (determined by quantum mechanics for the transition

corresponding to the spectral line). However, if we observe a region with spectral lines with a Landé factor of about 1 and of about 3, this proportionality relation does not hold. The degree of polarization of the line with the larger Landé factor is smaller than the theory predicts. There are several ways to explain this discrepancy. The most probable one (which is believed to be true today) is that the magnetic field is not uniform over the observed region (a pixel of a few arcsec in size); the magnetic field is concentrated in a small portion of the region, while the rest of the region has no magnetic field. For example, a pixel whose magnetic field is measured to be 10 gauss is actually made of a magnetic field of 1000 gauss occupying only 1% of the area. If the magnetic field strength is 1000 gauss or more, the polarization saturates for a spectral line with a large Landé factor, and the line exhibits a polarization that is lower than what the proportionality approximation predicts. It was also conjectured that the bright points with sizes of about 0.2–0.3 arcsec (about 200 km on the Sun) that are seen in the intergranular lanes might correspond to this concentrated magnetic field. Hence the name "intense flux tubes" was given to this, then hypothetical, object.

Even before *Hinode*, there had been attempts by ground-based observations to measure the magnetic field in flux tubes directly. However, the *Hinode* SOT has made it possible for the first time to measure accurately and reliably the magnetic field in small-scale flux tubes (Fig. 2.1). A process called "convective collapse," predicted by theory, was observed in which the magnetic field compressed by the granular motions turns into a flux tube with a field strength of about 1500 gauss (Nagata et al. 2008). When the magnetic field strength reaches 1500 gauss, the magnetic outward force (magnetic pressure) balances the inward pressure of the surrounding plasma, so that the internal volume of the flux tube may lose the plasma and still support the tube. Therefore, the density in the tube decreases, and the tube becomes a route through which radiation can escape easily. Because of this effect, the Sun is brighter when there is plenty of magnetic flux on the surface (i.e., during activity maximum periods). Therefore, the physical processes in the magnetic flux tubes are closely related to the amount of solar energy reaching the Earth.

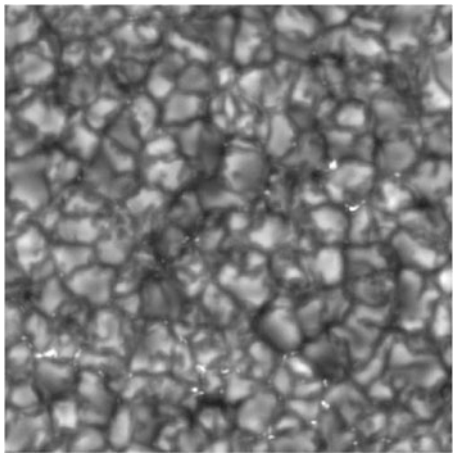

Fig. 2.1 High-resolution image of the Sun with *Hinode*/SOT at a wavelength of 430 nm (NAOJ, ISAS/JAXA)

2.1.2 Polar Magnetic Field

The regions with the strongest magnetic fields on the Sun are the sunspots; they have magnetic fields of about 2000–4000 gauss. The Zeeman effect of the spectral lines in sunspots was discovered by G.E. Hale of the Mt. Wilson Observatory in 1908 (Hale 1908). The magnetic field in the polar region is weak (only a few gauss) compared to that of the sunspots. Therefore we had to wait until a high-sensitivity magnetograph was developed (also at Mt. Wilson) in the 1950s. In 1957, a reversal of the polar magnetic field was observed (Babcock 1959). Continued observations show that the polar magnetic field is the strongest and most extended when the number of sunspots is small (in activity minimum periods) and weakens and reverses its sign in the active maximum periods. In the theory of solar magnetic field generation (the so-called dynamo mechanism), the polar magnetic field serves as the seed. It is stretched and amplified by the differential rotation of the Sun (i.e., the Sun rotates faster near the equatorial region compared to the high-latitude regions), and the magnetic field becomes oriented in the east-west direction, which is the source of the sunspots.

On the other hand, small point-like bright structures called "polar faculae" are known to exist in the polar region. Their number changes with the 11-year sunspot cycle, but they are out of phase, i.e., the polar faculae are more numerous in the activity minimum periods. It was conjectured that the polar field, which is on average a few gauss in strength, is also concentrated into flux tubes that are seen as polar faculae. There were fragmentary observations that the polar faculae have magnetic field of the order of 1000 gauss. The *Hinode* SOT has made it possible to observe for the first time that the magnetic field in the polar region is concentrated into flux tubes (Tsuneta et al. 2008) with a field strength exceeding 1000 gauss (Fig. 2.2). The orientation of the magnetic field vectors, and henceforth the magnetic flux in the polar region, is also accurately derived. Polar faculae are found to correspond to flux tubes with higher field strength and larger size; not all of the flux tubes show up as polar faculae (Kaithakkal et al. 2013).

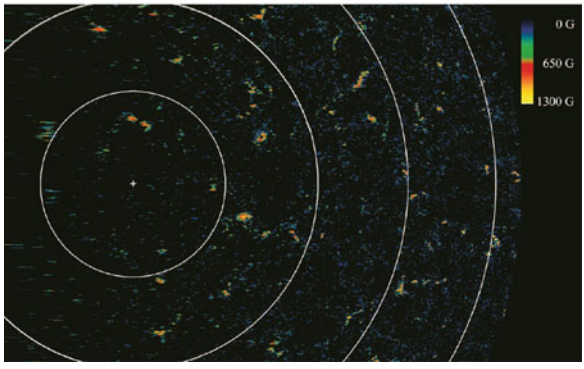

Fig. 2.2 Magnetic field of the Sun's south polar region in 2007 (NAOJ, ISAS/JAXA) (Tsuneta et al. 2008)

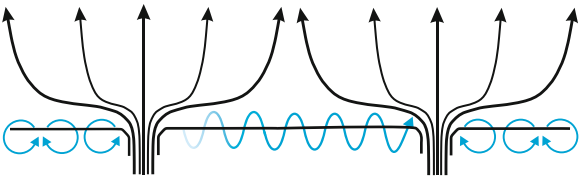

Fig. 2.3 Canopy structure and the horizontal magnetic fields. Whether the latter form a serpentine or rings is the author's imagination

2.1.3 Canopy Structure and Horizontal Magnetic Field

In the surface layer of the Sun (the photosphere with a temperature of about 6000 K), the atmospheric pressure rapidly decreases with height. Therefore the magnetic field in a flux tube cannot be confined in the tube as one goes up to higher layers. The magnetic field inevitably expands and fills the volume. The funnel-shaped structure made of magnetic field lines is called a canopy structure (Giovanelli 1980). Under the canopy, there is believed to be a nonmagnetic atmosphere where only (ineffective) nonmagnetic heating mechanisms might be in operation, and the temperature continues to decrease with height down to around 4200 K. Beyond this height the atmosphere is covered with canopy magnetic fields and heated to a million-degree temperature.

However, the *Hinode* SOT has discovered that the volume below the canopy is not nonmagnetic but is filled with magnetic fields of a few hundred gauss, directed nearly horizontally (Ishikawa and Tsuneta 2009) (Fig. 2.3). The amount of the horizontal field is not correlated with the amount of the vertical magnetic field coming from the magnetic flux tubes. Therefore, it will not follow the 11-year solar cycle. Theoretical studies suggest that the horizontal magnetic field is created by turbulent convection in the Sun's surface layer, not by a mechanism related to the rotation of the Sun or its Coriolis effect. Because the amount of the horizontal field is independent of the amount of magnetic flux in a region, it will not be responsible for the heating of the corona over regions of strong magnetic fields near sunspots (the so-called active regions). On the other hand, it may be that the heating of the corona in regions of weak magnetic field or the heating of the atmosphere of slowly rotating stars, which was thought to be due to sound waves, actually is caused by magnetic heating.

2.2 Discovery of Various Waves and Corona Heating

Although the surface of the Sun is only 6000 K, the corona of 1–2 million K (MK) is formed above the surface. How such a heating is possible is the problem of coronal heating, which is one of the most important and yet unresolved problems in solar and stellar physics. The temperature of the corona (1–2 MK) was identified around 1940. The first theory to explain the high temperature of the corona assumes that the pressure perturbation generated by the convective motion in the Sun's surface

layer is transmitted to the upper layers as sound waves. The amplitude of the sound waves increases as they propagate because the density of the atmosphere decreases with height. The sound waves evolve into shock waves and will be dissipated and heat the atmosphere. This theory is called the acoustic heating theory. When X-ray observations of the corona from satellites started in the 1970s, it became clear that the hot and dense part of the corona corresponds to the active regions with strong magnetic fields. The acoustic theory was then modified to theories using magnetic waves instead of acoustic waves.

On the other hand, in the corona around the active regions, an explosive phenomenon called a flare occurs intermittently, in which the plasma is heated to more than 10 MK, particles are accelerated to high energies, and a huge plasma cloud (called a coronal mass ejection, CME) is ejected. Large flares occur only rarely, but smaller flares are frequent. Parker (1972) proposed the microflare theory, which assumes that small flares are taking place all the time and are heating the corona.

Hinode has discovered various wave phenomena (Okamoto et al. 2007), and significant progress has been made in terms of using waves as a diagnostic tool. However, it is not yet clear whether the detected waves carry large enough energy to heat the corona (particularly the hot and high-pressure portion of the corona around the active regions). On the other hand, the microflare theory also has problems; the number of small flare events is insufficient to explain the heating of the corona (Shimizu 1995). According to the recent observation of hard X-ray spectra of an active region, the amount of plasma with a temperature exceeding 10 MK, which is supposed to be created by microflares, is small (Ishikawa et al. 2014),

Before the launch of *Hinode*, we expected that the coronal heating problem would be solved if data were available to show the relationship between the phenomena on the solar surface and the resultant heating in the corona. It turned out that this expectation was too naive, because the resolution of the X-ray and extreme ultraviolet (EUV) data of *Hinode* is still no better than 1 arcsec, and the diagnostic capability of *Hinode* in regions between the surface and the corona (the chromosphere with a temperature of about 10^4 K) is limited. The Interface Region Imaging Spectrograph (IRIS) satellite launched by NASA in 2013 has been carrying out high-resolution spectroscopic observations of the chromosphere, and joint observations with *Hinode* are expected to bring us closer to an answer.

2.3 Active Region Outflows and the Solar Wind

The solar corona, because of its high temperature, cannot be held by the gravity of the Sun and flows out into the interplanetary space as the solar wind. The high-speed wind comes from the polar region where the magnetic field lines are open to the interplanetary space and the plasma flows out easily. The high-speed wind in the vicinity of the Earth's orbit has a speed of about 800 km s^{-1}. On the other hand, a slow wind with a speed of about 300 km s^{-1} flows out from low-latitude

regions. It was not clear how the plasmas in the low-latitude regions could escape from the Sun because the magnetic field lines are mostly closed (not connected to the interplanetary space) there.

In 1992, using data from the Soft X-ray telescope (SXT) onboard *Yohkoh*, Uchida et al. (1992) discovered that the loops of magnetic field lines extending from the active regions expand into the interplanetary space. They advocated that this "active region expansion" is a source of the slow solar wind. It is widely accepted that such a phenomenon occurs when the magnetic loops rise one after another from below the surface in an emerging flux region. It is still debated whether this expansion continues after the flux emergence phase ends when an active region is matured or whether it provides enough mass flux into the slow wind.

On the other hand, the *Hinode* X-ray telescope (XRT), which has better temporal and spatial resolution than SXT onboard *Yohkoh*, discovered a pattern of continuous outflow from the edge of an active region (Sakao et al. 2007). The Doppler velocity was also measured by the *Hinode* Extreme Ultraviolet Imaging Spectrometer (EIS), and the flow of the plasma was confirmed (Harra et al. 2008). From the model calculation of the magnetic field lines, the flow is along the field lines that connect a small portion in the active region to the interplanetary space (He et al. 2010). Further study is needed to confirm whether this is the main source of the slow wind.

2.4 Outlook for the Future

Our understanding of the physics of solar flares has been significantly advanced by the *Yohkoh* satellite; this was brought by the combination of hard and soft X-ray observations (Masuda et al. 1994; Tsuneta 1996). In *Hinode*, the emphasis has been shifted to lower-energy phenomena, and in this sense, *Hinode*'s contributions to flare physics might be said to be incremental. Flares, particularly the big ones, are relatively rare events, and it is difficult to obtain synthetic data that combine multiwavelength and physically diverse observations under favorable conditions. This is still the case at present. Compared to this situation inherent to flare studies, investigations of the heating mechanisms of the corona can be well planned because the heating must be taking place everywhere continuously. If we are not yet at the goal of this research, it is not due to a lack of favorable events but is due either to incomplete planning (hope not) or to insufficient instrumentation because of limitations in budget or the capacity of the spacecraft. So, which way should we proceed after *Hinode*? Three important factors to consider are increases in spatial resolution, wavelength coverage (and height coverage in the solar atmosphere), and polarimetric measurement accuracy. Numerical simulations of the solar atmosphere with radiation and magnetic fields included will become indispensable to interpret the observations and to understand the underlying physics. Whether the goal is achieved by next-generation space observatories or by ground-based telescopes is hard to predict, but it will not take long because the problems are already quite narrowed down (Sakurai 2017).

Acknowledgements This work was supported by JSPS KAKENHI Grant Numbers JP15K05034 and JP15H05816. *Hinode* is a Japanese mission developed and launched by ISAS/JAXA, with NAOJ as a domestic partner and NASA and STFC (UK) as international partners. It is operated by these agencies in cooperation with ESA and NSC (Norway).

References

Babcock, H.D.: The Sun's polar magnetic field. Astrophys. J. **130**, 364–365 (1959)
Giovanelli, R.G.: An exploratory two-dimensional study of the coarse structure of network magnetic fields. Solar Phys. **68**, 49–69 (1980)
Hale, G.E.: On the probable existence of a magnetic field in sun-spots. Astrophys. J. **28**, 315–343 (1908)
Harra, L.K., Sakao, T., Mandrini, C.H., et al.: Outflows at the edges of active regions: contribution to solar wind formation? Astrophys. J. Lett. **676**, L147 (2008)
Harvey, J., Livingston, W.: Magnetograph measurements with temperature-sensitive lines. Solar Phys. **10**, 283–293 (1969)
He, J.-S., Marsch, E., Tu, C.-Y., Guo, L.-J., Tian, H.: Intermittent outflows at the edge of an active region – a possible source of the solar wind? Astron. Astrophys. **516**, A14 (2010)
Ishikawa, R., Tsuneta, S.: Comparison of transient horizontal magnetic fields in a plage region and in the quiet Sun. Astron. Astrophys. **495**, 607–612 (2009)
Ishikawa, S., Glesner, L., Christie, S., et al.: Constraining hot plasma in a non-flaring solar active region with FOXSI hard X-ray observations. Publ. Astron. Soc. Jpn. **66**, S15 (2014)
Kaithakkal, A.J., Suematsu, Y., Kubo, M., Shiota, D., Tsuneta, S.: The association of polar faculae with polar magnetic patches examined with Hinode observations. Astrophys. J. **776**, 122 (2013)
Masuda, S., Kosugi, T., Hara, H., Tsuneta, S., Ogawara, Y.: A loop-top hard X-ray source in a compact solar flare as evidence for magnetic reconnection. Nature **371**, 495–497 (1994)
Nagata, S., Tsuneta, S., Suematsu, Y., et al.: Formation of solar magnetic flux tubes with kilogauss field strength induced by convective instability. Astrophys. J. Lett. **677**, L145 (2008)
Okamoto, J.T., Tsuneta, S., Berger, T., et al.: Coronal transverse magnetohydrodynamic waves in a solar prominence. Science **318**, 1577–1580 (2007)
Parker, E.N.: Topological dissipation and the small-scale fields in turbulent gases. Astrophys. J. **174**, 499–510 (1972)
Sakao, T., Kano, R., Narukage, N., et al.: Continuous plasma outflows from the edge of a solar active region as a possible source of solar wind. Science **318**, 1585–1588 (2007)
Sakurai, T.: Heating mechanisms of the solar corona. Proc. Jpn. Acad. Ser. B **93**, 87–97 (2017)
Schwarzschild, M.: Photographs of the solar granulation taken from the stratosphere. Astrophys. J. **130**, 345–363 (1959)
Shimizu, T.: Energetics and occurrence rate of active-region transient brightenings and implications for the heating of the active-region corona. Publ. Astron. Soc. Jpn. **47**, 251–263 (1995)
Title, A.M., Tarbell, T.D., Topka, K.P., et al.: Statistical properties of solar granulation derived from the SOUP instrument on Spacelab 2. Astrophys. J. **336**, 475–494 (1989)
Tsuneta, S.: Structure and dynamics of magnetic reconnection in a solar flare. Astrophys. J. **456**, 840–849 (1996)
Tsuneta, S., Ichimoto, K., Katsukawa, Y., et al.: The magnetic landscape of the Sun's polar region. Astrophys. J. **688**, 1374–1381 (2008)
Uchida, Y., McAllister, A., Strong, K.T., et al.: Continual expansion of the active-region corona observed by the Yohkoh Soft X-ray Telescope. Publ. Astron. Soc. Jpn. **44**, L155–L160 (1992)

Chapter 3
Ten-Year Results of Solar Optical Telescope (SOT) Onboard *Hinode*

Yoshinori Suematsu

Abstract Since the scientific operation of *Hinode* started at the end of 2006 October, the Solar Optical Telescope onboard *Hinode* has provided unprecedentedly high-resolution and high-precision data on the magnetized solar photosphere and chromosphere. I review the achievements enabled by SOT observations in its first decade in terms of the *Hinode*'s scientific goals, such as understanding the formation and heating mechanism of the outer atmosphere and basic plasma processes such as magnetic reconnection occurring there.

Keywords Hinode · SOT · Sun: photosphere · Sun: chromosphere · Sun: magnetic field

3.1 Scientific Objectives of Solar Optical Telescope

The *Hinode* satellite (Kosugi et al. 2007; Shimizu 2018) was designed to answer the fundamental questions of how magnetic fields are formed and how they dissipate to create the solar chromosphere and corona and to explore the physical coupling between the photosphere and the upper layers in order to understand the mechanism of their dynamics and heating. These questions are ultimately related to all phenomena that have an impact on the Sun-Earth system, such as the formation of the solar winds, triggering of jets and flares with intense nonthermal particle acceleration and coronal mass ejections, and the formation and maintenance of prominences.

There are three instruments onboard *Hinode*, the Solar Optical Telescope (SOT), X-Ray Telescope (XRT), and Extreme-Ultraviolet (EUV) Imaging Spectrometer (EIS), each of which measures critical parts of the solar atmosphere from the photosphere to the chromosphere, the transition region, and finally the outer and

Y. Suematsu (✉)
National Astronomical Observatory of Japan, Mitaka, Tokyo, Japan
e-mail: suematsu@solar.mtk.nao.ac.jp

T. Shimizu et al. (eds.), *First Ten Years of Hinode Solar On-Orbit Observatory*,
Astrophysics and Space Science Library 449,
https://doi.org/10.1007/978-981-10-7742-5_3

hottest part of the atmosphere, the corona. The concept of *Hinode* is that the X-ray and EUV telescopes observe the dissipative part of the magnetic life cycle history and the optical telescope simultaneously observes the generation and transport of magnetic fields.

The SOT (Tsuneta et al. 2008a) is the largest optical telescope yet flown in space to observe the Sun. It has an aperture of 50 cm and achieves an angular resolution of 0.2–0.3 arcsec covering a wavelength range from 380 to 660 nm. It consists of two optical components, the Optical Telescope Assembly (OTA) (Suematsu et al. 2008a) and the Focal Plane Package (FPP). The FPP includes a narrowband filter imager (NFI) and a broadband filter imager (BFI) (Tsuneta et al. 2008a) and a Stokes spectropolarimeter (SP) at a pair of photospheric magnetic sensitive lines of Fe I 630.15/630.25 nm (Lites et al. 2013; Lites and Ichimoto 2013). Low-frequency pointing jitter is suppressed by an active image stabilization system consisting of a correlation tracker in the FPP, a tip-tilt mirror in the OTA, and a satellite pointing jitter controller (Shimizu et al. 2008). This complex instrument allows very accurate magnetic field measurements in both the longitudinal and transverse directions, Doppler shift measurements, and imaging in the range from the low photosphere through the chromosphere under precise polarimetric calibration (Ichimoto et al. 2008).

Magnetic fields carry kinetic energy through waves and fluctuations, can store energy that is dissipated via magnetic reconnection, and induces magnetohydrodynamic (MHD) instability and eruptions. Thus, to understand the origin of solar active phenomena, it is very important to observe their fine-scale structure and accurately measure their magnetic fields on the Sun. From this viewpoint, highlights of the new observational results from *Hinode* are described below.

This review summarizes how the new results from *Hinode*, in particular those from the SOT, are addressing these critical questions and probing fundamental physical processes such as magnetic reconnection.

3.2 Resolution of Photospheric Magnetic Structures in Quiet Sun

Photospheric magnetic flux tubes with kilogauss field strength and a spatial scale of a few hundreds of kilometers are ubiquitously found across the entire solar surface. These flux tubes appear as G-band bright or facular points. The field strength should be limited by the equipartition magnetic energy (typically 400 G) corresponding to the kinetic energy density of the granular flows (Katsukawa and Orozco Suarez 2012). Thus, further intensification is necessary to explain the kilogauss field strength flux tubes. One theory is that the plasma in flux tubes emerges from below, cools, and falls owing to suppression of heat and the flux tube narrows until the magnetic pressure of the evacuated flux tube balances the surrounding gas pressure. This process, referred to as convective collapse (Parker 1978; Spruit 1979), has

been studied for almost 30 years and was finally confirmed by *Hinode* (Nagata 2008). Good coincidence was found between the field strength intensification and the downward motion. SOT-SP observations indicate that the initial field strength of 400 G in the photosphere is intensified to 2,000 G as the downflow grows to 6 km s^{-1} in 150 s. The events are accompanied by a continuum bright point and nearly always by a brightening in the Ca II H images, and a strong downflow in Mg I b_2 line formed in the upper photosphere (Fischer et al. 2009). Convective collapse occurs ubiquitously, even in the Sun's polar regions (Tsuneta et al. 2008b), in the convective atmosphere, and is an essential ingredient in the formation of flux tubes with intense magnetic fields.

The magnetic field outside of active regions was thought to be organized mainly as flux tubes of kilogauss strength delineating the supergranular boundaries (network) with nearly field-free internetwork cells. This view changed when ubiquitous weak fields inside the internetwork cells were found by Trujillo Bueno et al. (2004) with ground-based observations. The *Hinode* observations by Lites, Ishikawa, and others (Lites et al. 2008; Ishikawa and Tsuneta 2009; Ishikawa et al. 2007; Ishikawa and Tsuneta 2010; Centeno et al. 2007; Orozco Suárez et al. 2007; Orozco Suárez and Katsukawa 2012) strengthened this finding considerably (Fig. 3.1). They found transient horizontal magnetic fields that are characterized by a horizontal field with random direction, a size as small as a granular cell, a lifetime as short as the convection turnover time, and a magnetic field strength smaller than the equipartition strength. These unique properties are completely different from those of the vertical magnetic elements. The horizontal fields are ubiquitous in both the quiet Sun and active regions (Ishikawa and Tsuneta 2010), and their total magnetic flux is larger than that of the vertical fields (Lites et al. 2008). It appears that the convection layer has an inherent property that produces these horizontal fields. We may call this the local dynamo process (Ishikawa and Tsuneta 2010; Lites 2011).

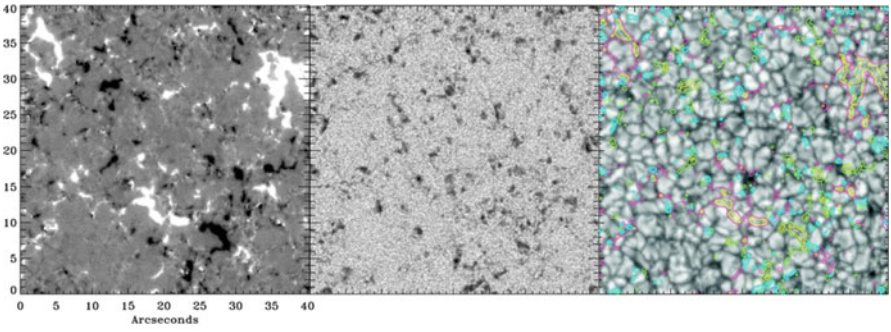

Fig. 3.1 *Hinode* SOT-SP observations revealing the existence of ubiquitous horizontal weak magnetic fields. The gray scale images are shown for the longitudinal (left panel), transverse field components (middle panel), and continuum intensity with contours of magnetic fields overlaid (right panel). Red and green contours indicate the longitudinal positive and negative components of 24 G level, respectively. Yellow and blue contours are for the longitudinal of 100 G and transverse component of 122 G level, respectively (Reproduced with permission by Lites et al. 2008)

However, the appearance and disappearance of magnetic features are still mysterious, since unipolar appearance and disappearance are common in the photosphere. It was confirmed using SOT-NFI 0.3-arcsec–resolution magnetograms at disk center that the apparent unipolar magnetic flux emergence is the coalescence of previously existing like-polarity diffused magnetic flux (Lamb et al. 2010) and that the dominant process of their disappearance is through flux dispersion (unipolar disappearance) (Lamb et al. 2013). The SOT-SP Doppler velocity measurements revealed that the polar magnetic patches are surrounded by a strong horizontal converging flow during the period of their formation, suggesting the concentration of like-polarity flux fragments by the converging flow field and the disintegration of the magnetic patch into like-polarity fragments (Kaithakkal et al. 2015). It is likely that the SOT does not resolve the fundamental scale of flux emergence: most new magnetic features seem to arise through coalescence of unresolved magnetic flux into larger concentrations that can be resolved by the SOT. Those SOT observations imply that processes on spatial scales smaller than those visible to the SOT dominate the processes of flux emergence and cancelation.

The supergranular boundary (network) harbors a sizable fraction of the total quiet-Sun flux, although its origin and maintenance are not well known. *Hinode* SOT-NFI long-duration (12–32 h) observations revealed that the internetwork magnetic fields contributed to the network flux (Orozco Suárez et al. 2012; Gošić et al. 2014, 2016). Internetwork fields, which tend to drift toward the supergranular boundaries with a nonconstant velocity, permeate the interior of supergranular cells and show large emergence rates (Fig. 3.2). Then, 14% of the quiet-Sun flux was found to be in the form of internetwork fields with little temporal variations, which

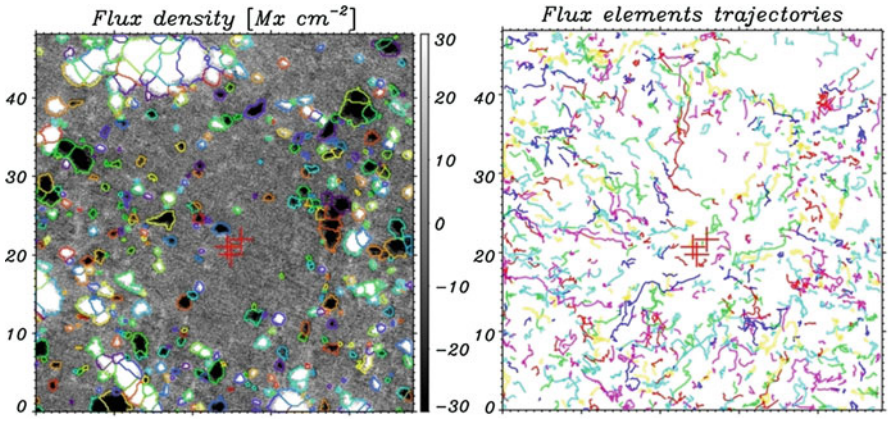

Fig. 3.2 Left: a snapshot from the time sequence of SOT-NFI high-resolution magnetograms in Na I D_1 589.6 nm line. Black and white indicate negative and positive magnetic flux. Colors outline magnetic features detected with a tracking algorithm. Axis units are in arcsecond. Right: paths of some of the internetwork magnetic elements detected and tracked. The locations of the centers for radial flow fields are represented by red crosses in each panels (Adapted from Orozco Suárez et al. (2012), reproduced by permission of the AAS)

interact with network patches and modify the flux budget of the network, either by adding flux through merging processes or by removing it through cancelation events (Iida et al. 2012). Coalescence appears to be dominant, so the net flux contribution of the internetwork is positive. Most of the internetwork flux is lost through fading and interactions with the network, at nearly the same rate. It appears, therefore, that the sources and sinks of internetwork magnetic flux are well balanced. The observed rate of flux transfer to the network is so large that the internetwork supplies as much flux as is present in the network in 9–13 h. Considering that not all the transferred fluxes are incorporated into the network, this indicates that the internetwork would be able to replace the entire network flux in approximately 18–24 h. This makes the internetwork the most important contributor to the network. It is likely that about 40% of the total internetwork flux eventually ends up in the network.

On the other hand, long-term SOT-SP observations during 2008–2013 revealed no evidence for systematic changes in the weakest observable magnetic flux at moderate latitudes, as a function of time and solar latitude in either the unsigned line-of-sight flux or in measures of the transverse flux (Lites et al. 2014; Jin and Wang 2015a,b). However, in the polar regions where strong magnetic patches are observed (Tsuneta et al. 2008b), changes are apparent in the measure of signed magnetic flux corresponding to reversal of the polarity of the poles (Shiota et al. 2012), changes that persist even for the weakest observed flux. Also evident in measures of the weakest signed flux are preferences for positive (negative) polarity at mid-north (mid-south) latitudes (20°–60°). Center-to-limb variations in various measures of the weak flux appear to be independent of the solar cycle. The results are consistent with the operation of a small-scale solar dynamo operating within and just below the solar photosphere, but measures of the weakest signed flux still contain small signatures of the global solar cycle.

It is totally unknown at this point how the local dynamo process and its resultant horizontal fields are related to the global dynamo process, which produces sunspots and the activity cycle of the Sun (Hotta et al. 2016).

Studies in short-term behavior of magnetic flux tubes are important to solve the coronal heating problem. There are basically two models: MHD wave heating model, in which the waves propagate along the magnetic flux tubes, and nanoflare heating model in which braiding of magnetic fields in the corona is supposed to be caused by the shuffles of the magnetic elements in the photosphere.

Regarding the wave heating, Fujimura and Tsuneta (2009) investigated the weak fluctuations in temporal behaviors of SOT-SP data in active-region plages and pores, suggesting that the phase relations of the photospheric fluctuations can be explained by longitudinal (sausage mode) and/or transverse (kink mode) MHD waves and by the dominant existence of standing waves at the photosphere with a small but sufficient leakage toward the chromosphere. Kanoh et al. (2016) extended the wave observations by performing simultaneous SOT-SP and *Interface Region Imaging Spectrograph (IRIS* De Pontieu et al. 2014*)* observations of a sunspot umbra to derive the upward energy fluxes at two different atmospheric layers (photosphere and lower transition region) and to estimate the energy dissipation. It was found

that the difference between the energy fluxes is larger than the energy required to maintain the chromosphere in the sunspot umbrae, suggesting that the observed waves can make a crucial contribution to the heating of the chromosphere in the sunspot umbrae. In contrast, the upward energy flux derived at the lower transition region level is smaller than the energy flux required for heating the corona, implying that another heating mechanism is necessary.

To study the propagation of Alfvén wave along the flux tubes, the so-called $k-\omega$ diagrams of the photospheric horizontal velocity are for the first time derived using SOT G-band movies (Matsumoto and Kitai 2010). The power spectra from the diagrams typically have a double power-law shape bent over at a frequency of 4.7 mHz. The numerical MHD simulations of 1.5 dimension suggested that torsional Alfvén waves generated by the derived power spectra transfer sufficient energy to heat the quiet corona, although there exist simplification and a number of assumptions in the simulations (Matsumoto and Shibata 2010).

The nanoflare models of coronal heating suppose that convective motions in the photosphere shuffle the footpoints of coronal magnetic fields and thereby inject sufficient magnetic energy upward to account for the observed coronal and chromospheric energy losses in active regions.

Using high-resolution observations of magnetic fields in an active-region plage made with the SOT, this idea was studied by estimating the upward transport of magnetic energy using the vertical Poynting flux across the photosphere in the plage region (Welsch 2015; Yeates et al. 2014). In this plage region, it was found that the average vertical Poynting flux varied spatially but was upward and sufficient to explain coronal heating, with values near 5×10^{7} erg cm^{-2} s^{-1}. The energy input per unit magnetic flux was found to be on the order of 10^{5} erg s^{-1} Mx^{-1}. A comparison of the intensity in a Ca II H filter image co-registered with one plage magnetogram shows stronger spatial correlations with both the total field strength and unsigned vertical field than either the average vertical Poynting flux or the horizontal flux density. The observed Ca II H brightness enhancement, however, probably contains a strong contribution from a near-photosphere hot-wall effect of kilogauss flux tubes, which is unrelated to heating in the solar atmosphere.

A similar study was made in a well-developed active region using the *Hinode* SOT, to determine what gives rise to the temperature difference between warm loops [T = 1–2 million Kelvin (MK)], which are coronal loops observed at EUV wavelengths, and hot loops ($T > 3$ MK), which are coronal loops observed in X rays (Kano et al. 2014). It was found that outside sunspots, the magnetic filling factor in the solar network varies with location and is anticorrelated with the horizontal random velocity. Provided that the observed magnetic features consist of unresolved magnetic flux tubes, this anticorrelation can be explained by the ensemble average of flux tube motion driven by small-scale random flows. The observed data are consistent with a flux tube width of about 77 km and horizontal flow at about 2.6 km s^{-1} with a spatial scale of about 120 km. It was also found that outside sunspots, there is no significant difference between warm and hot loops either in the magnetic properties (except for the inclination) or in the horizontal random velocity at their footpoints, which are identified using the *Hinode* XRT and the *Transition*

Region and Coronal Explorer (TRACE). The energy flux injected into coronal loops by the observed photospheric motion of the magnetic fields was estimated to be 2×10^6 erg s^{-1} cm^{-2}, which is the same for both warm and hot loops. This suggests that coronal properties play a more important role than photospheric parameters in giving rise to temperature differences between active-region coronal loops.

3.3 Resolution of Dynamical Phenomena in the Chromosphere

Hinode has higher temporal, spatial, and velocity resolution than any previous satellite and is probing wavelength regimes in which such continuous time coverage had never been available. This has allowed us to measure waves in the atmosphere in a way we were unable to do before. Previous attempts to detect Alfvén waves using previous ground-based observations have yielded ambiguous results, but *Hinode* appears to open the door to observation of these waves in many different circumstances.

A spectacular example is solar prominences. These are large-scale, cool structures that are surrounded by the hot corona. It has been suggested that they are caused by plasma maintained in coronal horizontal magnetic field line configurations. Observations show horizontal threads of plasma that exhibit oscillatory behavior with periods around 170 s. This is consistent with Alfvén wave propagation, which may possibly heat the surrounding corona (Okamoto et al. 2007). Surprisingly, prominences in the quiet Sun show dark upward flows that are likely turbulent and move at speeds of 20 km s^{-1} (Berger et al. 2011). The existence of these flows is a real challenge to the current MHD understanding of prominences, as they are inconsistent with the magnetic support of heavy low-temperature plasma against gravity.

The chromosphere is highly structured. At the solar limb, spiky features known as spicules are seen in abundance (Tsiropoula et al. 2012 and references therein). Now with *Hinode*, observations can be made continuously without concerns about the effect of seeing conditions, unlike the case with ground-based telescopes. For example, SOT-BFI observations in the Ca II H line revealed that the spicules are even more dynamic than previously thought, having lifetimes of a minute, with widths of less than 200 km, and are moving predominantly upward with speeds of more than 100 km s^{-1} (De Pontieu et al. 2007b). It is likely that the spicules fading out in Ca II H appear in hotter passband, showing parabolic trajectories at tops as a whole, and that they consist of a mix of chromospheric and transition region temperatures; heating seems to be occurring toward their tops (Skogsrud et al. 2015).

The spicules show a swaying behavior strongly indicative of Alfvén waves. They show amplitudes and periods that are consistent with those of 5-min oscillation (De Pontieu et al. 2007a), and they have enough energy to power the solar wind. Using high cadence (1.6 s) SOT observations, shorter-period (<100 s) waves were

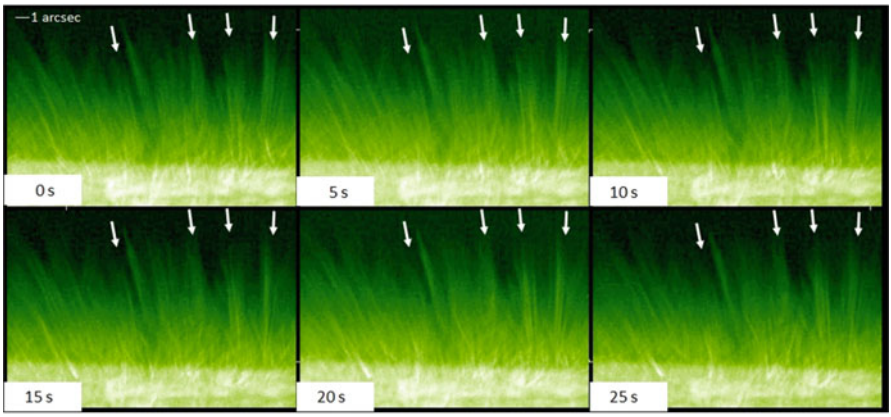

Fig. 3.3 High-resolution image time sequence of solar limb spicules taken with SOT-BFI in Ca II H filter. Arrows indicate prominent double-thread spicules that evolve with time

also found in the spicules, which are a mix of upward propagating, downward propagating, as well as standing waves (Okamoto and de Pontieu 2011). The observed high-frequency waves carry a significant energy flux enough to play a role in heating the corona. However, the observations suggest that most of these waves likely do not reach the corona in sufficient quantity because of the reflection off the transition region.

SOT high-resolution observations also revealed that most spicules have a double-thread structure during their life span (Suematsu et al. 2008b) (see, Fig. 3.3). It should be noted that the separation of some of the double-thread spicules changes with time, alternating between a single-thread phase and double-thread one. This change in separation can be interpreted by a spinning of spicules as a whole body: spin period of 1–1.5 min and velocity of 15 km s^{-1}. Rotation about the quasi-radial axis of spicules has been inferred in several spectroscopic studies from the tilts observed on slit spectra (e.g., De Pontieu et al. 2012), without fully resolving the components of spicules.

In addition, the SOT Ca II H observations indicate that many spicules tend to expand laterally or split into two or more strands after being ejected (Sterling et al. 2010). A possible explanation could be that many of the splitting or expanding spicules could be small-scale magnetic eruptions, analogous to coronal mass ejections.

The fine structure and lateral/spinning motion of the spicules suggest that they can be driven by spontaneous magnetic energy release (reconnection) at an unresolved spatial scale at their footpoints (Suematsu et al. 2008b). Most spicules emanate from seemingly unipolar magnetic regions, in contrast to the larger-scale jets associated with an emergence of small bipoles (e.g., Nishizuka et al. 2008), and the relevant magnetic reconnection must take place at a crossing field configuration (component reconnection) that was also suggested for penumbral microjets (see below), although there is no clear evidence for that.

In summary, the SOT observations have revealed dynamic nature of spicules than ever with little information on their formation mechanisms. Detailed spatial and temporal high-resolution observations of the magnetic and velocity fields at the photosphere-chromosphere boundary are crucial to understand the physics that governs the generation and dynamics of the chromospheric small-scale structures and to investigate their role in powering the Sun's outer atmosphere.

The SOT also revealed the ubiquitous presence of small-scale chromospheric jets outside sunspots in active regions (Shibata et al. 2007; Nishizuka et al. 2011). They are typically 2,000–5,000 km long and 150–300 km wide, showing velocities of 10–20 km s^{-1}. These jets have an inverted Y shape, similar to the shape of X-ray jets in the corona. These features imply that magnetic reconnection similar to that in the corona is occurring at a much smaller spatial scale throughout the chromosphere and suggest that heating of the solar chromosphere and corona may be related to small-scale ubiquitous magnetic reconnections.

One of the striking new findings from *Hinode* is small-scale jet-like features in the penumbral chromosphere (see details Katsukawa in this volume (Katsukawa 2018)). Penumbral microjets appear as transient brightenings in Ca II H broadband images, with a brightness about 10–20% greater than that of the underlying penumbral structures; they become invisible several tens of seconds after their appearance. They are ubiquitous in the penumbral chromosphere. Their length is typically between 1,000 and 4,000 km, and some have a length of up to 10,000 km. Their width is about 400 km or less. The most striking property of microjets is their duration of brightening. Almost all penumbral microjets have durations shorter than 1 min, which is much shorter than the time scales of the known dynamical phenomena yet observed. There are nearly horizontal magnetic fields along the dark penumbral filaments, and a penumbral microjet has its root between two dark penumbral filaments, where more vertical magnetic fields exist. The magnetic configuration possibly induces magnetic reconnection between the horizontal and vertical fields and generates transient jet-like brightenings.

Another striking finding of *Hinode* is chromospheric jets along a sunspot light bridge, which take appear intermittently and recurrently for more than 1 day (Shimizu et al. 2009) (Fig. 3.4). The apparent lengths of the jets are 1,500–3,000 km, which are much smaller than the typical length (10,000 km) of surges. The apparent upward velocity of the ejectors was estimated from positional changes in the top of the ejectors, which yield a wide distribution of 6–40 km s^{-1}; the actual upward velocity would be 26–180 km s^{-1}, considering the inclination of the magnetic field lines of the jets. The SOT-SP revealed obliquely oriented magnetic fields with vertical electric current densities higher than 100 mA m^{-2} along the light bridge, implying that current-carrying highly twisted magnetic flux tubes are trapped below a cusp-shaped magnetic structure along the light bridge. The presence of trapped current-carrying flux tubes is essential to the occurrence of long-lasting chromospheric plasma ejections at the interface with pre-existing vertically oriented umbral fields. A bidirectional jet was clearly detected there, suggesting magnetic reconnections occurring at very low altitudes, slightly above the height where the vector magnetic fields are measured.

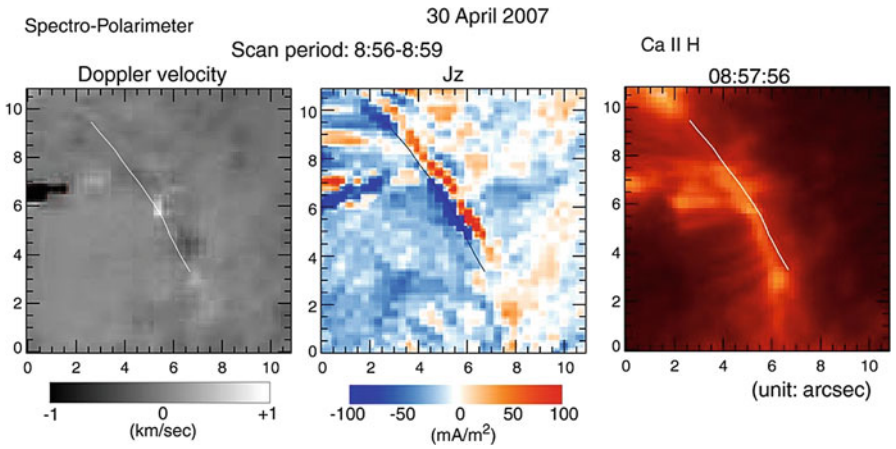

Fig. 3.4 Line-of-sight velocity (left) and vertical electrical current density (middle) derived from the *Hinode*-SP data and Ca II H image (right) showing a chromospheric ejection from the location where a downflow patch was detected in the line-of-velocity map. The positive values are red-shifted velocity, i.e., downward motion toward the photosphere. The solid line gives the location of the right edge of ejection footpoints (Reproduced with permission by Shimizu et al. 2009)

The Ellerman bombs (EBs) in active regions are interesting target to study magnetic reconnection at magnetic dips in undulatory magnetic field of emerging flux region. The SOT high-resolution observations showed that the Ca II H bright points identified with EBs were associated with the bipolar magnetic field structures and that the bright points consist of sub-arcsec core-halo structures: a central elongated bright core located along the magnetic neutral line and a diffuse halo as the models predict (Matsumoto et al. 2008). The observations of EBs suggest that a temperature enhancement region where the reconnection outflow and the U-shaped magnetic fields above the reconnection site collided with each other.

The SOT can observe jets in significantly more detail to study basic physical processes (Singh et al. 2012a,b; Yan et al. 2015). A report of a chromospheric jet presented complete observational evidence for the cause and consequence of chromospheric intermittent reconnection (Yan et al. 2015) (Fig. 3.5). The intermittent eruption of this jet showed two distinct quasiperiods, 50–60 s and 600–700 s. The short-period eruptions may be related to plasmoid-induced reconnection, and the long-period ones may be interpreted as sequences of cycles of energy storage and release during magnetic reconnections. The observations also reveal Alfvénic waves with a mean period of around 88 s and a maximum transverse displacement of around 0.26 arcsec. The jet is hosted by a loop moving smoothly with a horizontal speed of around 0.4 km s^{-1}. It is likely that these results provide observational evidence supporting the magnetic reconnection model of the formation of chromospheric jets with related products, in which loop advection drives intermittent magnetic reconnections, and reconnection outflows carrying plasmoids collide further with the ambient field lines and finally excite waves and jets.

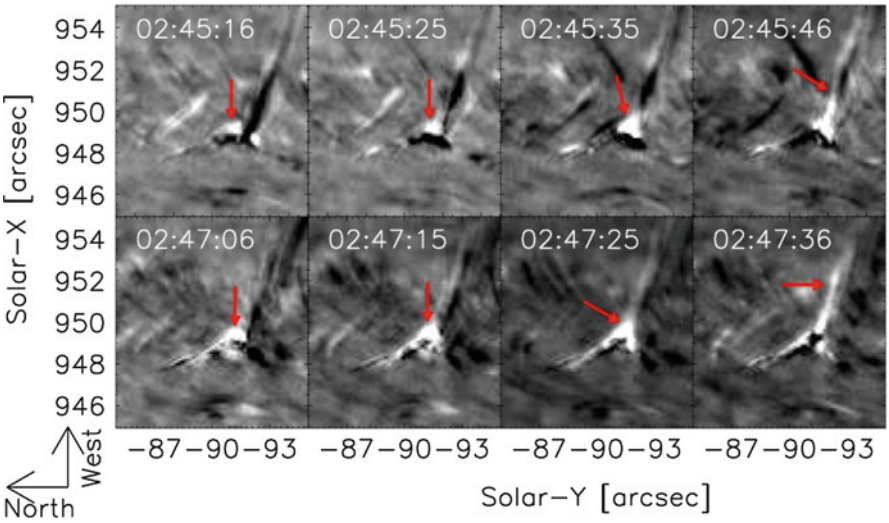

Fig. 3.5 Data sets obtained from SOT-BFI observations in the Ca II H filter between 00:00 and 03:45 UT on 2007 January 14. Running-difference images are shown, which were obtained with respect to the frame of three time steps prior. The arrows indicate bright blobs or plasma ejections (Adapted from Yan et al. (2015), reproduced by permission of the AAS)

3.4 Summary

The *Hinode* SOT has exhibited excellent performance on-orbit for more than 10 years. Many excellent papers have been published to date (most of which cannot be introduced here) using *Hinode*'s unprecedentedly high-quality data for the sub-photosphere (local helioseismology) through the corona.

Magnetic fields transfer kinetic energy to upper atmosphere by waves and fluctuations, can accumulate energy that is dissipated via magnetic reconnection and MHD instability, and induce heatings and eruptions. Thus, to understand the origin of solar active phenomena, it is very important to observe their fine-scale structure and accurately measure their magnetic fields on the Sun.

Hinode's higher temporal, spatial, and velocity resolution than any previous space-borne solar instruments has allowed us to measure waves in the atmosphere in a way we were unable to do before. Previous attempts to detect MHD waves have been ambiguous using ground-based observations which have yielded ambiguous results, but *Hinode* has opened the door to observation of these waves being observed in many different circumstances; the waves may carry enough energy to heat the corona and accelerate the solar wind in the quiet Sun.

SOT observations of active regions gave some evidence that an average vertical Poynting flux, in which photospheric motion shuffles the footpoints of coronal magnetic fields, varied spatially but was upward and sufficient to explain coronal heating.

High-resolution *Hinode* SOT observations also revealed that magnetic reconnection similar to that in the corona is occurring at a much smaller spatial scale throughout the chromosphere and suggested that heating of the solar chromosphere and corona may be related to small-scale ubiquitous magnetic reconnections. This finding promotes further study of magnetic reconnection in the atmosphere, where atoms are partially ionized and collisional (Singh et al. 2011), in contrast to the coronal conditions, and laboratory experiments of magnetic reconnection assimilating chromospheric jets (Nishizuka et al. 2012).

Unfortunately, the SOT filtergraph was terminated at the end of 2016 February, because of a short error in the filtergraph camera's electrical circuit. However, the SOT-SP is still healthy and performing various observations, focusing on higher resolution and a wider field of view. It should be stressed that the quality of SP polarization data is even superior in contrast to ground-based 1-meter class telescopes. New inversion techniques for deriving the magnetic field from polarimetric data are being advanced greatly by the application of spatial deconvolution techniques (Buehler et al. 2015; Quintero Noda et al. 2015) to enhance small-scale magnetic structure. Furthermore, the combination of SOT-SP with *IRIS* and ground-based advanced chromospheric (magnetic field) observations can provide three-dimensional view of magnetic structure, and we can expect more accurate quantitative analysis of evolving small-scale magnetic structure and the associated Poynting flux across the photosphere.

Acknowledgements I am much obliged to all those who actively contributed to the developments and completion of the *Hinode* SOT and the daily science operation of *Hinode*. I would like to thank the editors for their useful suggestion to improve the manuscript and Editage (www.editage.jp) for English language editing. *Hinode* is a Japanese mission developed and launched by ISAS/JAXA, in collaboration with NAOJ as a domestic partner and NASA and STFC (UK) as international partners. Scientific operation of the *Hinode* mission is conducted by the *Hinode* science team organized at ISAS/JAXA. This team consists mainly of scientists from institutes in the partner countries. Support for postlaunch operation is provided by JAXA and NAOJ (Japan), STFC, NASA, ESA, and NSC (Norway).

References

Berger, T., et al.: Magneto-thermal convection in solar prominences. Nature **472**, 197–200 (2011). https://doi.org.10.1038/nature09925

Buehler, D., et al.: Properties of solar plage from a spatially coupled inversion of Hinode SP data. A&A **576**, id.A27, 19 pp (2015). https://doi.org.10.1051/0004-6361/201424970

Centeno, R., et al.: Emergence of small-scale magnetic loops in the quiet-sun internetwork. ApJ **666**, L137–L140 (2007). https://doi.org.10.1086/521726

De Pontieu, B., et al.: Chromospheric Alfvénic waves strong enough to power the solar wind. Science **318**, 1574–1577 (2007a). https://doi.org.10.1126/science.1151747

De Pontieu, B., et al.: A tale of two spicules: the impact of spicules on the magnetic chromosphere. PASJ **59**, S655–S662 (2007b). https://doi.org.10.1093/pasj/59.sp3.S655

De Pontieu, B., et al.: Ubiquitous torsional motions in type II spicules. ApJ **752**, id.L12, 6 pp (2012). https://doi.org.10.1088/2041-8205/752/1/L12

De Pontieu, B., et al.: The interface region imaging spectrograph (IRIS). SoPh **289**, 2733–2779 (2014). https://doi.org.10.1007/s11207-014-0485-y

Fischer, C.E., et al.: Statistics of convective collapse events in the photosphere and chromosphere observed with the Hinode SOT. A&A **504**, 583–588 (2009). https://doi.org.10.1051/0004-6361/200912445

Fujimura, D., Tsuneta, S.: Properties of magnetohydrodynamic waves in the solar photosphere obtained with Hinode. ApJ **702**, 1443–1457 (2009). https://doi.org.10.1088/0004-637X/702/2/1443

Gošić, M., et al.: The solar internetwork. I. Contribution to the network magnetic flux. ApJ **797**, id.49, 11 pp (2014). https://doi.org.10.1088/0004-637X/797/1/49

Gošić, M., et al.: The solar internetwork. II. Flux appearance and disappearance rates. ApJ **820**, id.35, 8 pp (2016). https://doi.org.10.3847/0004-637X/820/1/35

Hotta, H., et al.: Large-scale magnetic fields at high Reynolds numbers in magnetohydrodynamic simulations. Science **351**, 1427–1430 (2016). https://doi.org.10.1126/science.aad1893

Ichimoto, K., et al.: Polarization calibration of the solar optical telescope onboard Hinode. SoPh **249**, 233–261 (2008). https://doi.org.10.1007/s11207-008-9169-9

Iida, Y., Hagenaar, H. J., Yokoyama, T.: Detection of flux emergence, splitting, merging, and cancellation of network field. I. Splitting and merging. ApJ **752**, id.149, 9 pp (2012). https://doi.org.10.1088/0004-637X/752/2/149

Ishikawa, R., Tsuneta S.: Comparison of transient horizontal magnetic fields in a plage region and in the quiet Sun. A&A **495**, 607–612 (2009). https://doi.org.10.1051/0004-6361:200810636

Ishikawa, R., et al.: Relationships between magnetic foot points and G-band bright structures. A&A **472**, 911–918 (2007). https://doi.org.10.1051/0004-6361:20066942

Ishikawa, R., Tsuneta, S., Jurčák, J.: Three-dimensional view of transient horizontal magnetic fields in the photosphere. ApJ **713**, 1310–1321 (2010). https://doi.org.10.1088/0004-637X/713/2/1310

Jin, C.L., Wang, J.X,: Solar cycle variation of the inter-network magnetic field. ApJ **806**, id.174, 6 pp. (2015a). https://doi.org.10.1088/0004-637X/806/2/174

Jin, C.L., Wang, J.X,: Does the variation of solar intra-network horizontal field follow sunspot cycle? ApJ **807**, id.70, 6 pp (2015b). https://doi.org.10.1088/0004-637X/807/1/70

Kaithakkal, A.J., et al.: Photospheric flow field related to the evolution of the sun's polar magnetic patches observed by Hinode solar optical telescope. ApJ **799**, id.139, 13 pp (2015). https://doi.org.10.1088/0004-637X/799/2/139

Kano, R., Ueda, K., Tsuneta, S.: Photospheric properties of warm EUV loops and hot X-ray loops. ApJ **782**, L32, 6 pp (2014). https://doi.org.10.1088/2041-8205/782/2/L32

Kanoh, R., Shimizu, T., Imada, S.: Hinode and IRIS observations of the magnetohydrodynamic waves propagating from the photosphere to the chromosphere in a sunspot. ApJ **831**, id.24, 10 pp (2016). https://doi.org.10.3847/0004-637X/831/1/24

Katsukawa, Y.: In this volume (2018)

Katsukawa, Y., Orozco Suarez, D.: Power spectra of velocities and magnetic fields on the solar surface and their dependence on the unsigned magnetic flux density. ApJ **758**, id.139, 9 pp (2012). https://doi.org.10.1088/0004-637X/758/2/139

Kosugi, T., et al.: The Hinode (solar-B) mission: an overview. SoPh **243**, 3–17 (2007). https://doi.org.10.1007/s11207-007-9014-6

Lamb, D.A., et al.: Solar magnetic tracking. III. Apparent unipolar flux emergence in high-resolution observations. ApJ **720**, 1405–1416 (2010). https://doi.org.10.1088/0004-637X/720/2/1405

Lamb, D.A., et al.: Solar magnetic tracking. IV. The death of magnetic features. ApJ **774**, id.127, 10 pp (2013). https://doi.org.10.1088/0004-637X/774/2/127

Lites, B.W.: Hinode observations suggesting the presence of a local small-scale turbulent dynamo. ApJ **737**, id.52, 9 pp (2011). https://doi.org.10.1088/0004-637X/737/2/52

Lites, B.W., Ichimoto K.: The SP_PREP data preparation package for the Hinode spectro-polarimeter. SoPh **283**, 601–629 (2013). https://doi.org.10.1007/s11207-012-0205-4

Lites, B.W., et al.: The horizontal magnetic flux of the quiet-sun internetwork as observed with the Hinode spectro-polarimeter. ApJ **672**, 1237–1253 (2008). https://doi.org.10.1086/522922
Lites, B.W., et al.: The Hinode spectro-polarimeter. SoPh **283**, 579–599 (2013). https://doi.org.10.1007/s11207-012-0206-3
Lites, B.W., Centeno, R., McIntosh, S.W.: The solar cycle dependence of the weak internetwork flux. PASJ **66**(SP1), id.S4, 14 pp (2014). https://doi.org.10.1093/pasj/psu082
Matsumoto, T., Kitai R.: Temporal power spectra of the horizontal velocity of the solar photosphere. ApJ **716**, L19–L22 (2010). https://doi.org.10.1088/2041-8205/716/1/L19
Matsumoto, T., Shibata K.: Nonlinear propagation of Alfven waves driven by observed photospheric motions: application to the coronal heating and spicule formation. ApJ **710**, 1857–1867 (2010). https://doi.org.10.1088/0004-637X/710/2/1857
Matsumoto, T., et al.: Cooperative observation of Ellerman bombs between the solar optical telescope aboard Hinode and Hida/Domeless solar telescope. PASJ **60**, 577–584 (2008). https://doi.org.10.1093/pasj/60.3.577
Nagata, S.: Formation of solar magnetic flux tubes with kilogauss field strength induced by convective instability. ApJ **677**, L145–L147 (2008). https://doi.org.10.1086/588026
Nishizuka, N., et al.: Giant chromospheric anemone jet observed with Hinode and comparison with magnetohydrodynamic simulations: evidence of propagating Alfven waves and magnetic reconnection. ApJ **683**, L83–L86 (2008). https://doi.org.10.1086/591445
Nishizuka, N., et al.: Statistical study of chromospheric anemone jets observed with Hinode/SOT. ApJ **731**, id.43, 11 pp (2011).https://doi.org.10.1088/0004-637X/731/1/43
Nishizuka, N., et al.: A laboratory experiment of magnetic reconnection: outflows, heating, and waves in chromospheric jets. ApJ **756**, id.152, 11 pp (2012). https://doi.org.10.1088/0004-637X/756/2/152
Okamoto, T.J., de Pontieu B.: Propagating waves along spicules. ApJ **736**, L24, 6 pp (2011). https://doi.org.10.1088/2041-8205/736/2/L24
Okamoto, T.J., et al.: Coronal transverse magnetohydrodynamic waves in a solar prominence. Science **318**, 1577–1580 (2007). https://doi.org.10.1126/science.1145447
Orozco Suárez, D., et al.: Quiet-sun internetwork magnetic fields from the inversion of Hinode measurements. ApJ **670**, L61–L64 (2007). https://doi.org.10.1086/524139
Orozco Suárez, D., Katsukawa, Y.: On the distribution of quiet-sun magnetic fields at different heliocentric angles. ApJ **746**, id.182, 15 pp (2012). https://doi.org.10.1088/0004-637X/746/2/182
Orozco Suárez, D., Katsukawa, Y., Bellot Rubio, L.R.: The connection between internetwork magnetic elements and supergranular flows. ApJ **758**, id.L38, 4 pp (2012). https://doi.org.10.1088/2041-8205/758/2/L38
Parker, E.N.: Hydraulic concentration of magnetic fields in the solar photosphere. VI – adiabatic cooling and concentration in downdrafts. ApJ **221**, 368–377 (1978). https://doi.org.10.1086/156035
Quintero Noda, C., et al.: Spatial deconvolution of spectropolarimetric data: an application to quiet Sun magnetic elements. A&A **579**, id.A3, 13 pp (2015). https://doi.org.10.1051/0004-6361/201425414
Singh, K.A.P., et al.: Chromospheric anemone jets and magnetic reconnection in partially ionized solar atmosphere. Phys. Plasmas **18**, 111210-1–111210-8 (2011). https://doi.org.10.1063/1.3655444
Singh K.A.P., et al.: Multiple plasma ejections and intermittent nature of magnetic reconnection in solar chromospheric anemone jets. ApJ **759**, id.33, 14 pp (2012a). https://doi.org.10.1088/0004-637X/759/1/33
Singh K.A.P., et al.: Systematic motion of fine-scale jets and successive reconnection in solar chromospheric anemone jet observed with the solar optical telescope/Hinode. ApJ **760**, id.28, 5 pp (2012b). https://doi.org.10.1088/0004-637X/760/1/28
Shibata, K., et al.: Chromospheric anemone jets as evidence of ubiquitous reconnection. Science **318**, 1591–1594 (2007). https://doi.org.10.1126/science.1146708
Shimizu, T.: In this volume (2018)

Shimizu, T., et al.: Image stabilization system for Hinode (solar-B) solar optical telescope. SoPh **249**, 221–232 (2008). https://doi.org.10.1007/s11207-007-9053-z

Shimizu, T., et al.: Hinode observation of the magnetic fields in a sunspot light bridge accompanied by long-lasting chromospheric plasma ejections. ApJ **696**, L66–L69 (2009). https://doi.org.10.1088/0004-637X/696/1/L66

Shiota, D., et al.: Polar field reversal observations with Hinode. ApJ **753**, id.157, 8 pp (2012). https://doi.org.10.1088/0004-637X/753/2/157

Skogsrud, H., et al.: On the temporal evolution of spicules observed with IRIS, SDO, and Hinode. ApJ **806**, id.170, 10 pp (2015). https://doi.org.10.1088/0004-637X/806/2/170

Spruit, H.C.: Convective collapse of flux tubes. SoPh **61**, 363–378 (1979). https://doi.org.10.1007/BF00150420

Sterling, A.C.; Moore, R.L.; DeForest, C.E.: Hinode solar optical telescope observations of the source regions and evolution of "Type II" spicules at the solar polar limb. ApJ **714**, L1–L6 (2010). https://doi.org.10.1088/2041-8205/714/1/L1

Suematsu, Y., et al.: The solar optical telescope of solar-B (Hinode): the optical telescope assembly. SoPh **249**, 197–220 (2008a). https://doi.org.10.1007/s11207-008-9129-4

Suematsu, Y., et al.: High resolution observations of spicules with Hinode/SOT. In: Matthews, S.A., Davis, J.M., Harra L.K. (eds.) First Results From Hinode. ASP Conference Series, vol. 397, pp. 27–30. Astronomical Society of the Pacific, San Francisco (2008b)

Trujillo Bueno, J., Shchukina, N., Asensio Ramos, A.: A substantial amount of hidden magnetic energy in the quiet Sun. Nature **430**, 326–329 (2004). https://doi.org.10.1038/nature02669

Tsiropoula, G., et al.: Solar fine-scale structures. I. Spicules and other small-scale, jet-like events at the chromospheric level: observations and physical parameters. Space Sci. Rev. **169**, 181–244 (2012). https://doi.org.10.1007/s11214-012-9920-2

Tsuneta, S., et al.: The solar optical telescope for the Hinode mission: an overview. SoPh **249**, 167–196 (2008a). https://doi.org.10.1007/s11207-008-9174-z

Tsuneta, S., et al.: The magnetic landscape of the sun's polar region. ApJ **688**, 1374–1381 (2008b). https://doi.org.10.1086/592226

Welsch, B.T.: The photospheric poynting flux and coronal heating. PASJ **67**, 18-1–18-17 (2015). https://doi.org.10.1093/pasj/psu151

Yan, L., et al.: Observational evidence for the causes and consequences of chromospheric reconnection. ApJ **804**, id.69, 6 pp (2015). https://doi.org.10.1088/0004-637X/804/1/69

Yeates, A.R., et al.: The coronal energy input from magnetic braiding. A&A **564**, id.A131, 10 pp (2014). https://doi.org.10.1051/0004-6361/201323276

Chapter 4
X-Ray Telescope (XRT) Aboard *Hinode*: Key Instrumental Features and Scientific Highlights

Taro Sakao

Abstract The X-ray Telescope (XRT) aboard *Hinode* was designed to observe the solar corona in its entire temperature range, spanning from below 1 million Kelvin (MK) to beyond 20 MK. In particular, the capability of observing low-temperature (below 2 MK) plasmas that were not accessible with the *Yohkoh* Soft X-ray Telescope (SXT), coupled with an order of magnitude higher cadence than SXT, has enabled XRT to make various discoveries on coronal activities. Furthermore, XRT has the unique strength of observing high-temperature plasmas in the corona that are not necessarily well observed with other coronal imagers. The scientific considerations made while designing the XRT and the key points of the instrumental features are reviewed, followed by some highlights of the scientific results obtained with XRT.

Keywords Sun: corona · Sun: activity · Sun: X-rays

4.1 Scientific Background of XRT and Key Instrumental Features

4.1.1 Background

Following the success of *Yohkoh*, a concept study for the next solar physics mission, SOLAR-B (named *Hinode* after launch), was intensively conducted starting from several years after the launch of *Yohkoh*. The X-ray telescope for SOLAR-B (XRT; Golub et al. 2007; Kano et al. 2008) was conceived to observe, in detail, activities in the corona in response to the magnetic activities of the photosphere, which was to be

T. Sakao (✉)
Institute of Space and Astronautical Science, Japan Aerospace Exploration Agency, Chuo-ku, Sagamihara, Kanagawa, Japan
e-mail: sakao@solar.isas.jaxa.jp

T. Shimizu et al. (eds.), *First Ten Years of Hinode Solar On-Orbit Observatory*, Astrophysics and Space Science Library 449,
https://doi.org/10.1007/978-981-10-7742-5_4

observed with the Solar Optical Telescope (SOT). The soft X-ray telescope aboard *Yohkoh* (SXT; Tsuneta et al. 1991) played a significant part in studying the activities of the corona such as those in X-ray-active regions near sunspots and in solar flares, with the aim to observe active and hot corona whose temperatures are above approximately 3 MK. Meanwhile, telescopes for imaging the corona at extreme ultraviolet (EUV) wavelengths around 200–300 Å [EUV imaging telescope (EIT) aboard *Solar and Heliospheric Observatory (SoHO)* (Delaboudinière et al. 1995) and *Transition Region and Coronal Explorer (TRACE)* (Handy et al. 1999)] started extensive observations from the middle of the 1990s. These EUV telescopes aimed at studying low-temperature corona of 1–2 MK and were powerful in investigating the quiet regions of the Sun away from sunspots and the low-temperature structure of the corona around hot loops during flares.

Based on this observational background, XRT was intended to be equipped with the temperature sensitivity of both *Yohkoh* SXT and EUV telescopes, to access the entire temperature range of the corona, covering quiet regions, active regions around sunspots, and flares.

4.1.2 Instrumental Features

To observe the corona in its entire temperature range, for its focal-plane imaging device, XRT adopted a backside-illuminated charge-coupled device (CCD), which was sensitive not only to X-rays but also EUV wavelengths. For the optics of XRT, there was a series of discussions during the concept study phase of the instrument on whether we should adopt grazing-incidence optics similar to *Yohkoh* SXT or normal-incidence optics such as EUV telescopes (or, to be more precise, have an EUV telescope for XRT). Normal-incidence optics can be employed for EUV wavelengths, with which a telescope of a compact size and high angular resolution can be built by introducing standard fabrication and measurement techniques established at visible-light wavelengths. Meanwhile, to have a good EUV reflectivity for nearly normal incidences to the mirror surface, a multilayer coating that is tuned to have a peak reflectivity at the target wavelength has to be applied to the mirror surface. As an intense EUV emission line needs to be chosen for such a target wavelength to ensure a good intensity for the reflected EUV light, a fabricated EUV telescope must inherently have a narrowband temperature response. For this reason, it is difficult for EUV telescopes to cover the entire temperature range of the corona even though one prepares multiple wavelength channels with different multilayer coatings. In this regard, EUV telescopes are not perfectly suited to observe all coronal activities that accompany the heating and cooling of plasmas. With the coverage of the entire coronal plasmas being a high priority of XRT, we adopted grazing-incidence optics (Fig. 4.1) for the telescope which provided a broadband temperature response covering a wavelength range of 5–200 Å. For performing temperature analysis with this telescope, XRT introduced a set of X-ray analysis filters made from thin metals, one of which was then inserted in the ray

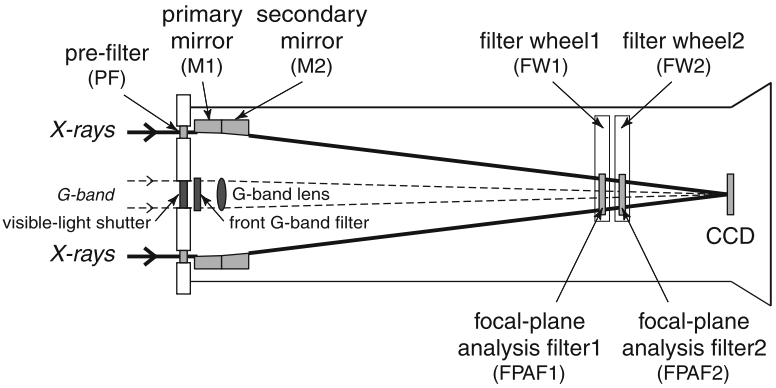

Fig. 4.1 Schematic diagram of the optics system of XRT (Narukage et al. 2011). X-ray incident from the left side of the figure reflects off the mirror twice (once on the primary mirror and again on the secondary), focusing on the focal-plane CCD. In addition to the X-ray optics, XRT is equipped with visible-light optics, which aids in the coalignment of the X-ray images with data from other instruments, both from the space and from the ground

path of the focusing X-rays, as was done in SXT. The representative temperature (weighted by the differential emission measure (DEM) distribution along the line of sight) was then derived from the ratio of X-ray count rates recorded with different filters for each CCD pixel (referred to as the "filter-ratio method" (Acton et al. 1999; Narukage et al. 2011, 2014)).

Besides the decision of employing grazing-incidence optics, the mirror diameter was enlarged to 35 cm to increase the effective area of the telescope. This ensured the necessary exposure times for each CCD pixel (1″/pixel for XRT), equivalent to those necessary for SXT (2.45″/pixel). Furthermore, through precise polishing, the mirror achieved the highest angular resolution of 2″ for a grazing-incidence telescope for solar observations. These features enabled XRT to observe, in detail, coronal plasmas of a wide temperature range from below 1 MK up to beyond 20 MK without any gap in temperature coverage. Precision polishing of the mirror was performed by Goodrich who also constructed the grazing-incidence mirrors of the *Einstein* and *Chandra* X-ray observatories as well as *Yohkoh* SXT, although the company does not fabricate precision grazing-incidence mirrors anymore.

During the concept study phase of the SOLAR-B mission, there was a consensus that a spatial resolution of approximately 1″/pixel would be sufficient for coronal instruments [XRT and EUV imaging spectrometer (EIS)] as elementary flux tubes rooted on the photosphere were likely to expand rapidly toward the upper atmosphere, increasing their diameters. However, as was recognized soon after the start of *Hinode* observations, the 2″ spatial resolution of XRT and EIS was insufficient to investigate the spatial and temporal relationship with the intensity and magnetic structures of the photosphere observed with SOT with a 0.2″ resolution. Fine-scale features observed in SOT were "too rich" in structure that it was not possible to investigate their correspondence with the coronal features observed

with XRT and EIS. The question then became whether we were able to identify the photosphere-corona connection if we had coronal instruments with a higher spatial resolution. I do not think this is the case. The magnetic field structure of the chromosphere, connecting the photosphere and the corona, appears to be quite different from that of the photosphere. This observation was once reported and alerted by a US solar physicist, Dr. Jack Harvey, in one of the SOLAR-B science study meetings during the concept study phase. For me, his message is hard to forget. After all, it would not be possible to identify the direct connection—cause and its consequence along magnetic field lines—between the corona and lower atmosphere (photosphere and chromosphere) unless the magnetic field structure of the chromosphere is simultaneously identified. This may be a subject for future solar observations.

4.1.3 Data Rate for Observations

Besides the difference in instrumental performance, a major difference between XRT and SXT is the data rate for observations. In particular, for observing the non-flaring corona XRT is capable of capturing images at a cadence about one order of magnitude higher than SXT for the same field of view size. This feature enabled XRT to reveal the unexpectedly frequent occurrence of various coronal activities, even though such activities themselves had been recognized previously. A good example of this is the frequent occurrence of X-ray jets in the polar regions of the Sun where no significant activities were thought to exist before *Hinode* observations.

Because of a malfunction with the X-band transmitting modulator of *Hinode* at the end of 2007, the downlink rate for observational data began to suffer severe limitations (Shimizu 2016). Despite this incidence, XRT, together with other *Hinode* instruments, has been maintaining a high cadence of observation by devising efficient ways of reducing the amount of data (although there are certainly restrictions on observations) by, for example, applying onboard data compression as much as it is acceptable from a scientific point of view.

4.1.4 International Collaboration

Hinode was realized under extensive international collaboration among Japan, the USA and UK, and also Europe (ESA) after the launch. For XRT, the Smithsonian Astrophysical Observatory (SAO) in the USA took part in the development of the telescope mirror and metering tube, as well as X-ray analysis filters with their drive mechanism and controlling electronics. The Japanese side [Institute of Space and Astronautical Science at Japan Aerospace Exploration Agency (ISAS/JAXA) and National Astronomical Observatory of Japan (NAOJ)] participated in the development of the focal-plane CCD camera and its electronics. After the CCD

camera was installed in the telescope tube at SAO, telescope-level tests were performed at NASA/GSFC for the mechanical and thermal environment tests and at NASA/MSFC for the X-ray optical verification tests. After the series of tests, XRT was then shipped to ISAS/JAXA for spacecraft-level flight model tests.

For science operations that started after the launch of *Hinode*, the US-Japan XRT team have been regularly holding international teleconference meetings every week to report XRT observations and the status of instruments and to review observational plans for the upcoming week. In addition, by utilizing annual *Hinode* international science conferences, a face-to-face team meeting is also held every year, thus maintaining team activities.

4.2 Some Scientific Highlights from XRT

As mentioned before, because of the broadband temperature response of the grazing-incidence optics, XRT is capable of observing not only the high-temperature plasmas created in flares and active regions but also low-temperature plasmas of 1–2 MK. Among the various scientific results from XRT, which were possible from the wide temperature coverage and high exposure cadence, two results will be introduced below.

4.2.1 Source Region of the Slow Solar Wind

Our solar system is filled with streams of charged particles from the Sun, which are referred to as the solar wind. The solar wind is composed of "fast" solar wind with velocities of around 600–700 km s^{-1} and "slow" solar wind with velocities of around 300–400 km s^{-1}. Observations with the *Ulysses* spacecraft identified that the former emanated from middle-to-high latitudes of the Sun including polar regions, while the latter from low latitudes (McComas et al. 1998). However, before *Hinode* there was no observation that directly indicated any particular locations in the low-latitude regions as the source of the slow solar wind.

It was revealed by XRT observation in February 2007 that there were patterns of continuous plasma flows that were emitting soft X-rays along magnetic field lines from the edge of an active region adjacent to a coronal hole (Sakao 2008), as indicated by the white circle in the right panel of Fig. 4.2. Note that the presence of flow patterns suggests that density nonuniformity is present in the flowing plasmas. Upward Doppler motion along the line of sight was also detected in Fe XII data obtained by EIS, confirming that the flow patterns observed with XRT were in fact due to the outflow of plasmas. In addition, potential magnetic field calculations indicated that magnetic field lines from this outflowing region were not connected to the Sun but extended toward the interplanetary space, suggesting that the outflowing plasmas could flow out as the solar wind. The temperature of the outflowing plasmas

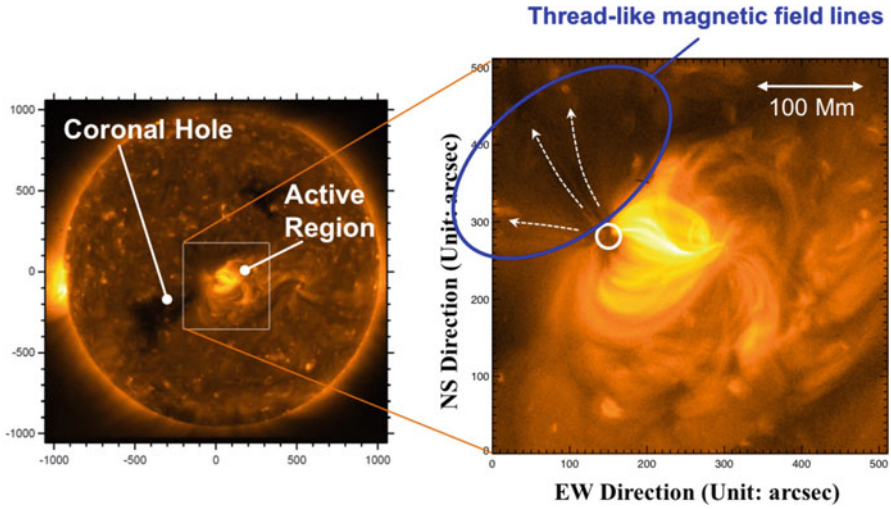

Fig. 4.2 Source region of the slow solar wind as identified with XRT (Sakao 2008). The white circle in the right panel indicates the source region

was estimated to be approximately 1.1 MK from the filter-ratio method. The low temperature of the outflowing plasmas implies that SXT was not able to detect such outflowing features.

The idea that the edge of an active region adjacent to a coronal hole could be a source of the slow solar wind had been postulated by radio interplanetary scintillation observations by a group at Nagoya University (Kojima et al. 1999; Ohmi 2003) and also by in situ observations of the solar wind with the *Advanced Composition Explorer (ACE)* spacecraft (Ko et al. 2006). The result with XRT can be viewed as a direct identification in images of the slow wind source. Source regions of the slow solar wind as well as the nature of the outflowing pattern observed in XRT images (it is likely that the pattern consists of real plasma flows and waves) have been extensively studied chiefly with EIS until today (Lee et al. 2016).

4.2.2 X-Ray Jets

X-ray jets were discovered by *Yohkoh* SXT as a collimated upward-propagating feature of hot plasmas along magnetic field lines from the lower portion of the corona. The X-ray jets are thought to be generated by magnetic reconnection around their footpoints. While SXT found that most of jets originated from active regions, XRT revealed that there were frequent jets also in the quiet regions of the corona and in coronal holes. In particular, the frequent occurrence of X-ray jets in polar coronal

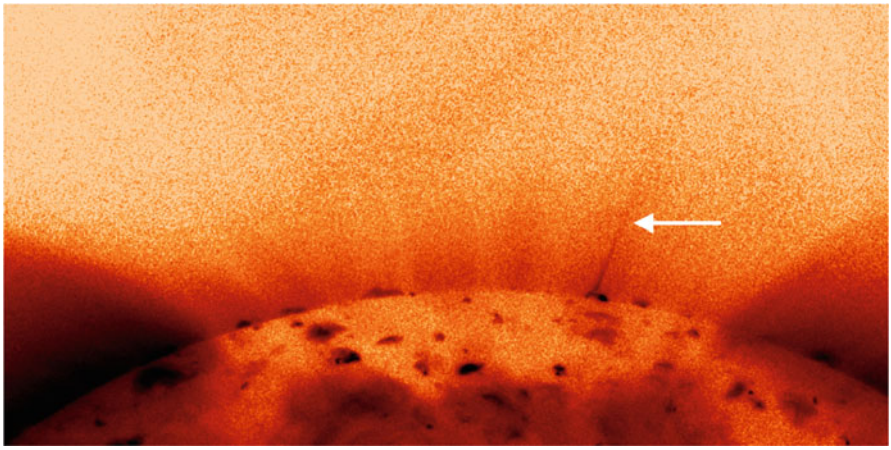

Fig. 4.3 Example of an X-ray jet whose frequent occurrence was revealed by XRT (Sakao 2008)

holes (Fig. 4.3) was so impressive that an XRT image of the Sun capturing such an X-ray jet was adopted for the cover figure of *Science* magazine in 2007 featuring scientific results from *Hinode*.

The occurrence frequency of X-ray jets, as observed by XRT, was typically 60/day for a polar coronal hole (Savcheva et al. 2007). Although direct comparison may not be adequate because of the difference in jet-producing regions, this number is significantly larger (10 times) than that reported by SXT. The finding of such a high occurrence frequency was made possible by the order-of-magnitude higher exposure cadence of XRT than SXT for non-flaring corona. In addition, a recent study (Sako 2014) indicated that among X-ray jets observed with XRT, there was a population of cool jets (1–2 MK) besides hot jets ($\geq$3 MK) that SXT could observe. While such cool jets can be observed with the recent EUV telescopes, such as Atmospheric Imaging Assembly (AIA) aboard *Solar Dynamics Observatory (SDO)*, by exploiting the unique strength of XRT that it can detect both hot and cool jets with a high exposure cadence, discussions are taking place regarding the dependence of hot/cool jets to their originating regions in the corona as well as the difference in the formation mechanism (jet formation by magnetic tension or evaporation flow) of those jets (Sako 2014).

4.2.3 Onboard Flare Detection

Although not a scientific result, I would like to stress here that XRT is also contributing a considerable amount to flare observations with *Hinode*. The onboard Mission Data Processor (MDP), which controls XRT observations, has the capability of detecting the occurrence of flares by monitoring the increase in X-ray intensity in

full-frame CCD images that are regularly recorded by XRT. The flare occurrence and its positional information are provided not only to XRT but also to other instruments, with which each instrument starts its own flare observations. As the field of view of SOT and EIS is small relative to the angular size of the XRT CCD, these instruments do not start their flare observation sequences if the flare location is outside their field of view. As for XRT, it can set the observing region on its CCD and start flare observations as the flare occurrence is detected by the XRT CCD itself.

As XRT serves as the flare monitor for the entire *Hinode* mission, it is crucial to optimize the flare detection performance. We have set a requirement of the detection performance such that the major flares whose peak *GOES (Geostationary Operational Environmental Satellite)* X-ray flux reaches at least a middle-M-class should be detected when the X-ray flux reaches 1/10 of the peak flux level. To meet this requirement, we conducted careful studies to optimize the parameters for the flare detection with MDP, including the time interval for flare monitor exposures, threshold for the X-ray increase, and weighting factor of the previous X-ray intensities. The study was conducted using multiple series of actual flare monitor images from XRT and a software simulator equipped with the flare detection logic of MDP. By identifying the optimal parameters for flare detection, the requirement was then met. An example of the resultant detection and observation performance of flares with the XRT-MDP system is shown in Fig. 4.4. The horizontal axis indicates the peak X-ray flux level of the flare from the *GOES* satellite, while the vertical axis is the percentage of flares observed with XRT relative to the total number of flares for each *GOES* flare class. (Those shown in red are events observed in flare-observing mode after flare detection, and those in orange were observed without transition to flare-observing mode as the flare detection was not triggered.) To derive the percentage in the figure, the total number of flares was used as the denominator for each *GOES* class, which includes those commenced during the periods that XRT was not observing because of, for example, CCD bakeout for the removal of contaminants accumulated on the CCD and *Hinode*'s passage of the South Atlantic Anomaly (SAA). In this regard, the percentage in the figure might not directly reflect the XRT performance of flare detection and observation; the percentage during the XRT-observing period should be even higher. Nonetheless, XRT performed well such that all major flares whose *GOES* class was at least M9 were successfully observed with XRT in flare-observing mode.

4.3 Summary

Thus far, I have discussed the scientific background for the concept of XRT and a portion of its scientific results. However, for the subject of observing the corona without a temperature gap, I have intentionally left the subject unaddressed because a paper relevant to this subject has yet to be published (refused by a referee claiming issues in the temperature analysis). The paper reports an interesting study on the filter ratio temperature distribution across the whole area of the Sun, including

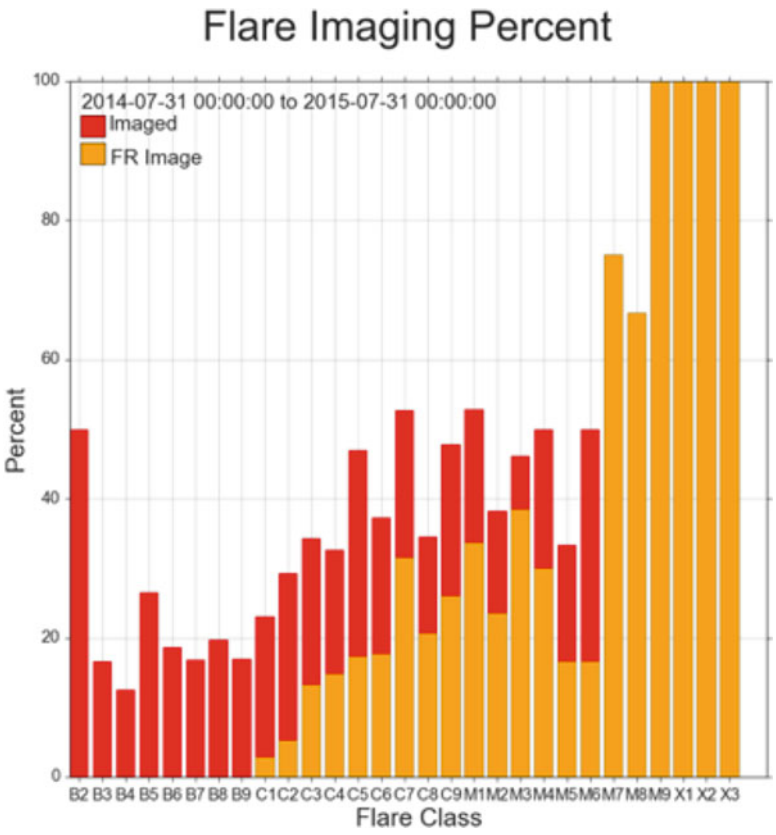

Fig. 4.4 Flare observation performance with XRT during a 1 year period from 2014 to 2015. The horizontal axis indicates the peak X-ray flux level of the flare from the *GOES* satellite, while the vertical axis indicates the percentage of flares observed with XRT relative to the total number of flares for each *GOES* flare class. The figure is courtesy of Drs. K. Reeves and N. Schanche of the Harvard-Smithsonian Center for Astrophysics

active regions, quiet regions, and coronal holes, and discusses the heating and cooling processes for each region. I very much hope that the first author of this paper revises the manuscript soon, resubmits, and makes the results public to the community. For investigating high-temperature components in active regions, XRT has a unique advantage over EUV telescopes (Ishikawa 2016) and holds its own scientific position in the observation of hot plasmas in the corona. As for higher-temperature plasmas created during flares, some interesting results have also been obtained, although care should be taken in deriving the filter ratio temperatures for the rapidly evolving X-ray structure of flares. This will be reported in a future study.

Ten years have passed since the launch of *Hinode*. I am pleased to report that XRT has been observing well up to now. I very much hope to continue the science operation of XRT to make new discoveries with unique observations and analyses.

Acknowledgements *Hinode* is a Japanese mission developed and launched by ISAS/JAXA, collaborating with NAOJ as a domestic partner and NASA and STFC (UK) as international partners. Scientific operation of the *Hinode* mission is conducted by the *Hinode* science team organized at ISAS/JAXA. This team mainly consists of scientists from institutes in the partner countries. Support for the postlaunch operation is provided by JAXA and NAOJ (Japan), STFC (UK), NASA, ESA, and NSC (Norway).

In addition, throughout the development and operation stage of *Hinode*, indispensable support was given by engineering researchers of JAXA and by our industrial partners, which made XRT observations possible for these 10 years with the expected observational performance. I hereby express my sincere gratitude and would appreciate continuous support to the *Hinode* mission.

References

Acton, L.W., Weston, D.C., Bruner, M.E.: Deriving solar X ray irradiance from Yohkoh observations. J. Geophys. Res. **104(A7)**, 14827–14832 (1999)

Delaboudinière, J.-P., Artzner, G.E., Brunaud, J., et al.: EIT: extreme-ultraviolet imaging telescope for the SoHO mission. Sol. Phys. **162**, 291–312 (1995)

Golub, L., DeLuca, E., Austin, G., et al.: The X-ray telescope (XRT) for the *Hinode* mission. Sol. Phys. **243**, 63–86 (2007)

Handy, B.N., Acton, L.W., Kankelborg, C.C., et al.: The transition region and coronal explorer. Sol. Phys. **187**, 229–260 (1999)

Ishikawa, S.: Hinode investigations of microflares and nanoflares. Tenmon Geppo **109**, 544–547 (2016)

Kano, R., Sakao, T., Hara, H., et al.: The *Hinode* X-ray telescope (XRT): camera design, performance and operations. Sol. Phys. **249**, 263–279 (2008)

Ko, Y.-K., Raymond, J.C., Zurbuchen, T.H., et al.: Abundance variation at the vicinity of an active region and the coronal origin of the slow solar wind. Astrophys. J. **646**, 1275–1287 (2006)

Kojima, M., Fujiki, K., Ohmi, T., et al.: Low-speed solar wind from the vicinity of solar active regions. J. Geophys. Res. **104(A8)**, 16993–17003 (1999)

Lee, K.-S., Brooks, D.H., Imada, S.: The origin of the solar wind observed by Hinode. Tenmon Geppo **109**, 700–704 (2016)

McComas, D.J., Bame, S.J., Barraclough, B.L. et al.: Ulysses' return to the slow solar wind. Geophys. Res. Lett. **25(1)**, 1–4 (1998)

Narukage, N., Sakao, T., Kano, R., et al.: Coronal-temperature-diagnostic capability of the *Hinode/X-Ray Telescope* based on self-consistent calibration. Sol. Phys. **269**, 169–236 (2011)

Narukage, N., Sakao, T., Kano, R., et al.: Coronal-temperature-diagnostic capability of the *Hinode/X-Ray Telescope* based on self-consistent calibration. II. Calibration with on-orbit data. Sol. Phys. **289**, 1029–1042 (2014)

Ohmi, T.: The origin of the low-speed solar wind. Ph.D. Thesis, Nagoya University (2003)

Sakao, T.: Source region of the solar Wind identified with Hinode X-ray telescope. Tenmon Geppo **101**, 491–496 (2008)

Sako, N.: Statistical study of X-ray jets using Hinode/XRT. Ph.D. Thesis, The Graduate University for Advanced Studies (SOKENDAI) (2014)

Savcheva, A., Cirtain, J., DeLuca, E.E., et al.: A study of polar jet parameters based on Hinode XRT observations. Publ. Astron. Soc. Jpn. **59**, S771–S778 (2007)

Shimizu, T.: Hinode's brief history–still active. Tenmon Geppo **109**, 524–528 (2016)

Tsuneta, S., Acton, L., Bruner, M., et al.: The soft X-ray telescope for the solar-A mission. Sol. Phys. **136**, 37–67 (1991)

Chapter 5
Solar Extreme Ultraviolet Spectroscopy: zur Nach*EIS*zeit

Tetsuya Watanabe

Abstract The extreme ultraviolet (EUV) imaging spectrometer (EIS) onboard the *Hinode* mission has been observing for more than a decade since its launch the profiles of EUV emission lines originating from high-temperature solar outer atmospheres with its high dispersion spectrograms for the first time in solar EUV spectroscopy. The EIS has been ice-breaking difficult problems and obtaining a plenty of important scientific results. The EIS has since entered an epoch of "sunrise" in solar EUV spectroscopy. Scientific outputs thawed out by EIS are briefly discussed, and key emission lines in hot and dynamic postglacial periods of solar EUV spectroscopy are highlighted.

Keywords Sun: UV radiation · Sun: transition region · Sun: corona

5.1 *EIS*berg Before *Hinode* (*"Sunrise"*)

After S082A (Tousey et al. 1977) experiment was onboard *Skylab*, the solar extreme ultraviolet (EUV) observation did not have good opportunities for flight, and the situation at the time of launching the *Hinode* mission seemed similar to cruising in an ocean at dawn shrouded with mist, avoiding the tips of icebergs representative of the uncertainty in scientific prospect and the technical difficulty, and waiting for the sunrise, i.e., a breakthrough. The first conceptual design of the EUV imaging spectrometer (EIS) onboard *Hinode* was nicknamed as TRENDY (transition region energetics and dynamics). It had a 20 cm aperture primary and a grating (groove density is 4,800 grooves/mm), which were set up 3 m (originally 4 m) apart, and tried to obtain solar EUV spectra only at wavelengths of 250–290 Å.

T. Watanabe (✉)
National Astronomical Observatory of Japan, Mitaka-shi, Tokyo, Japan
e-mail: watanabe@uvlab.mtk.nao.ac.jp

T. Shimizu et al. (eds.), *First Ten Years of Hinode Solar On-Orbit Observatory*,
Astrophysics and Space Science Library 449,
https://doi.org/10.1007/978-981-10-7742-5_5

Then the scientific purpose of the *Hinode* mission converged into the understanding of (a) the heating mechanisms of the outer atmosphere (chromosphere and corona), (b) dynamo mechanism of the fine magnetic flux tubes as the basic structure of the solar magnetic field, and (c) coronal dynamics and details of magnetic reconnection. We critically reviewed the solar EUV observations performed so far, reconsidered the scientific requirements of the EIS, and updated the EIS instrument specification, in which the combination of an off-axis paraboloid and a toroidal grating enabled image magnification and the observing wavelengths were doubled by introducing a multilayer coating to increase the spectral sensitivity. As a result, all constraints for the installation onto the spacecraft were cleared to satisfy the scientific requirements at the same time (Culhane et al. 2007). However, the size of the EIS was still larger than that of the Solar Optical Telescope (SOT), and many technical difficulties remained such as launch locks as a trivial example that could be ignored during the *Yohkoh* era.

Solar and Heliospheric Observatory (SoHO)/Coronal Diagnostic Spectrometer (CDS) (NIS – normal incidence spectrometer) and Solar Ultraviolet Measurements of Emitted Radiation (SUMER) held an unchallenged position in solar UV spectroscopy at that time before the launch of *Hinode*. However, both instruments were very slow spectrographs, and spectra taken by them were fairly still spectrograms. The grazing-incidence spectrometer (GIS) failed in CDS, and the *Hinode*/EIS observation quickly gained high expectation.

The first priority science mission of the EIS instrument was quantitative measurement of the energy transport from the photosphere to the corona and the understanding of the energy input to the corona via the observation of chromospheric and transition region (TR) emission lines.

Emission lines formed in the chromosphere and transition region exhibit excess line widths expected from thermal Doppler broadening (Teriaca et al. 1999). These excess line widths are thought to be a manifestation of the energy flows propagating from chromosphere – transition region – corona, and precise investigation of the EUV emission line profiles would be expected to draw a clear physical picture of the energy flux.

Another main scientific objective of the EIS is to diagnose physical quantities such as electron temperatures, electron densities, and velocities of plasmas at the sites of magnetic reconnection in solar flares. The *Yohkoh* observations established that the energy release mechanism in solar flares was magnetic reconnection. However, precise diagnostic measurements at and around the reconnection points were not performed, because the emission measure around the region was too low in the case of soft X-ray imaging (SXT) on board *Yohkoh*, and spatial information was not obtained in the case of soft X-ray spectroscopy [Bragg Crystal Spectrometer (BCS) on board *Yohkoh*]. Therefore, there were many theories based on morphology, though they remained a matter of speculation. The direct detection and quantitative observation of reconnection inflows and outflows were considered to be particularly important.

5.2 Ice-Breaking (*EIS*brechend) Scientific Problems

5.2.1 High-Resolution EUV Spectra

The EIS scientific achievement that we consider first is that this instrument continuously obtained high-dispersion solar EUV spectra in orbit with a spatial resolution of 2–3 arcsec in the EUV wavelengths (171–211Å and 245–291Å). In this context,"high dispersion" implies that we can analyze the emission line profiles as well as the line intensities. There are more than 500 emission lines originating from 54 ionization stages of 14 elements just in the two wavelength bands, and there still exists an abundance of unidentified emission lines (Brown et al. 2008). Moreover, EIS has begun observing dynamical phenomena occurring in a wide range of solar outer atmosphere beyond the chromosphere with a shutter speed of a second or two, with a combination of high dispersion and high spatial resolution, for active region observations. A few trifle accidents and trivial degradations in the performance were recognized more or less during these 10 year operation, but the EIS made epoch-making scientific achievements by steadily providing high-quality solar EUV spectral observations.

5.2.2 Active Region: Nonthermal Emission Line Widths and High-Speed Upflows

Ultraviolet (UV) emission lines originating from high-temperature solar plasma usually show excess line widths, larger than those expected from thermal motions. A rough estimate suggests that the energy for this excess velocity is comparable to that put into the solar corona and that the nonthermal line widths might imply the mechanism of coronal heating.

The emission line widths have been intensively measured since the launch of *Hinode*. Figure 5.1 shows a strong correlation between the nonthermal velocity and the blue-shifted line-of-sight (LOS) velocity for coronal loops in a non-flaring active region (AR10938) (Doschek et al. 2007; Hara et al. 2008b). Both of them cease when the active region approaches to the limb, which suggests that multiple velocity components along the magnetic field lines are mixed within an area smaller than the EIS spatial resolution and that the maxima of upflow and nonthermal velocities are located around the foot points of coronal loops (Hara et al. 2008b). High-velocity components are anticipated to have structures smaller than the EIS spatial resolution by comparing the intensity ratios of the main components to those of the high-velocity components. In addition, the theoretical simulation (Antolin et al. 2008) suggests that these high-velocity components have similar characteristics to those of plasma flows, which are triggered by intensive heating of microflares intermittently occurring at the lower part of the solar corona (Hara 2009). The spatial and temporal correlations of (high-speed) blue-shifted components of coronal emission lines

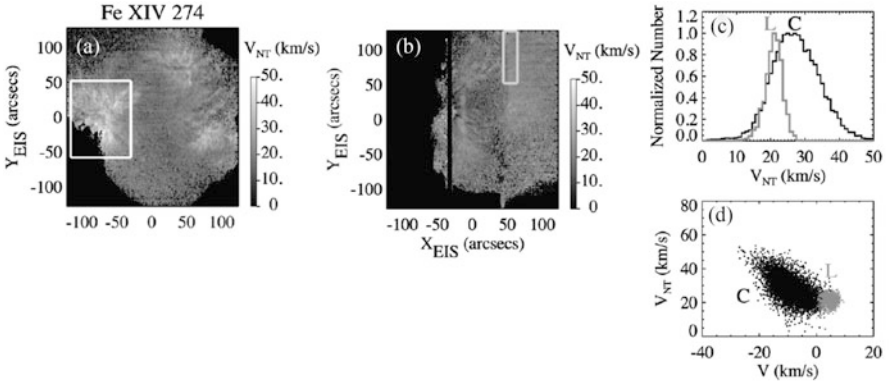

Fig. 5.1 AR10938 seen in Fe XIV λ274Å emission line: (from left to right) nonthermal velocity – (**a**) disk center, (**b**) limb, (**c**) histogram of the nonthermal line widths, (**d**) Doppler velocity vs. the nonthermal velocity. Capital letters C and L in panels (**c**) and (**d**) indicate the data sets extracted from white squares in panels (**a**) and (**b**), respectively (Reproduced from Hara et al. (2008b) by permission of the AAS)

(Fe XIV) and chromospheric jets suggest that the major part of coronal heating may occur at a height of the chromospheric layer to be transported to the corona with high-velocity upflows such as spicules (De Pontieu et al. 2009).

Reflecting these observational results, a scenario of nanoflare-like magnetic reconnection events possibly seen in the excess line widths at the loop foot points is thought to be responsible for the mechanism of coronal heating in the active regions, in which the coronal loop apices show no such line broadening. Nevertheless, we still need critical verification of the observational data acquired from precise spectroscopic instruments such as EIS. A new result of the detailed measurements of the excess broadening of emission lines originating from 15 non-flaring high-temperature coronal loops in the active regions was obtained this spring. The average excess line width was $17.6 \pm 5.3\,\mathrm{km\,s^{-1}}$ by carefully examining the instrumental width and the optical performance of the spectrograph (Brooks and Warren 2016). This value is not surprisingly large, and the widths do not have tight correlations with temperatures and magnetic fluxes of the active regions, which implies that these observation results are consistent with none of the models, chromospheric magnetic reconnection, chromospheric evaporation triggered by coronal magnetic reconnection, turbulent Alfvén waves, etc. It will take more time to make a definite conclusion about the heating mechanism of coronal loops.

5.2.3 Ubiquitous Flows and Waves in Solar Plasma

One of the major discoveries of the *Hinode* mission, not to say the EIS, is that plasma flows and waves occur everywhere in the solar atmosphere. High-speed

upflows are found as outlets of slow solar winds (Sakao et al. 2007; Harra et al. 2008a), and high-resolution SOT images detect oscillating magnetic field lines in solar prominences (Okamoto et al. 2007). It has become evident that the solar atmosphere is full of Alfvén(ic) waves.

Various kinds of oscillations are found by investigating the temporal behavior of the emission line intensities and LOS velocities. Simultaneous observations of the LOS velocity and the transverse motion combined with that of the line intensity have a possibility to identify the modes of the oscillations, so that we can estimate the magnetic flux density in the corona. The oscillations observed by the EIS so far are kink mode oscillations (Van Doorsselaere et al. 2008; Erdelyi and Taroyan 2008; Kitagawa et al. 2010), sausage mode oscillations (Erdelyi and Taroyan 2008; Kitagawa et al. 2010), standing waves of magnetohydrodynamics (MHD) slow mode (Kitagawa et al. 2010; Mariska et al. 2008), and propagating waves of the previous mode (Kitagawa et al. 2010; Wang et al. 2009a,b; Mariska and Muglach 2010).

5.2.4 Polar Jets and Outlets of High-Speed Solar Winds

Tiny but strong magnetic patches whose strength may reach 1 kG are found in both polar regions of the Sun (Tsuneta et al. 2008), and the X-Ray telescope (XRT) found that jet-like plasma eruptions happen frequently in these magnetic patches (Cirtain et al. 2007). The EIS observes these jets as structures of the LOS velocity moving upward (Kamio et al. 2009), and the jet speeds are estimated to be comparable to the sound velocities at the coronal temperatures. These polar jets are thought to appear as the result of magnetic reconnection between tiny emerging magnetic fluxes from below the photosphere and the pre-existing coronal open magnetic fields of opposite magnetic polarity. Combining the SOT observations of photospheric magnetic fields, X-ray jets in the polar regions blow up from the foot points of kilogauss magnetic patches, and short low-lying jets of TR temperatures appear in the closed magnetic structures.

In these polar regions diffusely bright elongated structures appear, and they are called polar plumes. The velocity structures of upflows in these plumes are measured by the EIS and compared with the EUV images taken by the atmospheric imaging assembly (AIA) instrument onboard NASA's *Solar Dynamics Observatory (SDO)* satellite. It is found that these plumes are not transient phenomena but stationary structures of radially accelerated upflows. Therefore, plumes are thought to be important mass suppliers for solar winds, namely, they correspond to be solar wind outlets (Fu et al. 2014).

5.2.5 *Solar Flares: Spectroscopic Diagnostics of Superhot Plasma*

The predecessor, *Yohkoh* mission, found that solar flares were explosively triggered by magnetic reconnection, but *Yohkoh* itself could not directly observe and diagnose the physical environment at and around the reconnection points. The subject was passed down to the *Hinode* mission. Using the EIS advantages of high throughput as well as high spectral and spatial resolutions, the instrument has been successful in pinning down the region where magnetic reconnection occurs and for understanding the physical conditions in its circumjacent area.

A small B9.5 flare occurred at the disk center associated with a coronal mass ejection (CME) event – the date was 2007 May 19. The flare shown in Fig. 5.2 was a long-duration event. The most fortunate things were that the EIS rastering slit was just on the apex of the loop, on the top of which this flare occurred, and that the EIS was prepared to choose a number of emission lines formed in various temperatures for simultaneous observations. This fortune enabled us to start measuring plasma temperatures and velocities immediately after the flare initiation and to locate the magnetic reconnection region that caused the flare. By combining information obtained from *Hinode*/XRT, *Reuven Ramaty High-Energy Solar Spectroscope Imager (RHESSI)*, *Solar Terrestrial Relations Observatory (STEREO)*, and *Transition Region and Coronal Explorer (TRACE)*, the structures

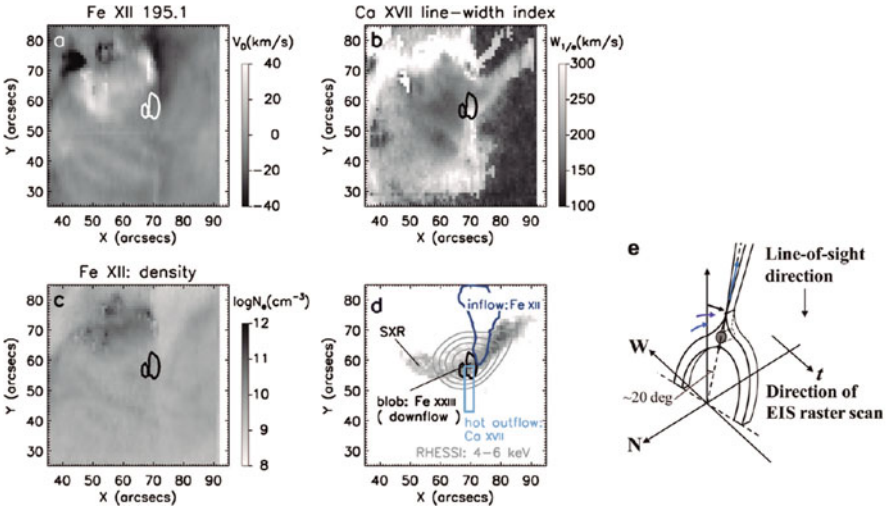

Fig. 5.2 The 2007 May 19 flare: (**a**) inflows measured from the LOS velocity of Fe XII around the region where superhot Fe XXIII emission lines show downflows (white circles). (**b**) Excess line broadening in Ca XVII lines showing hot gas outflows. (**c**) Electron density distribution measured from the Fe XII line intensity ratios. (**d**) XRT image of flaring loops superimposed on *RHESSI* (4–6 keV) image (contour) and velocity fields observed by the EIS. (**e**) Velocity structure inferred from panels from (**a**) through to (**d**) (Reproduced from Hara et al. (2011) by permission of the AAS)

of temperature, velocity, and density can be all determined around the area (Hara et al. 2011). It is confirmed that magnetic reconnection actually occurs to trigger this sort of tiny flares in B-class and that physical observations, especially spectroscopic observations around the reconnection region, were successfully performed.

The EIS also contributes to observations of reconnection outflows associated with solar flares (Imada et al. 2013). An X-class flare of 2012 January 27 is taken as an example. The EIS recognized superhot [$\sim$30 million Kelvin (MK)] and high-speed ($>500\,\mathrm{kms}^{-1}$) plasma flows above the flaring coronal loops. The 3-D structure of the region confirmed in the *SDO*/AIA and the *STEREO* observations could be explained as a feature of fast-mode shocks created by the interaction of reconnection outflows with surrounding plasma while travelling from the reconnection points.

After accelerated nonthermal electrons and/or thermal conduction front associated with solar flares reach the chromosphere, chromospheric plasma heats and chromospheric evaporation are initiated. The phenomenon of chromospheric evaporation was discovered, and its concept was established in the early 1980s, when *Hinotori* and the *Solar Maximum Mission (SMM)* actively participated in X-ray observations of the Sun from space. Nevertheless, the understanding of its spatially resolved temperature and velocity structures has not been drastically improved since then, and it has to wait for the *Hinode*/EIS launch (Watanabe et al. 2010; Milligan and Dennis 2009). All redshifts were measured in TR and chromospheric emission lines. As a result of violent energy deposition called "explosive" chromospheric evaporation (Fisher et al. 1985), the electron densities at the foot points of flaring loops increased to an order of $10^{10}\,\mathrm{cm}^{-3}$. The plasma upflow velocity of the chromospheric evaporation is found to show a strong temperature dependence (Fig. 5.3), and thus upflows that originate from magnetic

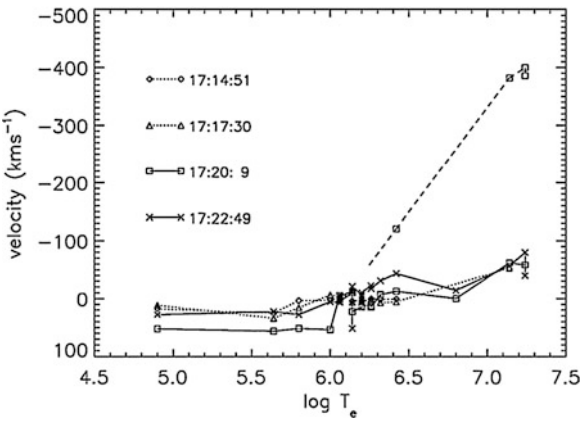

Fig. 5.3 Temperature dependence of plasma motions observed in the initial phases of a C9.7 flare of 2007 June 6 (positive sign for redshift): Significant blueshifts in high-temperature lines (Fe XVI, Fe XXIII, and Fe XXIV) and universal redshifts of $\sim$50 kms^{-1} in the emission lines formed below 10^6 K are only observed during the time interval when the flaring loop foot points start to brighten up (Reproduced from Watanabe et al. (2010) by permission of the AAS)

reconnection can be distinguished showing no such dependence on the temperature. However, when the structures of flaring coronal loops are not spatially resolved, it is difficult to determine whether the observed high-speed and high-temperature outflows are of reconnection origin or of thermal origin, namely, whether they are reconnection outflows or those associated with chromospheric evaporation (Matsui et al. 2012).

5.3 Scientific Objectives for Post-gracial Age (Nach*EIS*zeit)

The structure called "moss" is observed at the central parts of the active regions. By comparing the magnetic structure (by SOT observations) and the thermal evolution and temporal changes of the emission line intensities (by EIS observations), the moss structure has a size of 10–20% of the EIS spatial resolution (∼0.3 arcsec) (Brooks et al. 2010). Therefore, if we are able to build an instrument to have a spatial resolution of an order of magnitude better than that of the EIS, we can probe the solar atmosphere in wider temperature ranges, from the chromosphere to the corona. This approach could be similar to the one for prominence by collaborative observations of SOT and the *Interface Region Imaging Spectrograph (IRIS)* satellite (Okamoto et al. 2015). The behavior of energy transportation will be investigated in detail to understand the coronal heating mechanism of the active region corona.

The problem of the gaps in the temperature at which emission lines form will be highlighted, when we study the above-noted solar plasma physics in the coming era. In the 80Å EIS observing wavelength ranges are the emission lines formed at the temperatures from 80 kK to 16 MK, but their formation temperatures are not uniformly distributed. First, a group of emission lines formed at the upper TR temperatures (500 kK–1 MK) are all weak. An emission line of Ne VII λ465Å ($T_f \sim 5 \times 10^5$ K; T_f – line forming temperature) can act as a key in this situation, capable of providing very important diagnostic information on the energy transport from the chromosphere to the corona (Mariska and Dowdy 1992). There exists a wide temperature gap between those of O VI ($T_f \sim 3 \times 10^5$ K) and Ne VIII ($T_f \sim 7 \times 10^5$ K), where the fundamental structure on the solar surface substantially changes from chromospheric networks to coronal loops. It is expected that the relationship of chromospheric and coronal heating would be clarified if we could diagnose dynamical chromospheric plasma, observed with this Ne VII emission line, which has a narrow contribution curve peaked just at the temperature between those of the above-noted two lines.

It is also very important to understand the behavior of plasma, which has high temperatures close to the upper limit for the active regions. Collaborative observations of EIS/XRT and SUMER revealed that the distribution of emission measures extends to the temperature range, in which Fe XVIII emission lines form ($T_f \sim 8 \times 10^6$ K) (Teriaca et al. 2012). Therefore, new knowledge can be gathered

on the mechanism of high-temperature plasma creation in the active regions if we can observe the Fe XVIII λ975Å line in the core of the active regions.

The tasks for the post-EIS EUV spectroscopic instrument should be (a) observing with the best set of emission lines, besides the above-noted two lines, (b) increasing its throughput, (c) adopting the widest possible fields of view, and (d) following rapid changes in the electron temperature, electron density, velocity fields, magnetic field shapes, as well as abundances of various elements (Brooks et al. 2015).

References

Antolin, P., et al.: Predicting observational signatures of coronal heating by Alfvén waves and nanoflares. Astrophys. J. **688**, 669–682 (2008)

Brooks, D., Ugarte-Urra, I., Warren, H.P.: Full-Sun observations for identifying the source of the slow solar wind. Nat. Commun. **6**, 6947 (2015)

Brooks, D.H., Warren, H.P.: Measurements of non-thermal line widths in solar active regions. Astrophys. J. **820**, 63 (14pp) (2016)

Brooks, D.H., Warren, H.P., Winebarger, A.R.: Characteristics and evolution of the magnetic field and chromospheric emission in an active region core observed by *Hinode*. Astrophys. J. **720**, 1380–1394 (2010)

Brown, C.M., et al.: Wavelengths and intensities of spectral lines in the 171–211 and 245–291 Å ranges from five solar regions recorded by the Extreme-ultraviolet imaging spectrometer (EIS) on *Hinode*. Astrophys. J. Suppl. **176**, 511–535 (2008)

Cirtain, J.W., et al.: Evidence for Alfvén waves in solar X-ray jets. Science **318**, 1580–1582 (2007)

Culhane, J.L. et al.: The EUV imaging spectrometer for Hinode. Solar Phys. **243**, 19–61 (2007)

De Pontieu, B., et al.: Observing the roots of solar coronal heating – in the chromosphere. Astrophys. J. **701**, L1–L6 (2009)

Doschek, G.A., et al.: Nonthermal velocities in solar active regions observed with the Extreme-ultraviolet imaging spectrometer on *Hinode*. Astrophys. J. **667**, L109–L112 (2007)

Erdelyi, R., Taroyan, Y.: Hinode EUV spectroscopic observations of coronal oscillations. Astron. Astrophys. 489, L49–L52 (2008)

Fisher, G. II., Canfield, R.C., McClymont, A.N.: Flare loop radiative hydrodynamics – part six – chromospheric evaporation due to heating by nonthermal electrons. Astrophys. J. **289**, 425–433 (1985)

Fu, H., et al.: Measurements of outflow velocities in on-disk plumes from EIS/*Hinode* observations. Astrophys. J. **794**, 109 (9pp) (2014)

Hara, H.: Coronal plasma motions in active region loops observed with *Hinode* EIS. In: Lites B., Cheung, M., Magara, T., Mariska, J., Reeves, K. (eds.) The Second Hinode Science Meeting Beyond Discovery – Toward Understanding. Astronomical Society Pacific Conference Series, vol. 415, pp. 252–255. ASP, San Francisco (2009)

Harra, L.K., et al.: Outflows at the edges of active regions: contribution to solar wind formation? Astrophys. J. **676**, L147–L150 (2008a)

Hara, H., et al.: Coronal plasma motions near footpoints of active region loops revealed from spectroscopic observations with *Hinode* EIS. Astrophys. J. **678**, L67–L71 (2008b)

Hara, H., et al.: Plasma motions and heating by magnetic reconnection in a 2007 May 19 flare. Astrophys. J. **741**, 107 (20pp) (2011)

Imada, S., et al.: Evidence for hot fast flow above a solar flare arcade. Astrophys. J. **776**, L11 (5pp) (2013)

Kamio, S., et al.: Distribution of jets and magnetic fields in a coronal hole. Astron. Astrophys. **502**, 343–345 (2009)

Kitagawa, N., et al.: Mode identification of MHD waves in an active region observed with *Hinode*/EIS. Astrophys. J. **721**, 744–749 (2010)
Mariska, J.T., Dowdy, J.F. Jr.: Solar Doppler-shift measurements in the Ne VII 465 Å emission line. Astrophys. J. **401**, 754–758 (1992)
Mariska, J.T., Muglach, K.: Doppler-shift, intensity, and density oscillations observed with the Extreme ultraviolet imaging spectrometer on *Hinode*. Astrophys. J. **713**, 573–583 (2010)
Mariska, J.T., et al.: Observations of Doppler shift oscillations with the EUV imaging spectrometer on *Hinode*. Astrophys. J. **681**, L41–L44 (2008)
Matsui, Y., et al.: Multi-wavelength spectroscopic observation of extreme-ultraviolet jet in AR 10960. Astrophys. J. **759**, 15 (8pp) (2012)
Milligan, R., Dennis, B.R.: Velocity characteristics of evaporated plasma using *Hinode*/EUV imaging spectrometer. Astrophys. J. **699**, 968–975 (2009)
Okamoto, T.J., et al.: Coronal transverse magnetohydrodynamic waves in a solar prominence. Science **318**, 1577–1580 (2007)
Okamoto, J.T., et al.: Resonant absorption of transverse oscillations and associated heating in a solar prominence. I. Observational aspects. Astrophys. J. **809**, 71 (12pp) (2015)
Sakao, T., et al.: Continuous plasma outflows from the edge of a solar active region as a possible source of solar wind. Science **318**, 1585–1588 (2007)
Teriaca, L., et. al.: SUMER observations of Doppler shift in the quiet Sun and in an active region. Astron. Astrophys. **349**, 636–648 (1999)
Teriaca, L., Warren, H.P., Curdt W.: Spectroscopic observations of Fe XVIII in solar active regions. Astrophys. J. **754**, L40 (5pp) (2012)
Tousey, R., et al.: Extreme ultraviolet spectroheliograph ATM experiment S082A. Appl. Opt. **16**, 870–878 (1977)
Tsuneta, S., et al.: The magnetic landscape of the Sun's polar region. Astrophys. J. **688**, 1374–1381 (2008)
Van Doorsselaere T., et al.: Coronal magnetic field measurement using loop oscillations observed by Hinode/EIS. Astron. Astrophys. **487**, L17–L20 (2008)
Wang, T.J., et al.: Hinode/EIS observations of propagating low-frequency slow magnetoacoustic waves in fan-like coronal loops. Astron. Astrophys. **503**, L25–L28 (2009)
Wang, T.J., Ofman, L., Davila, J.M.: Propagating slow magnetoacoustic waves in coronal loops observed by *Hinode*/EIS. Astrophys. J. **696**, 1448–1460 (2009)
Watanabe, T., et al.: Production of high-temperature plasmas during the early phases of a C9.7 flare. Astrophys. J. **719**, 213–219 (2010)

Part II
Coronal Heating and Solar Wind

Chapter 6
Coronal Heating: Issues Revealed from *Hinode* Observations

Hirohisa Hara

Abstract The corona, which is observed around the Sun during total solar eclipses, has a temperature of a few million degrees. The temperature of the Sun monotonically decreases from the core to the surface that we call the photosphere, and then, the temperature rapidly increases outward by two orders of magnitude from the photosphere to the corona, which starts at a distance of a few thousand kilometers above the photosphere. In this article, I introduce the understanding that has recently been improved by observations from high-performance telescopes onboard *Hinode* regarding the site where coronal heating occurs.

Keywords Sun: corona · Coronal heating · Sun: magnetic field

6.1 Introduction

After the identification of emission lines radiating from the corona, it has been understood since the 1940s that the solar corona is a hot outer atmosphere with a temperature of a few million degrees. Identifying the mechanism by which the corona is heated is the coronal heating problem, and some theoretical research and observational studies have been conducted. The solar surface observed at visible wavelengths is covered with turbulent convective structures, called "granules," of about 1,000 km in diameter, which have temperatures two orders of magnitude lower than that of the corona. There is no doubt that the kinetic energy of granular motions is the energy source that heats the corona.

Sound waves are generated by the turbulent convection and propagate upward. The mechanism that was first proposed for coronal heating is the heating by the acoustic shock wave. The sound wave propagating upward forms the shock wave, and the wave energy is used for the heating of the atmosphere. However, it has

H. Hara (✉)
SOLAR-C Project Office, National Astronomical Observatory of Japan, Mitaka, Tokyo, Japan
e-mail: hirohisa.hara@nao.ac.jp

T. Shimizu et al. (eds.), *First Ten Years of Hinode Solar On-Orbit Observatory*,
Astrophysics and Space Science Library 449,
https://doi.org/10.1007/978-981-10-7742-5_6

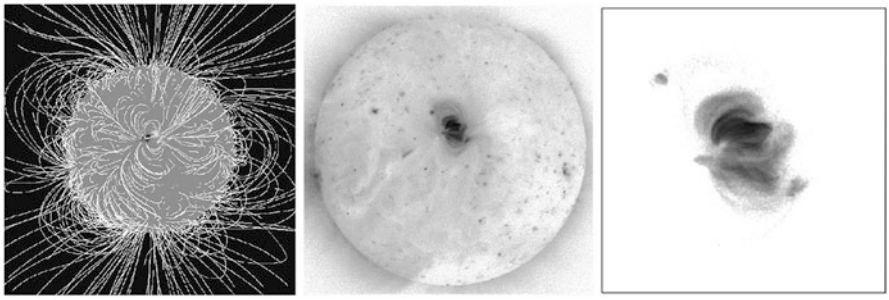

Fig. 6.1 (Left) Magnetic fields observed in the photosphere from *Solar and Heliospheric Observatory (SoHO)*/Michelson Doppler Imager (MDI) with calculated magnetic field lines by the potential field approximation. (Center) Sun in soft X-rays from *Hinode*/XRT(X-ray Telescope). (Right) Magnified view of the central part of the X-ray image (Figures reprinted from an article in The Astronomical Herald by permission of ASJ (The Astronomical Society of Japan))

been proven theoretically and observationally in the 1970s that the wave energy flux required for the coronal heating cannot reach the altitude of the corona by the shock waves because of its short damping scale. For this reason, the shock wave heating model has been excluded from candidates of the primary heating mechanism, and another model is required.

It is widely believed at present that the energy for coronal heating is transported through magnetic fields that extend from the photosphere to the corona. This concept was established from the property of coronal structures observed in X-rays (see the center panel of Fig. 6.1). Unlike the convective structures observed everywhere on the photosphere, structures similar to the magnetic field lines calculated from the observed surface magnetic fields (lines in the left panel of Fig. 6.1) are observed in the corona, as shown in the right panel of Fig. 6.1. The following correspondence is found; the stronger the magnetic field, the brighter the corona. However, the existence of a magnetic field and its strength alone are insufficient to generate the corona; the photospheric convections that force the magnetic field lines to move are also required. This is because a bright corona is not observed above a large sunspot known as a strong magnetic field region in which the photospheric convective motion is suppressed by the presence of the magnetic fields.

6.2 Before the Birth of *Hinode*

In the observations of the solar corona, we cannot ignore the achievements made with numerous sounding-rocket experiments, several *OSO (Orbiting Solar Observatory)* satellites, and the *Skylab* space station, which were executed by the USA in the 1960s and 1970s. These observations have shown that (a) the corona is magnetically heated, (b) the dark corona in the polar region observed in the center

panel of Fig. 6.1 is a global monopolar region that we call the "coronal holes" (CHs) where high-speed solar wind originates from, and (c) the corona is mostly covered by loop-shaped structures, which we call "coronal loops," that connect between the positive and negative magnetic polarities on the photosphere.

At that time, there were no two-dimensional electronic devices like charge-coupled device (CCD) and complementary MOS (CMOS) imaging sensors that we use at present; thus, a film with a small resolution was used as the detector for high-resolution observations. When highly sensitive observations were required, a single element detector with a high sensitivity was used in a particular configuration, in which an observing target is moved to the detector position by moving the solar image on the focal plane with a mechanism. Thus, the temporal cadence of space observations at that time was very low. From these observations, however, the energy flux required for coronal heating was derived (10^7 erg cm^{-2} s^{-1} in the active region (AR) that has a strong magnetic field and 10^5 erg cm^{-2} s^{-1} in the quiet-Sun (QS) region of the weak magnetic field region outside the AR) (Withbroe and Noyes 1977). The energy flux is still used as a reference, and a useful scaling relation among the temperature, pressure, and loop length was found for the case in which the coronal loop is heated steadily (Rosner et al. 1978).

Since the shape of a coronal loop resembles the coronal magnetic field structure that is calculated from the observed surface magnetic fields, (1) the dissipation of DC electric currents generated in the magnetic structure and (2) the dissipation of Alfvén waves propagating along the magnetic structures are regarded as the strong candidates for the heating mechanism. These are generated when the magnetic field lines extending toward the corona are translated, twisted, or braided by the surface convective motions. Because of the difference in the time scales of the motion of the magnetic fields, there are two different responses: it appears either as a DC electric current or as an alternating current (Alfvén wave). In the DC heating model, continuous excursions driven by the convective motions at the footpoints of magnetic fluxes constituting the coronal loops generate multiple locations where opposite-directed magnetic fields face each other in the corona. The restructuring of the magnetic field configuration by magnetic reconnection occurs at locations of high-current density, and the plasmas within the magnetic loops are heated to the coronal temperature. This is the heating mechanism that Parker proposed as "nanoflares" (Parker 1972, 1988).

The possibility of coronal heating by the ensemble of small-scale flares has seriously been considered by the detection of hard X-ray microflares that was first reported in the 1980s by a balloon-borne experiment with a high-sensitivity hard X-ray spectrometer (Lin et al. 1984). Although the number of microflares observed in hard X-rays was small, it was shown that the frequency distribution could resemble a power law against the flare energy with a steeper power-law index than that of larger flares. This observation has suggested the importance of small flares with a lower energy, and a serious discussion has started on whether it might be possible to understand the amount of energy for coronal heating by the ensemble of small flare events in the corona.

The first imaging observations of microflares were carried out by the X-ray telescope mounted on the Japanese solar flare observation satellite *Yohkoh*. The microflares observed with the *Yohkoh* soft X-ray telescope are small in size and released energy (Shimizu et al. 1992). Since multiple loop structures were found for relatively large microflares, it has been believed that magnetic reconnection between two small magnetic structures produces them. As a result, hot plasmas appear in the ARs. Depending on the magnetic field configuration, X-ray jets that *Yohkoh* first observed also occur simultaneously. However, the lifetime of the microflares is at most about 10 min and is much shorter than that of the other coronal loops. The frequency distribution of microflares $N(E)$, which follows a power-law against energy E, is located approximately on the low-energy extension of the frequency distribution of the flare, and the power index of the distribution is 1.7 ($N(E) \propto E^{-1.7}$) and is similar to that of larger flares. This distribution implies that the frequency of high-energy events determines the total energy. Since the total energy in the microflare energy range is found to be insufficient for AR heating from the *Yohkoh* observations, the smaller flares with the same property, even if they exist, cannot explain the amount of energy required for coronal heating (Shimizu 1995).

6.3 From *Yohkoh* to *Hinode*

The coronal loop structures observed by *Skylab* and *Yohkoh* in X-rays are apparently maintained in a period that is longer than the cooling time determined by radiation and thermal conduction. The coronal loops have also been routinely observed at extreme ultraviolet (EUV) wavelengths by the *SoHO* observatory at the L1 Lagrangian point, and EUV loops occupy different spaces in the corona from the X-ray loops. Although the spatial segregation by coronal loops with different temperatures is well-known from observations of emission lines with different ionization levels, it is important to understand the cause of this difference in temperature. A possibility is that there might be a difference in the magnetic and kinetic properties at the footpoints of coronal loops.

While we were executing the coronal observations with *Yohkoh*, extensive efforts to detect the small-scale flux tube of approximately 0.2 arcsecs in diameter on the photosphere have been made at the ground-based observatories since the 1970s. The existence has been inferred from the spectropolarimetry of multiple absorption lines with different responses to the photospheric magnetic field. The small object, which is sometimes observed in snapshot images with a good atmospheric seeing condition, could not be found in the magnetogram as an isolated magnetic element due to the optical turbulence of the Earth's atmosphere. The following was strongly desired to understand the formation of the corona: (1) clarify the property of fine-scale magnetic fields and its motion on the photosphere and (2) explore the variability and velocity structures of fine coronal features as a response to the motion of magnetic field structures. This is the mission of SOLAR-B (the code name of *Hinode*). See the article Kosugi et al. (2007) for the science objectives and science instruments on *Hinode*.

In terms of coronal heating, *Hinode* was proposed such that the following three points were tackled for the deep understanding:

I. Are Alfvén waves or DC electric currents sufficiently generated to heat the corona on the photosphere?
II. Do the waves transfer through the chromosphere toward the corona?
III. Where and how is the energy that is transferred from the lower atmosphere dissipated in the corona?

In the *Hinode* program, these were going to be answered by the high-resolution observations of the photospheric vector magnetic field and velocity field for the first question (I), by imaging observations of the chromosphere for the second question (II), and by the imaging and spectroscopic observations of the corona for the third question (III).

6.4 Achievements by *Hinode* on Coronal Heating

6.4.1 Characteristics of Photospheric Magnetic Fields and Energy Transfer

The Solar Optical Telescope (SOT) has established that elemental magnetic flux tubes of 0.2 arcsecs in diameter with a magnetic field of 1 kG actually exist at the boundaries of granules on the photosphere. The telescope has further revealed the formation process of these flux tubes from a weaker magnetic field (Nagata et al. 2008). The magnetic structure that is spread in the corona by its magnetic pressure is actually concentrated as a flux tube on the photosphere. The imaging observations by the *Hinode* SOT have shown that most of the observed elemental flux tubes have a width identical to the telescope's spatial resolution and that there is evidence for the existence of a smaller magnetic element from the spectropolarimetry data. It has thus been determined that the magnetic flux tubes on the photosphere have not been fully resolved in the *Hinode* SOT observations (Stenflo 2011).

From the viewpoint of coronal heating, the motion of the elemental flux tubes by photospheric convection is an important process for transporting energy upward. A standard method to evaluate the horizontal velocity on the photosphere is to use the morphological variation of the features on the photosphere such as granules from a series of imaging data, and the horizontal velocity is calculated from the cross-correlation of those local features between the consecutive images in time. The power spectrum of the horizontal velocity in the QS region has been estimated from the SOT observations. A magnetohydrodynamics (MHD) simulation using the seeing-free power spectrum of the photospheric horizontal velocity from *Hinode* has demonstrated that the Alfvén wave excited by the photospheric motion of the flux tube can transfer sufficient energy to heat of the QS region and CH where the average magnetic field is weak (Matsumoto and Shibata 2010). In addition,

the Alfvén wave energy flux toward the chromosphere, the 10^4 K atmosphere located between the photosphere and corona, has been estimated from the variation in the magnetic and velocity fields for the ensemble of flux tubes, which has shown that sufficient energy flux required for heating the QS corona is transported toward the chromosphere (Fujimura and Tsuneta 2009).

The slow photospheric motion of magnetic flux tubes in the time scale of an hour produces the electric currents in the upper atmosphere. At the footpoints of coronal loops, the energy flux upward from the photosphere has been estimated from the observations, and it has been shown that the required flux is expected. From the comparison between the data analysis and MHD simulation for magneto-convection, it has also been noted that the motion of the braiding process among flux tubes and its energy transport are underestimated due to the insufficient spatial resolution of the *Hinode* SOT (Yeates et al. 2014).

The property of the flux tubes as a footpoint of coronal loops and their motions on the photosphere have also been examined from the SOT observations to understand the cause of the difference in temperature of coronal loops over an AR, as shown in Fig. 6.2. At the footpoints of coronal loops, there are no major differences in the property of magnetic fields and their horizontal motion (Kano et al. 2014). The observed property of the photospheric flux tube from the *Hinode* observation is qualitatively consistent with the situation that the energy flux given to the hot loop is larger under the condition that the length of hot X-ray loops is shorter than that of the warm EUV loops. Further studies will reveal the relationship between the energy input on the photosphere and the energy required for a coronal loop.

Numerous small-scale bipolar structures over the disk of the Sun have been discovered by photospheric observations of the linear polarization that represent the presence of the horizontal magnetic field (Lites et al. 2007, 2008; Ishikawa

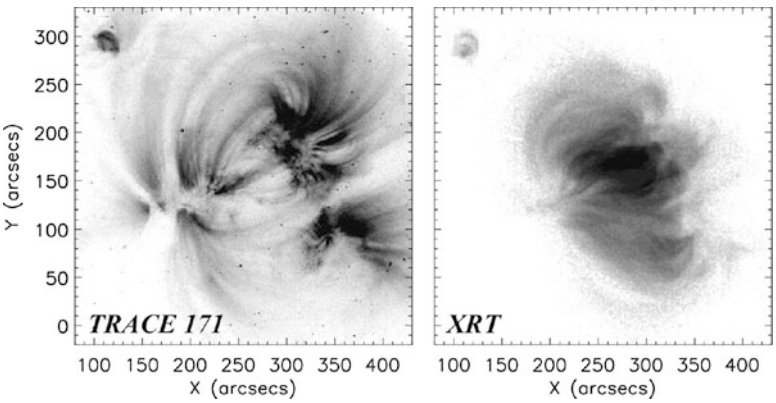

Fig. 6.2 Coronal loops in an AR. (Left) Warm loops [$T_e \sim 1$ million Kelvin (MK)] in the EUV image from *Transition Region and Coronal Explorer (TRACE)* and (Right) hot loops ($T_e > 2$ MK) in the soft X-ray image from the *Hinode* XRT (Figures reprinted from an article in The Astronomical Herald by permission of ASJ) are shown for comparison

et al. 2008). The interaction between these rapidly changing structures and larger pre-existing magnetic fields may be important in the heating of the chromosphere and corona because the number and magnetic energy of such emerging bipoles appear to be sufficient for the heating of the upper atmosphere (Ishikawa and Tsuneta 2009). It will be crucial to obtain evidence for magnetic reconnection in the chromosphere and the corona in association with the emergence of small bipoles in future observations.

6.4.2 Energy Transfer Through the Chromosphere

The chromosphere is an outer atmosphere of 10^4 K in temperature and is located between the photosphere and the corona. Vertically oriented jet-like features at the chromospheric height are called "spicules" (see the article by Suematsu in this volume). One of the outstanding achievements by the *Hinode* program is the clear observation of lateral motion of the spicule structures, which has not been reported from ground-based telescopes with larger mirror diameters than that of the *Hinode* SOT. This is a good example of the excellent performance of the space telescope that is free from the atmospheric seeing. Since the extended structures of spicules are believed to be aligned with the magnetic field lines, the lateral motion is interpreted as the detection of the Alfvénic waves that oscillates perpendicular to the magnetic field.

The energy flux toward the corona by the Alfvénic wave is derived from the analysis of the lateral motion of spicules located outside the sunspot region and is found to be sufficient for the heating of the QS and CH corona (Okamoto and De Pontieu 2011). While it is welcomed by the researchers who support the coronal heating by Alfvén waves, it has long been recognized that it might be difficult for the wave to reach the corona because of the large density gradient between the chromosphere and corona. If the energy flux of the Alfvénic waves in the corona that are located above spicules is measured in future observations, future measurements will make substantial progress in understanding the contribution of the wave that *Hinode* has revealed to coronal heating. To perform such observations, the corona needs to be observed by an instrument with a similar high spatial resolution to the *Hinode* SOT, i.e., by an instrument with a resolving performance 5–10 times better than those of the XRT and EUV Imaging Spectrometer (EIS) on *Hinode*.

6.4.3 Fine-Scale Structures and Velocity Field in the Corona

What fraction of volume in the observed coronal structure is filled with hot plasmas? The electron density of a coronal loop can be estimated from the EIS observations by the intensity ratio of a pair of emission lines. It is possible to derive the fraction of volume filling (a filling factor) from the emission line intensity across a loop,

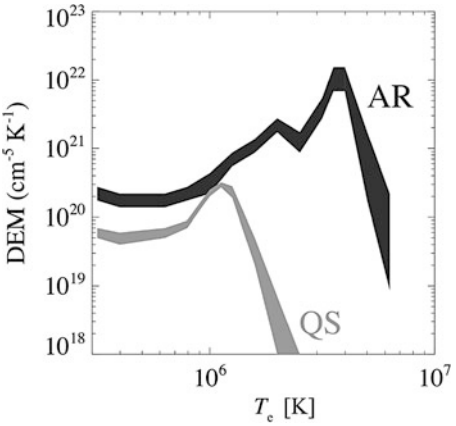

Fig. 6.3 Differential emission measures for the core of AR (black) and QS (gray). This figure is made from the studies in References; Warren et al. (2012), Winebarger et al. (2012), and Brooks et al. (2009) (Figure reprinted from an article in The Astronomical Herald by permission of ASJ)

apparent width of the coronal loop for a measure of the line-of-sight (LOS) length, and electron density. The filling factor has been found to be 0.05–0.1, depending on the position in the loop (Warren et al. 2008). Since the EIS spatial resolution is about 3 arcsecs, if the observed loop is a filamentary structure, the loop width may be 0.6–0.8 arcsecs, which cannot be resolved with the instruments on the operating science satellites.

If each structure cannot be resolved by the current instrumentation, it would be good to examine how much plasma exists in a unit volume and a temperature range to directly compare with observations. While the *Hinode* EIS can measure the amount of plasma in the temperature range of $10^{5.6}$–$10^{6.7}$ K by many emission lines, the XRT has an excellent sensitivity to temperatures above $10^{6.5}$ K. With the combination of the EIS and XRT, the differential emission measure (DEM), defined by $d(n_e^2 L)/dT_e$ (where n_e is the electron density, L is the LOS length, and T_e is the electron temperature), has been estimated for the core part of the AR and QS regions, as shown in Fig. 6.3 (Warren et al. 2012; Winebarger et al. 2012; Brooks et al. 2009). The DEM at a high-temperature region ($\log T_e > 6.6$) is not shown in Fig. 6.3 because of the large uncertainty. The DEM peak for the AR appears at $10^{6.5}$–$10^{6.6}$ K, and there is little emission measure at higher temperatures. The amount of plasma in the temperature range of DEM is given by the ensemble of small-scale loops that are independently in the heating or cooling phase. For the hot AR loop at $10^{6.6}$ K, which is short in length, it has been determined from the recent MHD simulations that there is a difficulty in heating it by Alfvén waves (Antolin and Shibata 2010). It has also been found that a larger velocity fluctuation than what is observed is required in the photosphere for the hot loop force to produce the Alfvén waves (Asgari-Targhi et al. 2014). The heating by Alfvén waves is becoming less preferred in explaining the production of hot coronal plasmas in the core of ARs. In the numerical simulation of the heating through the induced small-scale current structures, which is driven by the convective motions of flux tubes, the DEM calculated from the simulation is compared with the observed values for explaining both the fine-scale coronal structures and hot AR components simultaneously (Dahlburg et al. 2016).

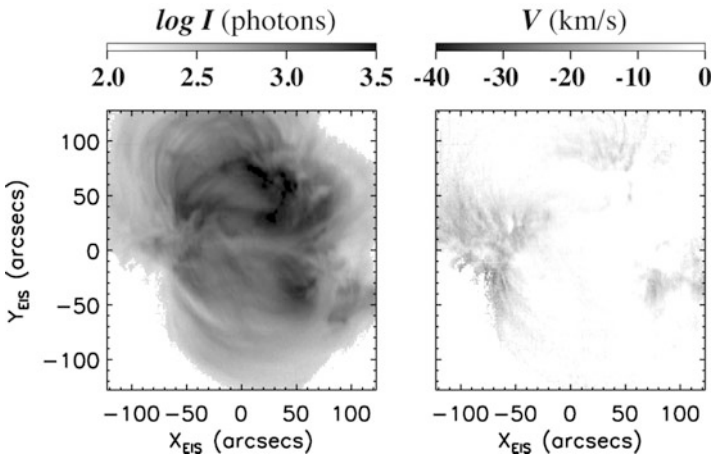

Fig. 6.4 Emission line observation by *Hinode* EIS. Line intensity in units of observed photons (left) and upflow components in Doppler velocity (right) (Figures reprinted from an article in The Astronomical Herald by permission of ASJ)

The newest point in the coronal observation by *Hinode* is the spectroscopy with the highest sensitivity in intensity and velocity (note: spectral data of a high spectral resolution have been obtained for the targets outside the solar limb from the ground during the total eclipse or with coronagraphs). If the corona is steadily heated, plasmas in the coronal loop should be static with no high-speed flow. If the energy input to the coronal loop is intermittent, as most researchers agree, a characteristic plasma flow occurs in the loop. The average flow speed over a wide area has only been reported before the start of the *Hinode* EIS observations.

The following properties of the coronal velocity fields have been found: (1) the presence of the subsonic upflows of 10–20 $\mathrm{km\,s^{-1}}$ along coronal loops near the footpoints (Fig. 6.4) with (2) faint $\sim$100 $\mathrm{km\,s^{-1}}$ upflows and (3) the fineness of fast upflows that are smaller than the instrument's spatial resolution (Hara et al. 2008; De Pontieu et al. 2009; Nishizuka and Hara 2011; Tian et al. 2011). Numerical simulations have suggested that an intermittent energy input enhanced at the footpoints is required (Antolin et al. 2008). Fast and slow upflows may be the response of the solar atmosphere in different phases after heating: the early phase for the former and late relaxation phase for the latter. In any case, the EIS observations have detected the process in which dense hot plasmas are supplied upward from the base of the corona. The thermal energy of the fast upflow is about 10^{23} erg ($\sim$0.1 nanoflare energy), which is nine orders of magnitude smaller than that of the largest solar flare (Hara 2009). The enhanced radiation by the occurrence of such a small energy release is so small that it cannot be detected by the X-ray monitor on the *GOES* satellite.

The motion measured by the Doppler shift of the EUV emission line contains the wave component in addition to the upflow. It has been found that the wave mostly

represents the slow mode wave propagating upward and that the energy flux in the AR loops is 10^3–10^5 erg cm^{-2} s^{-1}, which is insufficient by more than two orders of magnitude for the heating of AR loops (Nishizuka and Hara 2011; Wang et al. 2009; Kitagawa et al. 2010). Because of the amount of the wave energy, it is considered to be a by-product during the heating process. Direct evidence for the Alfvén wave has not been found in the EIS spectral data, which may be due to the insufficient spatial resolution. This is because the SOT and *IRIS* observations with an order of magnitude better spatial resolution than the EIS show the lateral motion of the prominence, which is a 10^4 K structure at the coronal height, as Alfvénic waves with an energy flux of 10^6 erg cm^{-2} s^{-1} (Okamoto et al. 2007, 2015). Although it may partially contribute to the heating of ARs, the wave with the evaluated energy flux appears not to play a primary role there because the spatial correlation between the hot coronal structures and 10^4 K structures with the lateral motion appears to be weak.

In the polar CHs where the magnetic field radially extends to the interplanetary space, however, the heating by Alfvén waves is considered to be a primary element. A study has reported from the EIS observation that the evidence for the damping of Alfvén waves propagating outward is detected at a distance beyond 0.2 solar radii (Hahn and Savin 2013). The nonthermal line broadening of the coronal emission line is interpreted as the result of plasma oscillations perpendicular to the magnetic field line due to Alfvén waves, and the energy flux of the wave appears to decrease at a distance beyond 0.2 solar radii. The energy flux given to the plasma is sufficient for the heating of the corona in the polar region and the acceleration of the fast solar wind.

6.5 Concluding Remarks

In this article, I have reviewed what we have learned from the *Hinode* observations on the topic of coronal heating. The essential differences from the previous observations are:

- High-resolution vector magnetic fields and velocity fields are obtained on the photosphere at the site of energy input for the heating of the upper atmosphere.
- Alfvénic waves, which are thought to play a primary role in the wave heating, are clearly detected in the chromosphere through the improvement of the spatial resolution.
- The volume filling fraction of coronal structures is measured by the coronal spectroscopy, which clarifies the presence of fine-scale coronal structures and the width of the elemental structure.
- The amount of hot coronal components in coronal loops is measured for comparison with coronal heating models.
- The high-precision velocity measurements in the corona from space have revealed the dynamics of coronal loops.

The implications of these observations on coronal heating will be slightly different among researchers. The author's personal view is that the primary heating mechanism in the ARs and CHs are the DC and AC heating, respectively. In the QS region, both may contribute to the heating of the corona in a similar amount. The contribution of the DC heating in the QS region and CHs may be changed depending on the estimation of energy input by magnetic reconnection in association with numerous small-scale emerging bipoles that *Hinode* has discovered from the vector magnetic field observations. The summary will be clarified through ongoing further verifications.

The details on microflares observed by *Hinode* are reported in the article of this volume by Ishikawa. In addition to the improvement in spatial resolution of the X-ray imaging observations, *Hinode* has also carried out simultaneous observations of photospheric vector magnetic fields. It has been found that half of the microflares occur at the site where a footpoint of a small magnetic loop, which emerges from the subsurface or moves horizontally near the sunspot region, collides with the magnetic structure that has an opposite polarity (Kano et al. 2010). While the mixed polarity condition observed at the site of microflares is common for the photosphere in the QS region or the region with many small emerging bipoles within ARs, the condition is different in the ARs where the coronal loops are rooted and the footpoints with a single polarity are shuffled by the convective motion of granules. The magnetic field configuration at footpoints of coronal loops in Fig. 6.2 is not the former case but the latter. The form of magnetic reconnection there, if the process occurs, is interchange reconnection and component reconnection for the former and the latter, respectively. Since the primary mechanism for coronal heating is magnetic reconnection for both cases with different magnetic configurations, the occurrence frequency of the heating events is expected to follow a power law with a power-law index of -1.7. However, the absolute value of occurrence frequency at a given energy may be different because the formation process of the magnetic configuration is different. This may also be revealed in the future analyses.

Multiple EUV imaging instruments with a slightly better spatial resolution of about 1 arcsec have been operated by the USA on the *Solar Dynamics Observatory (SDO)* since the few years of operation of *Hinode*. A further improved imaging quality of 0.3 arcsecs in resolution has been achieved in the High-Resolution Coronal Imager (Hi-C) sounding-rocket experiment, and fine-scale coronal loop structures, which are inferred from the EIS observations, have been observed (Cirtain et al. 2013; Brooks et al. 2013). This scale is similar to those of the electric currents formed by the photospheric motions of magnetic structures. It has also been observed as narrow cooling structures flowing down along magnetic loop structures (Scullion et al. 2014). To understand how structures of this scale are formed and how much energy is hidden in such small-scale structures in the form of Alfvén waves, it is becoming extremely crucial to observe the corona with imaging and spectroscopy with the spatial resolution of Hi-C from space. When the structure of coronal electric currents is measured from the magnetic fields in the photosphere and chromosphere simultaneously with high-resolution coronal observations, the coronal heating problem may finally be resolved.

References

Antolin, P., Shibata, K.: The role of torsional Alfvén waves in coronal heating. ApJ **712**, 494–510 (2010)
Antolin, P., et al.: Predicting observational signatures of coronal heating by Alfvén waves and nanoflares. ApJ **688**, 669–682 (2008)
Asgari-Targhi, M., van Ballegooijen, A.A., Imada, S.: Comparison of extreme ultraviolet imaging spectrometer observations of solar coronal loops with Alfvén wave turbulence models. ApJ **786**, 28 (13pp) (2014)
Brooks, D.H., et al.: Hinode/Extreme-ultraviolet imaging spectrometer observations of the temperature structure of the quiet corona. ApJ **705**, 1522–1532 (2009)
Brooks, D.H., et al.: High spatial resolution observations of loops in the solar corona. ApJ **772**, L19 (5pp) (2013)
Cirtain, J.W., et al.: Energy release in the solar corona from spatially resolved magnetic braids. Nature **493**, 501–503 (2013)
Dahlburg, R.B., et al.: Observational signatures of coronal loop heating and cooling driven by footpoint shuffling. ApJ **817**, 47 (15pp) (2016)
De Pontieu, B., et al.: Observing the roots of solar coronal heating – in the chromosphere. ApJ **701**, L1–L6 (2009)
Fujimura, D., Tsuneta, S.: Properties of magnetohydrodynamic waves in the solar photosphere obtained with Hinode. ApJ **702**, 1443–1457 (2009)
Hahn, M., Savin, D.W.: Observational quantification of the energy dissipated by Alfvén waves in a polar coronal hole: evidence that waves drive the fast solar wind. ApJ **776**, 78 (10pp) (2013)
Hara, H.: Coronal plasma motions in active region loops observed with Hinode EIS. ASPC **415**, 252–255 (2009)
Hara, H., et al.: Coronal plasma motions near footpoints of active region loops revealed from spectroscopic observations with Hinode EIS. ApJ **678**, L67–L71 (2008)
Ishikawa, R., et al.: Transient horizontal magnetic fields in solar plage region. A&A **481**, L25–L28 (2008)
Ishikawa, R., Tsuneta, S.: Comparison of transient horizontal magnetic fields in a plage region and in the quiet Sun. A&A **495**, 607–612 (2009)
Kano, R., Shimizu, T., Tarbell, T.D.: Hinode observation of photospheric magnetic activities triggering X-ray microflares around a well-developed sunspot. ApJ **720**, 1136–1145 (2010)
Kano, R., Ueda, K., Tsuneta, S.: Photospheric properties of warm EUV loops and hot X-ray loops. ApJ **782**, L32 (6pp) (2014)
Kitagawa, N., et al.: Mode identification of MHD waves in an active region observed with Hinode/EIS. ApJ **721**, 744–749 (2010)
Kosugi, T., et al.: The Hinode (Solar-B) mission: an overview. Solar Phys. **243**, 3–17 (2007)
Lin, R.P., et al.: Solar hard X-ray microflares. ApJ **283**, 421–425 (1984)
Lites, B.W., et al.: Hinode observations of horizontal quiet Sun magnetic flux and the "Hidden Turbulent Magnetic Flux". PASJ **59**, S571–S576 (2007)
Lites, B.W., et al.: The horizontal magnetic flux of the quiet-Sun internetwork as observed with the Hinode spectro-polarimeter. ApJ **672**, 1237–1253 (2008)
Matsumoto, T., Shibata, K.: Nonlinear propagation of Alfvén waves driven by observed photospheric motions: application to the coronal heating and spicule formation. ApJ **710**, 1857–1867 (2010)
Nagata, S., et al.: Formation of solar magnetic flux tubes with kilogauss field strength induced by convective instability. ApJ **677**, L145–L147 (2008)
Nishizuka, N., Hara, H.: Spectroscopic observations of continuous outflows and propagating waves from NOAA 10942 with extreme ultraviolet imaging Spectrometer/Hinode. ApJ **737**, L43 (7pp) (2011)
Okamoto, T., De Pontieu, B.: Propagating waves along spicules. ApJ **736**, L24 (6pp) (2011)

Okamoto, T., et al.: Coronal transverse magnetohydrodynamic waves in a solar prominences. Science **318**, 1577–1580 (2007)
Okamoto, T., et al.: Resonant absorption of transverse oscillations and associated heating in a solar prominence. I. Observational aspects. ApJ **809**, 71 (12pp) (2015)
Parker, E.N.: Topological dissipation and the small-scale fields in turbulent gases. ApJ **174**, 499–510 (1972)
Parker, E.N.: Nanoflare and the solar X-ray corona. ApJ **330**, 474–479 (1988)
Rosner, R., Tucker, W.H., Vaiana, G.S.: Dynamics of the quiescent solar corona. ApJ **220**, 643–665 (1978)
Scullion, E., et al.: Unresolved fine-scale structure in solar coronal loop-tops. ApJ **797**, 36 (10pp) (2014)
Shimizu, T.: Energetics and occurrence rate of active-region transient brightenings and implications for the heating of the active-region corona. PASJ **47**, 251–263 (1995)
Shimizu, T., et al.: Transient brightenings in active regions observed by the soft X-ray telescope on YOHKOH. ApJ **44**, L147–L153 (1992)
Stenflo, J.O.: Collapsed, uncollapsed, and hidden magnetic flux on the quiet Sun. A&A **529**, A42 (20pp) (2011)
Tian, H., et al.: Two components of the solar coronal emission revealed by extreme-ultraviolet spectroscopic observations. ApJ **738**, 18 (20pp) (2011)
Wang, T.J., Ofman L., Davila J.M.: Propagating slow magnetoacoustic waves in coronal loops observed by Hinode/EIS. ApJ **696**, 1448–1460 (2009)
Warren, H.P., et al.: Observations of active region loops with the EUV imaging spectrometer on Hinode. ApJ **686**, L131–L134 (2008)
Warren, H.P., et al.: A systematic survey of high-temperature emission in solar active regions. ApJ **759**, 141 (13pp) (2012)
Winebarger, A.R., et al.: Defining the "Blind Spot" of Hinode EIS and XRT temperature measurements. ApJ **746**, L17 (5pp) (2012)
Withbroe, G.L., Noyes, R.W.: Mass and energy flow in the solar chromosphere and corona. ARA&A **15**, 363–387 (1977)
Yeates, A.R., et al.: The coronal energy input from magnetic braiding. A&A **564**, A131 (10pp)(2014)

Chapter 7
Importance of MHD Waves Observed with *Hinode*

Takuma Matsumoto

Abstract Robust and high spatial resolution observations made by *Hinode* enable us to understand waves in the solar atmosphere. It also enables us to estimate the energy supplied by waves and to discover the dissipation processes of waves. Moreover, by specifying the wave modes and estimating plasma density using spectroscopy, precise measurements of the coronal magnetic field can be obtained, which are now available. However, if we interpret all periodic events as waves, we will miss out on some important features, such as mass flows. In this document, I will explain energy transfer and magnetic field estimation using waves and quasiperiodic upflows that have observational features similar to those of waves.

Keywords MHD waves · Solar granules · Coronal heating

7.1 Introduction

The *Hinode* satellite has provided us with amazing movies of complex and dynamic motions. The inhomogeneous atmosphere of the Sun is maintained by its magnetic field and by gravity, resulting in a variety of dynamic activities on the solar surface. For example, spicules are eruptive jet-like structures, prominences are cloud-like structures above the solar surface, coronal loops are representatives of the magnetic field lines, and X-ray jets are eruptive phenomena that can be seen almost everywhere on the Sun. Due to convection motion in the photosphere or the sudden release of magnetic energy, these inhomogeneous structures have been considered to exhibit magnetohydrodynamic (MHD) waves.

T. Matsumoto (✉)
Institute of Space and Astronautical Science, Japan Aerospace Exploration Agency, 3-1-1, Yoshinodai, Chuo-ku, Sagamihara, Kanagawa, 252-5210, Japan
e-mail: takuma.matsumoto@nagoya-u.jp

T. Shimizu et al. (eds.), *First Ten Years of Hinode Solar On-Orbit Observatory*,
Astrophysics and Space Science Library 449,
https://doi.org/10.1007/978-981-10-7742-5_7

One of the most basic motions of matter is wave motion. Moreover, more than 99% of baryonic matter exists as plasma. Considering these facts, it can be said that MHD waves in plasma are the most basic phenomena in astrophysics. The most important property of waves is the transfer of energy or momentum. Energy transfer by MHD waves is considered to be one of the most important processes in addressing the coronal heating problem: how to maintain the hot [1 million Kelvin (MK)] corona above the cool (6,000 K) photosphere. The momentum transport by MHD waves gives additional momentum to the solar wind, which is originally driven by the gas pressure gradient forces, resulting in a high-speed wind, which has a speed of 800 km s^{-1} at the Earth's orbit.

In this document, I will briefly review the discoveries made by the *Hinode* satellite in the areas of energy transfer, estimation of magnetic fields, and mass loss processes.

7.2 Discoveries of Waves

Among the nine papers published in Science in December 2007, three reported discoveries of MHD waves. These papers reported discoveries of waves along spicules (De Pontieu et al. 2007), prominences (Okamoto et al. 2007), and X-ray jets (Cirtain et al. 2007). They all claimed to have observed Alfvén waves, one specific mode of MHD waves. Alfvén waves were theoretically predicted by Hannes Olof Gö Alfvén, and he received the Nobel Prize in 1970 for this achievement. Before the *Hinode* satellite was launched, only some signatures of Alfvén waves could be observed. Therefore, researchers expected the *Hinode* satellite to discover clear evidence of Alfvén waves. After the aforementioned three papers were published, a lot of researchers reported the existence of MHD waves using the *Hinode* satellite. Although the discovery of Alfvén waves is not yet widely accepted, the research field of solar MHD waves is now growing, thanks to discoveries by *Hinode*.

MHD waves have the important and basic property that they can transfer energy. In the field of solar physics, MHD waves are considered to play an important role in transferring energy from the photosphere to the corona. Since the corona has a higher temperature than the photosphere, there are no thermal processes that can maintain the coronal temperature. Therefore, energy transfer by waves has, since the 1940s, been suggested as an explanation.

The magnetic flux tubes are buffeted by surface convection, which is considered to generate enough Poynting flux to heat the corona. This idea is called the wave heating theory and is well known in the context of the coronal heating problem. The total amount of energy required to heat the corona is at most one ten-thousandth of the solar luminosity. Even though the required energy is small, it is necessary for the wave heating theory to prove quantitatively that there is a sufficient amount of wave energy in the Sun.

There are three methods for detecting MHD waves using *Hinode* data. The first method is to derive the Poynting flux in MHD waves using the time series of the magnetic and velocity field measurements. By using this method, an energy flux of $2.7 \times 10^6\,\mathrm{erg\,cm^{-2}\,s^{-1}}$ is estimated to exist above magnetic concentrations at the photosphere (Fujimura and Tsuneta 2009). The second method is to trace the wave pattern from the movies and estimate the velocity amplitude and phase speed. Since the spicules that have thin threadlike structures can be observed ubiquitously, several studies were able to estimate the energy flux of the transverse waves that propagates along spicules (De Pontieu et al. 2007; He et al. 2009; Okamoto and De Pontieu 2011). According to these observations, the energy flux above the quiet Sun at the height of the photosphere and the chromosphere exceeds the energy flux required to heat the corona. The third method uses the nonthermal width of extreme ultraviolet (EUV) lines as a proxy for wave amplitude in the corona. From spectroscopic observation above the polar region, the wave amplitude can be estimated as a function of the height (Hahn et al. 2012).

Recent studies suggest that not only energy transfer processes but also energy dissipation processes can be observed (Okamoto et al. 2015; Antolin et al. 2015). One of the plausible dissipation processes for Alfvén waves is called resonant absorption. These studies suggest that evidence of resonant absorption can be obtained using cooperative observations between *Hinode* and *Interface Region Imaging Spectrograph (IRIS)*. Even though there is enough wave energy flux in the corona, it cannot be thermalized as long as Alfvén waves do not dissipate. We therefore have to find further and more evidence of the dissipation processes in the future.

7.3 Energy Flux Estimation Using Numerical Simulation

In this section, I will introduce our previous studies that estimated the energy flux at the bottom of the corona using *Hinode* observation as a boundary condition for numerical simulation. In Sect. 7.2, I mentioned that it is possible to quantitatively estimate the wave energy flux using *Hinode* observations. Although direct observations of MHD waves give us a great insight into the wave heating theory, the statistical properties of the MHD waves may be biased if only the spicular structures are considered. Moreover, it is still unknown how much energy in the chromospheric waves can reach the coronal height. At this point, the only way to derive the energy flux at the coronal height is to estimate the energy flux using MHD theory or numerical simulations.

In order to calculate the amount of wave energy that can reach the coronal height, it is necessary to formulate the velocity disturbances as a boundary condition. The solar surface is filled with convection cells called granules that can be the source of velocity disturbances (Fig. 7.1). It is generally accepted that the kinetic energy of these convection cells is the origin of the coronal heating. The flux tubes are buffeted by the neighboring convection cells, which can drive the upward

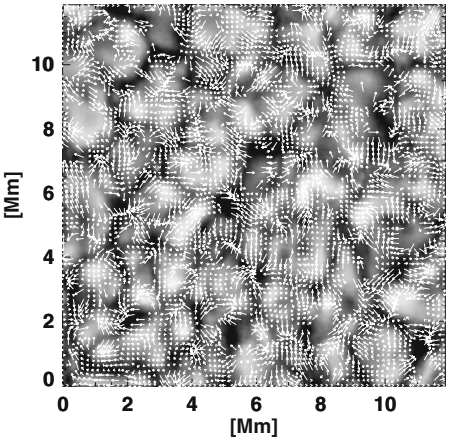

Fig. 7.1 The velocity field at the solar surface derived from the LCT method. The background image is a G-band image observed by *Hinode* Solar Optical Telescope (SOT). The arrow corresponds to the velocity at each point. The unit in the both axes is megameter (Mm)

propagating MHD waves. Among the MHD waves that can be generated by complex convection motions, Alfvén waves are considered to be the most important energy carrier. As the Alfvén waves may be generated by transverse or vortex motions, the horizontal velocity disturbances could be the most important component affecting the photospheric boundary condition.

In order to estimate the temporal power spectra of the horizontal velocity, it is necessary to analyze the time series images that are not affected by atmospheric seeing. By examining the correlation between two successive images, we can recognize where a specific structure like a granular cell moves from one image to the other image. If we know the displacement of the specific structure and the time difference, we can derive the horizontal velocity of the specific structure. This method is called local correlation tracking (LCT). Since the LCT method is severely affected by atmospheric seeing, it is difficult to obtain a reliable velocity field using ground-based telescopes. It was not until *Hinode* brought us time series of seeing-free images that reliable temporal power spectra of the horizontal velocity could be obtained using the LCT method (Matsumoto and Kitai 2010; Matsumoto and Shibata 2010). Among the space telescopes in operation at that time, only *Hinode* could observe at sufficiently high spatial resolution to resolve fine structures in granules that could be used for the LCT method. The root mean square velocity estimated by the LCT method is around 1.1 km s^{-1}, and the power spectra reveals a double power law, which has a break at around 3 min.

The propagation processes of Alfvén waves above the photosphere can be simulated using one-dimensional (1D) MHD simulations that use the observed photospheric velocity as a boundary condition. According to our 1D MHD simulations, the energy flux that can reach the coronal height is $3–4 \times 10^5$ erg cm^{-2} s^{-1}, which is sufficient to maintain the hot corona above the quiet region (Matsumoto and Shibata 2010). Moreover, there are 1D or two-dimensional (2D) MHD simulations using similar boundary conditions that can reproduce not only the propagation processes but also the dissipation processes (Suzuki and Inutsuka 2005; Matsumoto

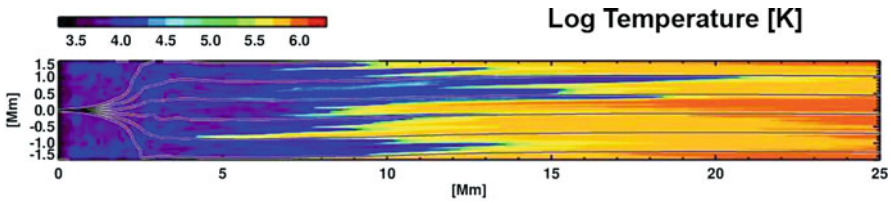

Fig. 7.2 The temperature distribution of 2D MHD simulation (Matsumoto and Suzuki 2014). The background color and white and black lines correspond to the temperature and magnetic field lines, respectively. The high temperature corona is reproduced above the photosphere

and Suzuki 2014). From these simulations, we found that the high temperature corona and the solar wind can be driven as a natural consequence of the photospheric disturbances (Fig. 7.2).

7.4 Estimation of Magnetic Field Using MHD Waves

In this section, I will introduce recent observations that can estimate the coronal magnetic field using MHD waves. The Solar Optical Telescope (SOT) on board *Hinode* can estimate the photospheric magnetic field using Zeeman splitting of the absorption lines. However, it is difficult to estimate the magnetic field in the corona as it does not contain enough photons.

Using MHD waves as a probe, we can estimate the coronal magnetic field without considering the Zeeman effect. The weak point of this method is that it results in large errors due to the uncertainty in the plasma density. The EUV imaging spectrometer (EIS) on board *Hinode* overcomes this weak point by using EUV spectroscopy for density diagnostics, which reduces the error in the magnetic field significantly. A coronal loop oscillation observed by the EIS was interpreted as the fundamental kink mode (Van Doorsselaere et al. 2008). Similar loop oscillations were also reported by past studies using EUV imaging observations (Aschwanden et al. 1999; Nakariakov et al. 1999). Thanks to the improvements in density diagnostics, it was possible to estimate the magnetic field to be 39 ± 8 G, reducing the error to half that of the previous studies. Estimation of the magnetic field using MHD waves is the most accurate way of determining the coronal field so far developed and will be an increasingly active research area in the future.

7.5 Waves or Mass Loss?

Finally, I will introduce an example of oscillations that appear to be wave phenomena but may in fact not be wave phenomena. Several oscillatory phenomena were observed by space solar telescopes before *Hinode* such as *Transition Region And*

Coronal Explorer (TRACE) and *Solar and Heliospheric Observatory (SoHO)*, using EUV imaging observations. One such phenomenon is the oscillation around the footpoints of the coronal loop. This phenomenon can be frequently observed in the coronal loop around the active region. From the oscillation period and the apparent propagation speed, this phenomenon is interpreted as slow magnetoacoustic waves (de Moortel et al. 2000).

However, the discoveries of upflows in the footpoint of the coronal loop gave rise to another interpretation for this oscillation. These upflows became widely known as a result of observation using the X-ray telescope (XRT) on board *Hinode* (Sakao et al. 2007). Quasiperiodic ejections of plasma from the loop footpoint are observed, which could be the origin of the slow solar wind (Brooks and Warren 2011). Besides the imaging observations, EUV spectroscopy using the EIS also reveals high-speed upflows (Hara et al. 2008). According to *Hinode* observations, these high-speed upflows are not rare events but are frequently observed around active region loops.

Taking into consideration these quasiperiodic upflows, the loop oscillations were reinterpreted by De Pontieu et al. (2010). They suggested that the loop oscillations are not caused by the MHD waves but are due to the upflows. Although the total amount of plasma that reveals upflows is small, the quasiperiodic nature of the upflows can reproduce the oscillatory features of the observations. This interpretation is also supported by oscillations in EUV line width observed by the EIS, for which it is difficult to find an explanation in terms of MHD waves. Although this interpretation is not always correct for similar observations, it is important to remember that not all oscillatory phenomena should be interpreted as waves.

7.6 Summary

The hot solar corona could be maintained by MHD waves. The *Hinode* satellite revealed to us many properties of MHD waves, such as their wave modes, amplitudes, and energy fluxes. From the hot corona, the solar wind blows against solar gravity, and this becomes the main contribution to solar mass loss. Mass loss by the stellar wind driven by MHD waves is also considered to be the dominant mass loss process in some types of star. For example, stellar winds in the main sequence stars later than B-type stars, low mass pre-main sequence stars, and post-main sequence giant or supergiant stars are considered to be driven by Alfvén waves (Lamers and Cassinelli 1999; Suzuki 2007). Mass loss due to the stellar wind affects not only the evolution of the stars themselves but also the evolution of surrounding planetary systems, gas, and dust in galaxies (Cranmer and Saar 2011). Therefore, the observations of MHD waves by *Hinode* should have a significant impact on the theory of stellar winds, which has many applications to the astrophysical problems.

Acknowledgements *Hinode* is a Japanese mission developed and was launched by ISAS/JAXA, with NAOJ as domestic partner and NASA and STFC (UK) as international partners. It is operated by these agencies in cooperation with ESA and NSC (Norway). The authors thank S.Imada and S.Ueno for their fruitful comments on this manuscript.

References

Antolin, P., et al.: Resonant absorption of transverse oscillations and associated heating in a solar prominence. II. Numerical aspects. ApJ **809**, 72 (2015)

Aschwanden, M., et al.: Coronal loop oscillations observed with the transition region and coronal explorer. ApJ **520**, 880–894 (1999)

Brooks, D.H., Warren, H.P.: Establishing a connection between active region outflows and the solar wind: abundance measurements with EIS/Hinode. ApJ **727**, L13 (2011)

Cirtain, J.W., et al.: Evidence for Alfvén waves in solar X-ray jets. Science **318**, 1580–1582 (2007)

Cranmer, A.R., Saar, S.H.: Testing a predictive theoretical model for the mass loss rates of cool stars. ApJ **741**, 54 (2011)

de Moortel, I., Ireland, J., Walsh, R.W.: Observation of oscillations in coronal loops. A&A **355**, L23–L26 (2000)

De Pontieu, B., et al.: Chromospheric Alfvénic waves strong enough to power the solar wind. Science. **318**, 1574–1577 (2007)

De Pontieu, B., McIntosh, S.W.: Quasi-periodic propagating signals in the solar corona: the signature of magnetoacoustic waves or high-velocity upflows? ApJ **722**, 1013–1029 (2010)

Fujimura, D., Tsuneta, S.: Properties of magnetohydrodynamic waves in the solar photosphere obtained with Hinode. Astrophys. J. **702**, 1443–1457 (2009)

Hahn, M., Landi, E., Savin, D.W.: Evidence of wave damping at low heights in a polar coronal hole. ApJ **753**, 36 (2012)

Hara, H., et al.: Coronal plasma motions near footpoints of active region loops revealed from spectroscopic observations with Hinode EIS. ApJ **678**, L67 (2008)

He, J.-S., et al.: Upward propagating high-frequency Alfvén waves as identified from dynamic wave-like spicules observed by SOT on Hinode. A&A **497**, 525–535 (2009)

Lamers, H.J.G.L.M., Cassinelli, J.P.: Introduction to Stellar Winds. Cambridge University Press, Cambridge (1999)

Matsumoto, T., Kitai, R.: Temporal power spectra of the horizontal velocity of the solar photosphere. ApJ **716**, L19–L22 (2010)

Matsumoto, T., Shibata, K.: Nonlinear propagation of Alfvén waves driven by observed photospheric motions: application to the coronal heating and spicule formation. ApJ **710**, 1857–1867 (2010)

Matsumoto, T., Suzuki, T.K.: Connecting the Sun and the solar wind: the self-consistent transition of heating mechanisms. MNRAS **440**, 971–986 (2014)

Nakariakov, V.M., et al.: TRACE observation of damped coronal loop oscillations: implications for coronal heating. Science **285**, 862–864 (1999)

Okamoto, T.J., De Pontieu, B.: Propagating waves along spicules. ApJ **736**, L24 (2011)

Okamoto, T.J., et al.: Coronal transverse magnetohydrodynamic waves in a solar prominence. Science **318**, 1577–1580 (2007)

Okamoto, T.J., et al.: Resonant absorption of transverse oscillations and associated heating in a solar prominence. I. Observational aspects. ApJ **809**, 71 (2015)

Sakao, T., et al.: Continuous plasma outflows from the edge of a solar active region as a possible source of solar wind. Science **318**, 1585–1588 (2007)

Suzuki, T.K.: Structured red giant winds with magnetized hot bubbles and the corona/cool wind dividing line. ApJ **659**, 1592–1610 (2007)

Suzuki, T.K., Inutsuka, S.-I.: Making corona and the fast solar wind: a self-consistent simulation for the low-frequency Alfvén waves from the photosphere to 0.3 AU. ApJ **632**, L49–L52 (2005)
Van Doorsselaere, T., et al.: Coronal magnetic field measurement using loop oscillations observed by Hinode/EIS. A&A **487**, L17–L20 (2008)

Chapter 8
Hinode Investigations of Microflares and Nanoflares

Shin-nosuke Ishikawa

Abstract Microflares and nanoflares are small energy release phenomena in the Sun. As their occurrence rate is high, these events may contribute to the heating of the solar atmosphere. The three instruments onboard the *Hinode* satellite enable us to investigate the physical processes and measure the energy releases of microflares and nanoflares. Based on the *Hinode* observations, some of the events can be explained by magnetic reconnection, particle acceleration, and chromospheric evaporation, similar to those for large flares. By precise differential emission measure estimations with multiwavelength observations, it is now possible to investigate the signatures of smaller flares with no individual flare detection.

Keywords Sun: corona · Sun: flares · Sun: X-rays · Sun: UV radiation

8.1 Small Flares in the Sun

Explosive multiwavelength brightenings, called solar flares, were known since the nineteenth century, and similar phenomena were detected by recent observations at smaller scales. The occurrence frequency of flares is higher for events with smaller energy releases, and there is a possibility that flares significantly contribute to the formation of the hot [about a few million Kelvin (MK)] upper atmosphere of the Sun, called the solar corona (coronal heating).

Small flares are classified based on the energy released by them compared to large flares [X-class flares in the flare classification by X-ray observations with the *Geostationary Operational Environmental Satellite (GOES)*]. For example, microflares release energy that is 3–6 orders of magnitude smaller and nanoflares release energy 6–9 orders of magnitude smaller than that of large flares. There

S.-n. Ishikawa (✉)
Institute of Space and Astronautical Science, Japan Aerospace Exploration Agency, Sagamihara, Kanagawa, Japan
e-mail: s.ishikawa@solar.isas.jaxa.jp

T. Shimizu et al. (eds.), *First Ten Years of Hinode Solar On-Orbit Observatory*, Astrophysics and Space Science Library 449,
https://doi.org/10.1007/978-981-10-7742-5_8

are observations of energy release events at the energy scale of nanoflares even in the lower solar atmosphere (photosphere, chromosphere, and transition region) (Shimizu 2005). I mainly describe coronal nanoflares in this article. There are also studies suggesting the existence of events with much smaller energy releases, known as picoflares, the energy released from which is at least 9 orders of magnitude smaller (Katsukawa and Tsuneta 2001; Katsukawa 2003; Ramesh et al. 2013). Small flares ranging from microflares to picoflares have very small radiative intensities and short durations. Therefore, it was difficult to observe them, and the details of the physical processes were not well investigated before the observations made by the *Hinode* satellite.

The aims of the *Hinode* satellite for small flares are (1) to reveal detailed features and physical processes and (2) to evaluate whether the total released energy is sufficient to heat the corona. For (1), the physical processes are understood, at least partially, for large flares. Therefore, we can interpret that small flares are phenomena equivalent to large flares if we observe similar physical process signatures. A combination of detailed magnetic field observations by the solar optical telescope (SOT), plasma flow observations by the extreme ultraviolet imaging spectrometer (EIS), and coronal observations by the X-ray telescope (XRT) can validate this. For (2), the total energy was estimated by investigating the relationship between the energy of individual events and the frequency (summarized in Hannah et al. (2011), shown in Fig. 8.1). However, it is known that the total estimated energy from individual detectable events is not sufficient to heat the corona; there are studies investigating the signatures of tiny flares with no individual flare detection.

8.2 Physical Processes of Microflares and Nanoflares

In a well-accepted standard model of solar flares, flares are thought to be an energy release phenomenon due to the reconnection of magnetic field lines (magnetic reconnection) in the solar corona. A portion of the energy released by reconnection accelerates charged particles in the plasma, and these accelerated particles precipitate toward the solar surface. The accelerated particles then heat the chromospheric plasma, and the heated plasma evaporates toward the corona (chromospheric evaporation). Hard X-ray emissions were observed to be associated with many microflares in the active regions, and this suggests that particle acceleration occurs, similar to large flares (Christe et al. 2008). Based on *Hinode*/EIS observations, upflows were detected as microflares and thought to be signatures of chromospheric evaporation (Chen and Ding 2010). Therefore, particle acceleration and chromospheric evaporation are suggested, which are identical physical processes to large flares.[1]

[1]Note that it is known that hard X-ray spectra depend on the scales of flares, and the physical process remains to be solved (Christe et al. 2008).

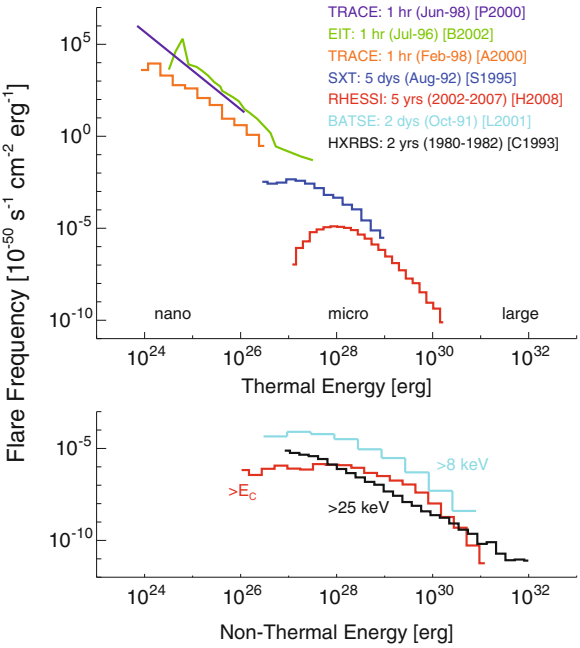

Fig. 8.1 Frequency distribution of solar flares from large flares to nanoflares (Reprinted from Hannah et al. 2011, with kind permission from Springer Science+Business Media)

One of the key questions is how the relationship forms between microflares and magnetic fields, which are candidates for the energy source. In large flares, it was reported that emergence of a magnetic field is responsible for the formation of complex magnetic structures and storing of magnetic energy, which led to a flare (Kubo et al. 2007). According to the results from the *Yohkoh* satellite, magnetic field activities were determined to be associated with about half of the microflares (Shimizu et al. 2002). In microflares observed by XRT, the SOT observed collisions of magnetic elements in about half of them (Kano et al. 2010). Chifor et al. (2008a,b) reported that the XRT and EIS observations of jet occurrences were associated with the decreasing magnetic fields observed by the SOT. X-ray jets associated with microflares were discovered by the *Yohkoh* observations and are considered to be plasma ejection phenomena caused by magnetic reconnection (Shimojo et al. 1996).

While all the observations described above were in active regions, there are observational studies of quiet regions and "coronal holes" with lower coronal plasma densities. Kamio et al. (2011) reported that the EIS and XRT observations showed that in nanoflares in quiescent regions and coronal holes, the plasma temperatures were high in the early phases, during which the plasma densities increased, and then the temperatures decreased gradually. These features match the scenario of chromospheric evaporation, and it is suggested that tiny flares occur in quiet regions and coronal holes with similar physical processes as those in the active regions. Many X-ray jets were also observed by XRT in polar coronal holes and quiet regions (Cirtain et al. 2007; Sako et al. 2013).

Conversely, it was reported that in some microflare observations, upflows were too weak to explain the events of chromospheric evaporation (Milligan 2008; Brosius 2013). In those events, there is no evidence of chromospheric evaporation, and they suggested that parts of the released energy could contribute directly to the heating of the plasma. There are many large flares that exhibit no signatures of chromospheric evaporation. Studies of these exceptions are important to better understand the conditions of the models. Still, there are currently not many reported events, and it is expected that more examples will be observed by *Hinode* and future missions.

8.3 Investigating Signatures of Unresolved Nanoflares

As already mentioned, although the total energy released by flares that are observed as brightening events, including those at the nanoflare scale, is not sufficient to heat the corona, it does not immediately dismiss the possibility of nanoflare heating. If we assume that a large amount of individually undetectable small energy releases occur, coronal heating by nanoflares could still be a possibility. There are several ways to investigate this, e.g., through the small time variations in X-rays (Testa et al. 2013; Terzo et al. 2011; Antolin et al. 2008), the coronal activities at fine spatial scales and resolving the braid components of coronal loop (Cirtain et al. 2013), and the temperature of the structures. Here, I describe the investigation of the temperature distribution.

When the corona is heated by nanoflares, simulations predict the existence of a hot plasma component above the typical coronal temperature of a few MK (Klimchuk et al. 2008). To investigate this, it is important to estimate the differential emission measure (DEM) temperature distributions to determine how much plasma exists and at what temperature. Spectroscopic observations by EIS and multi-filter observations by XRT are effective tools for estimating DEMs. Observational targets would include active regions with no obvious flares and quiescent regions to reduce the effects of individually detectable flares. Several DEM studies by *Hinode* observations suggest the existence of hot (>10 MK) plasma (Schmelz et al. 2009a; Reale et al. 2009). By using EIS observations of multiple spectral lines, DEMs of up to several megaKelvin can be estimated precisely (Winebarger et al. 2011; Warren et al. 2012). Conversely, spectral lines sensitive to temperatures above several MK are generally weak, and there are only a few detections by coordinated observations with *Hinode* and other instruments (Teriaca et al. 2012; Brosius et al. 2014). Therefore, XRT observations with thick filters were mainly used to investigate high-temperature components. However, it was reported that uncertainties remain in the XRT detector response with thicker filters even when applying the latest calibration (Narukage et al. 2014), and it was noted that large uncertainties remain in the quantitative evaluations of high-temperature components (Winebarger et al. 2012).

If hot plasma above 10 MK exists in the corona, it should emit hard X-rays with a higher energy than that of the sensitive wavelength of XRT. However, from the

hard X-ray observations by the *Reuven Ramaty High Energy Solar Spectroscopic Imager (RHESSI)* satellite, no hard X-ray imaging observation of individual regions was reported without flares (Schmelz et al. 2009b). By considering this fact, the estimated amount of hot component becomes smaller than that estimated only with *Hinode*/XRT. Note that the *RHESSI* data only represent the upper limits because of the lack of detections. Therefore, it is still not clear how much hot component exists in the corona without individual flare detection.

A hard X-ray instrument with a higher sensitivity than *RHESSI* is effective in answering this question. Recently, the technology of hard X-ray focusing optics has improved and has allowed for high-sensitivity hard X-ray observations. A sounding rocket experiment, Focusing Optics X-ray Solar Imager (FOXSI) (Krucker et al. 2014), observed an active region without obvious flare detection with a superior sensitivity with hard X-ray focusing optics, but there was no significant hard X-ray detection. This implies that the upper limit of the amount of hot component of the coronal plasma was smaller than that by *RHESSI* (Ishikawa et al. 2014) (Fig. 8.2). By considering this effect, it is still difficult to explain the coronal heating by nanoflares even when individually undetectable flares are included. The *Nuclear Spectroscopic Telescope Array (NuSTAR)* satellite with hard X-ray focusing optics and a high sensitivity comparable to FOXSI observed several active regions with no individual flare detection. So far, no significant hot component signature has been obtained (Hannah et al. 2016).

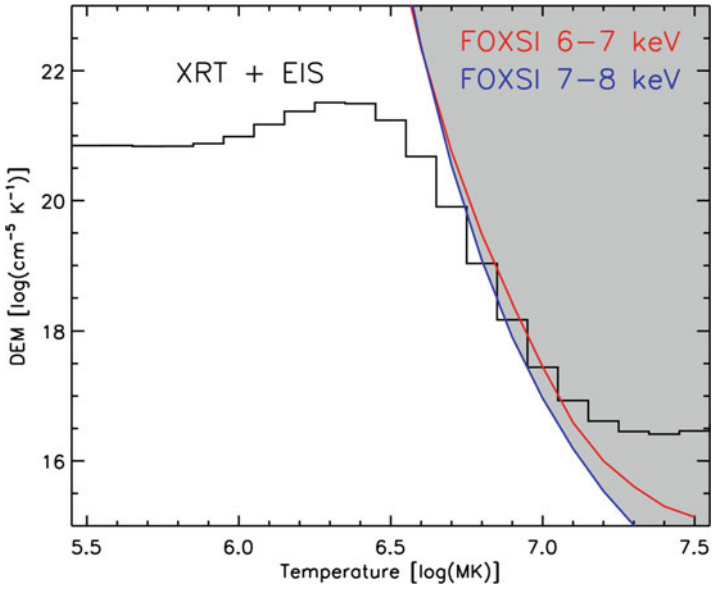

Fig. 8.2 DEM estimated by *Hinode* (Black) and upper limit by FOXSI (red and blue). Shaded area shows the forbidden area by the FOXSI observation (Reprint from Ishikawa et al. 2014 with permission from Oxford University Press)

Only a few observations of regions with no obvious flares were performed with the high-sensitivity hard X-ray instruments, and it is still not clear whether those samples are typical. Therefore, further observations with the FOXSI rocket or *NuSTAR* satellite and coordinated observations with *Hinode* are expected for the conduction of statistical studies on the hot plasma in the corona in regions with no individual flare detection. The second flight of FOXSI was successfully performed on December 2014, and the observational results were published recently (Ishikawa et al. 2017).

8.4 Summary and Future Observations

Small flares are important observational targets for *Hinode*, because the physical processes are not well known despite having a high occurrence frequency. Based on the *Hinode* observations, it can be inferred that microflares are energy release processes due to magnetic reconnection, similar to large flares, and chromospheric evaporations cause brightening events.

Investigations of signatures of individually undetectable nanoflares are performed by the temperature analysis of regions with no obvious individual flare detection by combining *Hinode*, extreme ultraviolet, soft X-ray observations, and hard X-ray observations. No significant hot component was detected so far with high-sensitivity hard X-ray observations such as the FOXSI rocket experiments. Statistical studies would be important for further investigations. To construct better models of active regions, detections and quantitative evaluations of high-temperature plasma are desired.

For both further understanding of physical processes of microflares and precise investigations of DEMs and fine spatial structures, observations with higher sensitivity and finer resolution are necessary. One of the effective methods is imaging and spectroscopic observations with a photon-counting soft X-ray telescope (Sakao et al. 2014). It enables us to evaluate coronal physical parameters quantitatively with a high temporal and spatial resolution. Progress in understanding microflares and nanoflares is expected with new instruments in the future.

References

Antolin, P., et al.: Predicting observational signatures of coronal heating by Alfvén waves and nanoflares. Astrophys. J. **688**, 669–682 (2008)

Brosius, J.W.: Rapid evolution of the solar atmosphere during the impulsive phase of a microflare observed with the extreme-ultraviolet imaging spectrometer aboard Hinode: hints of chromospheric magnetic reconnection. Astrophys. J. **777**, 135 (2013)

Brosius, J.W., et al.: Pervasive faint Fe XIX emission from a solar active region observed with EUNIS-13: evidence for nanoflare heating. Astrophys. J. **790**, 112 (2014)

Chen, F., Ding, M.D.: Evidence of explosive evaporation in a microflare observed by Hinode/EIS. Astrophys. J. **724**, 640–648 (2010)
Chifor, C., et al.: An active region jet observed with Hinode. Astron. Astrophys. **481**, L57–L60 (2008a)
Chifor, C., et al.: Magnetic flux cancellation associated with a recurring solar jet observed with Hinode, RHESSI, and STEREO/EUVI. Astron. Astrophys. **491**, 279–288 (2008b)
Christe, S., et al.: RHESSI microflare statistics. I. Flare-finding and frequency distributions. Astrophys. J. **677**, 1385–1394 (2008)
Cirtain, J.W., et al.: Evidence for Alfvén waves in solar X-ray jets. Science **318**, 1580 (2007)
Cirtain, J.W., et al.: Energy release in the solar corona from spatially resolved magnetic braids. Nature **493**, 501 (2013)
Hannah, I.G., et al.: Microflares and the statistics of X-ray flares. Space Sci. Rev. **159**, 263–300 (2011)
Hannah, I.G., et al.: The first X-ray imaging spectroscopy of quiescent solar active regions with NuSTAR. Astrophys. J. **820**, L14 (2016)
Ishikawa, S., et al.: Constraining hot plasma in a non-flaring solar active region with FOXSI hard X-ray observations. Publ. Astron. Soc. Jpn. **66**, S15 (2014)
Ishikawa, S. et al.: Detection of nanoflare-heated plasma in the solar corona by the FOXSI-2 sounding rocket. Nat. Astron. **1**, 771 (2017)
Kamio, S., et al.: Evolution of microflares associated with bright points in coronal holes and in quiet regions. Astron. Astrophys. **529**, A21 (2011)
Kano, R., et al.: Hinode observation of photospheric magnetic activities triggering X-ray microflares around a well-developed Sunspot. Astrophys. J. **720**, 1136–1145 (2010)
Katsukawa, Y.: Spatial and temporal extent of solar nanoflares and their energy range. Publ. Astron. Soc. Jpn. **55**, 1025–1031 (2003)
Katsukawa, Y., Tsuneta, S.: Small fluctuation of coronal X-ray intensity and a signature of nanoflares. Astrophys. J. **557**, 343–350 (2001)
Klimchuk, J.A., et al.: Highly efficient modeling of dynamic coronal loops. Astrophys. J. **682**, 1351–1362 (2008)
Krucker, S., et al.: First images from the focusing optics X-ray solar imager. Astrophys. J. **793**, L32 (2014)
Kubo, M., et al.: Hinode observations of a vector magnetic field change associated with a flare on 2006 December 13. Publ. Astron. Soc. Jpn. **59**, S779–S784 (2007)
Milligan, R.O.: A hot microflare observed with RHESSI and Hinode. Astrophys. J. **680**, L157 (2008)
Narukage, N., et al.: Coronal-temperature-diagnostic capability of the Hinode/X-ray telescope based on self-consistent calibration. II. Calibration with on-orbit data. Sol. Phys. **289**, 1029–1042 (2014)
Ramesh, R., et al.: Low-frequency radio observations of picoflare category energy releases in the solar atmosphere. Astrophys. J. **762**, 89 (2013)
Reale, F., et al.: Evidence of widespread hot plasma in a nonflaring coronal active region from Hinode/X-ray telescope. Astrophys. J. **698**, 756–765 (2009)
Sakao, T., et al.: The soft x-ray photon-counting telescope for solar observations. Proc. SPIE **9144**, 91443D (2014)
Sako, N., et al.: A statistical study of coronal active events in the North polar region. Astrophys. J. **775**, 22 (2013)
Schmelz, J.T., et al.: Hinode X-ray telescope detection of hot emission from quiescent active regions: a nanoflare signature? Astrophys. J. **693**, L131–L135 (2009a)
Schmelz, J.T., et al.: Some like it hot: coronal heating observations from Hinode X-ray telescope and RHESSI. Astrophys. J. **704**, 863–869 (2009b)
Shimizu, T.: 3D magnetic field configuration of small-scale reconnection events in the solar plasma atmosphere. Phys. Plasmas. **22**, 101207 (2005)

Shimizu, T., et al.: Photospheric magnetic activities responsible for soft X-ray pointlike microflares. I. Identifications of associated photospheric/chromospheric activities. Astrophys. J. **574**, 1074–1088 (2002)

Shimojo, M., et al.: Statistical study of solar X-ray jets observed with the YOHKOH soft X-ray telescope. Publ. Astron. Soc. Jpn. **48**, 123–136 (1996)

Teriaca, L., et al.: Spectroscopic observations of Fe XVIII in solar active regions. Astrophys. J. **754**, L40 (2012)

Terzo, S., et al.: Widespread nanoflare variability detected with Hinode/X-ray telescope in a solar active region. Astrophys. J. **736**, 111 (2011)

Testa, P., et al.: Observing coronal nanoflares in active region moss. Astrophys. J. **770**, L1 (2013)

Warren, H.P., et al.: A systematic survey of high-temperature emission in solar active regions. Astrophys. J. **759**, 141 (2012)

Winebarger, A., et al.: Using a differential emission measure and density measurements in an active region core to test a steady heating model. Astrophys. J. **740**, 2 (2011)

Winebarger, A., et al.: Defining the "Blind Spot" of Hinode EIS and XRT temperature measurements. Astrophys. J. **746**, L17 (2012)

Chapter 9
The Origin of the Solar Wind

Kyoung-Sun Lee, David H. Brooks, and Shinsuke Imada

Abstract The source regions of the solar wind, and its driver and acceleration mechanism, remain key topics of study in heliophysics. With its combination of high sensitivity and high spatial resolution measurements of Doppler flows, mass motions, and plasma composition, the *Hinode* satellite is uniquely equipped to investigate many of these issues. On the occasion of the tenth anniversary of the launch of *Hinode*, we here briefly review some of the scientific highlights on this subject from the mission over the last decade.

Keywords Solar wind · EUV spectroscopy · Abundances

9.1 Introduction

There is a continuous flow of charged particles from the Sun, and this is called the solar wind. It is usually classified into two types depending on the velocity: fast and slow. To understand the formation mechanism of the solar wind and its effects on Earth, the plasma properties have been investigated using in situ and remote sensing measurements. Since the ratio of plasma pressure to magnetic pressure is low in the solar wind source regions, the plasma is frozen-in to the magnetic field, and its properties do not change significantly when it propagates to Earth.

K.-S. Lee (✉)
National Astronomical Observatory of Japan, Mitaka, Tokyo, Japan
e-mail: ksun.lee@nao.ac.jp

D.H. Brooks
College of Science, George Mason University, Fairfax, VA, USA
e-mail: dhbrooks@ssd5.nrl.navy.mil

S. Imada
Institute for Space-Earth Environmental Research (ISEE), Nagoya University, Nagoya, Aichi, Japan
e-mail: shinimada@stelab.nagoya-u.ac.jp

T. Shimizu et al. (eds.), *First Ten Years of Hinode Solar On-Orbit Observatory*,
Astrophysics and Space Science Library 449,
https://doi.org/10.1007/978-981-10-7742-5_9

Parker (1958) proposed a one-dimensional isothermal and polytropic expansion model for the solar wind. The model assumes a steady and spherically symmetric solar wind. It is well known that Parker's thermally driven solar wind model, with a typical coronal temperature of 1–2 million Kelvin (MK), can produce the slow solar wind asymptotic speed of about 400 $\mathrm{km\,s^{-1}}$ but cannot explain the fast solar wind that is observed to reach 800 $\mathrm{km\,s^{-1}}$. Moreover, the cooler plasma, such as found in coronal holes, becomes more difficult to explain. Therefore, several researchers have investigated the acceleration mechanism further by, for example, including additional sources of momentum in the magnetohydrodynamics (MHD) equations, such as Alfvén waves in one- (1D) or 2.5-dimensional (2.5D) simulations, or multiple fluid simulations (Ofman and Davila 1998, 2001; Suzuki and Inutsuka 2005). For these models, identifying the solar wind source regions and measuring their plasma properties provide important initial conditions for studying the acceleration and heating processes of the solar wind plasma.

One of the most useful parameters for identifying the origin of the solar wind is the difference in elemental composition. The elemental compositions in the solar photosphere and corona are different, and the difference depends on their first ionization potential (FIP) energy. Coronal abundances show an enhancement of low FIP elements compared to the photosphere, and this is called the FIP effect. The composition of the fast solar wind is close to that of the solar photosphere, while the composition of the slow solar wind is similar to the corona (Geiss et al. 1995; von Steiger et al. 2000). From its polar orbit, Ulysses observed the solar wind from the pole to the equator using in situ measurements and found that the fast and slow solar winds come from the polar and equatorial regions, respectively. Remote spectroscopic observations of the solar atmosphere also showed that the relative abundances of the polar and equatorial regions are consistent with the observed abundances of the fast and slow solar wind (Feldman et al. 2005; Wilhelm and Bodmer 1998; Young et al. 1999).

However, due to the low sensitivity and spatial resolution, these observations only provide averaged information for the polar and equatorial regions so it was not possible to determine the specific features from which the solar wind streams. For example, polar coronal holes contain several sub-features (plumes, inter-plumes, and X-ray jets), and there are also several candidates for the origin of the slow solar wind from the equator such as active regions or streamers located at higher altitude (Fig. 9.1). After the launch of *Hinode*, multi-wavelength (X-ray to optical) and high-sensitivity spectral observations have allowed us to investigate the elemental composition of specific features with high spatial resolution. As a result, there have been several efforts to clarify the origin of the fast and slow solar wind with *Hinode* observations, especially using the Extreme Ultraviolet (EUV) Imaging Spectrometer (EIS).

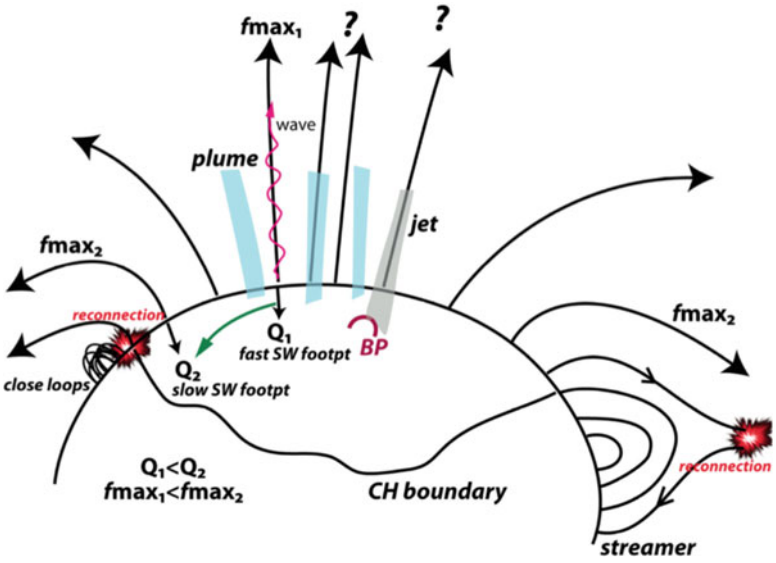

Fig. 9.1 Schematic illustration of the possible sources of the fast and slow solar wind. Arrows indicate magnetic fields. Cyan and gray color regions in the polar coronal hole represent plumes and jets, respectively (From Teriaca et al. 2012)

9.2 Fast Wind

Plumes, inter-plumes, and X-ray jets are all candidates to be the source of the fast solar wind in polar coronal holes. Indeed the magnetic field configuration in polar coronal holes and in those small-scale features are all known to be open, and it is thought that these open field lines connect to interplanetary magnetic fields and that the fast solar wind plasma is ejected along the field lines. However, how the plasma is accelerated and which structures in the polar region are the dominant sources of the fast solar wind are still open questions.

One of the most important findings from the *Hinode* X-ray Telescope (XRT) is that there are many more X-ray jets in the Sun's polar regions than was thought from previous observations. It has been suggested that these jets occur by magnetic reconnection (Shibata et al. 1992), and a fast velocity component (approx. $800\,\mathrm{km\,s^{-1}}$) was observed in X-ray jets using *Hinode*/XRT (Cirtain et al. 2007). From their observed speeds and masses, they suggested that jets can contribute to the solar wind and that reconnection accelerates the plasma into the solar wind. To confirm their possibility, the relative abundances were measured for a sample of polar X-ray jets (Lee et al. 2015). They found that the elemental composition of the jets is mostly photospheric, which is the same as the abundance of the fast solar wind (Fig. 9.2).

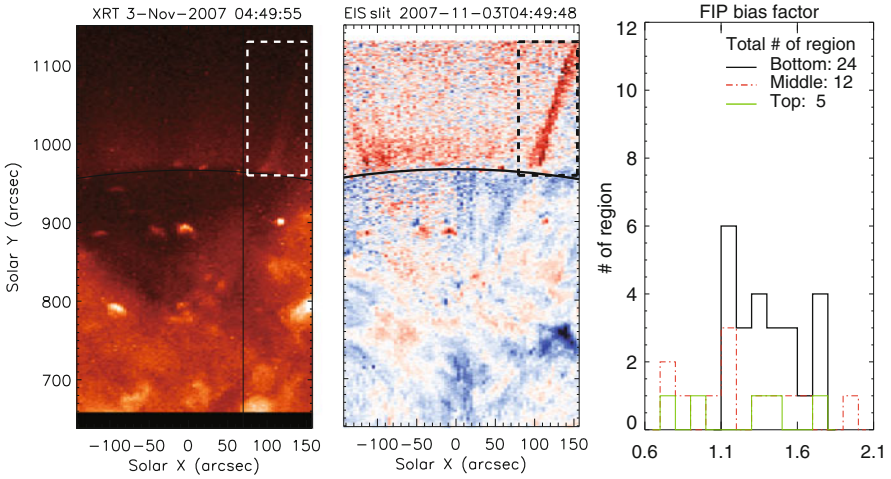

Fig. 9.2 Example of a polar X-ray jet observed by *Hinode*/XRT and EIS. Left panel: soft X-ray image. Middle panel: Doppler velocity image derived from an iron spectral line formed near 1.6 million degrees. Blue is toward the observer and red is away from the observer. The vertical line and the dashed box in both panels indicate the location of the EIS slit and the jet, respectively. Right panel: Histogram of the FIP bias factors (ratio of coronal to photospheric abundance) of the polar jets. Black, red, and green lines represent different regions of the polar jets. Most of the FIP bias factors fall in the range 0.7–1.5, which implies that the abundances of the polar jets are photospheric (fast solar wind) (Taken from Figure 1 and 3, Lee et al. 2015. Reproduced by permission of the AAS)

The abundances of plumes and inter-plume regions, which are the quite steady structures, have also been investigated by using EIS (Guennou et al. 2015). They showed that inter-plume regions have a photospheric composition, while the elemental composition of the low FIP elements in the plume is sometimes higher than in the inter-plume. They also found that the composition enhancement in the plume can be time-dependent.

These findings of photospheric abundances in polar jets, plumes, and inter-plumes are not surprising. The composition of polar coronal holes themselves also shows a photospheric composition (Brooks and Warren 2011), and it may imply that photospheric material is directly ejected along open magnetic field lines in those structures in polar regions. One interesting thing is that some X-ray jet bright points persist for a long duration (about a day) and these sometimes show a small enhancement of the elemental composition. It may be that the confinement time of the plasma is important for changing the elemental composition as previous studies have reported (Widing and Feldman 2001; Feldman and Widing 2003).

In summary, *Hinode* has discovered a possible source of the fast solar wind in X-ray jets, and new EIS measurements of elemental abundances have confirmed that these and other different structures in the polar regions, such as plumes and inter-plumes, have the correct composition to be fast wind sources.

9.3 Slow Wind

Hinode has also made many contributions to our understanding of the slow solar wind, and we will only cover a few of them briefly here. Perhaps the most exciting advance has been the discovery of high-temperature plasma outflows from dark areas at the peripheries of many active regions. These outflows were first noticed as propagating features in movies of active regions obtained by XRT (Sakao et al. 2007). Images can only show us apparent motions, but we can use EIS to accurately measure the Doppler velocities and determine whether the plasma is really upflowing or not. EIS measurements show that the motions are indeed blue-shifted, with speeds of tens of km per second (Del Zanna 2008; Harra et al. 2008; Doschek et al. 2008). EIS line profiles also show an asymmetric component (Hara et al. 2008) that reaches several hundred km per second in the outflows (Bryans et al. 2010) and increases with temperature (Brooks and Warren 2012).

An important clue as to whether the outflows are really sources of the slow solar wind comes from EIS elemental abundance measurements. As discussed, the slow solar wind can have a distinctive enhanced composition, so any source region should have an abundance signature that matches. EIS measurements do in fact confirm that the outflows have a slow wind composition, and indeed the remote observations made with EIS sometimes match the measurements made in situ near Earth by the *Advanced Composition Explorer (ACE)* observatory a few days later (Brooks and Warren 2011).

To form part of the solar wind, however, the plasma in the outflows must be able to escape into interplanetary space. It has been showed that the outflows in the active region they studied did lie on open magnetic fields inferred from a potential field extrapolation (Sakao et al. 2007). This is not always the case; however, Edwards et al. (2016) examined seven active regions and found that only one of them had an open field channel where the outflows could escape. In a well-studied case [active region (AR) 10978], the outflows appear to be completely covered by a helmet streamer, though it is possible that a multiple-step process involving magnetic reconnection can open up an alternative pathway (Culhane et al. 2014; Mandrini et al. 2014), and evidence of reconnection has been found in the form of radio noise storms near other active regions (Del Zanna et al. 2011).

Since the process of escaping from the solar atmosphere may be complex, it is important to ask whether enough plasma can flow from these regions to contribute substantially to the slow solar wind. By making a composition map of the entire disk (Fig. 9.3), Brooks et al. (2015) were able to identify enough active region outflows with the correct abundance to explain a significant fraction of the solar wind mass flux.

In summary, *Hinode* has discovered a possible new source of the slow solar wind in active region outflows, and new EIS measurements of elemental abundances have confirmed that these have the correct composition to be slow wind sources.

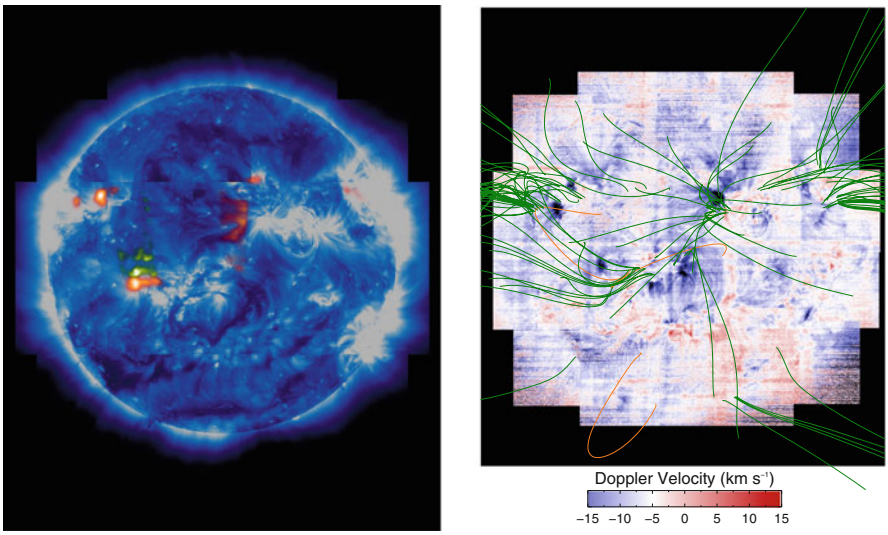

Fig. 9.3 EIS diagnostic maps of the entire disk of the Sun. Left panel: an abundance map. Brighter yellow and orange areas show where the elemental composition is enhanced. Right panel: Doppler velocity map. Blue is toward the observer and red is away from the observer. The overlaid green lines are from a magnetic field extrapolation and show where the field is open. By combining the measurements of composition and velocity with the magnetic field model, we can determine locations where plasma with a slow wind composition is outflowing on open magnetic field lines (From Brooks et al. 2015)

9.4 Future Prospects

Hinode observations have sparked significant advances in studies of the fast and slow solar wind, but ultimately there are two contradictory issues preventing further progress.

First, there is a need for high spatial resolution observations of the connection between coronal dynamics and magnetic field activity in the lower atmospheric layers such as the transition region and chromosphere. X-ray jets, for example, are thought to arise from the reconnection of emerging flux with the overlying field (but see Sterling et al. 2015); however, observing the detailed manifestation of the reconnection process at the jet footpoint requires higher spatial resolution measurements across a wider temperature range than currently possible. The same is true for detailed studies of plumes and inter-plumes and the footprints of the slow solar wind such as active region outflows. Coordinated observations between *Hinode* and *Interface Region Imaging Spectrograph (IRIS)* are currently developing this path. With high temporal resolution observations, moreover, non-equilibrium ionization may become an important effect, and further investigations are needed. In highly dynamic events related to the solar wind, such as coronal jets or reconnection processes in a low density plasma, the activity takes place on timescales shorter

than the ionization-relaxation timescale, and the plasma may not reach ionization equilibrium. In that case, composition or temperature measurements made assuming ionization equilibrium may be incorrect (Imada et al. 2011a,b; Mariska et al. 1982). So, in addition to high temporal and spatial resolution observations, time-dependent ionization calculations are needed for further progress.

Second, there is a need for improving our understanding of the connection between activity observed remotely in the lower atmosphere and the solar wind measured in situ. Structures in the corona may show the correct composition, but how do we connect those observations to measurements made in specific locations in the wind stream near Earth, or back-map those measurements to surface locations?

Two upcoming missions promise major advances in these areas. The successor to *Hinode*, Solar-C, is planned to perform high spatial resolution and high cadence observations covering the entire solar atmosphere from the photosphere, through the chromosphere and transition region, to the corona. This will compliment another mission, Solar-Orbiter (Muller et al. 2013), that will fly to within 0.3 AU and combine remote sensing observations with in situ measurements of the solar wind plasma and particles. We can expect significant breakthroughs from these missions in the coming decades.

Acknowledgements Figure 1 taken from Figure 6 in Teriaca et al. (2012). Figure 2 adapted from the original Figures 1 & 3 in Lee et al. (2015). Figure 3 adapted from the original Figures 6 and 8 in Brooks et al. (2015). Courtesy of Nature under Creative Commons Attribution 4.0 International license.

References

Brooks, D.H., Warren, H.P.: Establishing a connection between active region outflows and the solar wind: abundance measurements with EIS/Hinode. Astrophys. J. Lett. **727**, L13–L17 (2011)

Brooks, D.H., Warren, H.P.: The coronal source of extreme-ultraviolet line profile asymmetries in solar active region outflows. Astrophys. J. Lett. **760**, L5–L10 (2012)

Brooks, D.H., et al.: Full-sun observations for identifying the source of the slow solar wind. Nat. Commun. **6**, 5947 (2015). https://doi.org/10.1038/ncomms6947

Bryans, P., et al.: Multiple component outflows in an active region observed with the EUV imaging spectrometer on Hinode. Astrophys. J. **715**, 1012–1020 (2010)

Cirtain, J.W., et al.: Evidence for Alfvén waves in solar X-ray jets. Science **318**, 1580 (2007). https://doi.org/10.1126/science.1147050

Culhane, J.L., et al.: Tracking solar active region outflow plasma from its source to the near-Earth environment. Sol. Phys. **289**, 3799–3816 (2014)

Del Zanna, G.: Flows in active region loops observed by Hinode EIS. Astron. Astrophys. **481**, L49–L52 (2008)

Del Zanna, G., et al.: A single picture for solar coronal outflows and radio noise storms. Astron. Astrophys. **526**, 137–148 (2011)

Doschek, G., et al.: Flows and nonthermal velocities in solar active regions observed with the EUV imaging spectrometer on Hinode: a tracer of active region sources of heliospheric magnetic fields? Astrophys. J. **686**, 1362–1371 (2008)

Edwards, S.J., et al.: A comparison of global magnetic field skeletons and active-region upflows. Sol. Phys. **291**, 117–142 (2016)

Feldman, U., Widing, K.G.: Elemental abundances in the solar upper atmosphere derived by spectroscopic means. Space Sci. Rev. **107**, 665–720 (2003)
Feldman, U., et al.: On the sources of fast and slow solar wind. J. Geophys. Res. **110**, A07109 (2005). https://doi.org/10.1029/2004JA010918
Geiss, G., et al.: Origin of the solar wind from composition data. Space Sci. Rev. **72**, 49–60, (1995)
Guennou, C., et al.: Relative abundance measurements in plumes and interplumes. Astrophys. J. **807**, 145–158 (2015)
Hara, H., et al.: Coronal plasma motions near footpoints of active region loops revealed from spectroscopic observations with Hinode EIS. Astrophys. J. Lett. **678**, L67–L71 (2008)
Harra, L.K., et al.: Outflows at the edges of active regions: contribution to solar wind formation? Astrophys. J. Lett. **676**, L147–L150 (2008)
Imada, S., et al.: Magnetic reconnection in non-equilibrium ionization plasma. Astrophys. J. **742**, 70–80 (2011a)
Imada, S., et al.: One-dimensional modeling for temperature-dependent upflow in the dimming region observed by Hinode/EUV imaging spectrometer. Astrophys. J. **743**, 57–67 (2011b)
Lee, K.-S., et al.: Photospheric abundances of polar jets on the Sun observed by Hinode. Astrophys. J. **809**, 114–122 (2015)
Mandrini, C., et al.: Topological analysis of emerging bipole clusters producing violent solar events. Sol. Phys. **289**, 2041–2071 (2014)
Mariska, J.T., et al.: Solar transition region response to variations in the heating rate. Astrophys. J. **255**, 783–796 (1982)
Muller, D., et al.: Solar orbiter. Exploring the Sun-heliosphere connection. Sol. Phys. **285**, 25–70 (2013)
Ofman, L., Davila, J.M.: Solar wind acceleration by large-amplitude nonlinear waves: parametric study. J. Geophys. Res. **103**, 23677 (1998). https://doi.org/10.1029/98JA01996
Ofman, L., Davila, J.M.: Three-fluid 2.5-dimensional magnetohydrodynamic model of the effective temperature in coronal holes. Astrophys. J. **553**, 935–940 (2001)
Parker, E.N.: Dynamics of the interplanetary gas and magnetic fields. Astrophys. J. **128**, 664–676 (1958)
Sakao, T., et al.: Continuous plasma outflows from the edge of a solar active region as a possible source of solar wind. Science **318**, 1585 (2007). https://doi.org/10.1126/science.1147292
Shibata, K., et al.: Observations of X-ray jets with the YOHKOH soft X-ray telescope. Pub. Astron. Soc. Jpn. **44**, L173–L179 (1992)
Sterling, A.C., et al.: Small-scale filament eruptions as the driver of X-ray jets in solar coronal holes. Nature **523**, 437–440 (2015). https://doi.org/10.1038/nature14556
Suzuki, T.K., Inutsuka, S.-I.: Making the corona and the fast solar wind: a self-consistent simulation for the low-frequency Alfvén waves from the photosphere to 0.3 AU. Astrophys. J. Lett. **632**, L49–L52 (2005)
Teriaca, L., et al.: LEMUR: large European module for solar ultraviolet research. European contribution to JAXA's solar-C mission. Exp. Astron. **34**, 273–309 (2012)
von Steiger, R., et al.: Composition of quasi-stationary solar wind flows from Ulyssessolar wind ion composition spectrometer. J. Geophys. Res. **105**, 27217 (2000). https://doi.org/10.1029/1999JA000358
Widing, K.G., Feldman, U.: On the rate of abundance modifications versus time in active region plasmas. Astrophys. J. **555**, 426–434 (2001)
Wilhelm, K., Bodmer, R.: Solar EUV and UV emission line observations above a polar coronal hole. Space Sci. Rev. **85**, 371–378 (1998)
Young, P.R., et al.: Temperature and density in a polar plume – measurements from CDS/SOHO. Astron. Astrophys. **350**, 286–301 (1999)

Part III
Magnetism of Solar Atmosphere

Chapter 10
New Insights into Sunspots Through *Hinode* Observations

Masahito Kubo

Abstract Studies on sunspots have a very long history mostly supported by ground-based observations. However, the detailed evolution of sunspot magnetic field structures are revealed by *Hinode* observations of accurate photospheric magnetic fields at high spatial resolution under the seeing-free conditions. After the launch of *Hinode*, the radiative three-dimensional magnetohydrodynamic simulations successfully demonstrated sunspots. The combination of good observations and simulations results in rapid advancement in our knowledge about sunspots. Especially, fine-scale structures in sunspots are commonly understood as a manifestation of the magneto-convection.

Keywords Sunspots

10.1 Sunspot Studies Before *Hinode*

Sunspots appear as dark spots on the solar surface, and their temperature of about 4000 K is lower than their surroundings of about 6000 K. Sunspots are concentrations of strong magnetic field lines typically stronger than 1 kG. The strong magnetic fields suppress the convection and its heat transfer from the hot solar interior. Basic components of the sunspots are central dark area (umbra) and its peripheral semi-dark part (penumbra), as shown in Fig. 10.1. Observations of the sunspots have continued for more than 400 years since the era of Galileo, and tons of papers on sunspots have been published (Solanki 2003). When we observe the sunspots at low spatial resolution, they look like a simple fried egg. However, the sunspots that were observed at high spatial resolution are filled with fine-scale structures: fuzzy bright dots in the umbra, dark/bright filaments in the penumbra, and light bridges crossing the umbra.

M. Kubo (✉)
SOLAR-C Project Office, National Astronomical Observatory of Japan, Mitaka, Tokyo, Japan
e-mail: masahito.kubo@nao.ac.jp

T. Shimizu et al. (eds.), *First Ten Years of Hinode Solar On-Orbit Observatory*,
Astrophysics and Space Science Library 449,
https://doi.org/10.1007/978-981-10-7742-5_10

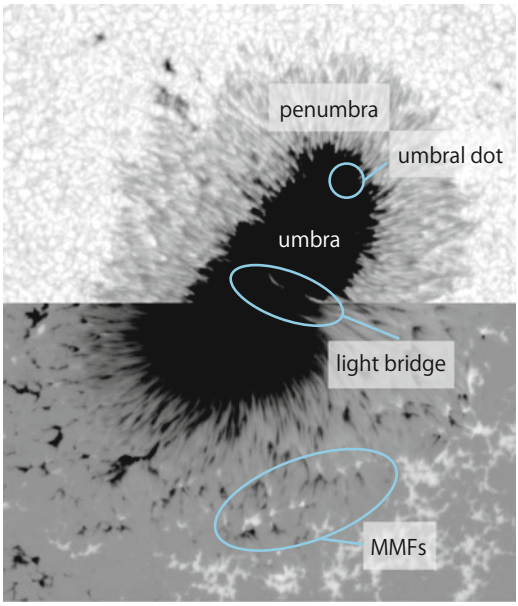

Fig. 10.1 First sunspot as observed with *Hinode*. The upper half shows the continuum intensity, and the lower half shows the line-of-sight magnetic fields. White (black) indicates positive (negative) magnetic polarity in the line-of-sight magnetic fields. The sunspot consists of an umbra with umbral dots, a penumbra, and a light bridge. Moving magnetic features (MMFs) are observed around the sunspot

From the latter half of the 1990s, a technology of an adaptive optics in solar observations was developed, and then fine-scale magnetic field structures were more clearly observed in the sunspots. The studies on the formation process of such fine-scale structures became active, and, in particular, the formation process of the fine-scale structures in the penumbra was a rather hot topic. In the penumbra, radial dark and bright filaments are alternatively located, and the inclination angle of magnetic fields in the photosphere varies at similar spatial scale. Evershed flows are observed as radial outward flows with speed of a few $\mathrm{km\,s^{-1}}$ along nearly horizontal magnetic fields in the penumbra. The flux tube embedded model (Solanki and Montavon 1993), in which the rising horizontal magnetic flux tubes embedded in the relatively vertical magnetic fields, was widely supported as one of scenarios to explain these observation results. Evershed flows were derived by hot gas rising along the horizontal flux tube (Schlichenmaier et al. 1998). However, this model was not able to explain the brightness of the penumbra because the heat input only along the horizontal thin flux tubes is insufficient. Another interesting scenario called the gappy-penumbral model (Scharmer and Spruit 2006) was proposed just before the launch of *Hinode*. The penumbral bright filaments are formed by protrusions of non-magnetized convecting hot gas in the gap between relatively vertical magnetic field lines in the penumbra. In the gap region, magnetic field lines have a cusp shape due to the protrusions of the hot gas. The magnetic fields are more inclined around the top of the cusp than their surroundings. In this model, horizontal magnetic field is not necessary to explain observed fluctuations of magnetic field inclination. Even with the development of the adaptive optics, it was still difficult to obtain the temporal evolution of accurate magnetic fields for the fine-scale structures with

ground-based telescopes at that time. It was expected to terminate chaotic sunspot studies by means of accurate magnetic field observations under the seeing-free conditions with the Solar Optical Telescope (SOT) of *Hinode*.

Hereafter, I briefly introduce a part of discoveries by *Hinode* on formation process of the fine-scale structures in the sunspots (Sect. 10.2), the sunspot formation (Sect. 10.3), and the sunspot decay (Sect. 10.4). Please see the reviews Borrero and Ichimoto (2011), Rempel and Schlichenmaier (2011), and Sakurai et al. (2018) to understand recent sunspot studies in more detail.

10.2 Sunspot Fine-Scale Structures

Evidence of convective motions along the bright filaments in the penumbra was obtained from the intensity images of the first sunspot observed by SOT (Ichimoto et al. 2007a). Inclined dark stripes along the bright filaments like a Japanese sacred straw festoon ("Shimenawa") are discovered in the space-time plot of bright filaments in the penumbra, as shown in Fig. 10.2. The direction of such dark stripes depends on the position angle of sunspot. This means that the inclined dark stripe is not an actual twist or turn of the bright filament. If the rising hot gas moves and cools down along the axis of the bright filament, such inclined dark stripes are not observed. However, if the convective cells are arranged along the filament axis, cooled plasma slightly veers away from the axis due to the lateral convective motions, and then the inclined dark stripes should be formed along the bright

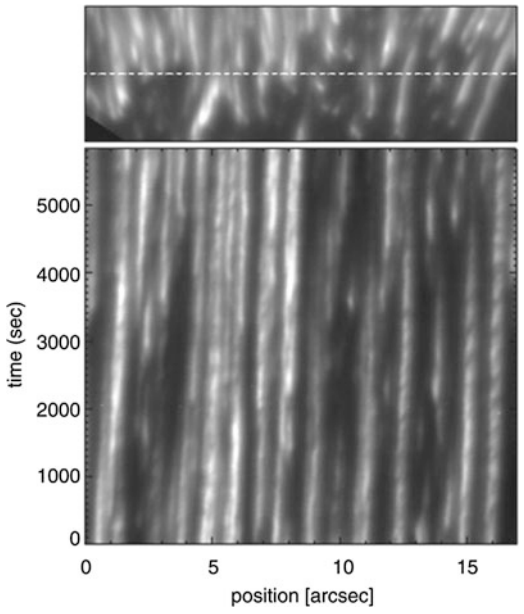

Fig. 10.2 Inclined dark stripes along bright filaments in the penumbra. The top panel is a snapshot of penumbral image, and the bottom panel shows the space-time plot along the dashed line in the top panel (From Ichimoto et al. 2007a (Fig. 2). Reprinted with permission from AAAS)

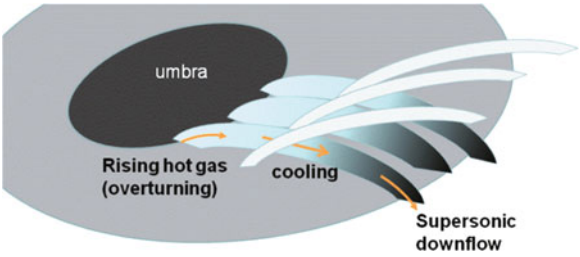

Fig. 10.3 Schematic illustrations for fine-scale magnetic field structures and Evershed flows in the penumbra (Reprinted from Borrero and Ichimoto 2011 (Fig. 35) by permission of Springer)

filaments. On the other hand, although the magnetic fields in the bright filaments are weaker than their surroundings, no evidence of the field-free gaps is obtained (Jurc et al. 2007; Borrero and Solanki 2008). Note that the existence of the field-free gaps or weak-field regions (weaker than 500 G) is still under discussions (Borrero et al. 2016). Based on the initial results of *Hinode*, a kind of a hybrid model combining the two models is rapidly supported: researchers added the convective cells into the horizontal flux tubes in the flux tube embedded model and added horizontal magnetic fields into the field-free gaps in the gappy-penumbral model. In addition, it is well confirmed that the Evershed flow starts at the leading edge of inwardly migrating bright points (penumbral grains) and turns to nearly a horizontal flow preferentially in the dark lanes of the penumbra (Ichimoto et al. 2007b). The upward and downward motions are observed at the start and end points of the Evershed flow, respectively. These results suggest that the hot gas rising from the solar interior in the inner penumbra cools down during its travel along the horizontal magnetic fields, and then the cooled gas returns into the interior in the outer penumbra (Fig. 10.3).

In the period around the launch of *Hinode*, researchers tried to demonstrate sunspots by use of 3D radiative magnetohydrodynamic (MHD) simulations. The targets of the 3D radiative MHD simulations so far were mainly magneto-convections in the quiet Sun. It was said that the calculations of the sunspots were difficult because they were unstable, large in size, and had strong magnetic field lines rooted in the deep convection zone. However, the dynamic behaviors of a large sunspot were shown by the numerical simulation (e.g., Rempel et al. 2009) (Fig. 10.4). The simulated sunspot is quite surprising to us, and we may feel that the simulated sunspot looks more advanced than the sunspot revealed by *Hinode* observations. Even in the strong magnetic field area as the sunspots, convective motions are not completely suppressed. If we focus on one convection cell, the magnetic fields are weaker in the vicinity of up-flowing regions, and more vertical strong magnetic fields are located along the outer boundary of the convection cell with the strong downflows. This is of interest because this dependence is commonly seen in the quiet Sun. The interaction between the convection and the magnetic fields with different environments and/or different physical parameters produces a large variety of the fine-scale structures in the sunspots (Katsukawa et al. 2007; Watanabe et al. 2009). Evershed flow along the horizontal magnetic fields in the penumbra is also successfully demonstrated in the simulated sunspots. Evershed flows can be explained as a result of anisotropic magneto-convection in the inclined magnetic

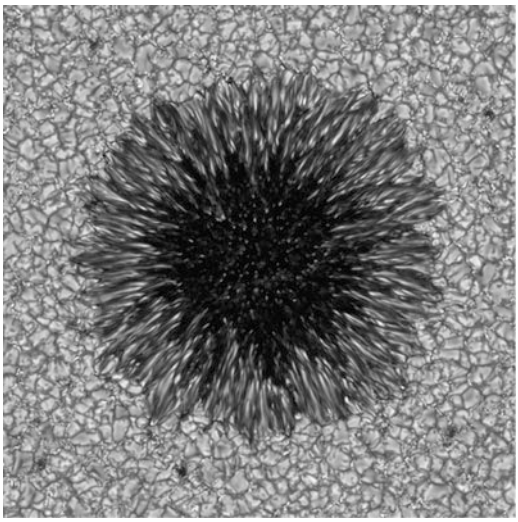

Fig. 10.4 Sunspot reproduced by 3D radiative MHD simulation (Reprinted from Rempel 2011 (Fig. 1) by permission of AAS)

field lines, and they are mainly derived through the horizontal component of the Lorentz force along the penumbral filament. Due to the synergy between the *Hinode* observations and the latest numerical simulations, we have an "almost" unified picture of fine-scale structures in the sunspots.

The convective upward and downward motions are clearly observed in the photospheric Dopplergrams of the quiet Sun. In the sunspots, the convective motions are not yet so clear from the Dopplergrams. The upward motions are commonly observed in bright structures in the sunspots, but the downward motions are vague. There are some reports on the downward convective motions in the sunspots (Ortiz 2010; Tiwari et al. 2013; Lagg et al. 2014), but not in the simple Dopplergram (bisector analysis of an absorption line or Dopplergrams with deconvolution assuming the point spread function). The reason why the downward convective motions are not so clearly observed in the comparison with the upward motions may be that the downward flows are very fine-scaled and are limited to the lower layer near the solar surface. We expect that the convective downward motions in the fine-scale structures of the sunspots are more clearly and more commonly detected in the Dopplergrams at ultrahigh spatial resolution by future ground-based telescope with a 4 m aperture (The Daniel K. Inouye Solar Telescope).

10.3 Sunspot Formation

The magnetic field lines in the sunspots originally emerge from the inside of the Sun. The magnetic field lines continuously emerge into the photosphere and then merge into each other. As a result, a small emerging magnetic bipole evolves to large magnetic elements with umbra and penumbra (i.e., sunspots). We have a rapid

progress on our understanding of the formation process of the fine-scale structures within the sunspots as mentioned in Sect. 10.2, but the formation process of the sunspots themselves, especially penumbra, are not yet well understood. This is due to the fact that detailed observations of growing sunspots are difficult. For understanding of the formation process of sunspots, three capabilities are necessary for an instrument: (1) spatial resolution to clearly observe magneto-convections that are essential for the formation of the fine-scale structures within the sunspots, (2) wide field-of-view to cover the entirety of the growing sunspots, and (3) continuous observations longer than several hours to trace the evolution from the small magnetic elements to the sunspots. We believe that SOT is still a unique instrument with these three capabilities. However, since a prediction of a birthplace of the sunspots is impossible now, SOT cannot yet perfectly capture the evolution of the sunspots from nothing in the quiet Sun.

On the other hand, interesting results on the formation of the penumbra have been obtained with SOT from a slightly different viewpoint. From the comparison of a time series of intensity images in the photosphere and chromosphere, it is found that semi-dark features appear in the chromosphere in an annular zone width 3–5 arcsec surrounding the umbra before the penumbra forms there in the photosphere (Fig. 10.5) (Shimizu et al. 2012). The follow-up observations with the ground-based telescope reveal downflows in the chromosphere in the regions with the precursor

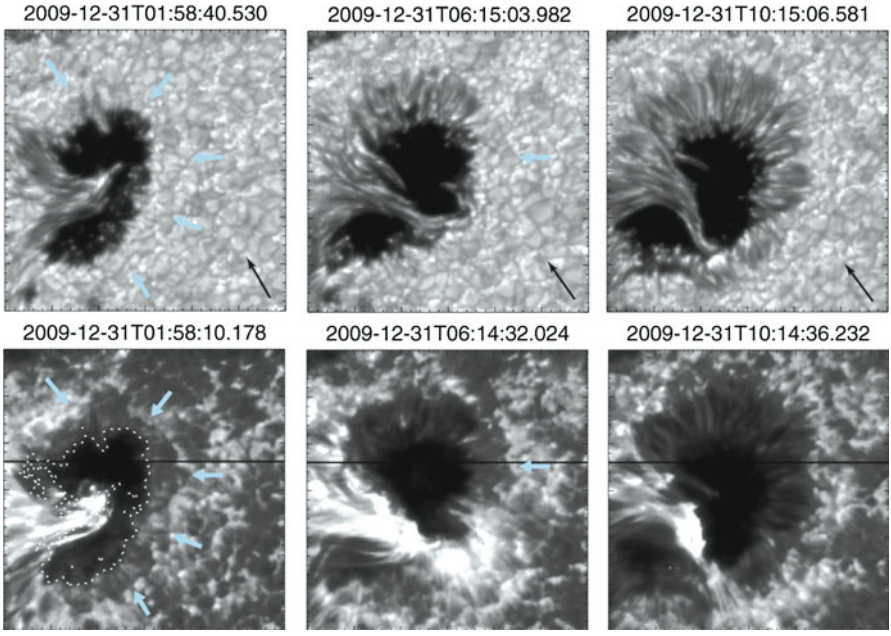

Fig. 10.5 Precursor of penumbral formation. The upper and lower panels show evolution of intensity in the photosphere and the chromosphere, respectively. In the regions as pointed by the blue arrows, dark structures appear in the chromosphere before the penumbra formation in the photosphere (Reprinted from Shimizu et al. 2012 (Fig. 1) by permission of AAS)

of the penumbral formation (Romano et al. 2013). Various possible processes have been proposed to explain the formation of the penumbral magnetic fields, and they roughly can be separated into two groups: (1) penumbral magnetic fields forming from the vertical magnetic fields in the umbra and (2) penumbral fields emerging from below the photosphere. The precursor of the penumbral formation with the downward motions in the chromosphere supports the former scenario.

The results with SOT tell us that measurements of the temporal variations of intensity, velocity, and magnetic field during the formation of the sunspot in the chromosphere in addition to the photosphere are necessary for understanding of the sunspot formation. It is one of important open questions for SOLAR-C (Chap. 21). The precursors of emerging flux regions are beginning to be obtained with the helioseismology (Ilonidis et al. 2011) or Doppler measurements in the photosphere (Toriumi et al. 2014). We hope that candidates for a birthplace of the sunspots will be predictable in the SOLAR-C era.

10.4 Sunspot Decay

Large mature sunspots are usually surrounded by a moat region whose width is comparable to the typical size of supergranular cells. The moat region was originally detected as the site of a radial outward flow called the moat flow. Many small magnetic features, called moving magnetic features (MMFs), are generally observed in the moat region. In most of the cases, the motion of MMFs is almost radial and is directed away from the sunspots. It was assumed that MMFs play an important role in the transportation of the sunspot magnetic flux, but there was no definite evidence. MMFs can be roughly classified into two types: bipolar MMFs and unipolar (single) MMFs. Most of studies on MMFs focus on the bipolar MMFs, although they basically do not contribute to the transportation of the sunspot magnetic flux, because the net flux carried by bipolar MMFs must be zero. SOT observations reveal that convective motions in the outer penumbra are related with the flux removal from the sunspot (Kubo et al. 2008a). The granular structures appear one after another in the outer penumbra, whereas unipolar MMFs are separated from penumbral "spines" (vertical component of interlaced penumbral magnetic fields), as shown in Fig. 10.6. We also obtain the clear evidence that bipolar MMFs correspond to the intersections of the solar surface with serpentine horizontal fields extending from the penumbra. It is confirmed that Evershed flows often produce bipolar MMFs around the outer boundary of the penumbra.

A time series of vector magnetic fields with SOT allow us to estimate the flux budget of a small sunspot (Kubo et al. 2008b). The amount of magnetic flux transported to the outer boundary of the moat region is comparable to the amount of magnetic flux that decreases in the sunspot. The flux loss rates of magnetic elements with opposite polarities balance each other around the outer boundary of the moat region. These results suggest that most of the magnetic flux in the sunspot is transported to the outer boundary of the moat region as MMFs and then removed from the photosphere by magnetic flux cancellation around the outer boundary of

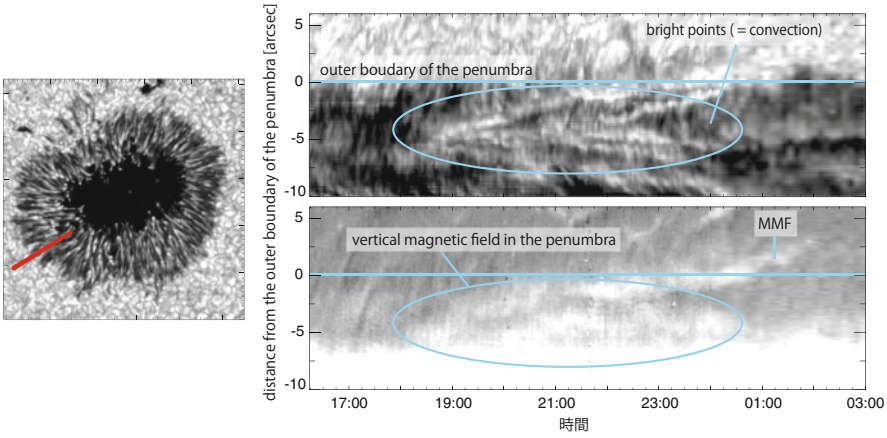

Fig. 10.6 The left panel is a snapshot of sunspot image. The right panels are space-time plots along the red solid line in the left panel for the intensity (top) and line-of-sight magnetogram (bottom)

the moat region. We believe that SOT observations give us the answers to most of questions about the sunspot decay raised from the ground-based observations, including in the author's PhD thesis, before *Hinode*. Certainly, we need to compare these results with the simulated sunspot in more details (Rempel and Cheung 2014) and also need statistical studies on the flux budget of sunspots for better understanding the sunspot decay.

One of the important advantages in SOT observations is that we can trace an accurate change of magnetic flux without any effects of atmospheric seeing. The studies on the magnetic flux budget maximize the advantage of SOT capabilities as well as fantastic movies with SOT at high spatial resolutions.

10.5 Future Works

From the viewpoint of understanding the sunspots themselves, it is necessary to investigate the three-dimensional magnetic field structures and convection in the sunspots. Especially, the magneto-convection in the convection zone is important because the sunspot magnetic fields originate from the convection zone and fine-scale structures in the sunspots are a manifestation of the subsurface magneto-convection. However, it is impossible to directly observe the interior of the Sun. The synergy between helioseismology and numerical simulations is the only way to investigate the magneto-convection in the convection zone. The local helioseismology in the sunspots is still under debate (Chap. 17) and further improvement is desired. Regarding the numerical simulation, we need to demonstrate the series of physical processes from amplification of magnetic fields due to dynamo process

inside the Sun to the formation of the sunspots on the solar surface. In addition, as mentioned in Sect. 10.3, measurements of magnetic fields and velocity fields in the chromosphere are also important. This is not limited to the formation process of sunspots. One of the important discoveries by *Hinode* is that various jet phenomena occur in the chromosphere in the sunspots (Chap. 18). It is relatively easy to observe the chromospheric magnetic fields in the sunspots in comparison with other areas with weaker magnetic fields. The sunspot is most probably the best place to investigate the evolution of magnetic fields related to magnetic reconnection that is considered to be the cause of the chromospheric jets.

The number of sunspots observed on the solar surface is used as an indicator of solar activity cycles. The process of a prolonged solar minimum like the Maunder Minimum in which the number of sunspots was very small over decades and the process to return to the normal solar activity cycles are long-standing questions in the stellar physics. It is believed that a global meridional circulation of magnetic flux is the key to understanding the solar cycle. The poleward motions of magnetic flux from the active region belt where sunspots likely appear are confirmed by long-term observations. When a sunspot appears on the solar surface, a huge amount of magnetic fluxes are apparently scattered from the sunspot to its surroundings, but the most of them disappear due to the magnetic flux cancellation before they reach the surrounding quiet region (Kubo et al. 2008b). It would be important to investigate how much sunspot magnetic flux really contribute to the solar cycle variations. In order to investigate the long-term variations of magnetic flux and/or irradiance in the quiet Sun, SOT monitors the areas along the central meridian of the Sun once a month (HOP79). There is a magnetic flux component with solar cycle variations even in the quiet Sun (Lites et al. 2014), and we need to know the proportion of the sunspot origin to this component. Now we have one cycle (11 years) variation of vector magnetic fields in the photosphere, and it will open a new research on the solar cycle. We hope that *Hinode* will give us excellent data sets of vector magnetic fields for the longest possible time.

Acknowledgements The rapid progress in our understanding of sunspots after the launch of *Hinode* proves that SOT provides us excellent data. We really appreciate all people who are involved in the development and operation of SOT.

References

Borrero, J.M., Ichimoto, K.: Magnetic structure of sunspots. Living Rev. Sol. Phys. **8**, 4 (2011). https://doi.org/10.12942/lrsp-2011-4

Borrero, J.M., Solanki, S.K.: Are there field-free gaps near $\tau = 1$ in Sunspot penumbrae? Astrophys. J. **687**, 668–677 (2008). https://doi.org/10.1086/591220

Borrero, J.M., Asensio Ramos, A., Collados, M., et al.: Deep probing of the photospheric Sunspot penumbra: no evidence of field-free gaps. A&A **596**, A2 (2016). https://doi.org/10.1051/0004-6361/201628313

Ichimoto, K., Suematsu, Y., Tsuneta, S., et al.: Twisting motions of Sunspot penumbral filaments. Science **318**, 1597 (2007a). https://doi.org/10.1126/science.1146337

Ichimoto, K., Shine, R.A., Lites, B., et al.: Fine-scale structures of the evershed effect observed by the solar optical telescope aboard Hinode. PASJ **59**, S593 (2007b). https://doi.org/10.1093/pasj/59.sp3.S593
Ilonidis, S., Zhao, J., Kosovichev, A.: Detection of emerging Sunspot regions in the solar interior. Science **333**, 993 (2011). https://doi.org/10.1126/science.1206253
Jurcák, J., Bellot Rubio, L., Ichimoto, K., et al.: The analysis of penumbral fine structure using an advanced inversion technique. PASJ **59**, S601 (2007). https://doi.org/10.1093/pasj/59.sp3.S601
Katsukawa, Y., Yokoyama, T., Berger, T.E., et al.: Formation process of a light bridge revealed with the Hinode solar optical telescope. PASJ **59**, S577 (2007). https://doi.org/10.1093/pasj/59.sp3.S577
Kubo, M., Lites, B.W., Ichimoto, K., et al.: Disintegration of magnetic flux in decaying sunspots as observed with the Hinode SOT. Astrophys. J. **681**, 1677–1687 (2008a). https://doi.org/10.1086/588040
Kubo, M., Lites, B.W., Shimizu, T., Ichimoto, K.: Magnetic flux loss and flux transport in a decaying active region. Astrophys. J. **686**, 1447–1453 (2008b). https://doi.org/10.1086/592064
Lagg, A., Solanki, S.K., van Noort, M., Danilovic, S.: Vigorous convection in a Sunspot granular light bridge. A&A **568**, A60 (2014). https://doi.org/10.1051/0004-6361/201424071
Lites, B.W., Centeno, R., McIntosh, S.W.: The solar cycle dependence of the weak internetwork flux. PASJ **66**, S4 (2014). https://doi.org/10.1093/pasj/psu082
Ortiz, A., Bellot Rubio, L.R., Rouppe van der Voort, L.: Downflows in Sunspot umbral dots. Astrophys. J. **713**, 1282 (2010). https://doi.org/10.1088/0004-637X/713/2/1282
Rempel, M.: Penumbral fine structure and driving mechanisms of large-scale flows in simulated sunspots. Astrophys. J. **729**, 5 (2011). https://doi.org/10.1088/0004-637X/729/1/5
Rempel, M., Cheung, M.C.M.: Numerical simulations of active region scale flux emergence: from spot formation to decay. Astrophys. J. **785**, 90 (2014). https://doi.org/10.1088/0004-637X/785/2/90
Rempel, M., Schlichenmaier, R.: Sunspot modeling: from simplified models to radiative MHD simulations. Living Rev. Sol. Phys. **8**, 3 (2011). https://doi.org/10.12942/lrsp-2011-3
Rempel, M., Schüssler, M., Cameron, R.H., Knölker, M.: Penumbral structure and outflows in simulated sunspots. Science **325**, 171 (2009). https://doi.org/10.1126/science.1173798
Romano, P., Frasca, D., Guglielmino, S.L., et al.: Velocity and magnetic field distribution in a forming penumbra. Astrophys. J. **771**, L3 (2013). https://doi.org/10.1088/2041-8205/771/1/L3
Sakurai, T., et al.: PASJ (Submitted) (2018)
Scharmer, G.B., Spruit, H.C.: Magnetostatic penumbra models with field-free gaps. A&A **460**, 605(2006). https://doi.org/10.1051/0004-6361:20066019
Schlichenmaier, R., Jahn, K., Schmidt, H.U.: Magnetic flux tubes evolving in sunspots. A model for the penumbral fine structure and the Evershed flow. A&A **337**, 897 (1998)
Shimizu, T., Ichimoto, K., Suematsu, Y.: Precursor of Sunspot penumbral formation discovered with Hinode solar optical telescope observations. Astrophys. J. **747**, L18 (2012). https://doi.org/10.1088/2041-8205/747/2/L18
Solanki, S.K.: Sunspots: an overview. A&ARv **11**, 153 (2003). https://doi.org/10.1007/s00159-003-0018-4
Solanki, S.K., Montavon, C.A.P.: Uncombed fields as the source of the broad-band circular polarization of sunspots. A&A **275**, 283 (1993)
Tiwari, S.K., van Noort, M., Lagg, A., Solanki, S.K.: Structure of Sunspot penumbral filaments: a remarkable uniformity of properties. A&A **557**, A25 (2013). https://doi.org/10.1051/0004-6361/201321391
Toriumi, S., Hayashi, K., Yokoyama, T.: Statistical analysis of the horizontal divergent flow in emerging solar active regions. Astrophys. J. **794**, 19 (2014). https://doi.org/10.1088/0004-637X/794/1/19
Watanabe, H., Kitai, R., Ichimoto, K., Katsukawa, Y.: Magnetic structure of umbral dots observed with the Hinode solar optical telescope. PASJ **61**, 193 (2009). https://doi.org/10.1093/pasj/61.2.193

Chapter 11
Three-Dimensional Coronal Magnetic Field Based on the Photospheric Magnetic Field by *Hinode*/SP Observation

Satoshi Inoue

Abstract Solar active phenomena observed in the solar corona are widely thought to be driven by the release of free magnetic energy accumulated in the coronal magnetic field. In order to understand these phenomena, we need to observe the three-dimensional (3D) coronal magnetic field. However, state-of-the-art instruments for solar observation can be used only for the photospheric magnetic field, as the 3D coronal magnetic field cannot be measured directly. Therefore, we need to numerically extrapolate the magnetic field above the photosphere as a boundary value problem based on the observed photospheric magnetic field. *Hinode* can provide the photospheric magnetic fields from space with unprecedented accuracy, which enables us to extrapolate the 3D magnetic field with the best possible accuracy. We report the several achievements based on the 3D extrapolated magnetic field.

Keywords Sun: magnetic field · Sun: corona · Sun: flares

11.1 Introduction

Solar active phenomena, particularly solar flares and coronal mass ejections (CMEs), are the biggest explosions in the solar system and are thought to be release phenomena of the free magnetic energy accumulated in the solar coronal magnetic field (Priest and Forbes 2002; Shibata and Magara 2011). Although knowledge of the 3D magnetic structure is required to understand the onset and dynamics of these solar explosive phenomena, observations are limited to measurements of the magnetic field at the photospheric level.

Except for the period during which solar flares occur, the coronal magnetic field can be assumed to show a temporal evolution on a time scale much longer than

S. Inoue (✉)
Institute for Space-Earth Environmental Research, Nagoya University, Nagoya, Japan
e-mail: inosato@nagoya-u.jp

T. Shimizu et al. (eds.), *First Ten Years of Hinode Solar On-Orbit Observatory*,
Astrophysics and Space Science Library 449,
https://doi.org/10.1007/978-981-10-7742-5_11

the Alfven time scale defined in the corona. Therefore, in order to determine the magnetic configuration before a flare, magnetohydrodynamic (MHD) equilibrium would be a suitable approximation for expressing the coronal magnetic field, as follows:

$$\mathbf{J} \times \mathbf{B} - \nabla P + \rho \mathbf{g} = 0, \tag{11.1}$$

$$\mathbf{J} = \nabla \times \mathbf{B}, \tag{11.2}$$

and

$$\nabla \cdot \mathbf{B} = 0, \tag{11.3}$$

where $\mathbf{B}$, $\mathbf{J}$, P, ρ, and $\mathbf{g}$ represent the magnetic field, current density, plasma pressure, plasma density, and gravity, respectively. However, as the low β $[= P/(B^2/2\mu)]$ condition (Gary 2001), where β is defined as the ratio of the gas pressure (P) to the magnetic pressure ($B^2/2\mu$, where μ is magnetic permeability), is well satisfied for the solar corona, the gas pressure and gravity terms can be neglected in the equilibrium state expressed in Eq. (11.1). Consequently, the balance of forces is maintained by the Lorentz force itself, i.e., the magnetic pressure and magnetic tension sustain the equilibrium. We call this simplified equilibrium state the force-free field. Under this approximation, the coronal magnetic field can simply be described by

$$\mathbf{J} \times \mathbf{B} = 0 \tag{11.4}$$

and the solenoidal condition (Eq. (11.3)). The force-free equation can be written in the following alternative form:

$$\nabla \times \mathbf{B} = \alpha(r)\mathbf{B}, \tag{11.5}$$

where $\alpha(r)$ corresponds to a coefficient but is typically a function of the space. This equation implies that α takes a constant value along each field line. Although the equation is simplified with respect to the original equilibrium state equation, it is a nonlinear equation. Therefore, it is difficult to obtain an analytical solution of Eq. (11.4), and hence either a further approximation or a numerical approach is required.

The most simple assumption for the force-free field is a potential field state for which it is assumed that the current density vanishes everywhere, i.e.,

$$\nabla \times \mathbf{B} = 0, \tag{11.6}$$

where the coefficient $\alpha(r)$ defined in Eq. (11.5) corresponds to zero. Although the potential field can be uniquely determined from only the normal component of the photospheric magnetic field (e.g., Sakurai 1989), it is the lowest energy state, i.e.,

there is no free energy to produce the solar flare, and therefore it cannot serve as a suitable model for the solar active region. In other words, the observed horizontal fields that deviate from the potential field are important for the accumulation of the free magnetic energy in the solar corona. Another approximation is the linear force-free field (LFFF) for which the coefficient α is constant everywhere. In that case, the Eqs. (11.4) and (11.5) become linear which enables us to seek their solution analytically. On the other hand, in general, observations support a nonconstant α derived from the photospheric magnetic field (e.g., Régnier et al. 2002), such that LFFF is not a suitable model either. In view of the above, we depend on the numerical approach to directly explore the solution of Eq. (11.4) without any approximations. We call this solution the nonlinear force-free field (NLFFF).

11.2 Nonlinear Force-Free Field Extrapolation

Solar observations can provide the three components of the magnetic field on the photosphere, and so we might try to obtain the 3D magnetic field solution from Eq. (11.4) as a boundary value problem. This means that the force-free solution is required in the solar corona, satisfying the photospheric magnetic field at the solar surface. The standard procedure is as follows: the potential field is first reconstructed from only the normal component of the photospheric magnetic field, for which a unique solution is mathematically guaranteed. Next, on the solar surface, the horizontal components derived from the potential field are changed to the observed ones, while the region above, an iteration process is executed until the solution converges to the force-free state. However, with regard to the iteration method, several such methods have been proposed up to now (e.g., Wiegelmann and Sakurai 2012), and we note that uniqueness is not guaranteed.

Schrijver et al. (2006) demonstrated the benchmark test of the NLFFF extrapolation methods using the semi-analytical force-free solution obtained from Low and Lou (1990) (hereafter, the LL solution). They measured the accuracy of the solution reconstructed only from the boundary conditions by using several proposed extrapolation methods. Consequently, the accuracy achieved was strongly dependent on the extrapolation methods. Since then, however, the methods used have been improved and polished. Recently, Inoue et al. (2014a) demonstrated the NLFFF extrapolation on the LL solution by using the MHD relaxation method. We first reconstructed the potential field from only the normal components of the magnetic fields at each boundary, and then the horizontal components of the potential field at each boundary were changed to the exact solution given by the LL solution. During this procedure the coronal magnetic field, initially reconstructed as the potential field, is according to the MHD evolution, described as

$$\rho = |\mathbf{B}|, \tag{11.7}$$

$$\frac{\partial \mathbf{v}}{\partial t} = -(\mathbf{v}\cdot\nabla)\mathbf{v} + \frac{1}{\rho}\mathbf{J}\times\mathbf{B} + \nu\nabla^2\mathbf{v}, \tag{11.8}$$

$$\frac{\partial \mathbf{B}}{\partial t} = \nabla\times(\mathbf{v}\times\mathbf{B} - \eta\mathbf{J}) - \nabla\phi, \tag{11.9}$$

$$\mathbf{J} = \nabla\times\mathbf{B}, \tag{11.10}$$

$$\frac{\partial \phi}{\partial t} + c_h^2\nabla\cdot\mathbf{B} = -\frac{c_h^2}{c_p^2}\phi, \tag{11.11}$$

where ϕ is a convenient potential. ν and η correspond to the viscosity and resistivity, respectively, while c_h and c_p are the coefficients controlling Eq. (11.11). The pseudo-density ρ is assumed to be proportional to $|\mathbf{B}|$ such that the Alfven speed undergoes the relaxation while traveling in space. The scalar ϕ was introduced in Dedner et al. (2002) to minimize any deviations from $\nabla\cdot\mathbf{B} = 0$. The detailed analysis is described in Inoue et al. (2014a) and Inoue (2016). The results are shown in Fig. 11.1. Figure 11.1a,b show the LL solution obtained from the semi-analytical approach and the NLFFF solution derived from the boundary conditions, respectively. We can see that the two solutions are apparently quite similar, which supports the reliability of our extrapolation method and numerical code.

On the other hand, the situation is very different if we apply the NLFFF extrapolation to the actual observed photospheric magnetic field. We first take notice of the fact that the photospheric magnetic field cannot satisfy the perfect force-free condition (Metcalf et al. 1995) because the low β approximation is broken at the photosphere. Even in this situation, iteration of the NLFFF extrapolation brings the magnetic field toward the force-free state in the inner region. Consequently, a strong discontinuity appears between the boundary and inner area of the numerical box. This discontinuity would reduce the accuracy of the solenoidal condition as well as that of the force-free condition. In order to relax this discontinuity, Wiegelmann et al. (2006) proposed a method for applying a prescription to the observed photospheric magnetic field according to which the observed transverse fields are modified within the limits of the measurement errors so as to approach the force-free state.

11.3 NLFFF Extrapolation Based on the Observed Magnetic Field

Hinode (Kosugi et al. 2007) was launched in September 2006 and has observed photospheric magnetic fields from space, which enables us to measure them with unprecedented accuracy, and consequently unprecedented accuracy can also be achieved for the NLFFF extrapolation. Soon after the launch, on December 13, a

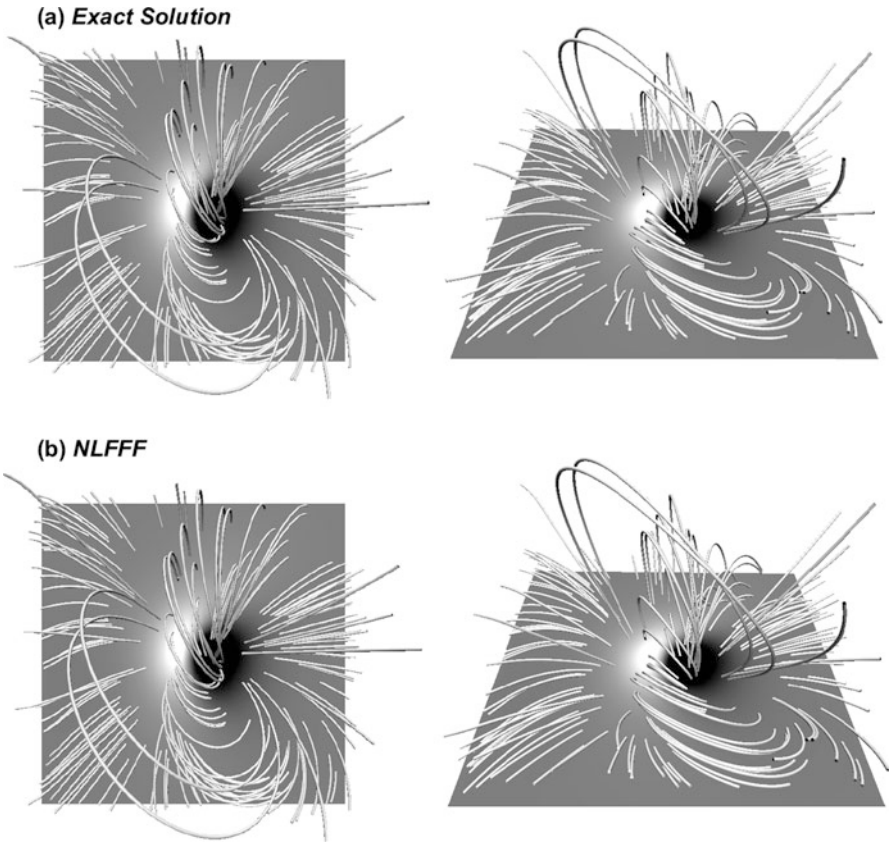

Fig. 11.1 (**a**) The field lines structure of the LL solution which is obtained from the semi-analytical approach. The B_z distribution is plotted in the gray scale where the white and black correspond to the positive and negative polarities, respectively. (**b**) The NLFFF solution derived from each boundary value of the LL solution, which is extrapolated based on the MHD relaxation method developed in Inoue et al. (2014a)

huge solar flare (X3.4 class) was observed in the solar active region (AR) 10930. The *Solar Optical Telescope* (Tsuneta et al. 2008) onboard *Hinode* could successfully take a time series of the photospheric magnetic field, covering before and after the flare. Schrijver et al. (2008) performed the NLFFF extrapolation using the observed photospheric magnetic field before and after the flare, by applying several different methods. Figure 11.2 shows the results of one of the NLFFF extrapolations performed in that study. We initially found that sheared field lines were formed before the flare on the polarity inversion line in the central area of the AR and that these field lines disappeared after the flare. The strong current density, which had been enhanced on the sheared field lines before the flare, also clearly disappeared after the flare. This is the first result that reveals the variation in the 3D coronal

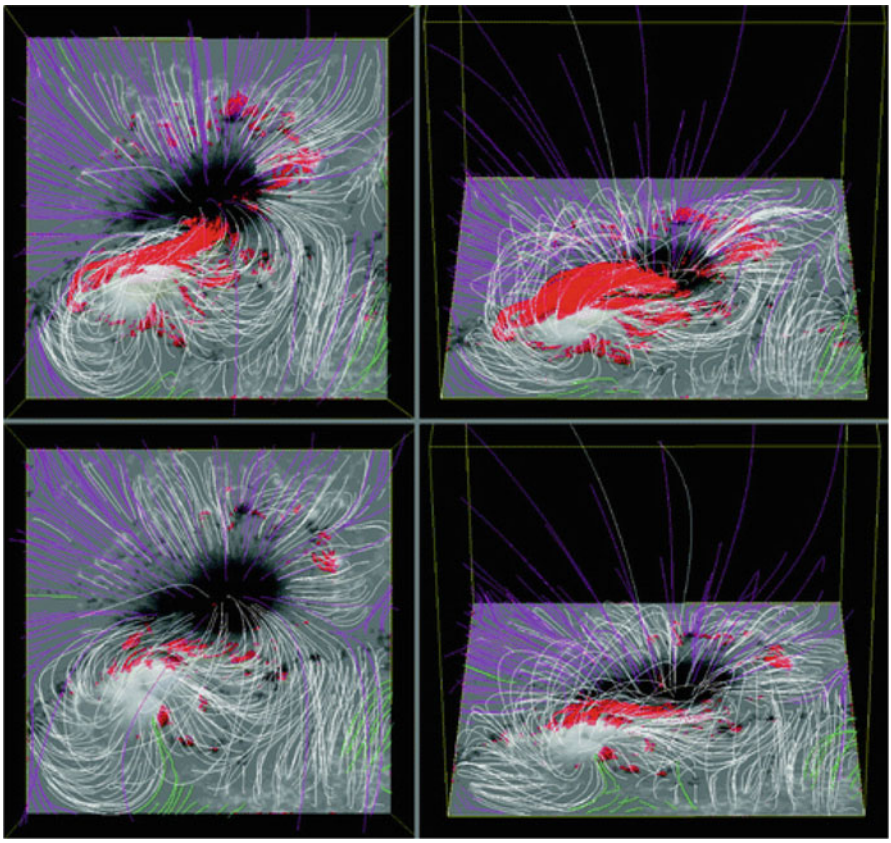

Fig. 11.2 Results from Schrijver et al. (2008) for the NLFFF before and after the X3.4 class flare occurred on December 13, 2006. The upper panels show the magnetic field lines and the strong current regions derived from the NLFFF where the field lines are plotted in white and the current density is drawn in red. The NLFFF was reconstructed from the photospheric magnetic field 6 h before the flare obtained from *Hinode*. The B_z distribution is plotted in gray scale. The lower panels show the NLFFF too but were reconstructed after the flare (All images are copyright AAS and are reproduced by permission)

magnetic field that accompanies a huge solar flare and therefore is one of the important results obtained from *Hinode*.

However, we also encountered several issues. For example, the value of the free energy strongly depended on the extrapolation methods, and it was pointed out in Schrijver et al. (2008) that most of the methods used could not reproduce enough free energy to explain the huge solar flares, even though the reconstruction was executed before the X3.4 class flare. Furthermore, De Rosa et al. (2009) pointed out that the extrapolated magnetic field structures differ considerably from each other, depending on the extrapolation technique used. Nevertheless, the NLFFF extrapolation suggested the temporal evolution of the 3D magnetic field in the

period leading up to the flare (Inoue et al. 2012; He et al. 2014) and the stability of the magnetic field prior to the flare (Inoue et al. 2011). Guo et al. (2008) inferred the dynamics during the flare by comparing the NLFFFs before and after the flare. As an example, the NLFFF extrapolation was applied in Inoue et al. (2011) using the photospheric magnetic field 6 h before the X3.4 class flare, based on the MHD relaxation method discussed above. The results are shown in Fig. 11.3, in which the selected sheared field lines are plotted superimposed on the Ca II images during

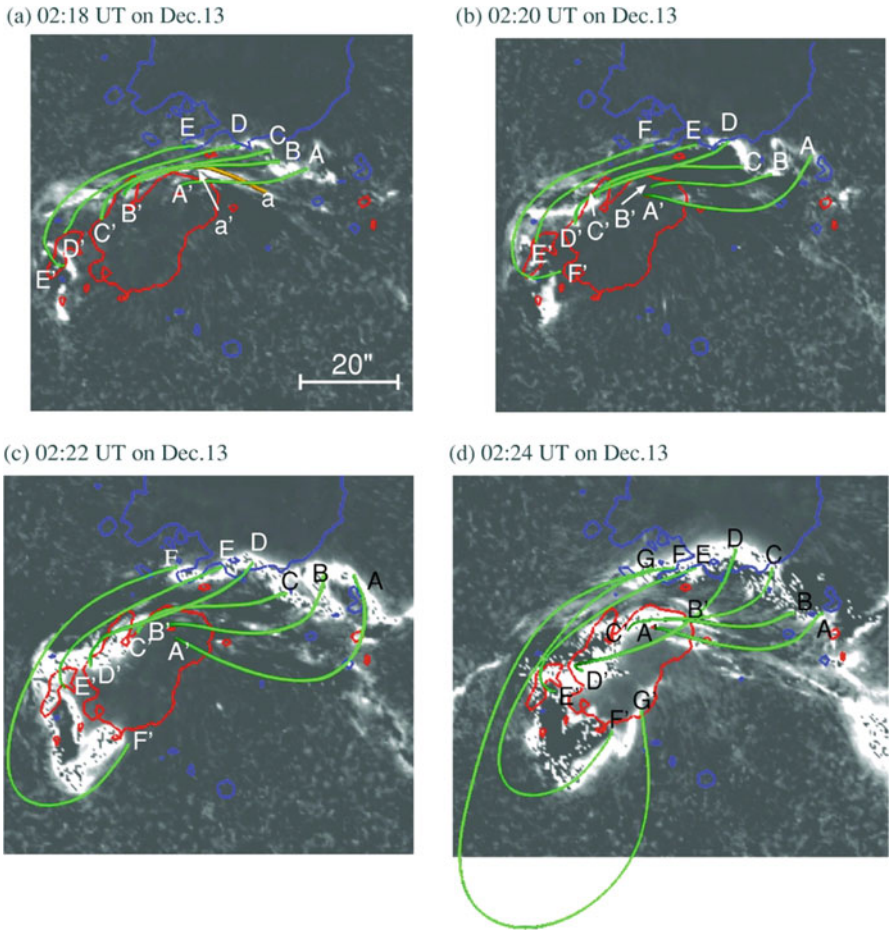

Fig. 11.3 Results from Inoue et al. (2011) for the NLFFF before the same flare shown in Fig. 11.2. The green lines correspond to the field lines of the NLFFF extrapolated 6 h before the X3.4 class flare, which are superimposed on Ca II images obtained during the flare. Both footpoints of the field lines are roughly anchored on the locations where the CaII images are enhanced as flare ribbons. The blue and red contours correspond to the locations of the negative and positive polarities. The NLFFFs are reconstructed using the MHD relaxation method developed in Inoue et al. (2014a) (All images are copyright AAS and are reproduced by permission)

the flare obtained from the *Hinode*. Since both of these footpoints are evidently anchored in the locations where the Ca II is strongly enhanced, i.e., corresponding to the flare ribbons, the authors of Inoue et al. (2011) suggested that these field lines caused the X3.4 class flare. They further discussed the stability of these field lines by estimating the magnetic twist defined as $(1/4)\int(\mathbf{B}\cdot\mathbf{J}/|\mathbf{B}|^2)dl$ where dl is a line element (Berger and Prior 2006). As a result they concluded that the NLFFF is stable to the kink instability. The diagnosis of the torus instability (Kliem and Török 2006) was also subsequently demonstrated later (Amari et al. 2014). These stability analyses were carried out based on the 3D coronal magnetic field extrapolated from the photospheric magnetic field obtained from *Hinode*. Therefore, these results also represent an important achievement by *Hinode*.

11.4 Current State and Future

Hinode can provide information on the photospheric magnetic field with unprecedented accuracy, which enables us to reconstruct the 3D coronal magnetic field with unprecedented accuracy and resolution. Although several problems still remain, such as the fact that the observed photospheric magnetic field cannot meet the perfect force-free condition, the 3D magnetic structure can be obtained with unprecedented accuracy, and the stability analysis for the MHD instability can also be executed, which enables us to discuss the onset and the dynamics of solar flares. Furthermore, MHD simulations initiated with the NLFFF have also been performed recently (Jiang et al. 2013; Inoue et al. 2014b; Amari et al. 2014; Inoue et al. 2015). Figure 11.4 is obtained from Inoue et al. (2014b), and Fig. 11.4a shows the results for the temporal evolution of the magnetic field obtained from the MHD simulation starting with the NLFFF. The orange lines are the twisted lines, which obviously show the launching away from the solar surface. The image in the left panel in Fig. 11.4b, which was taken by *Hinode*, corresponds to the two ribbons observed during the flare, while the middle and right panels show the flare ribbons obtained from the MHD simulation. The details of this simulation are described in Inoue et al. (2014b, 2015). We can see from these results that the simulation captures the observed features.

Recently, several other methods have been proposed to explore the force-free solution. The major feature of these methods is that the field lines are fitted to the observed Hα filament (van Ballegooijen 2004) or an extreme ultra violet image (Aschwanden 2016), without using the observed horizontal magnetic fields. Hence, these methods can avoid the discontinuity appearing close to the bottom surface in the NLFFF discussed above, at the expense of the observed horizontal field. Furthermore, the next solar physics satellite SOLAR-C plans to observe the chromospheric magnetic field, which will be better equipped to satisfy the force-free condition than the photospheric magnetic field, and is expected to act as a buffer zone smoothly connecting the photosphere to the corona. Therefore, a better force-free field or magnetohydrostatic field can be expected with an improvement in the observational technique.

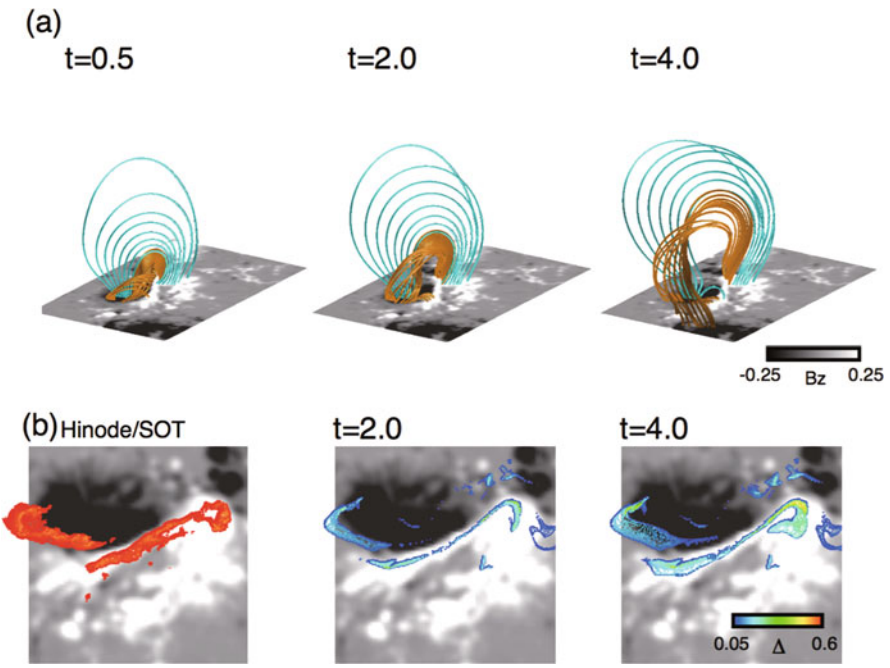

Fig. 11.4 Results from Inoue et al. (2014b). (**a**) Temporal evolution of the magnetic fields obtained from the MHD simulation starting with the NLFFF. The orange lines are twisted lines which can show the launching away from the solar surface. (**b**) Left panel shows the two flare ribbons observed during the flare, an observation which was taken by *Hinode*. The middle and right panels show the two flare ribbons too, but were obtained from the MHD simulation (All images are copyright AAS and are reproduced by permission)

Acknowledgements I'm grateful to Dr. T. Shimizu who carefully read this manuscript and gave constructive comments.

References

Amari, T., Canou, A., Aly, J.J., et al.: Characterizing and predicting the magnetic environment leading to solar eruptions. Nature **514**, 465 (2014)

Aschwanden, M.J.: The vertical-current approximation nonlinear force-free field code—description, performance tests, and measurements of magnetic energies dissipated in solar flares. Astrophys. J. Suppl. **224**, 25 (2016)

Berger, M.A., Prior, C.: The writhe of open and closed curves. J. Phys. A: Math. Gen. **39**, 8321 (2006)

Dedner, A., Kemm, F., Kroner, D., et al.: Hyperbolic divergence cleaning for the MHD equations. J. Comput. Phys. **175**, 645 (2002)

De Rosa, M.L., Schrijver, C.J., Barnes, G., et al.: A critical assessment of nonlinear force-free field modeling of the solar corona for active region 10953. Astrophys. J. **696**, 1780 (2009)

Gary, G.: Plasma beta above a solar active region: rethinking the paradigm. Sol. Phys. **203**, 71 (2001)
Guo, Y., Ding, M., Wiegelmann, T., et al.: 3D magnetic field configuration of the 2006 December 13 flare extrapolated with the optimization method. Astrophys. J. **679**, 1629 (2008)
He, H., Wang, H., Yan, Y., et al.: Variations of the 3-D coronal magnetic field associated with the X3.4-class solar flare event of AR 10930. J. Geophys. Res. **119**, 3286 (2014)
Inoue, S.: Magnetohydrodynamics modeling of coronal magnetic field and solar eruptions based on the photospheric magnetic field. Prog. Earth Planet. Sci. **3**, 19 (2016)
Inoue, S., Kusano, K., Magara, T., et al.: Twist and connectivity of magnetic field lines in the solar active region NOAA 10930. Astrophys. J. **738**, 161 (2011)
Inoue, S., Shiota, D., Yamamoto, T.T., et al.: Buildup and release of magnetic twist during the X3.4 solar flare of 2006 December 13. Astrophys. J. **760**, 17 (2012)
Inoue, S., Magara, T., Pandey, V.S., et al.: Nonlinear force-free extrapolation of the coronal magnetic field based on the magnetohydrodynamic relaxation method. Astrophys. J. **780**, 101 (2014a)
Inoue, S., Hayashi, K., Magara, T., et al.: Magnetohydrodynamic simulation of the X2.2 solar flare on 2011 February 15. I. Comparison with the observations. Astrophys. J. **788**, 182 (2014b)
Inoue, S., Hayashi, K., Magara, T., et al.: Magnetohydrodynamic simulation of the X2.2 solar flare on 2011 February 15. II. Dynamics connecting the solar flare and the coronal mass ejection. Astrophys. J. **803**, 73 (2015)
Jiang, C., Feng, X., Wu, S.T., et al.: Magnetohydrodynamic simulation of a sigmoid eruption of active region 11283. Astrophys. J. Lett. **771**, L30 (2013)
Kliem, B., Török, T.: Torus instability. Phys. Rev. Lett. **514**, 465 (2006)
Kosugi, T., Matsuzaki, K., Sakao, T. et al.: The Hinode (solar-B) mission: an overview. Sol. Phys. **243**, 3 (2007)
Low, B.C., Lou, Y.Q.: Modeling solar force-free magnetic fields. Astrophys. J. **352**, 343 (1990)
Metcalf, T.R., Jiao, L., MaClymont, A.N., et al.: Is the solar chromospheric magnetic field force-free? Astrophys. J. **439**, 474 (1995)
Priest, E., Forbes, T.: The magnetic nature of solar flares. Astron. Astrophys. Rev. **10**, 313 (2002)
Régnier, S., Amari, T., Kersalé, E.: 3D coronal magnetic field from vector magnetograms: non-constant-alpha force-free configuration of the active region NOAA 8151. Astron. Astrophys. **392**, 1119 (2002)
Sakurai, T.: Computational modeling of magnetic fields in solar active regions. Space Sci. Rev. **51**, 11 (1989)
Schrijver, C.J., De Rosa, M.L., Metcalf, T.R., et al.: Nonlinear force-free modeling of coronal magnetic fields part I: a quantitative comparison of methods. Sol. Phys. **235**, 161 (2006)
Schrijver, C.J., DeRosa, M.L., Metcalf, T., et al.: Nonlinear force-free field modeling of a solar active region around the time of a major flare and coronal mass ejection. Astrophys. J. **675**, 1637 (2008)
Shibata, K., Magara, T.: Solar flares: magnetohydrodynamic processes. Living Rev. Sol. Phys. **8**, 6 (2011)
Tsuneta, S., Ichimoto, K., Katsukawa, Y. et al.: The solar optical telescope for the Hinode mission: an overview. Sol. Phys. **249**, 167 (2008)
van Ballegooijen, A.A.: Observations and modeling of a filament on the Sun. Astrophys. J. **612**, 519 (2004)
Wiegelmann, T., Sakurai, T.: Solar force-free magnetic fields. Living Rev. Sol. Phys. **9**, 5 (2012)
Wiegelmann, T., Inhester, B., Sakurai, T.: Preprocessing of vector magnetograph data for a nonlinear force-free magnetic field reconstruction. Sol. Phys. **233**, 215 (2006)

Chapter 12
New Approach to Solar Flare Trigger Process with *Hinode*/Solar Optical Telescope

Yumi Bamba

Abstract Solar flares are explosive phenomena that release magnetic energy stored in the solar corona and affect our terrestrial environment at times. However, the triggering process of flares is still not completely understood. Here, I review the status of our theoretical understanding and observational examination of this process. In particular, I introduce the outcomes and new physical mechanisms emerging from our flare trigger study using the *Hinode*/Solar Optical Telescope.

Keywords Sun: flares · Flare-trigger process · *Hinode*/Solar optical telescope

12.1 Solar Flare Trigger Problem

Solar flares (Carrington 1859; Hodgson 1859) are explosive phenomena that release magnetic energy stored in the solar corona over solar active regions (sunspot regions). Flares are the largest explosive phenomena, which release 10^{29}–10^{32} erg of magnetic energy, in our solar system. The Carmichael, Sturrock , Hirayama, Kopp, and Pneuman (CSHKP) model (Carmichael 1964; Sturrock 1966; Hirayama 1974; Kopp and Pneuman 1976), in which the "magnetic reconnection" of antiparallel magnetic field lines is considered as the driver of energy release, is widely accepted as a standard model of solar eruptions including flares. Satellite observations such as *Yohkoh* (Ogawara et al. 1992) support the model through evidence of magnetic reconnection in the solar corona found during flares (Tsuneta et al. 1992; Masuda et al. 1994). However, an infinite number of antiparallel magnetic field lines exist in various magnetic field structures formed on the solar surface. Thus, the "solar flare trigger problem" of when, where, and how flares occur is still not completely understood.

Y. Bamba (✉)
SOLAR-B Project, Institute of Space and Astronautical Science (ISAS), Japan Aerospace Exploration Agency (JAXA), Sagamihara, Kanagawa, Japan
e-mail: y-bamba@nagoya-u.jp

T. Shimizu et al. (eds.), *First Ten Years of Hinode Solar On-Orbit Observatory*,
Astrophysics and Space Science Library 449,
https://doi.org/10.1007/978-981-10-7742-5_12

Multiple studies have attempted to reveal the flare-trigger process from theoretical and observational approaches so far. For instance, the emerging flux model (Chen and Shibata 2000) considers the situation where a small-scale emerging flux, which appears on the footpoint of magnetic arcades, traps a helical twisted magnetic flux tube (i.e., flux rope). Pre-existing magnetic arcades are weakened by magnetic reconnection with an emerging flux, and the flux rope then destabilizes and erupts. The Solar Optical Telescope (SOT, Tsuneta et al. 2008) onboard the *Hinode* satellite observed the emerging fluxes in a solar active region (AR) before a flare (Kubo et al. 2007; Toriumi et al. 2013). Another case, in which a flux rope is further twisted by horizontal motion on the photosphere, can also be considered. In this case, the electric current along the flux rope is strengthened, and the flux rope will erupt owing to the helical kink instability (Fan and Gibson 2003; Török and Kliem 2005). The strongly twisted flux rope is observed by the X-ray Telescope onboard *Hinode* as an S-shaped "sigmoid" structure, and a simulation illustrated its formation process (Amari et al. 2014). Moreover, it is conceivable that the horizontal component of the photospheric magnetic field is sheared (i.e., deviates from the potential field) on the footpoints of a flux rope. These strongly sheared photospheric horizontal fields are observed by *Hinode*/SOT before a flare onset (Magara and Tsuneta 2008). Conversely, it is also noted by observations that flares do not necessarily occur in a highly sheared AR (Leka and Barnes 2003).

Figure 12.1 shows a schematic of the physical processes leading to solar eruptive phenomena. A twisted flux rope is formed in the corona and grows. Antiparallel magnetic field lines (i.e., an electric current sheet) are formed by the magnetohydrodynamics instability in the flux rope, and then, magnetic reconnection occurs. The changes in magnetic topology by the reconnection further destabilize

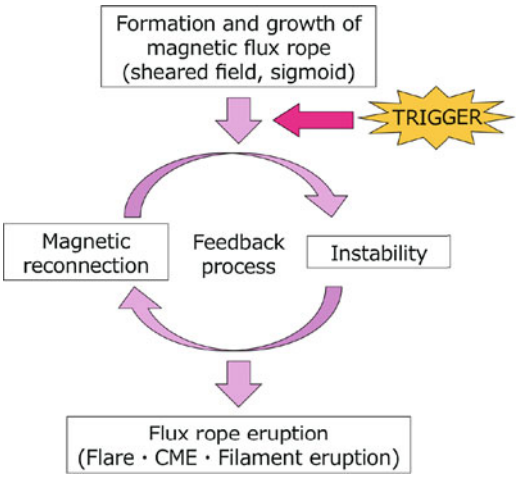

Fig. 12.1 Schematic of physical processes leading to solar eruption

the system. Thus, the magnetic reconnection and instability reinforce each other, accelerating the magnetic energy release and causing the flux rope to erupt. As mentioned earlier, many studies have been reported to approach the overview of the flare-trigger process using *Hinode* data. However, our physical understanding of some aspects of the flare-trigger process is still insufficient, e.g., the formation of erupting flux ropes, the mechanism through which the system moves onto the feedback process of magnetic reconnection and instability, etc. Hence, further detailed studies of the changes in photospheric magnetic fields in an AR before a flare using observational data are required to reveal the physical process of flare triggering.

12.2 Flare-Triggering Structure Observed by *Hinode*/SOT

12.2.1 Discovery of a Characteristic Magnetic Field Structure

Hinode/SOT is capable of an unprecedented high spatial resolution, high-cadence imaging observations, and high-accuracy magnetic field measurements (Ichimoto et al. 2008). Thus, SOT can capture quick changes in fine structures in the photospheric magnetic field and chromosphere. SOT has observed more than 1,000 flare events so far (Watanabe et al. 2012). However, I introduce an X3.4 flare that occurred on December 13, 2006, in this manuscript.

We precisely investigated the relationship between the photospheric magnetic field structures and pre-flare brightening in the chromosphere and the temporal evolution leading to the flare onset. Figure 12.2 displays the coalignment images of the photospheric line-of-sight (LOS) magnetic field (grayscale), polarity inversion lines (PILs, green), and strong brightening in the chromosphere (red). The flare ribbons appear as sheared two ribbons in the positive (white in the south) and negative (black in the north) polarity regions, just after the flare onset. There is an elongated, isolated, and small-scale bipolar field at the center of the sheared two-ribbon flares as marked by the yellow circle in Fig. 12.2d. In the small bipolar region, the positive polarity (north) is located above the negative (south), whereas, in the whole AR, the positive polarity (south) is located below the negative polarity (north). Therefore, the small-scale bipolar field has an opposite polarity pattern to the global magnetic field of the AR. The small-scale bipolar field originated from the isolated positive polarity region that appears in the large-scale negative polarity region, as indicated by the yellow arrow in Fig. 12.2a. Intermittent chromospheric pre-flare brightening is observed over the local PIL of the elongated bipolar field as the isolated positive region grows (see Fig. 12.2b). Therefore, we inferred that the small-scale isolated bipolar field that appears in the magnetic field structure of the AR before the flare onset plays an important part in triggering the flare.

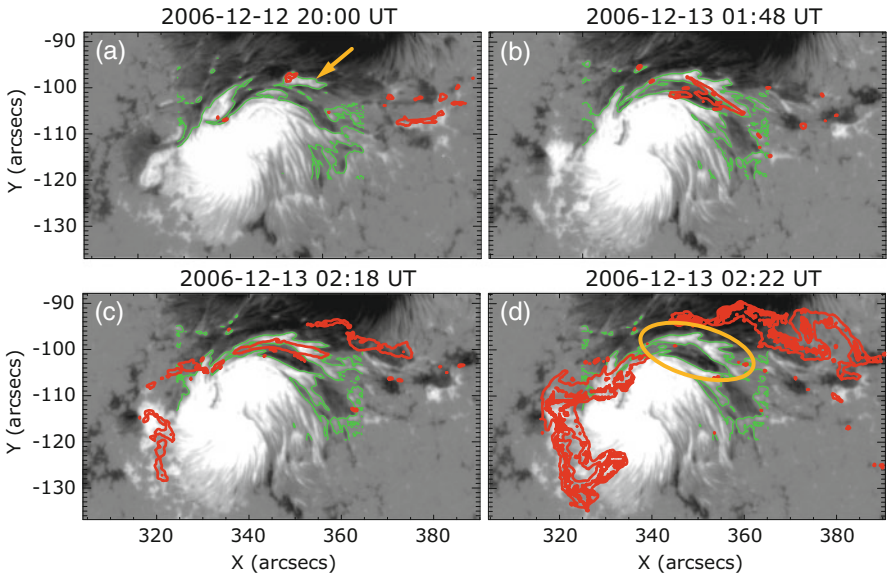

Fig. 12.2 Temporal evolution of the photospheric LOS magnetic field and chromospheric brightening leading to an X-class flare, captured by *Hinode*/SOT. White/black regions represent positive/negative polarities of the photospheric LOS magnetic field. The green and red lines indicate the PILs and strong chromospheric brightening, respectively. The small-scale magnetic island, which is marked by the yellow arrow in panel (**a**), grows and forms the flare-trigger field structure marked by the yellow circle in panel (**d**)

12.2.2 Consistency with Theoretical Model

We compared the observational findings described in Sect. 12.2.1 to the theoretical flare-trigger model based on the numerical simulations of Kusano et al. (2012, henceforth called "KB12 model"). The basic idea of the model is similar to that of the emerging flux model; a small-scale bipolar field (blue arcade in the upper schematic of Fig. 12.3) appears on the PIL of the global sheared magnetic field (red arcades in the upper schematic of Fig. 12.3). The shear angle θ_0 of the red magnetic arcades represents the deviation of the global magnetic fields in the AR from the potential field, and it characterizes the magnetic free energy stored in the corona. The azimuthal angle φ_e represents a small-scale magnetic disturbance, which is critical for flare occurrence. KB12 systematically investigated the flux rope formation, occurrence of magnetic reconnection, and physical processes leading to flux rope eruption using ensemble simulations with different combinations of (θ_0, φ_e). The KB12 model proposed quantitative conditions for flare triggering based on the simulation results, which are summarized in the bottom plot of Fig. 12.3. There are two types of small-scale bipolar fields that can trigger a flare, i.e., the "flare-trigger field": the "opposite polarity (OP) type" and the "reversed shear (RS) type."

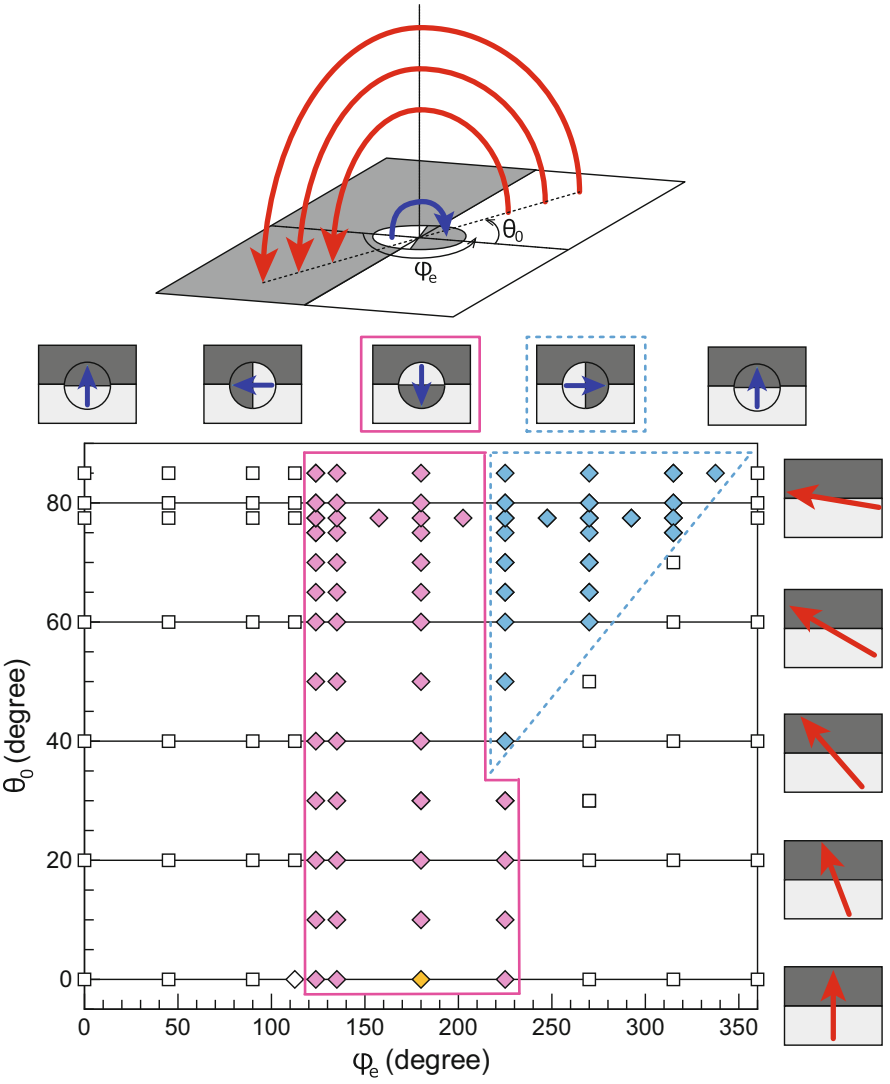

Fig. 12.3 Top: Schematic of the simulation setup in KB12. White/black regions represent positive/negative polarities of the magnetic field. The red and blue arrows represent the magnetic field lines in the pre-existing field and the small-scale injected field, which have rotation angles θ_0 and φ_e with respect to the large-sale potential field, respectively. Bottom: Flare phase diagram that summarizes the simulation results. The diamond symbols indicate the regions where the eruption has occurred under the θ_0 and φ_e conditions. The pink and blue diamonds indicate the types of dynamics considered "eruption-induced reconnection (OP-type)" and "reconnection-induced eruption (RS-type)," respectively. The yellow diamond corresponds to a special case where the potential field collapses because of reconnection with the small-scale injected field, which exhibits a completely antiparallel polarity compared with the initial potential field. The open square symbols indicate the regions where eruptions do not occur under the conditions

In the OP-type case, which is represented by the pink-colored diamonds in Fig. 12.3, the magnetic polarity pattern in the small-scale bipolar field is opposite to that of the global magnetic field, i.e., the azimuth angle φ_e is around 180°. Conversely, the RS-type case, in which the local magnetic shear in the small-scale bipolar field is opposite to the global magnetic shear in the AR (i.e., φ_e is around 270°), is represented by the blue-colored diamonds in Fig. 12.3.

Here, when we view the small-scale bipolar field that appears before the X3.4 flare described in Sect. 12.2.1, the small-scale bipolar field has a polarity pattern opposite to that of the global magnetic field in the AR. We measured the angles θ_0 and φ_e with the horizontal magnetic field data obtained by the spectropolarimeter of *Hinode*/SOT, and we obtained the results of $\theta_0 = 70° \pm 15°$ and $\varphi_e = 180° - 186°$. Therefore, we concluded that the X3.4 flare that occurred on December 13, 2006, was triggered by the OP-type bipolar field, which is marked by the yellow circle in Fig. 12.2d. It can be interpreted that the pre-flare brightening in Fig. 12.2b is caused by the minor magnetic reconnection between the OP-type flare-trigger field and the global magnetic field connecting the large-scale bipolar field. Moreover, we found the RS-type flare-trigger field for several major flares with *Hinode*/SOT (Bamba et al. 2013, 2014; Pesnell et al. 2012). Hence, the small-scale changes of the photospheric magnetic field are consistent with the KB12 model.

12.2.3 Further Suggestions from Hinode *Observation*

The OP-type flare-trigger field for the X3.4 flare formed and the (θ_0, φ_e) conditions were already satisfied at least three hours before the flare onset, as observed in Fig. 12.2. However, the flare did not immediately occur, and there are three hours of lag between the appearance of the flare-trigger field and the flare onset. Therefore, it is inferred that there may be another critical condition in addition to θ_0 and φ_e to trigger a flare. We thus investigated the temporal evolution of the magnetic flux contained within the flare-trigger field and the intensity variation of the pre-flare brightening. In Fig. 12.4, the magnetic flux (green) contained within the OP-type flare-trigger field gradually increases to the flare onset (vertical black solid line). The pre-flare brightening (red) follows the increase in the magnetic flux, and the flare finally occurs when the magnetic flux reaches a critical value. This suggests that the minor magnetic reconnection between the OP-type field and the global magnetic field of the AR gradually proceeds as the OP-type magnetic flux increase; then, the large-scale structure becomes unstable. Therefore, the flare-trigger field must satisfy both geometrical and quantitative magnetic flux conditions. In addition to enabling flare triggering, it should rapidly expand to drive the minor magnetic reconnection preceding the major reconnection that releases the magnetic energy as a flare.

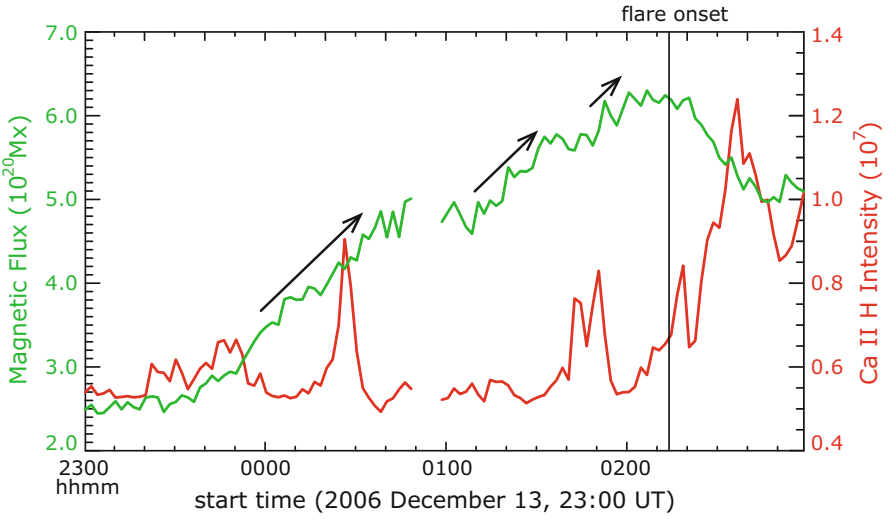

Fig. 12.4 Temporal evolution of magnetic flux (green) contained within the flare-trigger region and intensity of the pre-flare brightening (red) leading to an X-class flare. The vertical solid line indicates the flare onset time

12.3 Future Direction

12.3.1 Various Flare Events

We found several flare events, which have flare-trigger fields consistent with the KB12 model, with the *Hinode*/SOT data, as described in Sect. 12.2. We further suggested the existence of an additional critical parameter that likely determines the timing of a flare not included in the KB12 model. Conversely, flares occur not only in the central region but also in the peripheral region of an AR, where weak and small-scale magnetic structures are distributed, as exemplified in Fig. 12.5a. However, sometimes, flares occur in a magnetic field region more complex than the AR shown in Sect. 12.2, as observed in Fig. 12.5b. In these cases, the observable features, which are important to identify the flare-trigger regions such as "sheared two ribbons" and "chromospheric pre-flare brightening," may not be clear, or even too complicated. More statistical research with large samples is necessary to evaluate the applicability of the KB12 model to various flare events. The *Solar Dynamics Observatory* (*SDO*, Pesnell et al. 2012) is suitable for such kinds of statistical studies because it observes the full disk of the sun in multiple wavelengths with a high temporal resolution. *Hinode*/SOT has the highest spatial resolution and can measure the magnetic field with a high accuracy, which are powerful characteristics to analyze the detailed structure. Thus, *Hinode* and *SDO* can be complementary to each other for the study of the flare-trigger mechanism. We are now progressing to studies in order to comprehensively understand the physical mechanism of flare

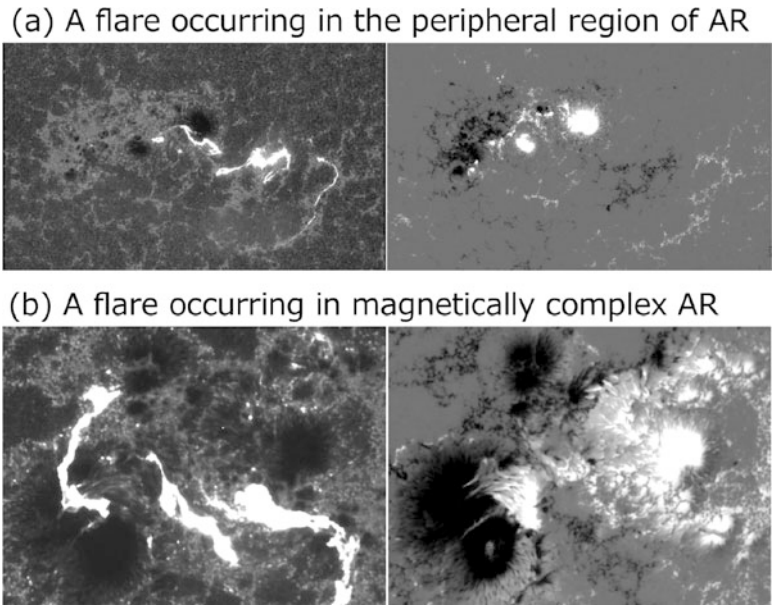

Fig. 12.5 Samples of various flare events. (**a**) A flare occurring in the peripheral region of AR and (**b**) a flare occurring in magnetically complicated AR. The left images were captured by *SDO*/Atmospheric Imaging Assembly 1600 Å which is sensitive to the emission from the upper photosphere and transition region. The right images are the photospheric LOS magnetic fields observed by *SDO*/Helioseismic and Magnetic Imager, and the white/black regions indicate positive/negative polarities

triggering by evaluating the consistency between the observations, such as those by *Hinode* and *SDO*, and theoretical models, such as the KB12 model.

12.3.2 Contribution to Space Weather Research

Eruptions of flux ropes are observed as flares, coronal mass ejections (CMEs), and filament eruptions, as summarized in Fig. 12.1. High-energy particles and interplanetary shock waves originate from flares, and CMEs sometimes disturb the space environment around Earth. It is widely known that CMEs are highly related to large X-class flares, but they do not necessarily occur simultaneously (Yashiro et al. 2006). There is a strong appeal to "space weather forecasts" that predict disturbances in the space environment such as flares and CMEs. This is important not only from a scientific research perspective, but from the perspective of the protection of infrastructure for our information-oriented society. There are various studies attempting to determine the physical parameters useful for the prediction of flares and CMEs by analyzing the huge number of flare events

observed by *SDO* in recent years (Bobra and Couvidat 2015; Bobra and Ilonidis 2016). These studies have found many parameters that are "empirically" related to flares and CMEs. However, the accuracy and reliability of our current flare or CME predictions have not improved dramatically. This is because our physical understanding of the parameters important to the various phases of the flare or CME triggers is not sufficient. In other words, it is essential to physically understand the triggering mechanism(s) of flares and CMEs to construct a new space weather forecast model with a much higher accuracy and reliability than those of conventional empirical methods. It is important to combine theoretical models, such as numerical simulations (Aulanier et al. 2012; Kusano et al. 2012), with observations, such as those from *Hinode* and *SDO* (Bamba et al. 2013, 2014), to gain an understanding of the flare-trigger mechanism. Moreover, new observational techniques to measure the magnetic field in the chromosphere and corona can be expected as improved approaches to understanding the details of how small-scale magnetic field disturbances in the photosphere affect large-scale changes in the magnetic field topology in the corona.

Acknowledgements This manuscript is based on my PhD thesis (Bamba 2016) and published papers (Bamba et al. 2013, 2014). I am deeply grateful to my PhD advisor Prof. Kanya Kusano at Nagoya University. I also appreciate my collaborators in Nagoya University, ISAS/JAXA, NAOJ, LMSAL, and NWRA. Ten years ago, when *Hinode* was launched, I was a high school student, and, at that time, I did not have a great interest in solar physics. However, I developed an interest after watching the fascinating *Hinode* videos. I would like to express my sincere gratitude to those who have made efforts to develop *Hinode* and those who perform the meaningful scientific operations.

References

Amari, T., et al.: Characterizing and predicting the magnetic environment leading to solar eruptions. Nature **514**(7523), 465–469 (2014). https://doi.org/10.1038/nature13815

Aulanier, G., et al.: The standard flare model in three dimensions. I. Strong-to-weak shear transition in post-flare loops. Astron. Astrophys. **543**, id.A110, 14 pp (2012). https://doi.org/10.1051/0004-6361/201219311

Bamba, Y.: Study on solar flare trigger process based on satellite observations. Ph.D. thesis, Nagoya University (2016)

Bamba, Y., et al.: Study on the triggering process of solar flares based on Hinode/SOT observations. Astrophys. J. **778**(1), article id. 48, 13 pp (2013). https://doi.org/10.1088/0004-637X/778/1/48

Bamba, Y., et al.: Comparison between Hinode/SOT and SDO/HMI, AIA data for the study of the solar flare trigger process. Publ. Astron. Soc. Jpn. **66**(SP1), id.S169 pp (2014). https://doi.org/10.1093/pasj/psu091

Bobra, M.G., Couvidat, S.: Solar flare prediction using SDO/HMI vector magnetic field data with a machine-learning algorithm. Astrophys. J. **798**(2), article id. 135, 11 pp (2015). https://doi.org/10.1088/0004-637X/798/2/135

Bobra, M.G., Ilonidis, S.: Predicting coronal Mass ejections using machine learning methods. Astrophys. J. **821**(2), article id. 127, 7 pp (2016). https://doi.org/10.3847/0004-637X/821/2/127

Carmichael, H.: A process for flares. The physics of solar flares. In: Greenbelt, M.D., Hess, W.N. (eds.) Proceedings of the AAS-NASA Symposium held 28–30 October, 1963 at the Goddard Space Flight Center. Washington, DC: National Aeronautics and Space Administration, Science and Technical Information Division, p. 451 (1964)

Carrington, R.C.: Description of a singular appearance seen in the Sun on September 1, 1859. Mon. Not. R. Astron. Soc. **20**, 13–15 (1859). https://doi.org/10.1093/mnras/20.1.13

Chen, P.F., Shibata, K.: An emerging flux trigger mechanism for coronal Mass ejections. Astrophys. J. **545**(1), 524–531 (2000). https://doi.org/10.1086/317803

Fan, Y., Gibson, S.E.: The emergence of a twisted magnetic flux tube into a preexisting coronal arcade. Astrophys. J. **589**(2), L105–L108 (2003). https://doi.org/10.1086/375834

Hirayama, T.: Theoretical model of flares and prominences. I: evaporating flare model. Sol. Phys. **34**(2), 323–338 (1974). https://doi.org/10.1007/BF00153671

Hodgson, R.: On a curious appearance seen in the Sun. Mon. Not. R. Astron. Soc. **20**, 15–16 (1859). https://doi.org/10.1093/mnras/20.1.15

Ichimoto, K., et al.: Polarization calibration of the solar optical telescope onboard Hinode. Sol. Phys. **249**(2), 233–261 (2008). https://doi.org/10.1007/s11207-008-9169-9

Kopp, R.A., Pneuman, G.W.: Magnetic reconnection in the corona and the loop prominence phenomenon. Sol. Phys. **50**, 85–98 (1976). https://doi.org/10.1007/BF00206193

Kubo, Y., et al.: Hinode observations of a vector magnetic field change associated with a flare on 2006 December 13. Publ. Astron. Soc. Jpn. **59**(SP3), S779–S784 (2007). https://doi.org/10.1093/pasj/59.sp3.S779

Kusano, K., et al.: Magnetic field structures triggering solar flares and coronal Mass ejections. Astrophys. J. **760**(1), article id. 31, 9 pp. (2012). https://doi.org/10.1088/0004-637X/760/1/31

Leka, K.D., Barnes, G.: Photospheric magnetic field properties of flaring versus flare-quiet active regions. I. Data, general approach, and sample results. Astrophys. J. **595**(2), 1277–1295 (2003). https://doi.org/10.1086/377511

Magara, T., Tsuneta, S.: Hinode's observational result on the saturation of magnetic helicity injected into the solar atmosphere and its relation to the occurrence of a solar flare. Publ. Astron. Soc. Jpn. **60**(5), 1181–1189 (2008). https://doi.org/10.1093/pasj/60.5.1181

Masuda, S., et al.: A loop-top hard X-ray source in a compact solar flare as evidence for magnetic reconnection. Nature **371**(6497), 495–497 (1994). https://doi.org/10.1038/371495a0

Ogawara, Y., et al.: The status of YOHKOH in orbit – an introduction to the initial scientific results. Pub. Astron. Soc. Jpn. **44**(5), L41–L44 (1992). ISSN:0004-6264

Pesnell, W.D., et al.: The solar dynamics observatory (SDO). Sol. Phys. **275**(1-2), 3–15 (2012). https://doi.org/10.1007/s11207-011-9841-3

Sturrock, P.A.: Model of the high-energy phase of solar flares. Nature **211**(5050), 695–697 (1966). https://doi.org/10.1038/211695a0

Toriumi, S., et al.: The magnetic systems triggering the M6.6 class solar flare in NOAA active region 11158. Astrophys. J. **773**(2), article id. 128, 10 pp (2013). https://doi.org/10.1088/0004-637X/773/2/128

Török, T., Kliem, B.: Confined and ejective eruptions of kink-unstable flux ropes. Astrophys. J. **630**(1), L97–L100 (2005). https://doi.org/10.1086/462412

Tsuneta, S., et al.: Observation of a solar flare at the limb with the YOHKOH soft X-ray telescope. Pub. Astron. Soc. Jpn. **44**(5), L63–L69 (1992). ISSN:0004-6264

Tsuneta, S., et al.: The solar optical telescope for the Hinode mission: an overview. Sol. Phys. **249**(2), 167–196 (2008). https://doi.org/10.1007/s11207-008-9174-z

Watanabe, K., et al.: Hinode flare catalogue. Sol. Phys. **279**(1), 317–322 (2012). https://doi.org/10.1007/s11207-012-9983-y

Yashiro, S., et al.: Different power-law indices in the frequency distributions of flares with and without coronal Mass ejections. Astrophys. J. **650**(2), L143–L146 (2006). https://doi.org/10.1086/508876

Chapter 13
Hinode Observations of Flows and Heating Associated with Magnetic Reconnection During Solar Flares

Katharine K. Reeves

Abstract The three instruments on the *Hinode* satellite give a wealth of information about the aftermath of reconnection in solar flares. As magnetic fields reconnect during solar flares, flows and heating are observed in the corona as well as in the chromosphere, where the magnetic fields are line tied. The X-Ray Telescope and the Extreme ultraviolet Imaging Spectrometer (EIS) have the temperature sensitivity and spatial resolution to observe these phenomena in the corona, and the Solar Optical Telescope and EIS can observe the signatures of heating and flows, respectively, at the flare footpoints. In this chapter, we will review the observational evidence for heating and flows in the corona and chromosphere in the aftermath of flare reconnection.

Keywords Reconnection · Sun: flares · Coronal mass ejections

13.1 Introduction

Magnetic reconnection is a fundamental process in solar flares that converts magnetic energy into thermal energy that heats the plasma and kinetic energy that results in plasma flows. Evidence for this energy transfer is seen in heating in the corona and flows that occur near the reconnection site. Since the magnetic fields in the corona are line tied to the Sun's surface, manifestations of this energy release are also seen at the footpoints of solar flares, where energy deposition causes heating and drives flows referred to as chromospheric evaporation.

The three instruments on the *Hinode* satellite (Kosugi et al. 2007) provide a unique perspective on the heating and flows that occur during solar flares. The X-Ray Telescope (XRT) (Golub et al. 2007; Kano et al. 2008) is sensitive to hot plasma, so it is ideal for viewing hot plasma that results from heating in the corona.

K. K. Reeves (✉)
Harvard-Smithsonian Center for Astrophysics, Cambridge, MA, USA
e-mail: kreeves@cfa.harvard.edu

T. Shimizu et al. (eds.), *First Ten Years of Hinode Solar On-Orbit Observatory*,
Astrophysics and Space Science Library 449,
https://doi.org/10.1007/978-981-10-7742-5_13

The Extreme ultraviolet (EUV) Imaging Spectrometer (EIS) (Culhane et al. 2007) can quantify line-of-sight flows using Doppler shift measurements and identify turbulence by measuring line broadening, both in the corona and at the footpoints of flares. The Solar Optical Telescope (SOT) (Tsuneta et al. 2008; Suematsu et al. 2008) can image the footpoints of flares in the lower layers of the Sun's atmosphere in unprecedented detail.

This chapter will discuss the *Hinode* contributions to observations of flows and heating precipitated by magnetic reconnection during solar flares. Section 13.2 will focus on flows observed by EIS via Doppler shift measurements and XRT measurements of flows in the plane-of-sky direction. Section 13.3 will focus on the heating that occurs in both the corona and at the footpoints during flares.

13.2 Flows

Reconnection constitutes a topological reordering of the magnetic fields and results in the conversion of some of the released magnetic energy into kinetic energy in the form of outflows from the reconnection site. There are also inflows into the reconnection site as magnetic fields are drawn into the reconnection region. Additionally, since magnetic fields in the corona are line tied to the lower parts of the atmosphere, energy deposition there creates flows at the flare footpoints. In the following sections, we will review results from *Hinode* regarding these reconnection-related flows.

13.2.1 Flows at or Near the Reconnection Site

One result of reconnection outflows in solar flares is the shrinking of cusp-shaped flare loops as the magnetic fields relax into a more potential state. This phenomena had been inferred previously during a flare observed by *Yohkoh* Soft X-ray Telescope (SXT) (Forbes and Acton 1996). The high-cadence and excellent spatial resolution of XRT allowed Reeves et al. (2008) to directly observe downflowing loops during two flares early in the *Hinode* mission, a B3.8 flare on May 2, 2007, and a C2.1 flare on December 17, 2006. The speeds of the shrinking loops in these flares were found to be on the order of a few km s^{-1}. These speeds are much slower than the expected reconnection outflow speeds (which should be on the order of the Alfvén speed), but they are consistent with models that show that the descending loops should slow down dramatically as they encounter the previously reconnected loops below (Lin 2004). Recent high-cadence observations with the Atmospheric Imaging Assembly (AIA) instrument on the *Solar Dynamics Observatory (SDO)* have confirmed these findings (Liu et al. 2013).

If reconnection is happening in a current sheet above a flare site, it is expected that there will be anti-sunward outflows as well as sunward flows. Savage et al.

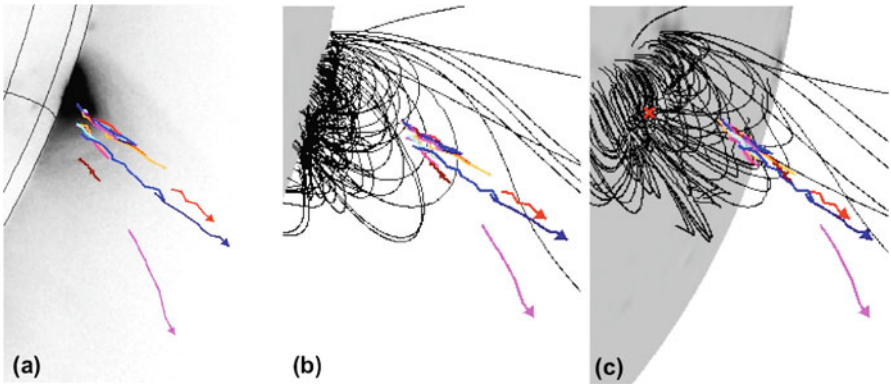

Fig. 13.1 Plane-of-sky velocities of outflows tracked from XRT data (colored arrows) superimposed on an XRT image taken on April 9, 2008, at 16:30:54 UT (panel **a**) and a potential field magnetic field model of the active region at two locations (panels **b** and **c**) (From Savage et al. 2010, reproduced by permission of the AAS)

(2010) analyzed the XRT data from a flare that occurred behind the west limb on April 9, 2008, and they are able to identify upward-moving flows in addition to sunward-shrinking loops, as shown in Fig. 13.1. These flows are between 100 and 200 km s^{-1}, and when tracked out to the field of view of LASCO (assuming no acceleration), they align with blobs of plasma seen flowing along a streamer-like structure. Other studies have attempted to connect post-CME (coronal mass ejection) blobs observed by LASCO with features observed lower in the corona in the EUV, without much success (Lin et al. 2005; Schanche et al. 2016). Thus this observation by Savage et al. (2010) may be unique due to XRT's broad temperature coverage and the long exposure times that occurred because the flare was occulted by the limb.

Reconnection inflows and outflows have also been observed by EIS. For example, Hara et al. (2011) analyzed the EIS data from a small flare that occurred on May 19, 2007, and found a blueshift in the Fe XVI line, formed at 3–5 million Kelvin (MK) during the flare, which they interpret as a hot outflow from the reconnection process. They also observed a blueshift in the cooler Fe XII line, which is interpreted as a reconnection inflow. In addition, the flare exhibited a bright loop-top source visible in the *STEREO-A* 195 Å channel, and in the EIS Fe XXIII line, which they interpret as evidence for a termination shock formed as the reconnection outflows impact the stationary loops below. Imada et al. (2013) analyzed EIS data from an X1.7 flare that occurred on the limb on January 27, 2012, and found Doppler shifts in the Fe XXIV line consistent with a 600 km s^{-1} outflow associated with shrinking loops as seen in AIA images. They also found opposing Doppler shifts in this line, possibly indicating transverse flows due to the termination shock formed as outflows collide with stationary loops. Examples of some of these flows are shown in Fig. 13.2.

Dark downflows have been observed above flare arcades during the decay phase of some flares. These flows, called supra-arcade downflows (SADs), were

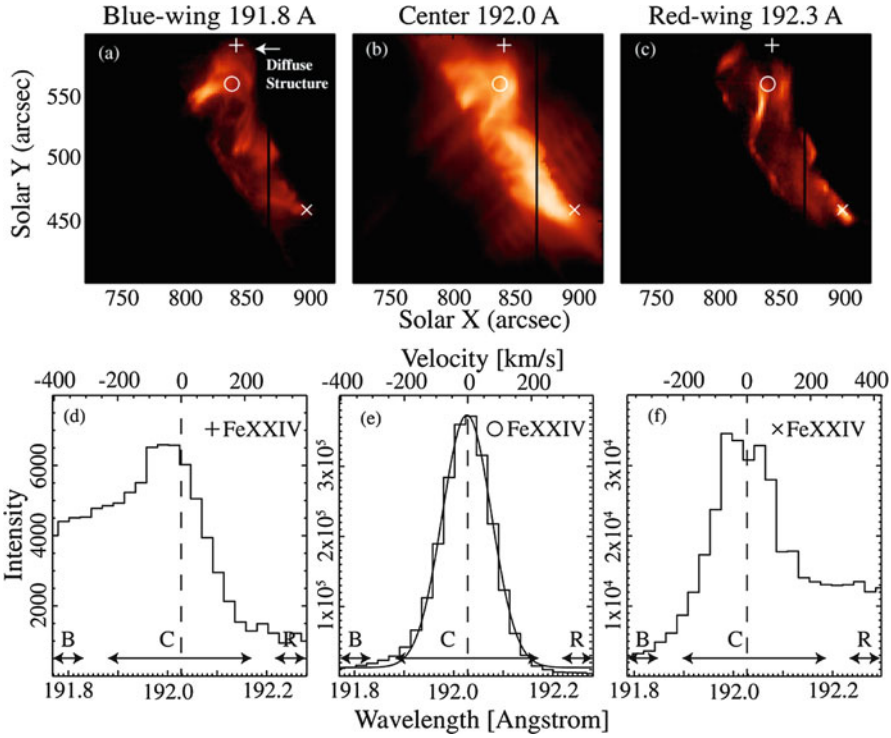

Fig. 13.2 Images from the blue wing (panel **a**), line center (panel **b**), and red wing (panel **c**) of the EIS Fe XXIV192 Å line for a flare that occurred on January 27, 2012. Examples of spectra from three different regions, marked with a cross (+), a circle (∘), and an x (×) are shown in panels (**d**)–(**f**) (From Imada et al. (2013), reproduced by permission of the AAS)

discovered during the *Yohkoh* era (McKenzie and Hudson 1999). They have been found to be voids that are cooler than the surrounding plasma (Innes et al. 2003a,b; Savage et al. 2012; Hanneman and Reeves 2014), and they are thought to be associated with the reconnection process (Asai et al. 2004). Statistical studies of these flows from a variety of telescopes, including XRT, show that the average velocity of these downflows is a few hundred km s^{-1} (Savage and McKenzie 2011), which is an order of magnitude lower than the commonly assumed Alfvén speed in the corona of 1000 km s^{-1}. These supra-arcade flows are often turbulent and full of vortices. McKenzie et al. (2013) applied a flow tracking algorithm to a rotating feature in the supra-arcade plasma imaged with XRT, shown in Fig. 13.3, and found that there is a significant vorticity in this feature, but it is unclear if the motion corresponds to the twisting or untwisting of a flux rope or if there is some other reason for the rotational motion. Measurements of the supra-arcade plasma with EIS show that there are significant nonthermal motions in the plasma that increase with height above the loop tops (Doschek et al. 2014). Large nonthermal widths have also been observed above the loop tops in other flares by Imada et al. (2013)

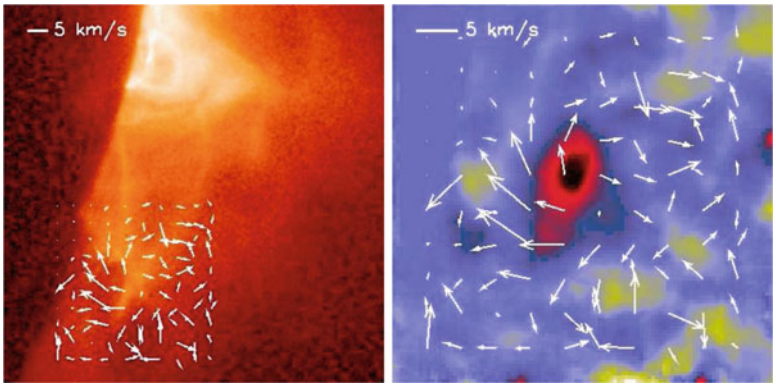

Fig. 13.3 Vortex flows observed using XRT for an event that happened on May 8, 2007. The background image in the left panel is an XRT Ti-poly image, and in the right panel, it is the vorticity calculated from the curl of the velocity field. The calculated velocity field is shown with arrows in both images (From McKenzie (2013), reproduced by permission of the AAS)

and Hara et al. (2008). This turbulence likely affects the magnetic fields and the reconnection rate in the current sheet region above the flare loops, as reconnection in the presence of turbulence is typically fast (Lazarian and Vishniac 1999).

13.2.2 Flows at the Chromosphere

In addition to inflows and outflows at the reconnection site, flows are expected at the footpoints of flares, where energy from the reconnection process heats the chromosphere, causing a pressure imbalance and driving upward and downward flows. These evaporation flows are difficult to image directly in large flares, but XRT has observed upflowing plasma in smaller events. Nitta et al. (2012) examined several small brightenings observed with XRT and found that there are symmetric upflows emanating from the footpoints in these events. The observed speeds are on the order of $100\,\mathrm{km\,s^{-1}}$ in most events, but a few events exhibit upflow speeds of up to $500\,\mathrm{km\,s^{-1}}$. This dichotomy may be due to the different energy deposition rates in the chromosphere, resulting in either gentle or explosive evaporation (Fisher et al. 1985a,b). XRT observations have also found evaporation speeds of around $100\,\mathrm{km\,s^{-1}}$ in coronal bright points, indicating that a gentle evaporation process is occurring (Zhang and Ji 2013).

Early spectroscopic observations of upflows from chromospheric evaporation almost always showed a stationary component along with the blueshifted component, e.g., Antonucci et al. (1987). Blueshifts near ribbons have been observed with Coronal Diagnostic Spectrometer (CDS) on *Solar and Heliospheric Observatory (SoHO)* (Czaykowska et al. 1999; Brosius and Phillips 2004; Milligan et al. 2006), but the spatial resolution of EIS, with its 1–2” slit width, has allowed for more

frequent observations of completely blueshifted lines at flare footpoints. The Fe XXIV line observed in the footpoint of a C9.7 flare examined by T. Watanabe et al. (2010b) is completely blueshifted, with no stationary component, and Doschek et al. (2015) also found completely shifted Fe XXIV profiles in the footpoints of an M3.7 flare. Brosius et al. (2013) found a completely blueshifted Fe XXIII line in the footpoint of a C1 flare. Most observations of chromospheric evaporation are still blended with a stationary component, however, indicating that the fundamental scale of flare loops is usually smaller than the EIS spatial resolution. Recent observations using the *Interface Region Imaging Spectrometer (IRIS)* have shown that its subarcsecond spatial resolution can resolve completely blueshifted lines in locations where EIS sees blended profiles (Polito et al. 2016).

EIS has been particularly useful for observing chromospheric evaporation flows because of its broad temperature coverage. Milligan and Dennis (2009) and Milligan (2011) examined the footpoints of a B-class flare and found a clear relationship between the temperature of the observed line and the velocity, with cooler temperatures redshifted, indicating a downward motion, and hotter temperatures blueshifted as hot plasma fills the loops, as shown in Fig. 13.4. The downflows are a result of explosive evaporation, but they occur at higher temperatures (∼1.35 MK) than

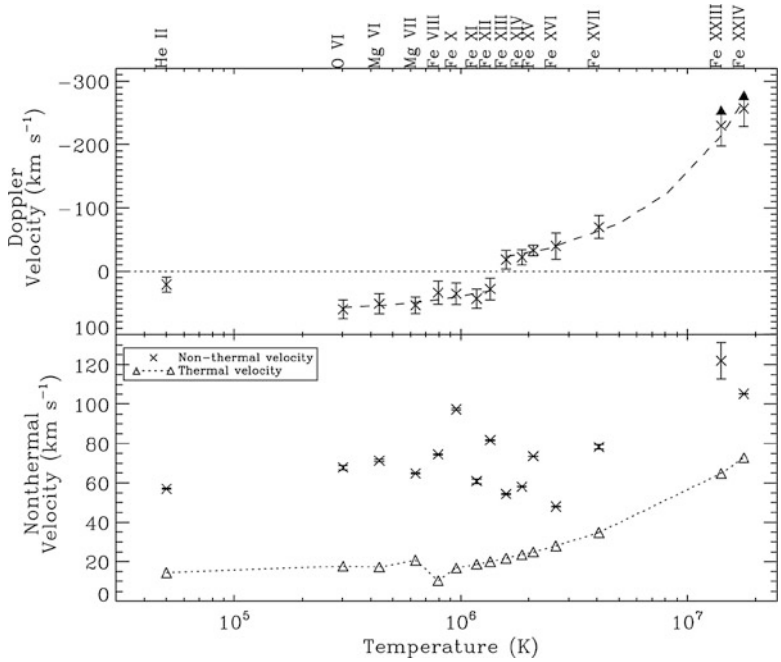

Fig. 13.4 Top panel: Doppler velocities from the footpoint of a flare that occurred on December 14, 2007. Positive velocities correspond to blueshifts, and negative velocities correspond to redshifts. Bottom panel: Corresponding thermal and nonthermal velocities for the same lines (From Milligan (2011), reproduced by permission of the AAS)

expected from hydrodynamic models (Fisher et al. 1985c). Similar results were observed in the footpoints of M1.1 flare by Young et al. (2013), who found a reversal at about 1.25 MK, and the flare observed by T. Watanabe et al. (2010b) exhibits high-speed blueshifts only in the hot Fe XXIII (T ∼14 MK) and Fe XXIV (T ∼17 MK) lines. Similarly, Imada et al. (2015) observed strong downflows in several EIS lines, including Fe XII, Fe XIV, Fe XV, and Fe XVI, during an M5.4 flare. Some ideas that might explain the high-temperature reversal are a suppression in the thermal conduction in the flare loop (Imada et al. 2015) and persistent electron deposition that continually heats the chromosphere (Liu et al. 2009).

13.3 Heating

Some of the magnetic energy release from reconnection is also channeled into thermal energy, heating the plasma at the reconnection site. Energy deposition at the footpoints also causes heating in the chromosphere, and the chromospheric evaporation process leads to hot plasma filling flare loops. The instruments on *Hinode* have observed many manifestations of these heating processes, which we will review in this section.

13.3.1 Heating at or Near the Reconnection Site

Heating is evident in supra-arcade plumes of plasma that have been observed with XRT. An example is shown in Fig. 13.5 from a flare that occurred on November 5, 2010 (Reeves and Golub 2011). The plasma above the flare loops is evident in all of the XRT filters, which are sensitive to plasma >2 MK, but it is only visible in the 131 and 94 Å AIA filters, which are sensitive to plasma at ∼10 MK and ∼8 MK, respectively. This plasma provides the medium that the supra-arcade downflows mentioned in the previous section flow through. The temperature structure of this plasma was investigated using DEMs from XRT and AIA data by Hanneman and Reeves (2014), who found that the supra-arcade plasma sheets typically have a peak temperature of about 10 MK.

Other examples of heating have been seen along with the eruption of a CME. The “cartwheel CME” event observed by Savage et al. (2010) exhibited a long, linear structure trailing the CME that was observed in XRT, but not visible in the *Transition Region and Coronal Explorer (TRACE)* 171 Å channel, which images cooler plasma at around 1 MK. Thus, it was inferred that this linear structure is hot and possibly associated with the reconnection current sheet. Fortuitously, the EIS slit was located just off limb during this event, enabling a detailed thermal structure of the CME and the current sheet region by Landi and coworkers (Landi et al. 2010, 2012, 2013). Using the Fe XIII-Fe XVI lines in EIS, these studies show that the current sheet region has a temperature that is peaked at about 3 MK and any plasma

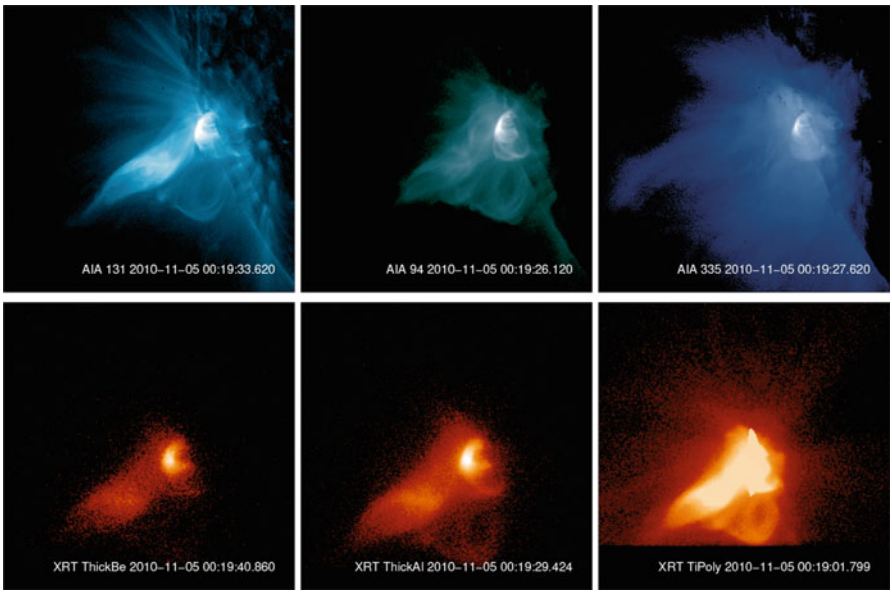

Fig. 13.5 Top row: Supra-arcade plasma plume from a flare that occurred on November 5, 2010, observed in AIA 131, 94, and 335 Å channels (from left to right). Bottom row: The same supra-arcade plume observed with the XRT Thin-Be, Thick-Al, and Ti-Poly filters (from left to right) (From Reeves and Golub (2011), reproduced by permission of the AAS)

above about 5 MK is faint. This hot plasma trailed the cooler CME, which EIS showed to have two parts: a colder and denser one (T = 125,000 K, log $N_e \approx 10$–11) and a hotter and less dense one (T = 500,000 K, log $N_e \approx 8.7$).

CMEs themselves have also shown evidence of heating. Seven eruptions were studied by Lee et al. (2015) using images from XRT. For four of these events, the estimated conductive cooling times were much shorter than the duration of the events, indicating that there must be additional heating occurring during these eruptions, possibly due to continual reconnection as the eruption progresses. Nindos et al. (2015) found that about half of CMEs imaged with the 131 Å channel on *SDO*/AIA showed evidence for hot flux ropes during the event. XRT was able to detect hot flux ropes in several events in their sample that were not visible in the AIA images, indicating that this proportion is a lower limit and that heating of the plasma associated with the CME is more the norm than the exception.

13.3.2 Heating in the Lower Atmosphere During Flares

Reconnection of coronal magnetic fields drives energy into the chromosphere, often in the form of accelerated particles, thus heating the lower layers of the atmosphere. The footpoint radiation in photospheric wavelengths observed in some

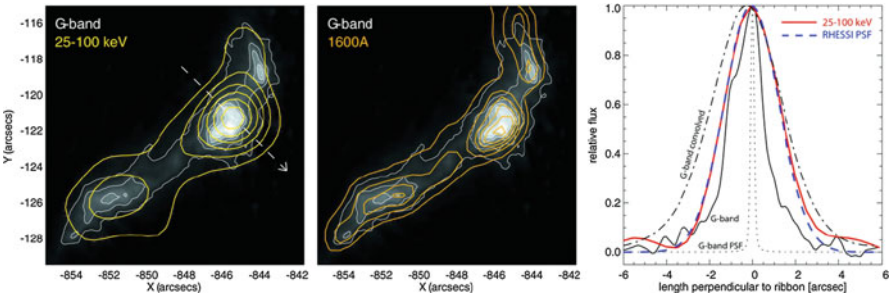

Fig. 13.6 Left panel: Background-subtracted G-band emission from SOT overlaid with 25–100 keV hard X-ray contours from RHESSI. Middle panel: Background-subtracted G-band emission overlayed with *TRACE* 1600 Å contours. Right panel: Spatial profiles of the ribbon emission taken along the dotted line in the left panel (From Krucker et al. 2011, reproduced by permission of the AAS)

flares is evidence for this heating. Several studies have correlated G-band emissions from SOT with hard X-ray emission from *Reuven Ramaty High Energy Solar Spectroscopic Imager (RHESSI)*. K. Watanabe et al. (2010a) analyzed an X class from December 14, 2006, and found that the G-band emissions and the hard X-rays from *RHESSI* are well-correlated in time and space and that the white light power and the power of the accelerated electrons are proportional, independent of the assumed cutoff energy. Krucker et al. (2011) examined the SOT G-band emissions and *RHESSI* hard X-rays from a different X-class flare and found that the G-band ribbon is wider than the HXR ribbon, once instrument point spread functions are taken into account. This result, shown in Fig. 13.6, indicates that the hard X-rays in this event come from the sharp leading edge of the G-band ribbon. Given the energy deposition rate in this observation, the electron beam density must be high, causing some problems for the thick target model. Even so, these studies indicate that the accelerated particles play an important role in heating the lower layers of the solar atmosphere.

Although the hard X-rays from accelerated particles and footpoint emission in photospheric wavelengths appear to be correlated, accelerated particles do not penetrate down to the photosphere, so some other mechanisms must be responsible for the white light flare emission. Some candidates are chromospheric free-bound emission or blackbody emission from enhanced H^-. Emission from SOT has been used to diagnose this footpoint emission. Kerr and Fletcher (2014) investigated the SOT optical continuum emission in broadband red, blue, and green filters taken during a X2.2 flare. They found that the temperature increases derived from the emission are consistent with blackbody emission from the photosphere, though a photospheric origin for a white light source is hard to explain. A chromospheric source is also possible, but the temperature findings indicate that this source must be heated if it exists. K. Watanabe et al. (2013) also look at the red, blue, and green continuum bands of SOT for a flare that occurred at the limb. They found that the heights of the sources in these three channels are consistent with heating in the

photosphere. Nevertheless, this question is far from solved, and measurements from *IRIS* and advanced modeling of the chromosphere are expected to shed more light on this issue in the near future.

13.4 Conclusions and Future Prospects

The last 10 years of *Hinode* data has provided a wealth of insight into the reconnection process. Reconnection outflows have been observed directly by XRT, and EIS has been instrumental in characterizing flows in the footpoint regions. Both of these instruments have been well suited to explore the turbulence that can occur in the supra-arcade region. The temperature coverage of EIS allows for a thorough characterization of footpoint flows as a function of temperature, and the high spatial resolution of SOT has provided insights into the energy deposition at flare footpoints. Evidence for heating in the plasma above the flare loops has been recorded by XRT and EIS.

For all of these advances, there are still discoveries to be made. For example, *IRIS*, with its high spatial and temporal resolution, has been able to explore the evolution of hot plasma in the footpoint region via the Fe XXI line formed at around 10 MK (Young et al. 2015; Tian et al. 2015; Polito et al. 2015, 2016). This line is the only strong coronal line available to *IRIS*, however, so there is currently no understanding of how the footpoint plasma evolves thermally on short timescales during flares. Understanding this evolution could give valuable insight to the energy release process during reconnection. Similarly, high-resolution imaging of hot supra-arcade plasma could give insight into the fundamental size scale of supra-arcade downflows. These features have been observed down to the resolution of current instrumentation (McKenzie and Savage 2009; Savage et al. 2012), and an accurate cataloging of their sizes could give insight into the reconnection process that creates them. Finally, detailed knowledge of the magnetic field structure higher in the atmosphere would be extremely useful for understanding the reconnection process. These measurements are starting to be explored by the COSMO (Coronal Solar Magnetism Observatory) telescope at Mauna Loa Solar Observatory and will be probed by the NSO (National Solar Observatory)'s DKIST (Daniel K. Inouye Solar Telescope) facility in the future.

References

Antonucci, E., Dodero, M.A., Peres, G., Serio, S., Rosner, R.: Simulations of the CA XIX spectral emission from a flaring solar coronal loop. I – thermal case. Astrophys. J. **322**, 522–543 (1987). https://doi.org/10.1086/165748

Asai, A., Yokoyama, T., Shimojo, M., Shibata, K.: Downflow motions associated with impulsive nonthermal emissions observed in the 2002 July 23 solar flare. ApJL **605**, L77–L80 (2004). https://doi.org/10.1086/420768

Brosius, J.W.: Chromospheric evaporation in solar flare loop strands observed with the extreme-ultraviolet imaging spectrometer on board Hinode. Astrophys. J. **762**, 133 (2013). https://doi.org/10.1088/0004-637X/762/2/133

Brosius, J.W., Phillips, K.J.H.: Extreme-ultraviolet and x-ray spectroscopy of a solar flare loop observed at high time resolution: a case study in chromospheric evaporation. Astrophys. J. **613**, 580–591 (2004). https://doi.org/10.1086/422873

Culhane, J.L., Harra, L.K., James, A.M., Al-Janabi, K., Bradley, L.J., Chaudry, R.A., Rees, K., Tandy, J.A., Thomas, P., Whillock, M.C.R., Winter, B., Doschek, G.A., Korendyke, C.M., Brown, C.M., Myers, S., Mariska, J., Seely, J., Lang, J., Kent, B.J., Shaughnessy, B.M., Young, P.R., Simnett, G.M., Castelli, C.M., Mahmoud, S., Mapson-Menard, H., Probyn, B.J., Thomas, R.J., Davila, J., Dere, K., Windt, D., Shea, J., Hagood, R., Moye, R., Hara, H., Watanabe, T., Matsuzaki, K., Kosugi, T., Hansteen, V., Wikstol, Ø.: The EUV imaging spectrometer for Hinode. Sol. Phys. **243**, 19–61 (2007). https://doi.org/10.1007/s01007-007-0293-1

Czaykowska, A., de Pontieu, B., Alexander, D., Rank, G.: Evidence for chromospheric evaporation in the late gradual flare phase from SOHO/CDS observations. ApJL **521**, L75–L78 (1999). https://doi.org/10.1086/312176

Doschek, G.A., McKenzie, D.E., Warren, H.P.: Plasma dynamics above solar flare soft X-ray loop tops. Astrophys. J. **788**, 26 (2014). https://doi.org/10.1088/0004-637X/788/1/26

Doschek, G.A., Warren, H.P., Dennis, B.R., Reep, J.W., Caspi, A.: Flare footpoint regions and a surge observed by Hindode/EIS, RHESSI, and SDO/AIA. Astrophys. J. **813**, 32 (2015). https://doi.org/10.1088/0004-637X/813/1/32

Fisher, G.H., Canfield, R.C., McClymont, A.N.: Flare loop radiative hydrodynamics – part seven – dynamics of the thick target heated chromosphere. Astrophys. J. **289**, 434–441 (1985a). https://doi.org/10.1086/162903

Fisher, G.H., Canfield, R.C., McClymont, A.N.: Flare loop radiative hydrodynamics – part six – chromospheric evaporation due to heating by nonthermal electrons. Astrophys. J. **289**, 425–433 (1985b). https://doi.org/10.1086/162902

Fisher, G.H., Canfield, R.C., McClymont, A.N.: Flare loop radiative hydrodynamics. V – Response to thick-target heating. VI – chromospheric evaporation due to heating by nonthermal electrons. VII – dynamics of the thick-target heated chromosphere. Astrophys. J. **289**, 414–441 (1985c). https://doi.org/10.1086/162901

Forbes, T.G., Acton, L.W.: Reconnection and field line shrinkage in solar flares. Astrophys. J. **459**, 330–341 (1996)

Golub, L., Deluca, E., Austin, G., Bookbinder, J., Caldwell, D., Cheimets, P., Cirtain, J., Cosmo, M., Reid, P., Sette, A., Weber, M., Sakao, T., Kano, R., Shibasaki, K., Hara, H., Tsuneta, S., Kumagai, K., Tamura, T., Shimojo, M., McCracken, J., Carpenter, J., Haight, H., Siler, R., Wright, E., Tucker, J., Rutledge, H., Barbera, M., Peres, G., Varisco, S.: The X-ray telescope (XRT) for the Hinode mission. Sol. Phys. **243**, 63–86 (2007). https://doi.org/10.1007/s11207-007-0182-1

Hanneman, W.J., Reeves, K.K.: Thermal structure of current sheets and supra-arcade downflows in the solar corona. Astrophys. J. **786**, 95 (2014). https://doi.org/10.1088/0004-637X/786/2/95

Hara, H., Watanabe, T., Matsuzaki, K., Harra, L.K., Culhane, J.L., Cargill, P., Mariska, J.T., Doschek, G.A.: 2006 December 17 long duration flare observed with the Hinode EUV imaging spectrometer. PASJ **60**, 275– (2008)

Hara, H., Watanabe, T., Harra, L.K., Culhane, J.L., Young, P.R.: Plasma motions and heating by magnetic reconnection in a 2007 May 19 flare. Astrophys. J. **741**, 107 (2011). https://doi.org/10.1088/0004-637X/741/2/107

Imada, S., Aoki, K., Hara, H., Watanabe, T., Harra, L.K., Shimizu, T.: Evidence for hot fast flow above a solar flare arcade. ApJL **776**, L11 (2013). https://doi.org/10.1088/2041-8205/776/1/L11

Imada, S., Murakami, I., Watanabe, T.: Observation and numerical modeling of chromospheric evaporation during the impulsive phase of a solar flare. Phys. Plasmas **22**(10), 101206 (2015). https://doi.org/10.1063/1.4932335

Innes, D.E., McKenzie, D.E., Wang, T.: Observations of 1000 km s^{-1} Doppler shifts in 10^7 K solar flare supra-arcade. Sol. Phys. **217**, 267–279 (2003a)
Innes, D.E., McKenzie, D.E., Wang, T.: SUMER spectral observations of post-flare supra-arcade inflows. Sol. Phys. **217**, 247–265 (2003b)
Kano, R., Sakao, T., Hara, H., Tsuneta, S., Matsuzaki, K., Kumagai, K., Shimojo, M., Minesugi, K., Shibasaki, K., Deluca, E.E., Golub, L., Bookbinder, J., Caldwell, D., Cheimets, P., Cirtain, J., Dennis, E., Kent, T., Weber, M.: The Hinode X-ray telescope (XRT): camera design, performance and operations. Sol. Phys. **249**, 263–279 (2008). https://doi.org/10.1007/s11207-007-9058-7
Kerr, G.S., Fletcher, L.: Physical properties of white-light sources in the 2011 February 15 solar flare. Astrophys. J. **783**, 98 (2014). https://doi.org/10.1088/0004-637X/783/2/98
Kosugi, T., Matsuzaki, K., Sakao, T., Shimizu, T., Sone, Y., Tachikawa, S., Hashimoto, T., Minesugi, K., Ohnishi, A., Yamada, T., Tsuneta, S., Hara, H., Ichimoto, K., Suematsu, Y., Shimojo, M., Watanabe, T., Shimada, S., Davis, J.M., Hill, L.D., Owens, J.K., Title, A.M., Culhane, J.L., Harra, L.K., Doschek, G.A., Golub, L.: The Hinode (solar-B) mission: an overview. Sol. Phys. **243**, 3–17 (2007). https://doi.org/10.1007/s11207-007-9014-6
Krucker, S., Hudson, H.S., Jeffrey, N.L.S., Battaglia, M., Kontar, E.P., Benz, A.O., Csillaghy, A., Lin, R.P.: High-resolution imaging of solar flare ribbons and its implication on the thick-target beam model. Astrophys. J. **739**, 96 (2011). https://doi.org/10.1088/0004-637X/739/2/96
Landi, E., Raymond, J.C., Miralles, M.P., Hara, H.: Physical conditions in a Coronal Mass ejection from Hinode, stereo, and SOHO observations. Astrophys. J. **711**, 75–98 (2010). https://doi.org/10.1088/0004-637X/711/1/75
Landi, E., Raymond, J.C., Miralles, M.P., Hara, H.: Post-coronal Mass ejection plasma observed by Hinode. Astrophys. J. **751**, 21 (2012). https://doi.org/10.1088/0004-637X/751/1/21
Landi, E., Miralles, M.P., Raymond, J.C., Hara, H.: Hot plasma associated with a coronal Mass ejection. Astrophys. J. **778**, 29 (2013). https://doi.org/10.1088/0004-637X/778/1/29
Lazarian, A., Vishniac, E.T.: Reconnection in a weakly stochastic field. Astrophys. J. **517**, 700–718 (1999). https://doi.org/10.1086/307233
Lee, J.Y., Raymond, J.C., Reeves, K.K., Moon, Y.J., Kim, K.S.: Mass and energy of erupting solar plasma observed with the X-ray telescope on Hinode. Astrophys. J. **798**, 106 (2015). https://doi.org/10.1088/0004-637X/798/2/106
Lin, J.: CME-flare association deduced from catastrophic model of CMEs. Sol. Phys. **219**, 169–196 (2004)
Lin, J., Ko, Y.K., Sui, L., Raymond, J.C., Stenborg, G.A., Jiang, Y., Zhao, S., Mancuso, S.: Direct observations of the magnetic reconnection site of an eruption on 2003 November 18. Astrophys. J. **622**, 1251–1264 (2005). https://doi.org/10.1086/428110
Liu, W., Petrosian, V., Dennis, B.R., Holman, G.D.: Conjugate hard X-ray footpoints in the 2003 October 29 X10 flare: unshearing motions, correlations, and asymmetries. Astrophys. J. **693**, 847–867 (2009). https://doi.org/10.1088/0004-637X/693/1/847
Liu, W., Chen, Q., Petrosian, V.: Plasmoid ejections and loop contractions in an eruptive M7.7 solar flare: evidence of particle acceleration and heating in magnetic reconnection outflows. Astrophys. J. **767**, 168 (2013). https://doi.org/10.1088/0004-637X/767/2/168
McKenzie, D.E.: Turbulent dynamics in solar flare sheet structures measured with local correlation tracking. Astrophys. J. **766**, 39 (2013). https://doi.org/10.1088/0004-637X/766/1/39
McKenzie, D.E., Hudson, H.S.: X-ray observations of motions and structure above a solar flare arcade. ApJL **519**, L93–L96 (1999). https://doi.org/10.1086/312110
McKenzie, D.E., Savage, S.L.: Quantitative examination of supra-arcade downflows in eruptive solar flares. Astrophys. J. **697**, 1569–1577 (2009). https://doi.org/10.1088/0004-637X/697/2/1569
Milligan, R.O.: Spatially resolved nonthermal line broadening during the impulsive phase of a solar flare. Astrophys. J. **740**, 70 (2011). https://doi.org/10.1088/0004-637X/740/2/70
Milligan, R.O., Dennis, B.R.: Velocity characteristics of evaporated plasma using Hinode/EUV imaging spectrometer. Astrophys. J. **699**, 968–975 (2009). https://doi.org/10.1088/0004-637X/699/2/968

Milligan, R.O., Gallagher, P.T., Mathioudakis, M., Bloomfield, D.S., Keenan, F.P., Schwartz, R.A.: RHESSI and SOHO CDS observations of explosive chromospheric evaporation. ApJL **638**, L117–L120 (2006). https://doi.org/10.1086/500555

Nindos, A., Patsourakos, S., Vourlidas, A., Tagikas, C.: How common are hot magnetic flux ropes in the low solar corona? A statistical study of EUV observations. Astrophys. J. **808**, 117 (2015). https://doi.org/10.1088/0004-637X/808/2/117

Nitta, S., Imada, S., Yamamoto, T.T.: Clear detection of chromospheric evaporation upflows with high spatial/temporal resolution by Hinode XRT. Sol. Phys. **276**, 183–197 (2012). https://doi.org/10.1007/s11207-011-9890-7

Polito, V., Reeves, K.K., Del Zanna, G., Golub, L., Mason, H.E.: Joint high temperature observation of a small C6.5 solar flare with Iris/Eis/Aia. Astrophys. J. **803**, 84 (2015). https://doi.org/10.1088/0004-637X/803/2/84

Polito, V., Reep, J.W., Reeves, K.K., Simões, P.J.A., Dudík, J., Del Zanna, G., Mason, H.E., Golub, L.: Simultaneous IRIS and Hinode/EIS observations and modelling of the 2014 October 27 X2.0 class flare. Astrophys. J. **816**, 89 (2016). https://doi.org/10.3847/0004-637X/816/2/89

Reeves, K.K., Golub, L.: Atmospheric imaging assembly observations of hot flare plasma. ApJL **727**, L52 (2011). https://doi.org/10.1088/2041-8205/727/2/L52

Reeves, K.K., Seaton, D.B., Forbes, T.G.: Field line shrinkage in flares observed by the X-ray telescope on Hinode. Astrophys. J. **675**, 868–874 (2008). https://doi.org/10.1086/526336

Savage, S.L., McKenzie, D.E.: Quantitative examination of a large sample of supra-arcade downflows in eruptive solar flares. Astrophys. J. **730**, 98 (2011). https://doi.org/10.1088/0004-637X/730/2/98

Savage, S.L., McKenzie, D.E., Reeves, K.K., Forbes, T.G., Longcope, D.W.: Reconnection outflows and current sheet observed with Hinode/XRT in the 2008 April 9 "Cartwheel CME" flare. Astrophys. J. **722**, 329–342 (2010). https://doi.org/10.1088/0004-637X/722/1/329

Savage, S.L., McKenzie, D.E., Reeves, K.K.: Re-interpretation of supra-arcade downflows in solar flares. Astrophys. J. **747**, L40 (2012)

Schanche, N.E., Reeves, K.K., Webb, D.F.: The blob connection: searching for low coronal signatures of solar post-CME blobs. Astrophys. J. **831**, 47 (2016). https://doi.org/10.3847/0004-637X/831/1/47

Suematsu, Y., Tsuneta, S., Ichimoto, K., Shimizu, T., Otsubo, M., Katsukawa, Y., Nakagiri, M., Noguchi, M., Tamura, T., Kato, Y., Hara, H., Kubo, M., Mikami, I., Saito, H., Matsushita, T., Kawaguchi, N., Nakaoji, T., Nagae, K., Shimada, S., Takeyama, N., Yamamuro, T.: The solar optical telescope of solar-B (Hinode): the optical telescope assembly. Sol. Phys. **249**, 197–220 (2008). https://doi.org/10.1007/s11207-008-9129-4

Tian, H., Young, P.R., Reeves, K.K., Chen, B., Liu, W., McKillop, S.: Temporal evolution of chromospheric evaporation: case studies of the M1.1 flare on 2014 September 6 and X1.6 flare on 2014 September 10. Astrophys. J. **811**, 139 (2015). https://doi.org/10.1088/0004-637X/811/2/139

Tsuneta, S., Ichimoto, K., Katsukawa, Y., Nagata, S., Otsubo, M., Shimizu, T., Suematsu, Y., Nakagiri, M., Noguchi, M., Tarbell, T., Title, A., Shine, R., Rosenberg, W., Hoffmann, C., Jurcevich, B., Kushner, G., Levay, M., Lites, B., Elmore, D., Matsushita, T., Kawaguchi, N., Saito, H., Mikami, I., Hill, L.D., Owens, J.K.: The solar optical telescope for the Hinode mission: an overview. Sol. Phys. **249**, 167–196 (2008). https://doi.org/10.1007/s11207-008-9174-z

Watanabe, K., Krucker, S., Hudson, H., Shimizu, T., Masuda, S., Ichimoto, K.: G-band and hard X-ray emissions of the 2006 December 14 flare observed by Hinode/SOT and Rhessi. Astrophys. J. **715**, 651–655 (2010a). https://doi.org/10.1088/0004-637X/715/1/651

Watanabe, T., Hara, H., Sterling, A.C., Harra, L.K.: Production of high-temperature plasmas during the early phases of a C9.7 flare. Astrophys. J. **719**, 213–219 (2010b). https://doi.org/10.1088/0004-637X/719/1/213

Watanabe, K., Shimizu, T., Masuda, S., Ichimoto, K., Ohno, M.: Emission height and temperature distribution of white-light emission observed by Hinode/SOT from the 2012 January 27 X-class solar flare. Astrophys. J. **776**, 123 (2013). https://doi.org/10.1088/0004-637X/776/2/123

Young, P.R., Doschek, G.A., Warren, H.P., Hara, H.: Properties of a solar flare kernel observed by Hinode and SDO. Astrophys. J. **766**, 127 (2013). https://doi.org/10.1088/0004-637X/766/2/127

Young, P.R., Tian, H., Jaeggli, S.: The 2014 March 29 X-flare: subarcsecond resolution observations of Fe XXI λ1354.1. Astrophys. J. **799**, 218 (2015). https://doi.org/10.1088/0004-637X/799/2/218

Zhang, Q.M., Ji, H.S.: Chromospheric evaporation in sympathetic coronal bright points. A&A **557**, L5 (2013). https://doi.org/10.1051/0004-6361/201321908

Chapter 14
The First Decade of *Hinode*: Understanding Coronal Mass Ejections

Louise Harra

Abstract In 2016, the *Hinode* spacecraft completed ten successful years of operations. This paper aims to summarise the observations of coronal mass ejections that have been made, using *Hinode*'s three instruments. The three instruments have allowed measurements of magnetic field changes, and plasma dynamics, in the time before the eruption and during the eruption itself. This has provided us with key boundary conditions for the models and has opened up new understanding of the process of triggering an eruption.

Keywords Sun:activity · Coronal mass ejections

14.1 Introduction

This paper aims to describe the novel observations of coronal mass ejections (CMEs) that have been produced from *Hinode*'s three instruments – the extreme ultraviolet (EUV) Imaging Spectrometer (EIS), the X-Ray Telescope (XRT) and the Solar Optical Telescope (SOT). Between them, the three instruments cover much of the solar atmosphere, being able to measure the flows and magnetic fields in the photosphere, the chromosphere through imaging and the corona through spectroscopy and imaging. These observations will be discussed in the context of constraining models of CMEs and highlighting observations that change the way we view what CMEs are and what they are made of.

There are a number of models that have been developed to explain how CMEs erupt (or become failed eruptions). The eruptions tend to start off slowly and have a rapid acceleration phase. The models that can potentially explain this are summarised below.

L. Harra (✉)
UCL-Mullard Space Science Laboratory, Dorking, Surrey, UK
e-mail: l.harra@ucl.ac.uk

T. Shimizu et al. (eds.), *First Ten Years of Hinode Solar On-Orbit Observatory*,
Astrophysics and Space Science Library 449,
https://doi.org/10.1007/978-981-10-7742-5_14

- flux emergence: magnetic field is key to any CME model, and new emergence is often seen hours or days ahead of a CME.
- flux cancellation: shearing, convergence and reconnection in the photosphere can lead to the formation of a flux rope through flux cancellation e.g. van Ballegooijen and Martens (1989)
- kink instability: the flux rope develops significant rotation or writhing, with the twist exceeding a critical value Török and Kliem (2005)
- torus instability: the flux rope which is embedded in an ambient field shows an outward expansion, which along with a rapid decrease in vertical magnetic field strength with height above the flux rope allows an eruption to proceed e.g. Kliem and Török (2006)
- tether-cutting: slow reconnection occurring at the footpoints of a sheared loop system which results the weakening of the overlying magnetic field, allowing the eruption to proceed e.g. Moore et al. (2001)
- breakout model: reconnection occurs above a sheared arcade at a magnetic null point created between the arcade and overlying field, weakening the overlying field to allow the eruption to occur e.g. Antiochos et al. (1999)

There could potentially be several of these occurring to create an eruption. We will refer to these different options throughout this paper. Although the author has attempted to cover as broad a range of publications as possible, it is inevitable that works will be missed during this decade of discovery.

14.2 The Build-Up to a CME

The first stage of a CME is the build-up phase. Flux ropes are a likely initial magnetic configuration of a CME – filling the whole volume of a dark coronal cavity that is so frequently seen in coronagraph data. When and where flux ropes are formed have been a subject of debate for many years. There are two possibilities:

- The flux rope is formed during the eruption: this can happen if there is a sheared arcade, which can lead to the formation of a flux rope through the process of reconnection during the eruption.
- The flux rope is formed before the eruption: this can happen through reconnection low in the atmosphere creating a flux rope that could contain filament material.

During this article, there will be many references to flux ropes and when they form.

One of the most recognisable structures that are related to CMEs in the corona are 'S'-shaped structures which were discovered in X-rays during the *Yohkoh* era. The XRT observations of sigmoids have illustrated that the structure is complex, consisting of many differently orientated loops that form two opposite J-like bundles giving an overall S-shaped structure (McKenzie and Canfield 2008). The erupting structure showed the rising of a flux ropelike structure from the middle of the

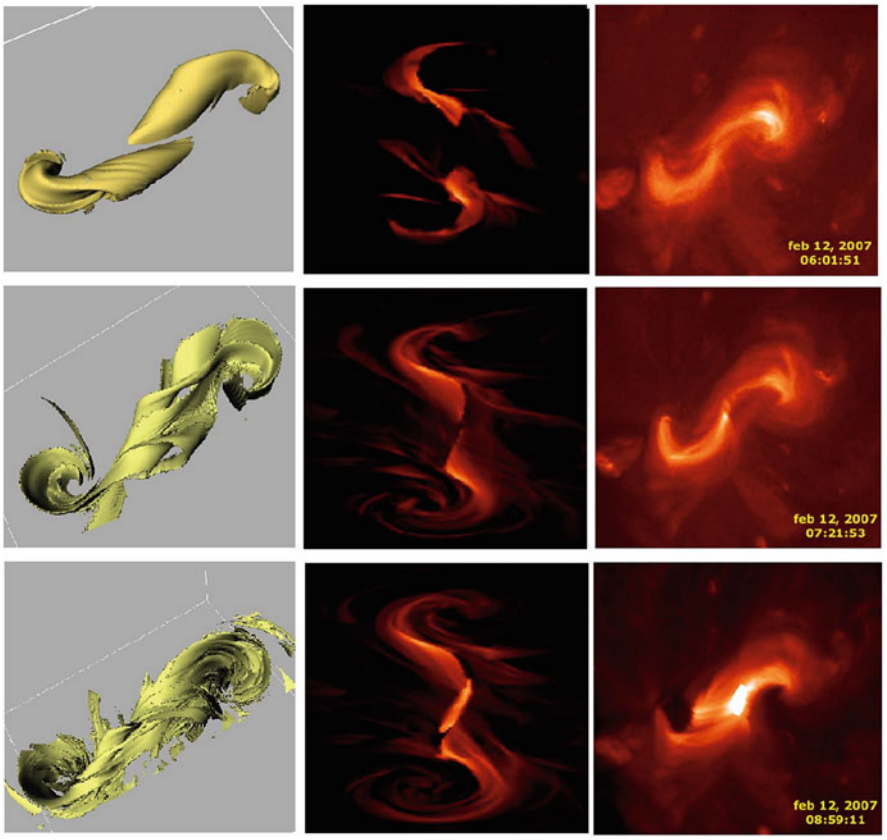

Fig. 14.1 A comparison between the simulations (left and middle) and observations (right). The left panels show the constant current surfaces, and the middle shows the heating term (Adapted from Figure 11 in Archontis et al. (2009) by permission of the AAS)

sigmoid and X-ray flaring between the two J-shaped structures. This new world of X-ray observations has led to advancement of boundaries in modelling. A flux emergence model was developed by Archontis et al. (2009) that is consistent with the observations. The model begins with a twisted flux rope below the surface that rises. The expanding field lines emerge into the photosphere at bald patches and form two separatrix surfaces where current sheets can form. Originally the separatrix surfaces have a J-like shape as is seen in the observations as can be seen in Fig. 14.1. Expansion of the sigmoidal active region has also been observed by (Baker et al. 2012) who found spectroscopic signatures of increased velocities 4 h before the CME occurred. The upflows in and around an active region were studied over days by Imada et al. (2014). The outer part of the active region loops that have a low density expands around a day before the eruption, and the high-density inner active region loops expand a few hours before the onset.

A sigmoid has been observed to appear 2 h before a CME by James et al. (2017). In this example, they also had spectroscopic data from *Hinode*/EIS providing information on the composition of the flux rope. Understanding the composition is key to determining where the flux rope was formed. In this example, the composition was found to be coronal indicating that the flux rope was formed in the corona. There have been many observations of the critical few hours before a CME erupts. One of the best observed flares and CMEs was the X-class flare on March 29, 2014. This event was observed by virtually all available space- and ground-based observations providing valuable spectroscopic and imaging information. A filament eruption was observed above a region where flux emergence had previously occurred (Kleint et al. 2015). The filament eruption appeared to change the magnetic configuration such that the large flare occurred – the hard X-ray emission was seen just 1 min after the eruption occurred. Flows in the chromosphere appeared at least an hour before the flare occurred, and their speed increased just 15 min before the filament erupted. The filament lifted off with a speed of 600 km s^{-1} measured in the chromosphere – which is consistent with the average speeds of CMEs. The early phase of this flare was further explored by Woods et al. (2017) who found that 40 min before the flare strong flows were seen throughout the atmosphere and at spatially discrete locations along the filament that would soon erupt. The speeds are fast reaching up to 200 km s^{-1} (see Fig. 14.2). Modelling work was also carried out indicating that a

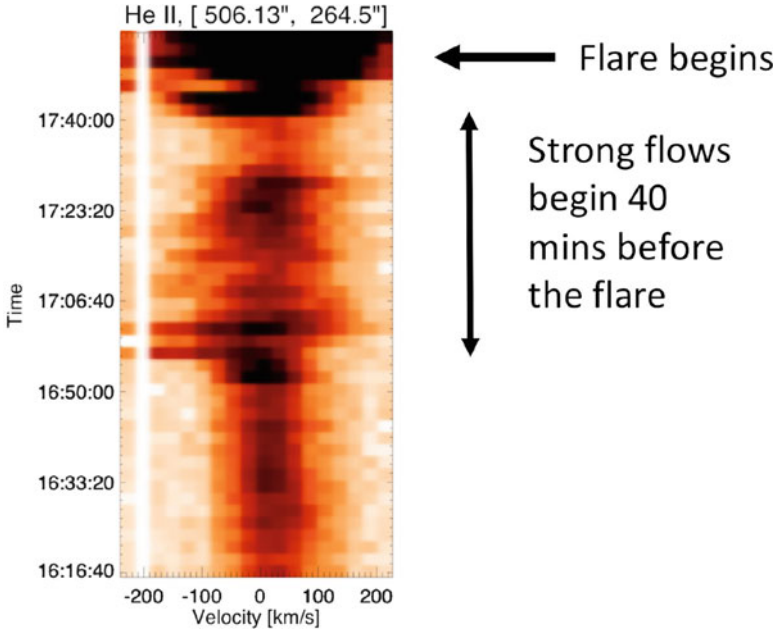

Fig. 14.2 Pre-event flows observed for SOL2014-03-29T17:48 as measured by *Hinode*-EIS. These show very fast flows 40 min before the eruption took place (Adapted from Woods et al. (2017) by permission of the Springer)

flux rope existed for days before the CME. They conclude that these observations and modelling are consistent with internal reconnection in the flux rope, early onset of the flare reconnection or tether-cutting reconnection along the filament.

XRT observations of sigmoids have also been compared to a model of torus-unstable flux ropes (Aulanier et al. 2010). In their MHD simulation, sheared arcades are formed through flux cancellation photospheric reconnection. The sheared arcades slowly rise and form a stable flux rope. As the flux rope grows, tether-cutting reconnection occurs in the corona. However the transition to eruption occurs only when the criterion for the torus instability is fulfilled. So in this work, they describe tether-cutting and flux cancellation as key to form rising flux ropes, but the torus instability actually causes the eruption.

The importance of sigmoids has been highlighted by the development of a sigmoid catalogue by Savcheva et al. (2014) that includes two long-lasting sigmoids. From this catalogue, it has been possible to characterise their magnetic and plasma properties. It has been found that flux cancellation is seen more frequently than flux emergence during the eruptive stages. This is important feedback for any CME model. Sigmoids are not a necessary configuration for a CME but are providing useful constraints for models because of their strong correlation with CMEs.

The pre-eruptive characteristics for two very fast CMEs were analysed by Syntelis et al. (2016), and it was found that in part of the region, the mean differential emission measure (DEM) in the hot temperature range increased by an order or magnitude 5 h before the first CME. This was associated with the gradual rise of the flux rope, which has associated dynamics observed with it of the order of $12\,\mathrm{km\,s^{-1}}$. Often the CMEs analysed are associated with large solar flares; however in the work by Reeves et al. (2015), a small prominence eruption was studied combining data from *Hinode*, *Interface Region Imaging Spectrograph (IRIS)* and *Solar Dynamics Observatory (SDO)*. They found the 'typical' slow rise ($0.4\,\mathrm{km\,s^{-1}}$) followed by a fast rise ($250\,\mathrm{km\,s^{-1}}$). During the transition period between these two phases, small-scale brightenings were observed which were consistent with a tether-cutting rather than a breakout mechanism. Evidence for the kink instability process was found by Williams et al. (2009) who measured Doppler shifts axisymmetric along the filament which are consistent with an expanding, untwisting flux rope that occurred minutes before the flare began.

Early signatures of coronal emission enhancements in nonthermal velocity (enhanced line widths) have been observed for many years, but the source has been debated. *Hinode*-EIS provides the spatial as well as spectral information to determine where and what these enhancements are. Four flares were analysed by Harra et al. (2013), and it was found that the pre-event nonthermal velocity signatures were located where the later dimming regions would be found following the eruption of the CME (Fig. 14.3). This spectroscopic signature highlights the activation of a coronal flux rope before the event and could be a useful way to determine whether a region will erupt or not.

Other modelling work has been carried out by Kusano et al. (2012), using the SOT magnetograms as input. They found that both stored free energy and a disturbance of the magnetic field are required to obtain an eruption. The latter can be

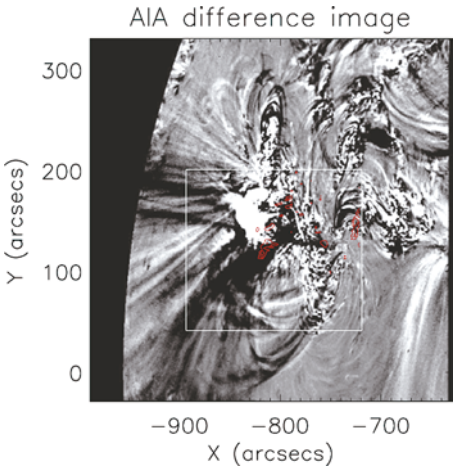

Fig. 14.3 An AIA difference image for the flare on 24 September. The red contours show where the pre-event enhanced coronal nonthermal velocities determined by *Hinode* EIS are, which are at the ends of the flux rope, which is highlighted post-eruption through dimming (Adapted from Figure 5 in Harra et al. (2013) by permission of the AAS)

caused by small magnetic elements, which means that the prediction timescale for an eruption is linked to the lifetime and behaviour of these small magnetic elements – which is a few hours. Many of the observational enhancements seen related to flows and nonthermal velocity are on similar short timescales.

In addition to these pre-event signatures, it is also observed that precursor CMEs can happen. Analyses by Sterling et al. (2011) have shown that two eruptions occurred before the famous December 13, 2006, X-flare and CME. The two earlier eruptions are offset to the main CME but form part of the destabilisation process.

14.3 Observations of the CME

A key element of any CME model is the magnetic field. The high-resolution magnetograms from *Hinode* have been combined with Helioseismic and Magnetic Imager (HMI) data to construct the three-dimensional (3D) coronal magnetic field using non-linear force-free field assumptions by Liu et al. (2012). They were able to measure rapid changes in the mean horizontal field at the centre of the sigmoid. They also found that strong currents are observed immediately above the region and that the coronal current collapsed after the sigmoid eruption. The results are consistent with tether-cutting reconnection producing the flare and implosion of the coronal field following the energy release.

Coronal dimming is an on-disc signature that indicates where the plasma comes from to form the CME. It is observed in the EUV and X-ray as a sudden depletion of coronal plasma and may last several hours. The dimming had been observed with imagers, until the launch of *Hinode*, when it was observed with the EIS instrument (Harra et al. 2007). This event was the first major flare and CME observed by the *Hinode* spacecraft on December 13, 2006. The region that showed strong coronal

dimming could be measured spectroscopically, and upflows of tens of $\mathrm{km\,s^{-1}}$ were measured – demonstrating that dimming regions are regions where coronal plasma is hurled upwards. This work was expanded on by Imada et al. (2007), and they found a temperature dependence of the dimming. There are weak upflows for low-temperature plasma, but once the plasma is more than a million Kelvin (MK), then the flows begin. This behaviour is consistent with coronal heating and solar wind formation models. They carried out models for these temperature-dependent upflows in Imada et al. (2011) and found that they are suggestive of strong heating occurring about 7 Mm in altitude above the surface in the dimming region. The strongest flows are seen for the fastest temperatures. It has also been found that the dimming line profiles can be caused by the superposition of a weak high-speed component and a strong low-speed component (Tian et al. 2012). The high-speed component can reach $100\,\mathrm{km\,s^{-1}}$. In the same paper, Tian et al. (2012) found that outflows existed immediately outside the deepest dimming region, which may be caused by evaporation flows from recently reconnected field lines. In addition to blueshift found in the dimming region, (Chen et al. 2010) found that the widths of all four spectral lines they analysed increase at the outer edge of the dimmings. They suggest that these may be generated by the successive stretching of the closed field lines.

14.4 Propagation of the CME

The CMEs propagate into interplanetary space. It is challenging linking the observations made on the Sun, with those from in situ measurements that are taken at only one point in space. It is important nonetheless to try and characterise the CME, as it propagates away from the Sun, as it will travel through the heliosphere, encountering planets on its way. Observations from the *Hinode*, *Solar and Heliospheric Observatory (SoHO)* and *Solar Terrestrial Relations Observatory (STEREO)* missions allowed analysis of a CME up to 22 solar radii by Landi et al. (2010). Understanding the acceleration and heating provides key boundary conditions to CME models. From the combination of data analysed, they could determine the heating required to maintain the plasma temperatures observed up to 1.9 solar radii. This was found to be several times that of kinetic energy and hence has to be factored in to the energy budget. Magnetic heating, shocks generated from outflows from the reconnection region and energetic particles all could be consistent with this level of heating. Seven eruptive events were analysed by Lee et al. (2015), and it was found that the CME mass in X-rays (determined by *Hinode*/XRT) was lower than that in white light (determined by *SoHO*/LASCO). The XRT data only shows the hot temperature plasma, whereas the white-light data covers all temperatures, so this difference can be explained. They also studied the thermal conduction time and found in some cases that this was shorter than the duration of the event so additional heating is needed.

Reconnection flows have been measured through the observations of supra-arcade downflows that have been observed in flares since the *Yohkoh* era. A correlation is found by Savage et al. (2010) between the reconnection outflows observed with XRT and the outgoing flows in the CME observed by *SoHO*/LASCO. In this observation, there was evidence of a current sheet extending between the flare arcade and the CME. Most models for CMEs predict a current sheet that develops beneath the erupting flus rope due to the expansion of the overlying magnetic field. Since they are such key aspects of CMEs, modelling has been carried out by Ko et al. (2010) who were able to replicate the observations in *SoHO*'s Ultraviolet Coronagraph Spectrometer (UVCS) and XRT and found a reconnection inflow speed of $10\,\mathrm{km\,s^{-1}}$ and a reconnection rate of 0.01.

One way to observe the propagation of the CME is through the observations of 'EUV coronal waves' (previously known as EIT[1] waves) e.g. Patsourakos and Vourlidas (2012). These coronal waves are always observed with CMEs, which are an important element to understanding CMEs. Spectroscopic measurements in the corona have been carried out at the edge of the coronal wave, and it was found that the line widths increase at the outer edge of the propagation. This is consistent with the field line stretching model, which suggests that the EIT waves are created by moving brightenings produced by the successive stretching of the closed magnetic fields as the CME lifts off. Other work by Balasubramaniam et al. (2010) has found that the CME drove a coronal shock which was responsible for a Moreton wave (observed in the chromosphere).

The rapid increase in the nonthermal velocity is followed by a slow decrease as observed by Attrill et al. (2008). This appears to be the result of the closing and gradual filling of the corona as the CME leaves the Sun. The behaviour of dimming has many analogies with coronal holes, and McIntosh (2009) has involved Alfvén waves and suggested that the dynamic evolution of nonthermal velocity is due to the growth of Alfvén wave amplitudes in the open magnetic field dimming region. Alternative work by Dolla and Zhukov (2011), studying the line profiles in detail, has found that the broadening and asymmetries found in the line profiles can be explained by inhomogeneities of flow velocities along the line of sight. An increase in the amplitude of the Alfvén waves could not explain all of the observed features. Models have been developed to fit the pre-eruption state and then progress to eruption by Su et al. (2011). The footpoints of the erupting flux rope are located around the coronal dimming regions, reinforcing their importance. The motion of the dimmings changes with time. In one example, (Miklenic et al. 2011) found that this motion reflects not only the eruption of a flux rope but also the stretching of the overlying arcade. These dimmings were also compared with the CME mass loss itself. Analysis by Jin et al. (2009) explored the relationship of the upflows in dimming regions and the magnetic field and found a positive correlation. They also

[1]Extreme ultraviolet Imaging Telescope

measured the mass loss based on height-dependent EUV dimmings and found it smaller than the CME mass derived from white-light observations. This may be due to the atmospheric model chosen.

A new technique has been developed from the observations of these coronal waves to probe the magnetic field in the corona – a parameter that is extremely hard to measure directly. Using kinematics from Atmospheric Imaging Assembly (AIA) and spectroscopic measurements of density from *Hinode*/EIS, the magnetic field strength in the corona was determined to be 2-6G in the quiet corona (Long et al. 2013). Modelling was used to indicate that these waves are global phenomena influenced by the global magnetic field. The overlying magnetic field is an important element in understanding whether a CME can become eruptive. However, using SOT and *SDO*/HMI, Nindos et al. (2012) found that although how fast the magnetic field decreases with height (the decay index) is important, the actual initiation of the eruption does not depend on the temporal evolution of the change in the overlying magnetic field.

Analysis of the dimming region, using spectroscopic data in the corona, allowed an accurate measurement of the CME source. Rather than using an intensity difference method often used in dimming measurements, Harra et al. (2011) used a velocity difference method. This guarantees that the region that is actually lifting off can be isolated. The problem with relying on dimming measurements from imagers alone is that some of the changes seen may be due to temperature changes. The magnetic flux underneath the regions of velocity enhancement was used as a proxy for the ejected flux, compared with the magnetic cloud flux, and found to be consistent. This method does rely on large field of view observations using a spectrometer.

14.5 Summary

Hinode observations have allowed a decade of discoveries from small to large CMEs and are successfully providing constraints on many models. As we move into the second decade of observing with *Hinode*, with new fast modes of measuring magnetic fields, new plasma diagnostic techniques being developed and the rapidly developing models, we expect results to start to answer the key question of 'Can we predict when a CME will happen?' We look forward to the next decade!

Acknowledgements *Hinode* is a Japanese mission developed and launched by ISAS/JAXA, collaborating with NAOJ as a domestic partner and NASA and STFC(UK) as international partners. Scientific operations of the *Hinode* mission are conducted by the *Hinode* science team organised at ISAS/JAXA.

References

Antiochos, S.K., DeVore, C.R., Klimchuk, J.A.: A model for solar coronal Mass ejections. ApJ **510**, 485–493 (1999)

Archontis, V., Hood, A.W., Savcheva, A., Golub, L., Deluca, E.: On the structure and evolution of complexity in sigmoids: a flux emergence model. ApJ **691**, 1276–1291 (2009)

Attrill, G.D.R., et al: The recovery of CME-related dimmings and the ICME's enduring magnetic connection to the Sun. ApJ **252**, 349–372 (2008)

Aulanier, G., Török, T., Démoulin, P., DeLuca, E.E.: Formation of torus-unstable flux ropes and electric currents in erupting sigmoids. ApJ **708**, 314–333 (2010)

Baker, D., van Driel-Gesztelyi, L., Green, L.M.: Forecasting a CME by spectroscopic precursor? Sol. Phys. **276**, 219–239 (2012)

Balasubramaniam, K.S., et al.: On the origin of the solar Moreton wave of 2006 December 6. ApJ **723**, 587–601 (2010)

Chen, F., Ding, M.D., Chen, P.F.: Spectroscopic analysis of an EIT wave/dimming observed by Hinode/EIS. ApJ **720**, 1254–1261 (2010)

Dolla, L.R., Zhukov, A.N.: On the nature of the spectral line broadening in solar coronal dimmings. ApJ **730**, 113(14pp) (2011)

Harra, L.K., Hara, H., Imada, S., Young, P.R., Williams, D.R., Sterling, A.C., Korendyke, C., Attrill, G.D.R.: Coronal dimming observed with Hinode: outflows related to a Coronal Mass ejection. PASJ **59**, S801-S806 (2007)

Harra, L.K., Mandrini, C.H., Dasso, S., Gulisano, A.M., Steed, K., Imada, S.: Determining the solar source of a magnetic cloud using a velocity difference technique. Sol. Phys. **268**, 213–230 (2011)

Harra, L.K., Matthews, S.A., Culhane, J.L., Cheung, M.C.M., Kontar, E.P., Hara, H.: The location of non-thermal velocity in the early phases of large flares—revealing pre-eruption flux ropes. ApJ **774**, 122 (2013)

Imada, S., Hara, H., Watanabe, T., Kamio, S., Asai, A., Matsuzaki, K., Harra, L.K., Mariska, J.T.: Discovery of a temperature-dependent upflow in the plage region during a gradual phase of the X-class flare. PASJ **59**, S793-S799 (2007)

Imada, S., Hara, H., Watanabe, T., Murakami, I., Harra, L.K., Shimizu, T., Zweibel, E.G.: One-dimensional modeling for temperature-dependent upflow in the dimming region observed by Hinode/EUV imaging spectrometer. ApJ **743**, 57 (2011)

Imada, S., Bamba, Y., Kusano, K.: Coronal behavior before the large flare onset. PASJ **66**, S1711 (2014)

James, A.W., Green, L.M., Palermo, E., Valori, G., Reid, H.A.S., Baker, D., Brooks, D.H., van Driel-Gesztelyi, L., Kilpua, E.K.J.: On-disc observations of flux rope formation prior to its eruption. Sol. Phys. **292**, 71 (2017)

Jin, M., Ding, M.D., Chen, P.F., Fang, C., Imada, S.: Coronal Mass ejection induced outflows observed with Hinode/EIS. ApJ **702**, 27–38 (2009)

Kleint, L., Battaglia, M., Reardon, R., Sainz Dalda, A., Young, P.R., Krucker, S.: The fast filament eruption leading to the X-flare on 2014 March 29. ApJ **806**, 9 (2015)

Kliem, B., Török, T.: Torus instability. Phys. Rev. Lett. **96**, 25 (2006)

Ko, Y.-K., Raymond, J.C., Vršnak, B., Vujíc, E.: Modeling UV and X-ray emission in a post-coronal Mass ejection current sheet. ApJ **722**, 625 (2010)

Kusano, K., Bamba, Y., Yamamoto, T.T., Iida, Y., Toriumi, S., Asai, A.: Magnetic field structures triggering solar flares and coronal Mass ejections. ApJ **760**, 31 (2012)

Landi, E., Raymond, J.C., Miralles, M.P., Hara, H.: Physical conditions in a coronal Mass ejection from Hinode, stereo, and SOHO observations. ApJ **711**, 75 (2010)

Lee, J.-Y., Raymond, J.C., Reeves, K.K., Moon, Y.-J., Kim, K.-P.: Mass and energy of erupting solar plasma observed with the X-ray telescope on Hinode. ApJ **798**, 106 (2015)

Liu, C., Deng, N., Liu, R., Lee, J., Wiegelmann, T., Jing, J., Xu, Y., Wang, S., Wang, H.: Rapid changes of photospheric magnetic field after tether-cutting reconnection and magnetic implosion. ApJ **745**, L4 (2012)

Long, D.M., Williams, D.R., Régnier, S., Harra, L.K.: Measuring the magnetic-field strength of the quiet solar corona using "EIT waves. Solar Phys. **288**, 567–583 (2013)

McIntosh, S.W.: The inconvenient truth about coronal dimmings. ApJ **693**, 1306 (2009)

McKenzie, D.E., Canfield, R.C.: Hinode XRT observations of a long-lasting coronal sigmoid. ApJ **481**, 65–68 (2008)

Miklenic, C., Veronig, A.M., Temmer, M., Möstl, C., Biernat, H.K.: Coronal dimmings and the early phase of a CME observed with STEREO and Hinode/EIS. Solar Phys. **273**, 125 (2011)

Moore, R.L., Sterling, A.C., Hudson, H.S., Lemen, J.R.: Onset of the magnetic explosion in solar flares and coronal Mass ejections. ApJ **552**, 833 (2001)

Nindos, A., Patsourakos, S., Wiegelmann, T.: On the role of the background overlying magnetic field in solar eruptions. ApJL **748**, L6 (2012)

Patsourakos, S., Vourlidas, A.: On the nature and genesis of EUV waves: a synthesis of observations from SOHO, STEREO, SDO, and Hinode (Invited Review). Sol. Phys. **281**, 187–222 (2012)

Reeves, K.K., McCauley, P.I., Tian, H.: Direct observations of magnetic reconnection outflow and CME triggering in a small erupting solar prominence. ApJ **807**, 12 (2015)

Savage, S.L., McKenzie, D.E., Reeves, K.K., Forbes, T.G., Longcope, D.W.: Reconnection outflows and current sheet observed with Hinode/XRT in the 2008 April 9 "Cartwheel CME" Flare. ApJ **722**, 329 (2010)

Savcheva, A.S., McKillip, S.C., McCauley, P.I., Hanson, E.M., DeLuca, E.E.: A new sigmoid catalog from Hinode and the solar dynamics observatory: statistical properties and evolutionary histories. Sol. Phys. **289**, 329 (2014)

Sterling, A.C., Moore, R.L., Harra, L.K.: Lateral offset of the coronal Mass ejections from the X-flare of 2006 December 13 and its two precursor eruptions. ApJ **743**, 63 (2011)

Su, Y., Surges, V., van Ballegooijen, A., Deluca, E., Golub, L.: Observations and magnetic field modeling of the flare/coronal Mass ejection event on 2010 April 8. ApJ **734**, 53 (2011)

Syntelis, P., Gontikakis, C., Parsourakos, S., Tsinganos, K.: The spectroscopic imprint of the pre-eruptive configuration resulting into two major coronal mass ejections. A&A **588**, A16 (2016)

Tian, H., McIntosh, S., Xia, L., He, J., Wang, X.: What can we learn about solar coronal mass ejections, coronal dimmings, and extreme-ultraviolet jets through spectroscopic observations? ApJ **748**, 106 (2012)

Török, T., Kliem, B.: Confined and ejective eruptions of kink-unstable flux ropes. ApJL **630**, L97 (2005)

van Ballegooijen, A.A., Martens, P.C.H.: Formation and eruption of solar prominences. ApJ **343**, 971 (1989)

Williams, D.R., Harra, L.K., Brooks, D.H., Imada, S., Hansteen, V.H.: Evidence from the extreme-ultraviolet imaging spectrometer for axial filament rotation before a large flare. PASJ **61**, 493–497 (2009)

Woods, M.M., Harra, L.K., Matthews, S.A., Dacie, S., Long,D.M.: Observations and modelling of the pre- are period of the 29-March-2014 X1 flare. Sol. Phys. **292**, 38 (2017)

Chapter 15
Understanding Magneto-convection on Solar Surface with *Hinode* Satellite Observation

Yusuke Iida

Abstract The *Hinode* satellite observations revealed that solar surface magneto-convection is more active than previously expected. *Hinode* helped enhance our knowledge of small-scale structures with its high temporal and spatial resolution data. In particular, the granular element structure of the magnetic field was observed, and the related phenomena have been widely investigated in the past decade since its launch. In this paper, we examine the observational results of such small-scale magneto-convection fields using the *Hinode* satellite data and propose future tasks in the following 10 years.

Keywords Sun: photosphere · Sun: surface magnetism · Sun: convection

15.1 Why Do We Prefer Smaller Scale?

For a long time, the reason why stars in the universe have a hot atmosphere has been an interesting question. The Sun, which is located close to us and can be observed in more detail, is the best object to investigate in order to answer this question. It is known that the origin of the active outer atmosphere of the Sun is tied to the surface magnetic field. Considering the age of the Sun and the dissipation timescale for magnetohydrodynamic diffusion, the existence of a magnetic field on the solar surface at present is dubious. Despite considerable research to identify the mechanism essential to create and maintain the surface magnetic field, the following fundamental questions remain unanswered: How much magnetic field is present on the surface of the Sun? How much magnetic energy is present over there? How is the magnetic field transported?

Y. Iida (✉)
Kwansei Gakuin University, Hyogo, Japan
e-mail: iida@kwansei.ac.jp

T. Shimizu et al. (eds.), *First Ten Years of Hinode Solar On-Orbit Observatory*,
Astrophysics and Space Science Library 449,
https://doi.org/10.1007/978-981-10-7742-5_15

There are two difficulties for observational solutions of these issues. One difficulty is that small-scale magnetic fields and convective structures may play important roles. The element structure of the convection is a granule. It has a size of approximately 1,000 km, which is roughly slightly larger than 1 arcsec if observed from the Earth. The elemental structure of the magnetic field is smaller than that of the convection structure, because it is, in general, being suppressed by convection. Therefore, it is necessary to observe these elemental structures with a high spatial resolution of 1 arcsec or more in order to capture them. The other difficulty is that the magneto-convection system on the solar surface exhibits a "complex" turbulent field. As mentioned earlier, it is generally assumed that the magnetic field is being touched by convection. However, a strong magnetic field, known as the network field, is present locally. It is a relatively large in size and reaches the upper atmosphere. Therefore, it is expected to play an important role in the energy transport between the surface and the upper atmosphere. Thus, both convection and magnetic fields may have important roles in the magneto-convection field on the solar surface. We should have consider both the fields on the solar surface, which is theoretically "complex" turbulent field. In short, it is essential to observe the magnetic field and the convective elemental structure with small spatial scale.

With this background, the *Hinode* satellite was launched in September 2006. Three telescopes are onboard the *Hinode* satellite. One of them, the solar optical telescope (SOT), captures the surface magneto-convection field by the filtergram (FG) and spectropolarimeter (SP). The significant feature of the SOT is its high spatial resolution and capability of the stable observation. It has a diameter of 50 cm, achieving a spatial resolution of 0.2 arcsec and a temporal resolution of 30 s. Furthermore, as it is a satellite observation using polar orbits and seeing-free condition, it is possible to acquire observational data stably. Thus, optimal observation is performed for the investigation of the magneto-convection on the solar surface. In this paper, we examine the results on such small-scale magneto-convection, particularly magnetic field, through the 10-year SOT observation.

15.2 Observational Results and New Knowledge Obtained by *Hinode*

Observational data with high spatial resolution by *Hinode* revealed the appearance of a small-scale magneto-convection field that is considerably active than that we expected. In this paper, I have explained the phenomena in terms of convective collapse, horizontal magnetic field, magnetic element dynamics, magnetic flux amount, and surface magnetic field transport.

15.2.1 Convective Collapse

It is observationally known that a magnetic field, which exhibits a magnetic field strength higher than that can be produced by gas pressure, exists on the solar surface. In a standard image of a magnetic field forced by surrounding convection, it is difficult to explain the existence of such magnetic field strength. The novel mechanism is essential for explaining the phenomenon. Parker (1978) proposed convective collapse as a mechanism for creating such unlikely magnetic field strength. First, consider a small magnetic field area swept away by convection. The magnetic field hinders the heat exchange between the area and the surroundings by the movement of the gas. Furthermore, if the area is sufficiently small, it is impossible to absorb the light from the surrounding area with sufficient heat. Therefore, the heat transports owing to both gas and light are hindered, and this area is thermally isolated from the surroundings. On the other hand, the light is emitted into the space and the internal energy is conducted. As a result, the temperature in this area becomes lower than the surroundings, and the gas falls down. The gas pressure decreases owing to the decrease of the gas, thereby collapsing the pressure balance and crushing the region to generate the unlikely strong magnetic field. On the other hand, Spruit (1979) proved that such instability can occur in the magnetic field strength less than 1270 Gauss. However, the observational proof required long years. The key to this phenomenon is not only the magnetic field but also the region that is sufficiently small so that light cannot be sufficiently absorbed. Therefore, its verification requires high spatial resolution, which indicates the proficient target for the SOT.

Nagata et al. (2008) explored the temporal change in the magnetic field strength and the Doppler velocity in the small-scale magnetic field region using the highly precise spectropolarization data obtained by the SOT/SP. As a result, it is observed for the first time that the magnetic field strength becomes stronger after the descending flow was observed, as expected, by using convective collapse model. Furthermore, similar analysis was performed statistically by Fischer et al. (2009), and they observed that the convective collapse occurs everywhere on the solar surface. It can be said that the existence of the convection collapse process proposed by Parker was confirmed after 30 years.

15.2.2 Horizontal Magnetic Field

The majority of the magnetic field was considered to be perpendicular to the solar surface until the middle of 1990s. Meanwhile, there are some indirect observational evidence indicating that there are small-scale magnetic fields parallel to the solar surface, e.g., horizontal magnetic field, before the *Hinode* launch. Lites et al. (1996) found the predominantly horizontal magnetic flux in the spectropolarimetric

observation, namely, Stokes Q and U signals, using the advanced Stokes polarimeter. The order of the polarimetric signal they observed was 1–2% with a noise level of 0.5% in their observation. Although it is not sufficient for the stable observation of the feature, they discussed that the solar surface is covered with weak (less than 1000 Gauss) and short-lived (approximately 5 min) horizontal magnetic field. It is also discussed that although the horizontal magnetic field has only a weak magnetic field, the total amount of magnetic flux reaches 10^{24} Mx, which is equivalent to the vertical flux on the entire solar surface. Harvey et al. (2007) revealed the nature of the horizontal field in a more direct manner. The magnetic field of the solar surface generates polarized light based on the Zeeman effect as a principle. According to it, the solar horizontal magnetic field perpendicular to the line of sight appears as a linearly polarized light. However, its degree of polarization is considerably small with respect to the solar plane perpendicular magnetic field parallel to the line of sight, and high accuracy is required for direct detection. They analyzed the Stokes V signal, e.g., the line-of-sight magnetic field, around the edge of the solar disk instead of the Stokes Q and U signals. By analyzing the Stokes V signal, the noise level is reduced than the Stokes Q and U signals. Thus, they analyzed the temporal power spectra of the horizontal magnetic field with high accuracy, 1.7 Gauss with a spatial resolution of 3 arcsec, and concluded that the dynamic horizontal field exists ubiquitously on the solar surface.

The spectroscopic polarimeter onboard the *Hinode*/SOT measures not only the circularly polarized light but also the linearly polarized light with high accuracy (see Fig. 15.1). Such high-precision observation helped us to observe the horizontal magnetic field directly with the Stokes Q and U signals. Lites et al. (2008) analyzed

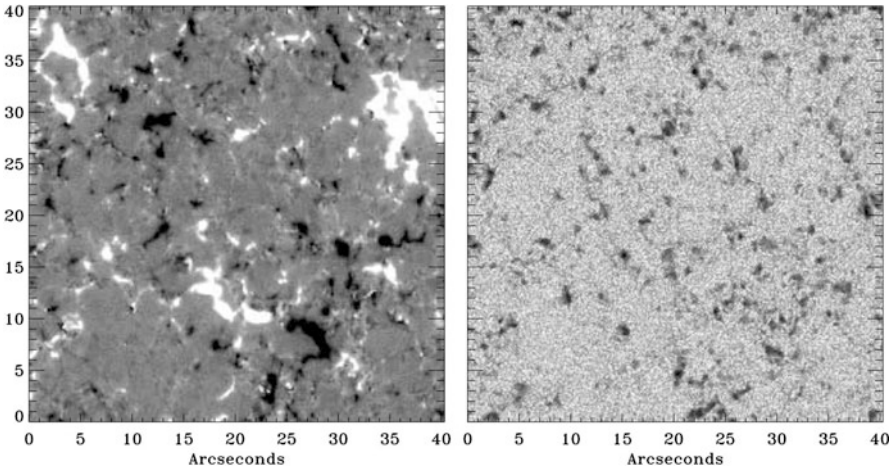

Fig. 15.1 Longitudinal (left) and transverse (right) magnetic flux density observed with *Hinode* from Lites et al. (2008). Field of view of each image is $40'' \times 40''$. The gray scale is saturated at ± 50 Mx cm^{-2} in the left image and at 200 Mx cm^{-2} in the right image (© AAS. Reproduced with permission)

the isolated horizontal field with the SOT data. They derived the average horizontal apparent flux density as 55 Mx cm^{-2}, which is larger than of the vertical flux density, 11 Mx cm^{-2}. It is also mentioned that the horizontal fields are likely the source of the seething field of the quiet Sun and may contribute to its hidden flux. Ishikawa et al. (2008) investigated two cases of the horizontal fields in detail. The time series of the full Stokes signals are tracked, and the Doppler velocity is measured. Furthermore, Danilovic et al. (2010) analyzed the characters of the horizontal field through rocket or ground-based observations with higher spatial resolution than that of *Hinode*.

15.2.3 Magnetic Flux Budget

How much magnetic flux exists on the surface of the Sun is a fundamental problem, but it is a mystery for a long time. Total magnetic flux amount increased as the spatial resolution of observation increased. One key to answer this question exists in the observation. Before the observation by the *Hinode* satellite, patchy magnetic field structures swept away by convection, which are called magnetic flux concentrations or magnetic elements, were observed on the solar surface. Based on this fact, one solution is to investigate the scale dependence of the magnetic elements.

Parnell et al. (2009) examined the flux distribution of magnetic elements by combining the observations of the *Solar and Heliospheric Observatory (SoHO)* and *Hinode*. The *SoHO* satellite observes the entire solar disk regularly and is suitable for examining a large-scale magnetic field. On the other hand, *Hinode* observes the Sun partially with higher spatial resolution. By using these two satellite data complementarily, they were able to investigate the range of five orders of magnitude in the magnetic flux amount. According to the results, from the largest to the smallest, the same magnetic flux distribution was obtained (see Fig. 15.2). The flux distribution has a form of a power-law, and the power-law index is a -1.85. The value of the power-law index, which is slightly larger than -2, indicates that the larger-scale magnetic field is more important for the total magnetic flux budget. Furthermore, they discussed that the same generation mechanism exists for both large- and small-scale magnetic fields. Several papers reported the same results within the error bars after their paper.

15.2.4 Magnetic Element Activities

The magnetic elements exhibit dynamic activities such as coalescence, splitting, emergence, and cancellation (see Fig. 15.3). Here, emergence indicates that equal amounts of magnetic elements appear with different polarities, and cancellation indicates that all or part of the magnetic elements with different polarities disappears owing to collision between them. The surface magnetic fields around which

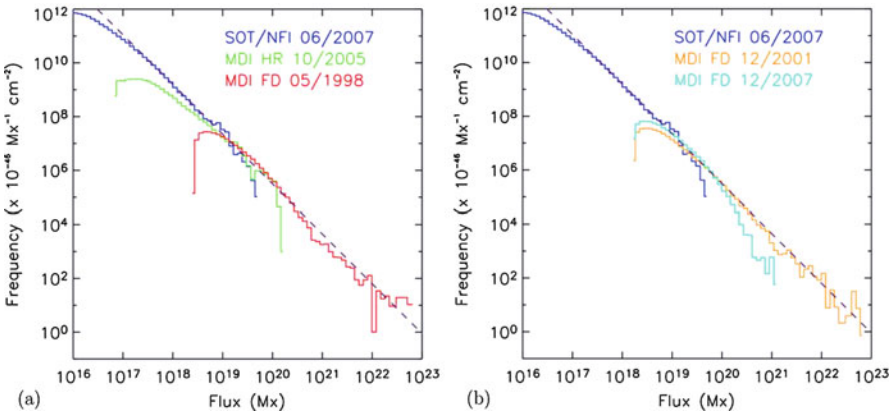

Fig. 15.2 Frequency distribution of magnetic flux contained in the recognized magnetic elements from Parnell et al. (2009). (**a**) Those in the *Hinode* and the *SoHO* observation. (**b**) Same as (**a**) but include the two results from different *SoHO* observation, 2001 December and 2007 December, for comparison. The dashed line in both graphs represents a fitting result of (**a**), which has slope of −1.85 (© AAS. Reproduced with permission)

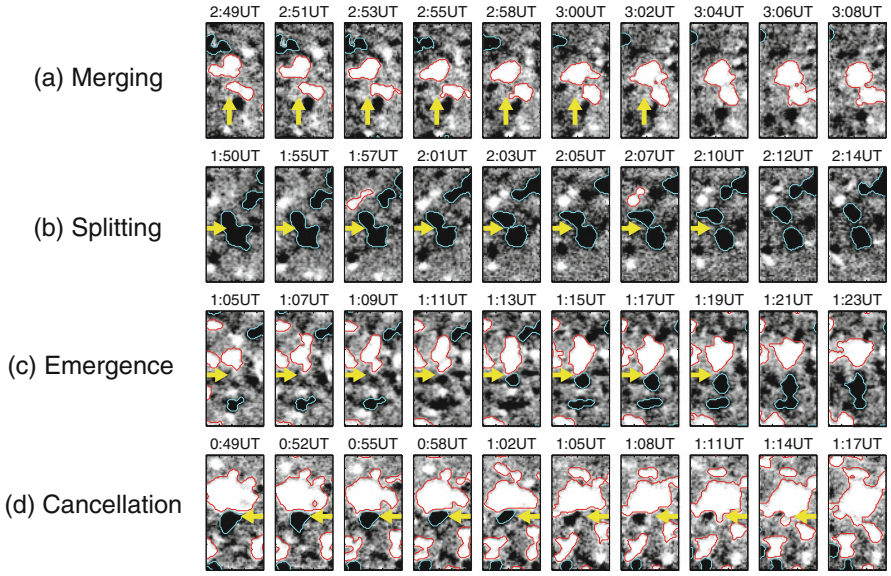

Fig. 15.3 Examples of recognized magnetic element interactions using feature tracking method in the *Hinode* observation (This figure is designed by Y Iida)

such magnetic elements moves dynamically is called a magnetic carpet from the *SoHO* era. Schrijver et al. (1997) suggested a model equation including the abovementioned four processes. In the *SoHO* era, relatively large magnetic flux

concentrations, which are larger than 10^{18} Mx, are captured. It was only a relatively large magnetic concentration, but it was not realistic to follow every concentration with human eyes. Hence, Hagenaar et al. (1999) investigated the dynamics of the magnetic elements using the feature tracking technique.

In the *Hinode* satellite era, the number of observable magnetic elements explosively increased, and the feature tracking technique of magnetic poles became more important. DeForest et al. (2007) conducted a comparative study on several automatic discrimination software developed in the era of *SoHO* satellite for the *Hinode* data analysis. Furthermore, Lamb et al. (2010) applied them to the *Hinode* magnetic field observation. They changed the spatial resolution of magnetograms artificially and found that the unipolar emergence observed in the lower-resolution magnetogram corresponds to the coalescence of the small magnetic elements in the higher-resolution one. On the other hand, Iida et al. (2012) developed a feature tracking method of magnetic elements and investigated the timescales of the four activities. Their results revealed that coalescence and splitting exhibit considerably shorter timescales than those of emergence and cancellation. It also deduces that the magnetic structures on the solar surface are generated on the surface and not in the inner Sun. Gosic et al. (2014) tracked small intra-network magnetic fields using Southwest Automatic Magnetic Identification Suite (SWAMIS), which is one of the magnetic element tracking codes. They investigated the contribution of the intra-network field to the network field through coalescence. It contributes 1.5×10^{24} Mx day^{-1} of flux on the entire surface. This value agrees that the intra-network field replaces the surface magnetic field in only 9−13 h. The magnetic element tracking observed in the *Hinode* era revealed that the frequencies of coalescence and splitting are considerably larger than our expectation and that they greatly contributed to the generation and maintenance of the surface magnetic field.

On the other hand, emergence and cancellation correspond to the exchanges of the magnetic field between the inside and the surface of the Sun and cause the magnetic energy release in the upper atmosphere. Regarding cancellation, two theoretical models have been proposed: sinking of the omega-shaped magnetic loop and levitation of the U-shaped magnetic loop. Chae et al. (2004) found submerging motion in the Doppler velocity around the canceling site using the polarization spectrum with high spatial resolution by the ground telescope. It corresponds to the sinking of the omega-shaped magnetic loop. However, the problem encountered was that the time evolution could not be tracked owing to the lack of the temporal resolution. Iida et al. (2010) took advantage of the better temporal resolution of FG observation. They derived the time evolution of the Doppler velocity field around the cancellation site and found the persistent submerging flow. Note that Kubo et al. (2014) reported the anomalous Stokes V profile at the cancellation site, and it can be produced by adding the symmetric Stokes V profiles observed at pixels immediately adjacent to the polarity inversion line where cancellation occurs. This suggests that the Doppler velocity observed at the cancellation site is apparent. Furthermore Iida et al. (2015) investigated the flux dependence of cancellation occurrence by using the feature tracking method. They observed a power-law distribution with a steep

index of -2.48 ± 0.26, such that the total flux amount of cancellations is dominated by the smaller-scale ones. On the other hand, there are a plenty of small-scale emergences observed in the *Hinode* data. Otsuji et al. (2011) performed a statistical study from the small one with a size of 2 arcsec to the large one with a size of 100 arcsec. They observed the power-law scaling relation between the maximum spatial distance between the main polarities, the magnetic flux growth rate, and the mean separation speed. Thornton and Parnell (2011) also found the power-law frequency distribution of the emerging flux content. The obtained power-law index is -2.7, which is sufficiently steep such that smaller emergences dominate the total flux amount of emergence. To summarize the observational results for cancellation and emergence in the *Hinode* era, we observed considerably more events than that obtained in the *SoHO* era and observed the power-law scaling ranging from the smallest to the large magnetic flux concentrations.

15.2.5 Surface Flux Transport

Surface flux transport is one of the important processes for flux transport dynamo. However, the transport process of magneto-convection in the global scale is not clear, namely, standard diffusion, sub-diffusion, or super-diffusion. Typically, the surface flux transport is treated as the standard diffusion. In the case, the diffusion coefficient is constant. However, in other cases, the diffusion coefficient is not constant, and it cannot be treated with the classical diffusion equation. By observing the elemental structures, the transport process can be evaluated by treating them as a cork. The relation between the squared displacement and the elapsed time is one of the most important relations for the evaluation of flux transport. Bright points in the photospheric images are proficient features for flow patterns in the earlier age. Later when the *SoHO* satellite started the observation, the magnetic element became the more proficient features for the investigation of the surface transport. Abramenko et al. (2011) compared their results obtained using the ground-based telescopes with the previous studies. They exhibit super-diffusion on short and small scales, which was obtained in their study, and continue until the scale of diffusion obtained in the past studies. *Hinode* provides the data with high spatial resolution where we can also trace such a small-scale magnetic field. Furthermore, *Hinode* can perform continuous observation for a longer time than the ground telescope. Giannattasio et al. (2014) analyzed 25 h continuous magnetogram and observed the change of the power-law index for a network field at a temporal scale of 600 s. The index changes from the super-diffusion domain (1.44 ± 0.08) to the classical diffusion domain (1.08 ± 0.11). Iida (2016) evaluated the transport process using the 5-day continuous observation, which is the longest continuous magnetogram data. It is observed that the diffusion coefficient changes from the super-diffusion domain to the sub-diffusion domain at a spatial scale corresponding to the network scale (see Fig. 15.4). Hence, they discussed that the stagnation of the magnetic field flow by network structure is significant when the global transport is considered.

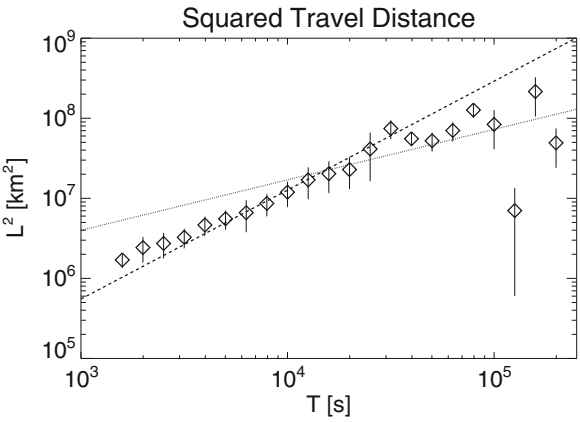

Fig. 15.4 Relationship between the elapsed time and the squared displacement of the magnetic elements in the *Hinode* observation. Bars show the one-sigma error, and the dashed/dotted lines are the fitting results below/above the timescale of 2×10^4 s (Reprinted with the permission from Iida 2016)

15.3 Future Tasks in the Following 10 Years

With the SOT onboard the *Hinode*, small-scale magneto-convection on the solar surface is revealed to be considerably more active than that expected before the *Hinode* launch, and some fundamental processes, such as convective collapse and horizontal magnetic field, could be observed directly due to the high spatial resolution of the SOT. However, the studies have not completely unveiled the magneto-convection field on the solar surface so far.

The most important task is to clarify the connection between the small-scale magneto-convection and the global-scale solar activity. The reason is that the *Hinode* satellite has the advantage of high spatial resolution, while the observable field of view is limited to approximately 1/40 of the solar disk. The strong magnetic field generated by the convective collapse is not clear, as the horizontal magnetic field and the other features described in this paper have influence on the global-scale activity. To solve this problem, the data accumulated for 10 years by the *Hinode* satellite is a big key. The observation data accumulated using the SOT is more than 15 TB. It is important to compare these data systematically with the observation by *SoHO* satellite and *Solar Dynamics Observatory*, which constantly captures the global-scale structure. The problem is a method to analyze these enormous data. One plausible method is the image recognition technique, which is already used in the past studies. We think that the expansion of the analysis method and more systematic research are essential to connect the relation between small-scale magneto-convection and global-scale solar activity.

Moreover, there exist important problems with the smaller scale than the *Hinode* reaches. For example, the estimate of total magnetic flux amount of the solar surface is not completely solved using the *Hinode*. According to the estimates by Stenflo and Collapsed (2011), the flux amount of the magnetic field disturbed by the turbulence is larger than that of the magnetic field swept up to concentration by convection, which has been studied using the *Hinode* observation so far. In order to observe

such turbulent magnetic field, it is essential to observe polarized spectra with higher spatial resolution and better temporal resolution beyond the *Hinode*. Telescopes such as Daniel K. Inouye Solar Telescope (DKIST), which is sharpened to a smaller scale, are expected to provide answers to these questions.

Acknowledgements I am grateful to all the editors who helped write this article. Moreover, I appropriate everyone involved in the development and operation of the *Hinode* satellite for providing the best analytical data so far and for the future.

References

Abramenko, V.I., Carbone, V., Yurchyshyn, V., Goode, P.R., Stein, R.F., Lepreti, F., Capparelli, V., Vecchio, A.: Turbulent diffusion in the photosphere as derived from photospheric bright point motion. Astrophys. J. **743**, 133–142 (2011)

Chae, J., Moon, Y.-J., Pevtsov, A.A.: Observational evidence of magnetic flux submergence in flux cancellation sites. Astrophys. J. **602**, L65–L68 (2004)

Danilovic, S., Beeck, B., Pietarila, A., Schussler, M., Solanki, S.K., Martinez Pillet, M., Bonet, J.A., del Toro Iniesta, J.A., Domingo, V., Barthol, P., Berkefeld, T., Gandorfer, A., Knolker, M., Schmidt, W., Title, A.M.: Transverse component of the magnetic field in the solar photosphere observed by Sunrise. Astrophys. J. **723**, L149–L153 (2010)

DeForest, C.E., Hagenaar, H.J., Lamb, D.A., Parnell, C.E., Welsch, B.T.: Solar magnetic tracking. I. Software comparison and recommended practices. Astrophys. J. **666**, 576–587 (2007)

Fischer, C.E., de Wijn, A.G., Centeno, R., Lites, B.W., Keller, C.U.: Statistics of convective collapse events in the photosphere and chromosphere observed with the Hinode SOT. Astron. Astrophys. **504**, 583–588 (2009)

Giannattasio, F., Stangalini, M., Berrilli, F., Del Moro, D., Bellot Rubio. L.: Diffusion of magnetic elements in a supergranular cell. Astrophys. J. **788**, 137–141 (2014)

Gosic, M., Bellot Rubio, L.R., Orozco Suarez, D., Katsukawa, Y., del Toro Iniesta, J.C.: The solar internetwork. I. Contribution to the network magnetic flux. Astrophys. J. **797**, 49–59 (2014)

Hagenaar, H.J., Schrijver, C.J., Title, A.M., Shine, R.A.: Dispersal of magnetic flux in the quiet solar photosphere. Astrophys. J. **511**, 923–944 (1999)

Harvey, J.W., Branston, D., Henney, C.J., Keller, C.U.: Seething horizontal magnetic fields in the quiet solar photosphere. Astrophys. J. **659**, L177–L180 (2007)

Iida, Y.: Tracking of magnetic flux concentrations over a five-day observation, and an insight into surface magnetic flux transport. J. Space Weather Space Clim. **6**, A27 (2016)

Iida, Y., Yokoyama, T., Ichimoto, K.: Vector magnetic fields and Doppler velocity structures around a cancellation site in the quiet Sun. Astrophys. J. **713**, 325–329 (2010)

Iida, Y., Hagenaar, H.J., Yokomaya, T.: Detection of flux emergence, splitting, merging, and cancellation of network fields. I. Splitting and merging. Astrophys. J. **752**, 149–157 (2012)

Iida, Y., Hagenaar, H.J., Yokoyama, T.: Detection of flux emergence, splitting, merging, and cancellation of network fields. II. Apparent unipolar flux change and cancellation. Astrophys. J. **814**, 134–142 (2015)

Ishikawa, R., Tsuneta, S., Ichimoto, K., Isobe, H., Katsukawa, Y., Lites, B.W., Nagata, S., Shimizu, T., Shine, R.A., Suematsu, Y., Tarbell, T.D., Title, A.M.: Transient horizontal magnetic fields in solar plage regions. Astron. Astrophys. **481**, L25–L28 (2008)

Kubo, M., Low, B.C., Lites, B.W.: Unresolved polarity magnetic fields at flux cancellation site in solar photosphere at $0''.3$ spatial resolution. Astrophys. J. **793**, L9 (2014)

Lamb, D.A., DeForest, C.E., Hagenaar, H.J., Parnell, C.E., Welsch, B.T.: Solar magnetic tracking. III. Apparent unipolar flux emergence in high-resolution observations. Astrophys. J. **720**, 1405–1416 (2010)

Lites, B.W., Leka, K.D., Skumanich, A., Pillet, V.M., Shimizu, T.: Small-scale horizontal magnetic fields in the solar photosphere. Astrophys. J. **460**, 1019–1026 (1996)

Lites, B.W., Kubo, M., Socas-Navaro, H., Berger, T., Frank, Z., Shine, R., Tarbell, T., Title, A., Shimizu, T., Nagata, S.: The horizontal magnetic flux of the quiet-Sun internetwork as observed with the Hinode spectro-polarimeter. Astrophys. J. **672**, 1237–1253 (2008)

Nagata, S., Tsuneta, S., Suematsu, Y., Ichimoto, K., Katsukawa, Y., Shimizu, T., Yokoyama, T., Tarbell, T.D., Shine, R.A., Berger, T.E., Title, A.M., Bellot Rubio, L.R., Orozco Suarez, D.: Formation of solar magnetic flux tubes with kilogauss field strength induced by convective instability. Astrophys. J. **677**, L145–L147 (2008)

Otsuji, K., Kitai, R., Ichimoto, K., Shibata, K.: Statistical study on the nature of solar-flux emergence. Publ. Astron. Soc. Jpn. **63**, 1047–105 (2011)

Parker, E.N.: Hydraulic concentration of magnetic fields in the solar photosphere. IV. Adiabatic cooling and concentration in downdrafts. Astrophys. J. **211**, 368–377 (1978)

Parnell, C.E., DeForest, C.E., Hagenaar, H.J., Johnston, B.A., Lamb, D.A., Welsch, B.T.: A power-law distribution of solar magnetic fields over more than five decades in flux. Astrophys. J. **698**, 75–82 (2009)

Schrijver, C.J., Title, A.M., van Ballegooijen, A.A., Hagenaar, H.J., Shine, R.A.: Sustaining the quiet photospheric network: the balance of flux emergence, fragmentation, merging, and cancellation. Astrophys. J. **487**, 424–436 (1997)

Spruit, H.C.: Convective collapse of flux tubes. Sol. Phys. **61**, 363–378 (1979)

Stenflo, J.O.: Collapsed, uncollapsed, and hidden magnetic flux on the quiet Sun. Astron. Astrophys. **529**, A42 (2011)

Thornton, L.M., Parnell, C.E.: Small-scale flux emergence observed using Hinode/SOT. Sol. Phys. **269**, 13–40 (2011)

Chapter 16
Hinode Observation of the Sun's Polar Magnetic Field and Solar Cycle Variation

Daikou Shiota

Abstract The Sun's polar magnetic field can play important roles in several physical processes such as solar dynamos, solar coronal heating, and solar wind acceleration. The first *Hinode* Solar Optical Telescope observations of the polar areas revealed the existence of many patches with intrinsic field strengths of over 1 kG distributed across the entire polar region. *Hinode* monitoring of both polar areas revealed that the distribution of the magnetic patches consists of two different components: a polarity-imbalanced component that consists of large patches and varies with the solar cycle and a stable well-balanced components consisting of small patches. It is important to continue monitoring of the polar regions to understand the formation process of the polar field in the current solar cycle.

Keywords Sun: magnetic field · Solar cycle

16.1 Introduction

Much of the high-resolution and high-sensitivity spectropolarimetry by the Solar Optical Telescope (SOT) onboard the *Hinode* satellite has been revealing a large number of features of the solar atmosphere that had been unknown or undetected before the *Hinode* launch. In particular, although the Sun's polar regions remained poorly understood because of observational difficulties such as foreshortening and limb-darkening effects, understanding of them has been dramatically improved by the *Hinode* polar region observations (Tsuneta et al. 2008). In this article, I focus on

D. Shiota (✉)
Institute for Space-Earth Environmental Research, Nagoya University, Chikusa, Nagoya, Aichi, Japan

National Institute of Information and Communications Technology (NICT), Koganei, Tokyo, Japan
e-mail: shiota@isee.nagoya-u.ac.jp

T. Shimizu et al. (eds.), *First Ten Years of Hinode Solar On-Orbit Observatory*,
Astrophysics and Space Science Library 449,
https://doi.org/10.1007/978-981-10-7742-5_16

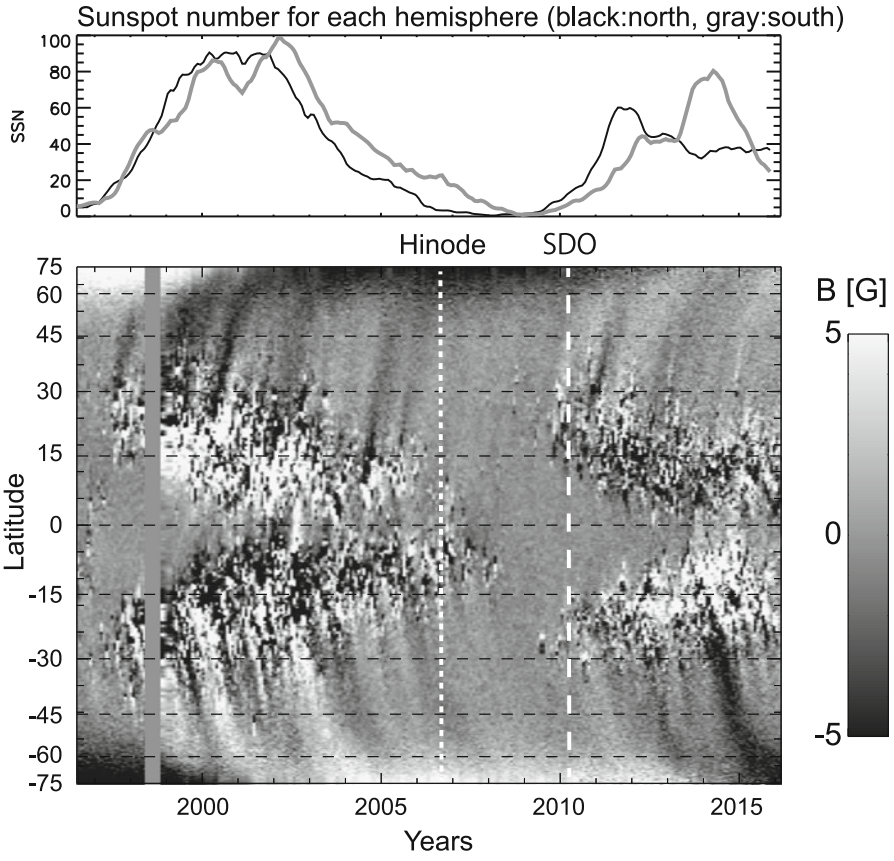

Fig. 16.1 Sunspot number variation of each hemisphere (top) and the butterfly diagram (bottom) synthesized from *SoHO*/Michelson Doppler Imager (MDI) and *SDO*/Helioseismic and Magnetic Imager (HMI) observations

recent progress in observations of the polar region magnetic fields and their long-term variations relevant to the solar cycle variation of the global solar magnetic field generated by the solar dynamo mechanism.

The magnetic field strength in the Sun's polar regions exhibits variations that are anticorrelated with those of the sunspot cycle. Figure 16.1 shows the profiles of the sunspot numbers in each hemisphere and the evolution of the longitudinally averaged magnetic field distribution of the photosphere (the so-called butterfly diagram), since the beginning of the previous solar cycle. At around 1996 (solar minimum), positive- and negative-polarity (unipolar) regions cover the north and south polar regions, respectively, and both region can be seen to extend around 60° in latitude. As the solar activity increases, magnetic flux opposite to that occupying the polar region in each hemisphere is transferred from the lower-latitude region where sunspots appear to the polar region. As the transferred magnetic flux cancels the preexisting flux, the unipolar region at the pole shrinks, and the central averaged

field strength decreases. Finally, the preexisting unipolar region disappears around the time that the solar activity becomes maximum, and the averaged field strength becomes almost zero. As flux transport from the lower-latitude region continues during the decline phase of solar activity, the flux forms and extends into a new opposite-polarity unipolar region. When the solar activity becomes minimum, the polar unipolar region becomes largest. Figure 16.1 shows that both unipolar regions at the poles (negative in the north and positive in the south) were most extended around 2008.

The polar magnetic fields have been monitored by ground-based observations since the late 1970s (Svalgaard et al. 1978). The long-term observation data show good correlation between the polar magnetic field strength at solar activity minimum (i.e., the axial magnetic dipole moment of the Sun) and the maximum sunspot number of the following solar activity maximum (Schatten et al. 1978; Svalgaard et al. 2005). This fact implies that the polar magnetic field can play a significant role in the solar dynamo mechanism that generates the Sun's global magnetic field in the interior of the Sun. In addition, understanding the evolution of the polar field will enable us to predict the solar activity of the next cycle in the future.

The solar polar region is also important for understanding the fast solar wind acceleration and solar coronal heating. When each polar region is covered by a large unipolar region around solar minimum, in the solar corona above the unipolar region, there is a large, stable coronal hole where the density is very low and from which a fast solar wind emanates. Although it has been suggested that the solar wind acceleration is affected by magnetic fields on a large spatial scale coronal hole or by coronal activities such as coronal jets, the actual mechanism of solar wind acceleration and coronal heating remains poorly understood. Thus, advancing our understanding of the polar regions is considered to be one of the most important goals in solar physics.

16.2 Polar Region Monitoring by *Hinode*

The *Hinode* satellite has a very high spatial resolution telescope, the SOT, and the Spectropolarimeter (SP) (Lites et al. 2013) in the SOT enables space-borne high-polarization-sensitivity and high-accuracy observation of the photosphere. SP observation mitigates the difficulties of polar magnetic field observations and can resolve fine magnetic elements in a region near the solar limb. By selecting a good time (March for the south pole and September for the north pole) in terms of the $\sim 7^\circ$ inclination of the solar rotation angle to the ecliptic, we can observe the magnetic field distribution near the center of the pole (Tsuneta et al. 2008).

Hinode first observed the south polar region in 2007 March (Tsuneta et al. 2008). Figure 16.2 shows a map of the magnetic field normal to the solar surface obtained in the observation. The magnetic map was transformed into a polar map when we observed the region above the pole. There are many patchy magnetic concentrations over the entire polar region. These magnetic structures are called magnetic patches. Although the average magnetic field strength in the entire observed region is 3.1 G,

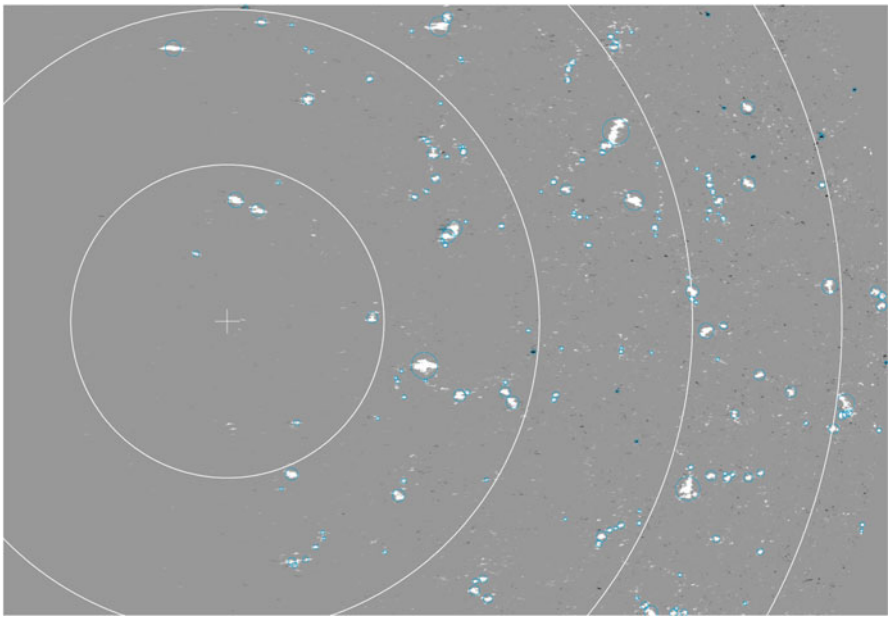

Fig. 16.2 Polar map of vertical magnetic fields in the south polar region on 2007 March 16 observed by *Hinode* SP. Colors show the local magnetic flux density. The cross indicates the center of the pole, and bold circles display colatitude lines for every 5°. Small thin circles display detected magnetic patches (Reproduced from The Astronomical Herald by permission of ASJ)

the magnetic patches contain internal structures whose magnetic field strengths exceed 1000 G. Such magnetic patches are called as kG patches. We identified a single magnetic patch as a continuous structure of the same polarity in the polar vertical magnetic map (indicated with small blue circles in Fig. 16.2). We analyzed the distribution of magnetic patches of different magnetic flux content and each magnetic polarity and made a histogram that shows the relative total magnetic flux (Fig. 16.3). In Fig. 16.2, we can see a small number of small negative (black) magnetic patches, in contrast that a large number of the dominant positive-polarity (white) patches are distributed at various spatial scales. The large kG patches are found to contain polar faculae, which are patchy brighter features seen in continuum observations.

In the previous section, we mentioned unipolar regions in the polar regions. They appear in a low-spatial-resolution observation that observes only the average field strength. As seen in the *Hinode* observation (Fig. 16.2) and the distribution of the patches (the left panel of Fig. 16.3), the patches of medium and high magnetic flux correspond to kG patches, which have the dominant positive polarity. On the other hand, there is almost the same amount of total magnetic flux in the low-flux ($\sim 10^{16}$ Mx) patches of each polarity. When we take the average, these fluxes cancel each other. Therefore, the local average magnetic polarity depends on the large

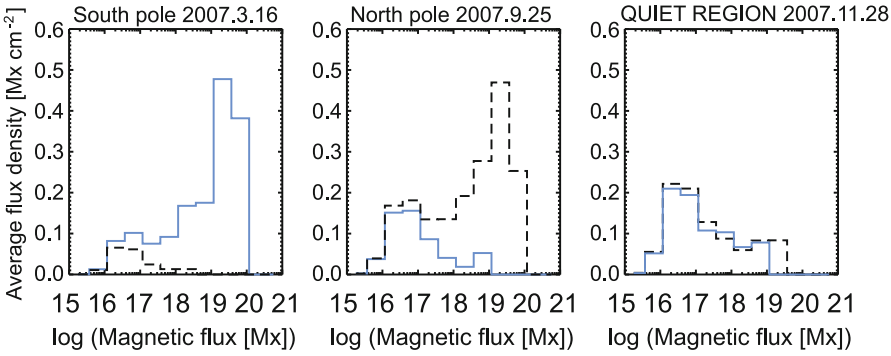

Fig. 16.3 Histogram of vertical magnetic patches in equatorial quiet region and both polar regions. Blue and black indicate positive and negative polarity, respectively (Shiota et al. 2012) (Reproduced from The Astronomical Herald by permission of ASJ)

magnetic patches ($\geq 10^{18}$ Mx). We analyzed the observation of the north polar region taken in 2007 September in the same way. In contrast to the south polar region, the negative-polarity kG patches were dominant in the north polar region, whereas the total magnetic fluxes of the low-flux ($\sim 10^{16}$ Mx) patches of each polarity commonly balanced each other.

The existence of a wide range of magnetic patches of both polarities is a ubiquitous feature of any region of the photosphere, not only the polar regions. In a quiet region of the Sun, photospheric convection motions (vortices) are formed on several spatial scales. Among them, those whose diameter is $\sim$30 megameter (Mm) are called supergranules. Because a supergranular pattern is observed as divergent horizontal motion, magnetic flux tends to flow out around the boundary of supergranules, forming a networked distribution of relatively large magnetic patches, which is called a network field. Within a supergranule, there are smaller-scale distributions of smaller patches, which are associated with smaller-scale convection patterns called intranetwork field. The intranetwork fields consist of the same quantity of patches of both polarities and are associated with transient horizontal magnetic fields that emerge from below the photosphere. These facts imply the existence of a local dynamo where magnetic fields are amplified by convective motion. Network fields have magnetic patches larger than 10^{18} Mx. These distributions of magnetic patches in network and intranetwork fields are consistent with the observations of the polar regions mentioned above. Magnetic patches repeatedly appear, disappear, become integrated, and disintegrate depending on convective motion. The association of larger magnetic patches with larger-scale convection patterns might imply that larger patches are rooted in a deeper layer below the photosphere.

Do the large magnetic patches in quiet regions have the same properties as those in polar regions? We conducted the same analysis in a quiet region near the equator near the solar limb: the patch distribution is plotted in the right panel of Fig. 16.3.

In the quiet region, the patches of both polarities are almost balanced in all the magnetic flux ranges, whereas the negative-polarity patches are dominant in the north polar region. The observations of the north polar region and the quiet region shown in Fig. 16.3 were conducted with the same quality and therefore can be compared quantitatively. Figure 16.3 shows that the amount of magnetic flux in small patches of both polarities is almost the same in the north polar region and the equatorial quiet region. This result implies that the small magnetic patches are maintained by a physical process common to the two regions. On the other hand, the maximum value of the magnetic flux in the large patches is higher in the north polar region than in the equatorial quiet region. This result might be interpreted as meaning that, if the size of a patch is related to the connection depth below the photosphere, as suggested above, the kG patches in the polar regions might be connected to a deeper layer.

Hinode has been monitoring the polar regions since 2008 September. We investigated the yearly variation in the distributions of the magnetic patches, as shown in Fig. 16.4. The result shows that only the distribution of larger vertical patches of the dominant polarity decreases in years when the solar cycle increases. In contrast, the distribution of small vertical patches of both polarities remains almost the same in both polar regions and in different years (Fig. 16.4). The distribution of horizontal magnetic patches does not vary by years, similar to that of small vertical ones.

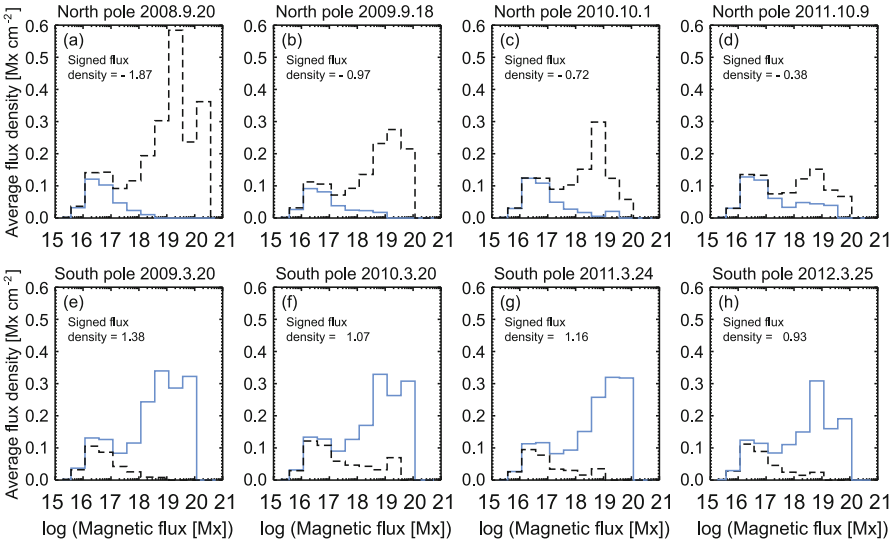

Fig. 16.4 Histogram showing yearly variation of vertical magnetic patches in both polar regions. Blue and black indicate positive and negative polarity, respectively (Shiota et al. 2012) (Reproduced from The Astronomical Herald by permission of ASJ)

The above results indicate the possibility that the distributions of magnetic patches consist of the following two components:

- Larger vertical patches that vary with the solar cycle activity, that is, the magnetic flux accumulated in the polar region
- Small vertical patches and horizontal patches maintained by a ubiquitous process independent of the location and solar cycle activity

16.3 Future Solar Cycle Variation and Polar Region Monitoring

In this solar cycle (Cycle 24), the solar activity became maximum in 2014 February and is currently declining. The top panel of Fig. 16.1 shows the variation of the sunspot number in each hemisphere. The sunspot number in the current cycle varies in a range lower than that in the previous cycle, and the asymmetry between the sunspot numbers in the northern and southern hemispheres is larger than that in the previous cycle. The activity in the northern hemisphere became maximum around 2011, whereas that in the southern hemisphere became around 2013–2014.

Hinode has conducted an observational program to monitor the entire polar region since 2012. Figure 16.5 shows the entire magnetic landscape of both polar regions obtained in the observation program. In 2012 September, there were medium-sized patches of negative polarity around the center of the north polar region, whereas their density was much lower compared with that in solar minimum

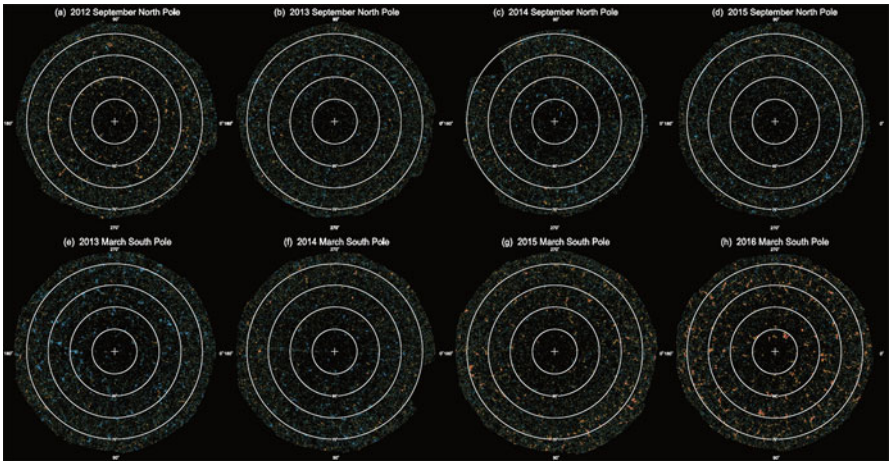

Fig. 16.5 Vertical magnetic field maps of the entire polar region of both poles for 4 years. Colors show the local magnetic flux density (blue and green, positive, and yellow and red, negative). Each map was synthesized from 1 month of *Hinode* observations

(Fig. 16.2) or in the south polar region in 2013 March or 2016 March. If there are almost no kG patches, the average magnetic field strength of the entire polar region becomes ∼0 G. In 2013 September, the negative kG patches disappeared, and small positive patches started to appear. However, the distribution did not change in the north polar region until 2015 September. This indicates that the condition of ∼0 G in the north polar region continued for 3 years. This fact can be seen in the butterfly diagram (Fig. 16.1) as the absence of the unipolar region in the north polar region.

The south polar region, in contrast, changed dramatically. In 2013 March, there were many kG patches of positive polarity, and the number of the positive kG patches decreased rapidly in 2014 March. In 2015 March, negative patches started to appear in the lower-latitude region. A large number of the negative kG patches appeared over the entire south polar region in 2016 March. Thus, the polarity reversal of the south polar region was complete. The evolution can also be seen in Fig. 16.1 as a surge of negative-polarity flux toward the south pole that remains in the south polar region after its arrival at the south pole.

As shown above, each hemisphere has evolved very differently in the current solar cycle. In terms of polarity reversal, the average magnetic field strength of the north polar region remained around 0 G for 3 years around the maximum of this cycle. On the other hand, the polarity reversal proceeded abruptly in 2014–2015. The formation of the positive unipolar region in the north polar region is currently delayed, and therefore the formation of the axial dipole moment is also considered to be delayed. It is quite interesting how the axial dipole of the next solar minimum is formed from the present asymmetric magnetic condition. The evolution process may improve our understanding of the solar dynamo and our prediction of the solar activity in the next cycle.

The previous solar minimum had the longest duration among several recent cycles. An extended cycle period is reported to have occurred around the beginning of the Spörer and Maunder Minima (Miyahara et al. 2004, 2010). A north–south asymmetry is also reported in the Maunder Minimum (Sokoloff and Nesme-Ribes 1994). It is important to keep monitoring the solar activity in the current and next solar cycle.

The launches of two inner heliosphere probe missions, Solar Orbiter and Parker Solar Probe, are scheduled in 2018. Coordinated observations between the *Hinode* polar region observations and these probe missions will provide much information for understanding the solar wind acceleration mechanism.

References

Lites, B.W., et al.: The Hinode spectro-polarimeter. Sol. Phys. **283**, 579 (2013). https://doi.org/10.1007/s11207-012-0206-3

Miyahara, H., et al.: Cyclicity of solar activity during the Maunder minimum deduced from radiocarbon content. Sol. Phys. **224**, 317 (2004). https://doi.org/10.1007/s11207-005-6501-5

Miyahara, H., et al.: Is the Sun heading for another Maunder minimum? – Precursors of the grand solar minima. J. Cosmol. **8**, 1970 (2010)

Schatten, K.H., Scherrer, P.H., Svalgaard, L., Wilcox, J.M.: Using dynamo theory to predict the sunspot number during solar cycle 21. Geophys. Res. Lett. **5**, 411 (1978). https://doi.org/10.1029/GL005i005p00411

Shiota, D., et al.: Polar field reversal observations with Hinode. ApJ **753**, 157 (2012). https://doi.org/10.1088/0004-637X/753/2/157

Sokoloff, D., Nesme-Ribes, E.: The Maunder minimum: a mixed-parity dynamo mode? A&A **288**, 293 (1994)

Svalgaard, L., Duvall, T.L. Jr, Scherrer, P.H.: The strength of the Sun's polar fields. Sol. Phys. **58**, 225 (1978). https://doi.org/10.1007/BF00157268

Svalgaard, L., Cliver, E.W., Kamide, Y.: Sunspot cycle 24: smallest cycle in 100 years? Geophys. Res. Lett. **32**, L01104 (2005). https://doi.org/10.1029/2004GL021664

Tsuneta, S., et al.: The magnetic landscape of the Sun's polar region. ApJ **688**, 1374–1381 (2008). https://doi.org/10.1086/592226

Chapter 17
Local Helioseismology Analyses with *Hinode*/SOT Datasets

Kaori Nagashima

Abstract The solar internal structure and dynamics have been probed by examining the oscillations of the Sun, or by "listening to the Sun"; helioseismology provides us with unique tools for these analyses. Starting from a brief introduction on local helioseismology, in this article I will describe what were our goals and what has been achieved, in learning from the local helioseismology analyses using observations by the Solar Optical Telescope aboard *Hinode*. This includes the detection of helioseismic signatures of flows in the solar atmosphere, study of supergranular cell structures in the solar polar regions, and sunspot seismology.

Keywords Sun: helioseismology · Sun: oscillations

17.1 Introduction

Helioseismology is a unique way to probe the solar interior by examining the "sound" of the Sun.

17.1.1 Solar Oscillations and Helioseismology

Oscillations with a period of about 5 min were first discovered in the 1960s (Leighton et al. 1962) and were interpreted as standing acoustic waves trapped in the Sun (e.g., Ulrich 1970; Deubner 1975). By examining these solar eigenmodes, the global structure and dynamics, such as sound speed and differential rotation profiles, have been revealed (see the review by Christensen-Dalsgaard 2002 for details); this is the discipline of *global helioseismology*.

K. Nagashima (✉)
Max-Planck-Institut für Sonnensystemforschung, Göttingen, Germany
e-mail: nagashima@mps.mpg.de

T. Shimizu et al. (eds.), *First Ten Years of Hinode Solar On-Orbit Observatory*,
Astrophysics and Space Science Library 449,
https://doi.org/10.1007/978-981-10-7742-5_17

Solar oscillations are observed in surface velocity fields (Dopplergrams), which are measured via the Doppler effect. But they are also observed in the visible light intensity (filtergrams); the compression and expansion of the gas caused by the oscillations result in the intensity fluctuations. To analyze these oscillations, continuous and stable observations are necessary. In the 1990s, modern instruments dedicated for helioseismic observations, such as the Global Oscillation Network Group (GONG; Harvey et al. 1996) and the Michelson Doppler Imager (MDI; Scherrer et al. 1995) onboard the *Solar and Heliospheric Observatory* (*SOHO*; Domingo et al. 1995), started providing months or even years of continuous full-disk observations with a sufficient quality to fulfill the requirements of helioseismology analyses. This resulted in the significant development of the global helioseismology as well as the launch of a new branch, *local helioseismology*, which exploits the spatially resolved observations to infer the three-dimensional subsurface structure of the Sun (see the review by Gizon et al. 2005 for details on local helioseismology).

In 2006 the Solar Optical Telescope (SOT; Tsuneta et al. 2008b) onboard the *Hinode* satellite (Kosugi et al. 2007) started observations. Although it is not designed specifically for helioseismology, its stable and high-resolution data have advantages in oscillation analysis: see Sect. 17.2. In this article, I will demonstrate that *Hinode* has provided valuable opportunities to carry out local helioseismology with high-resolution datasets, especially before the launch of the *Solar Dynamics Observatory* (*SDO*; Pesnell et al. 2012) in 2010, which carries the successor to MDI, the Helioseismic and Magnetic Imager (HMI; Schou et al. 2012).

17.1.2 Time–Distance Helioseismology

There are several local helioseismic analysis techniques; here, I focus only on the time–distance helioseismology technique (Duvall et al. 1993) as it was mainly used to examine the *Hinode* observations.

17.1.2.1 Basic Concept

In time–distance analysis, the travel times of acoustic waves measured on the solar surface are used to probe the solar interior.

The solar convection zone is full of acoustic waves excited by turbulent convection. As the sound speed in the Sun increases with depth, acoustic waves are refracted in the interior back toward the surface where they are then reflected back inward by the strong density gradient (see the ray paths in Fig. 17.1).

The travel times of these acoustic waves on the surface can tell us about the sound-speed anomaly and/or flows along the path of the acoustic waves. If there is a sound–speed anomaly on the ray path of the acoustic wave, it is observed as a travel-time anomaly. For example, in the case of Fig. 17.1, if we compare the travel

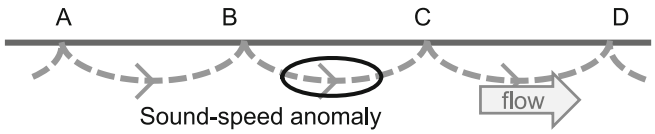

Fig. 17.1 Illustrative sketch of the ray paths of acoustic waves in the solar interior (gray-dashed curves) reflecting from the solar surface (solid line). The four points (A, B, C, D) in this figure are uniformly spaced. A change in sound speed or a flow lying along the ray path can be detected by observing the travel times of the waves at the surface

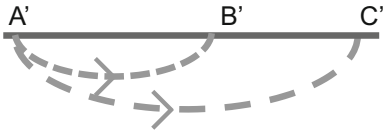

Fig. 17.2 Illustrative sketch of ray paths (gray-dashed curves) under the solar surface (solid line), showing that the waves with reflection points separated by longer distances at the surface penetrate deeper layers

time from A to B, $\tau_{A\to B}$, and the travel time from B to C, $\tau_{B\to C}$, the travel-time difference between these two can be detected: $\tau_{A\to B} > \tau_{B\to C}$, if the sound speed is larger in the anomaly area (and the reverse if the sound speed is less). If there is a flow along the ray path, it is observed as a travel-time anisotropy. In the case of Fig.17.1, the travel time between C and D has an anisotropy, namely, $\tau_{C\to D} < \tau_{D\to C}$.

Moreover, in general, waves that have reflection points separated by larger distances at the surface penetrate the deeper layers, as shown in Fig. 17.2.

In this way, by using wave travel times separated by different distances on the surface, we can infer the three-dimensional structure and dynamics of the solar interior.

17.1.2.2 How to Measure the Travel Time

To determine the travel time between a pair of points on the surface, we compute the cross-covariance function between the signals at two points. Figure 17.3 displays an example cross-covariance function calculated from the *Hinode*/SOT Ca II H line filtergrams between two points on the surface separated by approximately 15 megameter (Mm). The wave travel time is defined as the time lag at which the cross-covariance reaches its maximum, but usually, in helioseismology, we are only interested in travel-time perturbations: the travel-time shift compared to the travel time of the reference cross-covariance function. This reference cross-covariance function can be calculated from a solar model or from the average over the full field of view of the quiet-Sun observation.

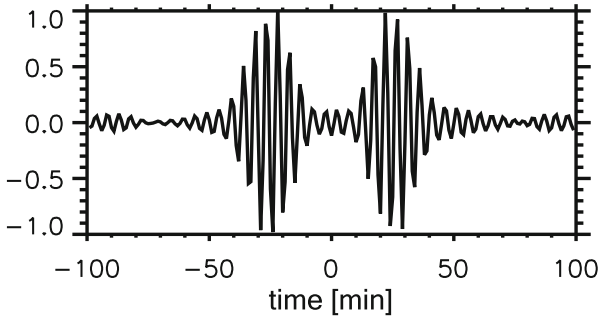

Fig. 17.3 Example cross-covariance function calculated using *Hinode*/SOT Ca II H line filtergrams averaged over the quiet-Sun region for waves whose traveling distance is about 15 Mm

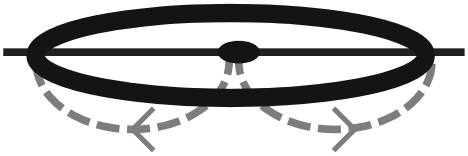

Fig. 17.4 Illustrative sketch of center-to-annulus geometry. The oscillation signal at the central point and averaged signal over the surrounding annulus are used to calculate the cross-covariance. Gray-dashed curves indicate example ray paths from the central point to the annulus

Because of the stochastic nature of wave excitations, the point-to-point cross-covariance function contains substantial noise. Therefore, we average the cross-covariance functions for one distance over some area. The geometry of the averaging depends on the purpose of the analysis. For example, point-to-annulus geometry (Fig. 17.4) is often used (e.g., Kosovichev and Duvall 1997) to detect the inward and outward flows in large cells of convection, called supergranules (e.g., Nagashima et al. 2011); or, the annulus surrounding the central point can be divided into four quadrants (north, south, east, and west) to derive the north-south and east-west flows (e.g., Kosovichev and Duvall 1997; Zhao et al. 2001).

17.2 Advantages of SOT Local Helioseismology

The SOT (Tsuneta et al. 2008b) onboard the *Hinode* satellite (Kosugi et al. 2007) is not designed specifically for helioseismology observations. Therefore, the SOT datasets are different from the usual helioseismology datasets in many aspects. Especially as the field of view of SOT is limited and does not cover the full disk, the depth investigated by time–distance helioseismology is limited to about 8 Mm (Sekii 2004), because the distance between pair points is limited in the field of view (see Fig.17.2). Nevertheless, SOT datasets have several advantages in oscillation analyses.

Firstly, the continuous and stable images of the Sun are free from blurring by the Earth's atmosphere and nighttime interruptions, unlike other high-resolution solar telescopes. Secondly, the spatial resolution (diffraction limit) of SOT is approximately $0.2''$, or 150 km on the Sun near the disk center (compared to approximately $1''$ for HMI and MDI high-resolution observations or $4''$ for MDI full-disk observations), and waves with a spherical harmonic degree ℓ up to about 4000 can be resolved (Sekii 2004). At the time the *Hinode* satellite was launched, only 1-arcsecond resolution observations were available from the high-resolution mode observations of *SOHO*/MDI, and, therefore, SOT provided a unique opportunity for high-resolution helioseismology studies.

Most measurements of the surface velocity have been performed using absorption lines that have non-zero Landé g-factors, because these lines can also be used to measure the magnetic field. The effect of the magnetic field on the line used to measure surface velocities is, therefore, a concern for helioseismic analysis in the regions with strong magnetic fields. The Narrowband Filter Imager (NFI; Tsuneta et al. 2008b) of SOT has a tunable Lyot filter, and one of the lines for Dopplergram observations, Fe I 5576 Å absorption line, is insensitive to magnetic fields, as the Landé g-factor of this absorption line is 0. Hence, SOT/NFI would have provided the only Dopplergrams free from this concern, and it was anticipated that it could be used to measure the surface velocities in the regions with strong magnetic fields, such as sunspots. Unfortunately, the availability of NFI datasets was limited because of a problem with the NFI filter. Hence, helioseismic analyses have been carried out mainly with filtergrams (intensity images) obtained by the Broadband Filter Imager (BFI; Tsuneta et al. 2008b) of SOT.

17.3 Significant Results of SOT Helioseismology

In this section, I summarize the four main SOT helioseismology results.

17.3.1 Oscillation Analysis Using Intensity Observations

In the paper on the initial SOT helioseismology results (Sekii et al. 2007), they reported the detection of oscillation signals suitable for helioseismic analysis using the photospheric G band and lower-chromospheric Ca II H line filtergrams obtained by BFI. Although the noise level of the SOT filtergram power spectrum is higher than that calculated from the MDI Dopplergrams, this study showed great potential for high-resolution helioseismic observations by *Hinode*. Though I will not go into detail here, let me mention a study of the phase between these two oscillation signals (Mitra-Kraev et al. 2008). They reported an unexpected property: the surface gravity waves (f mode) and acoustic waves (p modes) behave differently.

17.3.2 *Chromospheric Flow Detection by Multiwavelength Helioseismic Observations*

Two emerging active regions were observed with the photospheric nonmagnetic (Fe I 5576 Å line) Dopplergrams by NFI as well as Ca II H line filtergrams by BFI. By combining these multiwavelentgh observation datasets, the signature of chromospheric downflows in emerging active regions was detected via the time–distance helioseismology technique (Nagashima et al. 2009a).

In this subsection, let me simply assume that the chromosphere represents the formation layer of the Ca II H line, though the photosphere and chromosphere are thick layers in the solar atmosphere, and the line formation layer of the Ca II H line is extended to a certain height range centered around 250 km above the photosphere in the lower chromosphere.

Nagashima et al. (2009a,b) measured the center-to-annulus travel times using an annulus with a radius of approximately 15 Mm to illustrate the supergranular flow structure around the emerging active regions. As Fig. 17.5 shows, the travel-time maps from the photospheric Dopplergram and chromospheric filtergram had no significant difference in the quiet-Sun region. However, they are different in the bright area in the chromospheric-line filtergram (the plage region), where the magnetic field is stronger than the surroundings (i.e., the cross-section of the emerging flux tube. See Fig. 17.6): only the chromospheric data show a travel-time anomaly. In the plage region, the outward travel time is shorter than the inward travel time. As multiwavelength datasets had not been used in the time–distance helioseismology analysis before, this was the first time it was possible to study the wave propagation between different formation heights.

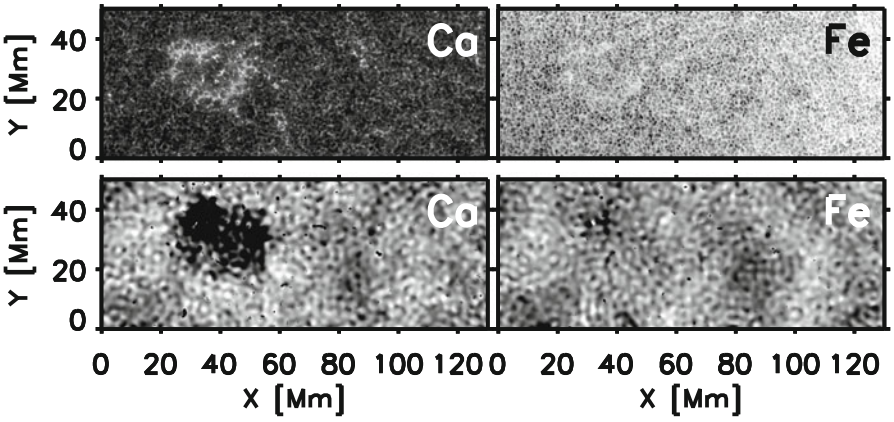

Fig. 17.5 Top row: Sample Ca II H line filtergram (left) and Fe I 5576 Å Dopplergram (right). Bottom row: Outward–inward travel-time difference maps. The gray scale ranges from −0.5 (black) to +0.5 min (white) (Reproduced from Nagashima et al. 2009b (Fig. 1) with permission from Astronomical Society of the Pacific)

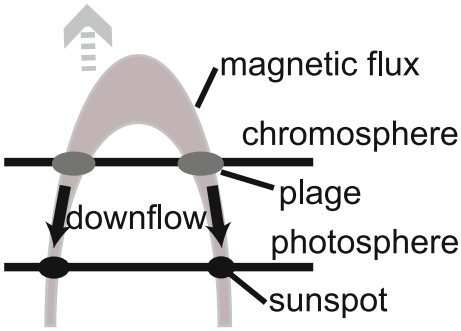

Fig. 17.6 Illustration of an emerging active region

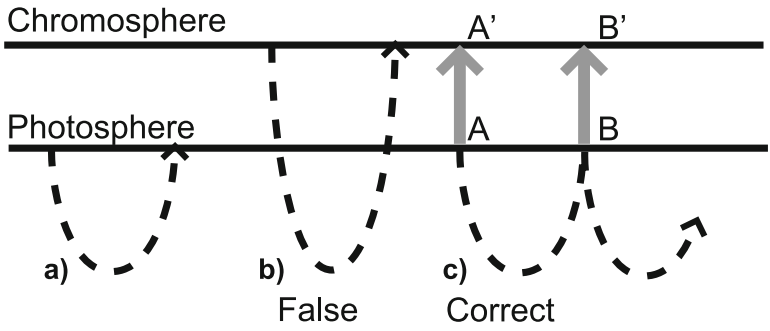

Fig. 17.7 Illustrative sketch of the propagation paths for the wave detected in the chromospheric data

From the chromospheric travel-time maps, at first glance there seems to be a horizontal divergent flow in the plage region. However, as there is no such signal in the photosphere, one would imagine that it might not indicate the simple divergent flow and might indicate that the source of the travel-time anomaly is located somewhere above the photosphere. Ultimately, this was the case, but it was more complicated than we had expected, because the waves used in the analysis are evanescent above the photosphere.

What does this anomaly that exists only in the chromosphere imply? To interpret this, it is necessary to review what is the travel time measured in the chromosphere.

When one thinks about the wave propagation between two points in the chromosphere, one tends to imagine path b in Fig. 17.7 in a similar way to the photospheric one, path a. However, this is incorrect. A wave with a wavelength larger than the scale height cannot propagate upward anymore. In other words, at a certain height, there is a cutoff frequency, and the waves with a frequency lower than the cutoff will be reflected. The cutoff frequency in the photosphere is 5.4 mHz (e.g., Nagashima 2010), and the waves used in the analysis (Nagashima et al. 2009a) are around 3 mHz (the period is around 5 min). Therefore, the waves are evanescent above the photosphere.

However, only the standing waves become evanescent, i.e., have infinite vertical phase speed. In reality, the oscillations on the Sun are constantly excited and damped. In this case, the information on the perturbations that occur on the reflection surface can be propagated upward with finite speed (Nagashima 2010), as is illustrated by the gray arrows in Fig. 17.7c. Therefore, the measured "travel time" in the chromosphere $\tau_{A'\to B'}$ actually corresponds to the difference in time of the signals, namely, $\tau_{A'\to B'}$ is not a real travel time from A' to B', but the difference between the times at which the information from the same starting point (A) arrives at the two points on the chromosphere (A' and B'). (Hereafter, for simplicity we refer to this as chromospheric travel time.)

If the propagation time from the photosphere to chromosphere is identical at both A and B, i.e., $t_{A\to A'} = t_{B\to B'}$, then the photospheric travel time $\tau_{A\to B}$ and chromospheric travel time $\tau_{A'\to B'}$ will be identical. In the observations, this is true in the quiet-Sun region. This is also an observational demonstration that path b in Fig. 17.7 is false.

If the propagation time from the photosphere to the chromosphere (e.g., $t_{A\to A'}$ in Fig. 17.7) is longer in the plage region than the quiet-Sun region, this will cause the travel-time anomaly which was observed in the study (Nagashima et al. 2009a). There are several possible causes for this longer propagation time above the photosphere. One possibility is a lower propagation speed, namely, a lower sound speed. However, this can be rejected, because the effective sound speed in the region with strong magnetic field, such as the plage region, is larger. The plausible source is the downflow in the chromosphere (see Fig. 17.6). It is well known from observations and numerical simulations of emerging flux tubes in the past that plasma falls along the flux tube as the flux tube rises. The downflow speed estimated from the chromospheric travel-time anomaly in the plage region is about 8 km s^{-1} (Nagashima et al. 2009a), and this is consistent with other studies. This might be underestimated, though, because the higher (effective) sound speed and the larger height difference between the chromosphere and photosphere in the plage might cancel the effect of the downflow on the chromospheric travel times.

In this way, this SOT helioseismology study demonstrated a new aspect of local helioseismology using multiwavelength observations: flow detection in the solar atmosphere.

17.3.3 Supergranular Cell Structure in Polar Regions

The SOT high-resolution datasets were utilized in the study of the solar polar regions as well.

The dynamics in the solar polar regions are essential to understanding the solar dynamo mechanism; the polar regions are the places where magnetic field reversal occurs at the solar maximum. Not only helioseismologists but also other solar physicists are interested in the polar regions, and some (e.g., Tsuneta et al. 2008a) have studied them using the *Hinode* datasets taken by SOT in combination with those taken by the X-Ray Telescope (XRT; Golub et al. 2007)

Compared to the area near the disk center, it is difficult to observe the polar regions because of foreshortening; the Earth and most sun-observing satellites are located on the solar ecliptic plane. No solar images were taken from outside the ecliptic plane, and to obtain them, we must wait for Solar Orbiter, which is planned to be launched in 2019 into a tilted polar orbit (Müller et al. 2013). Therefore, the high-resolution SOT datasets are, though obtained on the ecliptic plane, expected to be useful in revealing the fine structures in the polar regions, which were never detected before.

Time–distance helioseismology analysis of the SOT polar-region observations has revealed a peculiar supergranular cell structure in the polar regions (Nagashima et al. 2011). In this study, to maximize the use of the high-resolution datasets, the polar regions were observed when the B_0 angle was at its maximum. As the rotation axis of the Sun is tilted relative to the orbital axis of the Earth, the heliographic latitude of the apparent solar disk center varies with time up to approximately $\pm 7°$; this is the B_0 angle. Therefore, the southern and northern polar regions were observed around March and September, respectively.

Using these datasets, the travel times with the center-to-annulus geometry (Fig.17.4) were measured, and the convection cell structure in the polar regions was investigated. The parameters of the analyses were adjusted to detect convection cells with radii of about 2×10^4 km, namely, supergranular cells. Figure 17.8 displays the supergranular map in the northern polar region obtained from the month-long

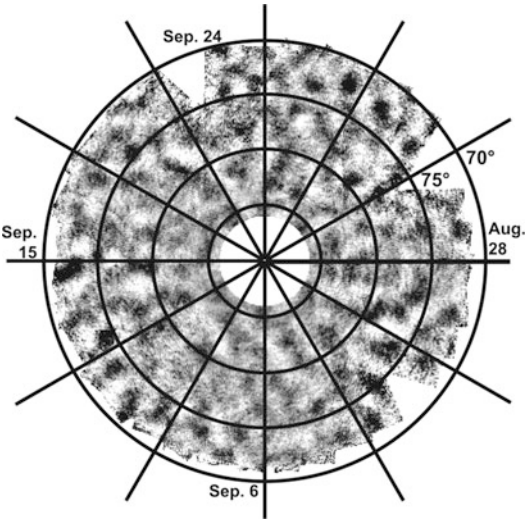

Fig. 17.8 Combined northern polar-region map obtained from month-long observation starting from the end of August 2010. From "Aug. 28" on the 3 o'clock direction, the data are displayed clockwise in chronological order. The concentric circles represent latitudinal lines marking every 5° starting from 70°, and the central point of this map is the solar north pole. The outward–inward travel-time difference is indicated in the gray scale: the diverging flow regions, which correspond to the supergranular cell center, are indicated in black (where the outward travel time is shorter than the inward one), and the converging flow regions are in white

campaign observation around September 2010. These polar maps (including the northern and southern polar regions in the figures in Nagashima et al. 2011) show the north-south alignment trend of the cells. Numerical convection simulations show this type of alignment only near the equatorial region (Miesch et al. 2006), though no global simulation can yet resolve the supergranular scale. Neither the cause of this alignment nor the relationship between the alignment and the solar activity is understood yet.

17.3.4 Sunspot Analyses

Sunspots and active regions are notable features in the Sun; solar activity events such as flares are often associated with the presence of sunspots at the surface. However, the subsurface structure of sunspots is poorly understood. In the first phase of *Hinode* observations, the Sun showed an unexpectedly low number of sunspots. Because of this low activity level in addition to the problem of the NFI filter, the originally planned sunspot study with the nonmagnetic Dopplergram was not carried out. However, SOT high-resolution filtergrams have been used in studies of oscillation phenomena in and around sunspots.

17.3.4.1 Umbral Oscillation

Nagashima et al. (2007) examined oscillations in a sunspot and detected the fine structure of the oscillation pattern thanks to the SOT stable and high-resolution observations.

Umbral flashes are the transient brightenings observed in the umbra of sunspots in chromospheric lines (Beckers and Tallant 1969). SOT observed a fairly circular (i.e., axisymmetrical) sunspot in the active region NOAA (National Oceanic and Atmospheric Administration) 10935 and detected typical umbral flashes in the Ca II H line filtergrams. As Fig. 17.9 shows, the oscillation power around the 5.5-mHz (3-min) band was enhanced in the umbra, though the power was suppressed around the center of the umbra (about 6″ in diameter). Umbral flashes are interpreted as upward-propagating shocks along the funnel-shaped magnetic field in the sunspot umbra (e.g., Rouppe van der Voort et al. 2003). Thus, a possible explanation of this tiny low-power area is as follows: as the magnetic field line of this axisymmetrical sunspot is nearly vertical around the center of the umbra, the (apparent) horizontal propagation speed is large, and the brightening period can be too short to observe, which results in this tiny low-power area. The mechanism is not fully understood, though. Observations taking Dopplergrams instead of filtergrams or radiative-transfer calculations in such a sunspot might help us solve the riddle of the mechanism.

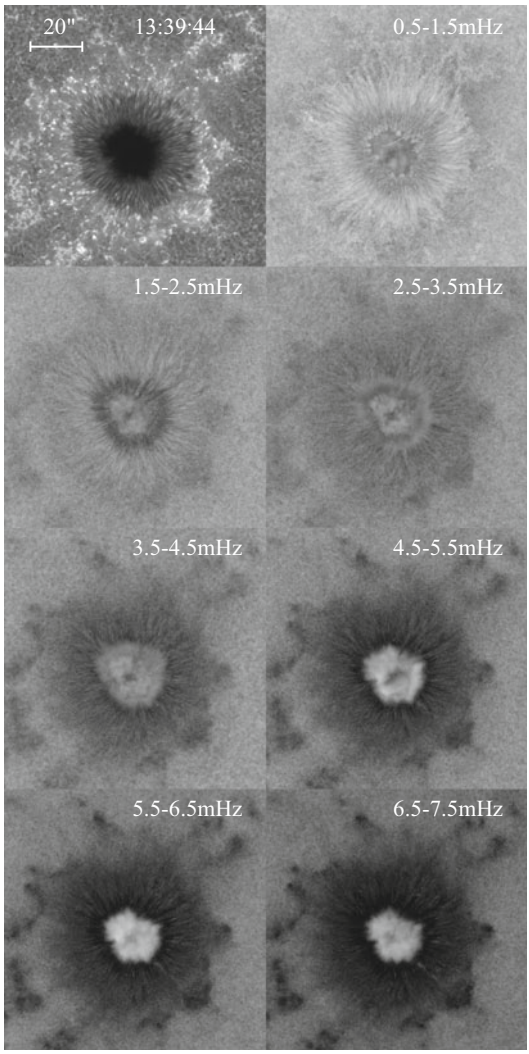

Fig. 17.9 Intensity snapshot in Ca II H line (top left) and power maps in various frequency bands calculated from the Ca II H line filtergrams of active region NOAA 10935. The power is indicated by a logarithmic gray scale where white indicates a large power. In the umbra power above 4.5 mHz is enhanced, except in the very central area (Reprinted from Nagashima et al. 2007 (Fig. 3) by permission of Oxford University Press)

17.3.4.2 Detection of Sunquake

A *sunquake* was detected in the SOT/BFI Ca II H line filtergram (Kosovichev and Sekii 2007). In some rare cases of strong flares, oscillations propagating from the flare site and showing the concentric circles around the epicenter are also observed. This type of rare earthquake-like oscillation on the Sun is the so-called sunquake. From previous studies of sunquake properties, it is thought that sunquakes are manifestations of magnetoacoustic waves. This implies that by examining how the sunquake propagates around the active region, one can investigate the magnetic structure in the regions where the sunquake propagates. Thus, sunquakes are not

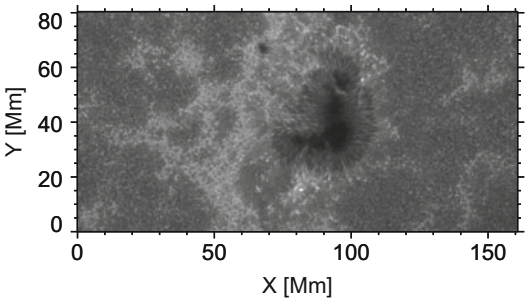

Fig. 17.10 Example Ca II H line intensity image of active region NOAA 10953 taken by *Hinode*/SOT. The light bridge is located around $(X, Y) = (95, 50$ Mm) between the small and big umbrae

only an interesting phenomenon but also a possible tool to probe the extremely complicated magnetic structure around active regions.

17.3.4.3 Sunspot Seismology

The interior structure of sunspots is important and of interest to a wide range of solar physicists. Many helioseismology studies of sunspots have been carried out, although the results thus far are still controversial (e.g., Moradi et al. 2010). This is partly because the effect of the strong magnetic field in the sunspot on Dopplergrams cannot be removed completely. Moreover, unlike the sophisticated global quiet-Sun model, the interior structure model of a sunspot is not well established. Hence, the deviation from the "reference" model (sometimes even the quiet-Sun model is used as reference) is not small enough to be treated in the linear regime, although the inversion using the travel time usually handles the linear perturbations of the interior parameters.

Thus, sunspot seismology is still difficult. A challenge to depict the interior structure of a complicated sunspot by helioseismology using SOT datasets was reported (Zhao et al. 2010). The sunspot has a complicated shape like the Japanese archipelago (active region NOAA 10953; see Fig. 17.10), and several fine structures in the sunspot were reported in Zhao et al. (2010). Especially, under the light bridge (the bright feature in the sunspot umbra), the region with high sound speed (i.e.,"hot" region) and a diverging flow was found.

17.4 Outlook

As you have read so far, *Hinode* provides unique observations for helioseismology studies. Not only have they provided new insights into the Sun but also reminded us of what we have overlooked in the analysis as well as they have revealed new possibilities for helioseismology analysis. Before I conclude this article, I would like to briefly mention the remaining issues in general helioseismic analysis.

One of the main challenges facing local helioseismology is the helioseismic analysis of regions with strong magnetic fields (Schunker et al. 2013). Another important one I consider is the center-to-limb variation.

The measured physical quantities obtained from the helioseismology analyses, such as travel times and interior velocities, tend to depend on the distance from the disk center. This systematic center-to-limb-variation effects are not negligible (Zhao et al. 2012). If the analysis would be carried out without calibration taking account into the systematics, for example, even the solar rotation speed at a certain latitude in the quiet-Sun region would exhibit significant longitudinal dependence, although it should be constant on the same latitudinal line. This is not limited to the results of the time–distance helioseismology analysis but is observed in other local helioseismology results as well. In addition, this is not instrumental systematics of a certain instrument but is seen in various instruments datasets. The behavior, however, depends on the observables (Zhao et al. 2012).

Though the origin of these systematic effects is not yet understood, there are several possible sources. For instance, the anisotropic foreshortening could be part of the cause. The formation height variation might affect it as well; as the line-of-sight depth of the atmosphere is longer as the observed region approaches the limb, we obtain information of the shallower layers of the atmosphere in the regions closer to the limb from the observation even in an identical absorption line. However, it has been turned out that the problem is not so simple such that we can explain it by one, or a simple combination, of these effects.

When the full-disk datasets are obtained and used in the analyses, such as HMI data analysis, a priori calibrations could be applicable, for example, subtracting the longitudinal trend on the equator from the latitudinal trend on the meridional line (Zhao et al. 2012). However, in the case of the analysis of limited field-of-view data, such as the *Hinode*/SOT datasets, calibration cannot be performed unless the cause is understood. Hence, the polar-region analysis requires careful consideration, and the SOT polar-region analysis could not proceed any further after the supergranulation study (Nagashima et al. 2011).[1]

Although we expect no new observations for helioseismology by SOT any more, the legacy of *Hinode*/SOT leaves us with observations that are unique and may still be exploited for new insights once helioseismic analysis techniques are improved. I also would like to improve the analysis technique, which I had acquired during my PhD study using *Hinode*/SOT datasets.

[1] As I discussed in Sect. 17.3.3, the signal averaged over the annulus was used in the travel-time calculation of the polar supergranulation study (Nagashima et al. 2011). This alleviates the systematic effect, and the results in Nagashima et al. (2011) are robust. However, if we aim to measure the rotation speed or the meridional flow in the polar region, calibration taking account of the systematics is crucial.

Acknowledgements I thank Aaron C. Birch, Hannah Schunker, Takashi Sekii, and Masahito Kubo for useful comments on this article. *Hinode* is a Japanese mission developed and launched by ISAS/JAXA, with NAOJ as domestic partner and NASA and STFC (UK) as international partners. It is operated by these agencies in cooperation with ESA and NSC (Norway). I would like to thank Editage (www.editage.jp) for English language editing.

References

Beckers, J.M., Tallant, P.E.: Chromospheric inhomogeneities in sunspot umbrae. Sol. Phys. **7**, 351–365 (1969). https://doi.org/10.1007/BF00146140

Christensen-Dalsgaard, J.: Helioseismology. Rev. Mod. Phys. **74**, 1073–1129 (2002). https://doi.org/10.1103/RevModPhys.74.1073

Deubner, F.L.: Observations of low wavenumber nonradial eigenmodes of the Sun. A&A **44**, 371–375 (1975)

Domingo, V., Fleck, B., Poland, A.I.: The SOHO mission: an overview. Sol. Phys. **162**, 1–37 (1995). https://doi.org/10.1007/BF00733425

Duvall, T.L. Jr, Jefferies, S.M., Harvey, J.W., Pomerantz, M.A.: Time-distance helioseismology. Nature **362**, 430–432 (1993). https://doi.org/10.1038/362430a0

Gizon, L., Birch, A.C.: Local helioseismology. Living Rev. Sol. Phys. **2**, 6 (2005). https://doi.org/10.12942/lrsp-2005-6

Golub, L., Deluca, E., Austin, G., Bookbinder, J., Caldwell, D., Cheimets, P., Cirtain, J., Cosmo, M., Reid, P., Sette, A., Weber, M., Sakao, T., Kano, R., Shibasaki, K., Hara, H., Tsuneta, S., Kumagai, K., Tamura, T., Shimojo, M., McCracken, J., Carpenter, J., Haight, H., Siler, R., Wright, E., Tucker, J., Rutledge, H., Barbera, M., Peres, G., Varisco, S.: The X-ray telescope (XRT) for the Hinode mission. Sol. Phys. **243**, 63–86 (2007). https://doi.org/10.1007/s11207-007-0182-1

Harvey, J.W., Hill, F., Hubbard, R.P., Kennedy, J.R., Leibacher, J.W., Pintar, J.A., Gilman, P.A., Noyes, R.W., Title, A.M., Toomre, J., Ulrich, R.K., Bhatnagar, A., Kennewell, J.A., Marquette, W., Patron, J., Saa, O., Yasukawa, E.: The global oscillation network group (GONG) project. Science **272**, 1284–1286 (1996). https://doi.org/10.1126/science.272.5266.1284

Kosovichev, A.G., Duvall, T.L. Jr: Acoustic tomography of solar convective flows and structures. In: Pijpers, F.P., Christensen-Dalsgaard, J., Rosenthal, C.S. (eds.) SCORe'96: Solar Convection and Oscillations and Their Relationship. Astrophysics and Space Science Library, vol. 225, pp. 241–260. Springer, Dordrecht (1997). https://doi.org/10.1007/978-94-011-5167-2_26

Kosovichev, A.G., Sekii, T.: Initial observations of sunspot oscillations excited by solar flare. ApJL **670**, L147–L149 (2007). https://doi.org/10.1086/524298

Kosugi, T., Matsuzaki, K., Sakao, T., Shimizu, T., Sone, Y., Tachikawa, S., Hashimoto, T., Minesugi, K., Ohnishi, A., Yamada, T., Tsuneta, S., Hara, H., Ichimoto, K., Suematsu, Y., Shimojo, M., Watanabe, T., Shimada, S., Davis, J.M., Hill, L.D., Owens, J.K., Title, A.M., Culhane, J.L., Harra, L.K., Doschek, G.A., Golub, L.: The Hinode (Solar-B) mission: an overview. Sol. Phys. **243**, 3–17 (2007). https://doi.org/10.1007/s11207-007-9014-6

Leighton, R.B., Noyes, R.W., Simon, G.W.: Velocity fields in the solar atmosphere. I. Preliminary report. Astrophys. J. **135**, 474 (1962). https://doi.org/10.1086/147285

Miesch, M.S., Brun, A.S., Toomre, J.: Solar differential rotation influenced by latitudinal entropy variations in the tachocline. Astrophys. J. **641**, 618–625 (2006). https://doi.org/10.1086/499621

Mitra-Kraev, U., Kosovichev, A.G., Sekii, T.: Properties of high-degree oscillation modes of the Sun observed with Hinode/SOT. A&A **481**, L1–L4 (2008). https://doi.org/10.1051/0004-6361:20079042

Moradi, H., Baldner, C., Birch, A.C., Braun, D.C., Cameron, R.H., Duvall, T.L., Gizon, L., Haber, D., Hanasoge, S.M., Hindman, B.W., Jackiewicz, J., Khomenko, E., Komm, R., Rajaguru, P., Rempel, M., Roth, M., Schlichenmaier, R., Schunker, H., Spruit, H.C., Strassmeier, K.G., Thompson, M.J., Zharkov, S.: Modeling the subsurface structure of sunspots. Sol. Phys. **267**, 1–62 (2010). https://doi.org/10.1007/s11207-010-9630-4

Müller, D., Marsden, R.G., St. Cyr, O.C., Gilbert, H.R.: Solar orbiter: exploring the Sun-heliosphere connection. Sol. Phys. **285**, 25–70 (2013). https://doi.org/10.1007/s11207-012-0085-7

Nagashima, K.: Local helioseismology with solar optical telescope onboard Hinode. Ph.D. thesis, The Graduate University for Advanced Studies (2010)

Nagashima, K., Sekii, T., Kosovichev, A.G., Shibahashi, H., Tsuneta, S., Ichimoto, K., Katsukawa, Y., Lites, B., Nagata, S., Shimizu, T., Shine, R.A., Suematsu, Y., Tarbell, T.D., Title, A.M.: Observations of sunspot oscillations in G band and Ca II H line with solar optical telescope on Hinode. PASJ **59**, S631–S636 (2007). https://doi.org/10.1093/pasj/59.sp3.S631

Nagashima, K., Sekii, T., Kosovichev, A.G., Zhao, J., Tarbell, T.D.: Helioseismic signature of chromospheric downflows in acoustic travel-time measurements from Hinode. ApJL **694**, L115–L119 (2009a). https://doi.org/10.1088/0004-637X/694/2/L115

Nagashima, K., Sekii, T., Kosovichev, A.G., Zhao, J., Tarbell, T.D.: Travel-time analyses of an emerging-flux region. In: Lites, B., Cheung, M., Magara, T., Mariska, J., Reeves, K. (eds.) The Second Hinode Science Meeting: Beyond Discovery-Toward Understanding. Astronomical Society of the Pacific Conference Series, vol. 415. pp. 417–420. Astronomical Society of the Pacific, San Francisco (2009b)

Nagashima, K., Zhao, J., Kosovichev, A.G., Sekii, T.: Detection of supergranulation alignment in polar regions of the Sun by helioseismology. ApJL **726**, L17 (2011). https://doi.org/10.1088/2041-8205/726/2/L17

Pesnell, W.D., Thompson, B.J., Chamberlin, P.C.: The solar dynamics observatory (SDO). Sol. Phys. **275**, 3–15 (2012). https://doi.org/10.1007/s11207-011-9841-3

Rouppe van der Voort, L.H.M., Rutten, R.J., Sütterlin, P., Sloover, P.J., Krijger, J.M.: La Palma observations of umbral flashes. A&A **403**, 277–285 (2003). https://doi.org/10.1051/0004-6361:20030237

Scherrer, P.H., Bogart, R.S., Bush, R.I., Hoeksema, J.T., Kosovichev, A.G., Schou, J., Rosenberg, W., Springer, L., Tarbell, T.D., Title, A., Wolfson, C.J., Zayer, I., MDI Engineering Team: The solar oscillations investigation – Michelson Doppler imager. Sol. Phys. **162**, 129–188 (1995). https://doi.org/10.1007/BF00733429

Schou, J., Scherrer, P.H., Bush, R.I., Wachter, R., Couvidat, S., Rabello-Soares, M.C., Bogart, R.S., Hoeksema, J.T., Liu, Y., Duvall, T.L., Akin, D.J., Allard, B.A., Miles, J.W., Rairden, R., Shine, R.A., Tarbell, T.D., Title, A.M., Wolfson, C.J., Elmore, D.F., Norton, A.A., Tomczyk, S.: Design and ground calibration of the helioseismic and magnetic imager (HMI) instrument on the solar dynamics observatory (SDO). Sol. Phys. **275**, 229–259 (2012). https://doi.org/10.1007/s11207-011-9842-2

Schunker, H., Gizon, L., Cameron, R.H., Birch, A.C.: Helioseismology of sunspots: how sensitive are travel times to the Wilson depression and to the subsurface magnetic field? A&A **558**, A130 (2013). https://doi.org/10.1051/0004-6361/201321485

Sekii, T.: SOT local-helioseismology programme. In: Sakurai, T., Sekii, T. (eds.) The Solar-B Mission and the Forefront of Solar Physics. Astronomical Society of the Pacific Conference Series, vol. 325. pp. 87–92. Astronomical Society of the Pacific, San Francisco (2004)

Sekii, T., Kosovichev, A.G., Zhao, J., Tsuneta, S., Shibahashi, H., Berger, T.E., Ichimoto, K., Katsukawa, Y., Lites, B., Nagata, S., Shimizu, T., Shine, R.A., Suematsu, Y., Tarbell, T.D., Title, A.M.: Initial helioseismic observations by Hinode/SOT. PASJ **59**, S637–S641 (2007). https://doi.org/10.1093/pasj/59.sp3.S637

Tsuneta, S., Ichimoto, K., Katsukawa, Y., Lites, B.W., Matsuzaki, K., Nagata, S., Orozco Suárez, D., Shimizu, T., Shimojo, M., Shine, R.A., Suematsu, Y., Suzuki, T.K., Tarbell, T.D., Title, A.M.: The magnetic landscape of the Sun's polar region. Astrophys. J. **688**, 1374–1381 (2008a). https://doi.org/10.1086/592226

Tsuneta, S., Ichimoto, K., Katsukawa, Y., Nagata, S., Otsubo, M., Shimizu, T., Suematsu, Y., Nakagiri, M., Noguchi, M., Tarbell, T., Title, A., Shine, R., Rosenberg, W., Hoffmann, C., Jurcevich, B., Kushner, G., Levay, M., Lites, B., Elmore, D., Matsushita, T., Kawaguchi, N., Saito, H., Mikami, I., Hill, L.D., Owens, J.K.: The solar optical telescope for the Hinode mission: an overview. Sol. Phys. **249**, 167–196 (2008b). https://doi.org/10.1007/s11207-008-9174-z

Ulrich, R.K.: The five-minute oscillations on the solar surface. Astrophys. J. **162**, 993–1002 (1970). https://doi.org/10.1086/150731

Zhao, J., Kosovichev, A.G., Duvall, T.L. Jr: Investigation of mass flows beneath a sunspot by time-distance helioseismology. Astrophys. J. **557**, 384–388 (2001). https://doi.org/10.1086/321491

Zhao, J., Kosovichev, A.G., Sekii, T.: High-resolution helioseismic imaging of subsurface structures and flows of a solar active region observed by Hinode. Astrophys. J. **708**, 304–313 (2010). https://doi.org/10.1088/0004-637X/708/1/304

Zhao, J., Nagashima, K., Bogart, R.S., Kosovichev, A.G., Duvall, T.L. Jr: Systematic center-to-limb variation in measured helioseismic travel times and its effect on inferences of solar interior meridional flows. ApJL **749**, L5 (2012). https://doi.org/10.1088/2041-8205/749/1/L5

Part IV
Newly Opened Physics and Future Observations

Chapter 18
Penumbral Microjets in Sunspot Chromospheres: Evidence of Magnetic Reconnection

Yukio Katsukawa

Abstract It is not too much to say that the greatest achievement of the *Hinode* Solar Optical Telescope is observational demonstration of active plasma ejections (i.e., jets) occurring everywhere in the solar chromosphere. Among them, the penumbral microjets newly discovered by *Hinode* are a small-scale jet phenomenon that occurs frequently in the chromosphere above a sunspot penumbra. They are important because we can show strong evidence supporting magnetic reconnection as a driver of chromospheric jets because we can observe in detail the magnetic field and velocity structures around the site where a penumbral microjet occurs. The observation of penumbral microjets gave rise to strong recognition of the importance of magnetic reconnection in driving transient energy release even when the magnetic fields are not completely antiparallel. Recent progress in high-resolution observations of transition regions and coronae suggests the possible influence of penumbral microjets in the atmosphere outer than the chromosphere.

Keywords Sun · Hinode · Sun: chromosphere · Jets · Sunspots

18.1 Dynamic Chromosphere Revealed by *Hinode*

The Solar Optical Telescope (SOT) aboard *Hinode* has a unique capability for high-resolution and stable observations unaffected by atmospheric seeing. This capability has been clearly demonstrated in studies of active phenomena in the solar chromosphere and prominences above the visible surface. If we watch a movie taken through the ionized calcium (Ca II) H-band filter (396 nm), which is sensitive to the chromosphere, we can immediately notice plasma blowing up from several thousands of kilometers to often higher than 10,000 km everywhere

Y. Katsukawa (✉)
Solar Science Observatory, National Astronomical Observatory of Japan, Mitaka, Tokyo, Japan
e-mail: yukio.katsukawa@nao.ac.jp

T. Shimizu et al. (eds.), *First Ten Years of Hinode Solar On-Orbit Observatory*,
Astrophysics and Space Science Library 449,
https://doi.org/10.1007/978-981-10-7742-5_18

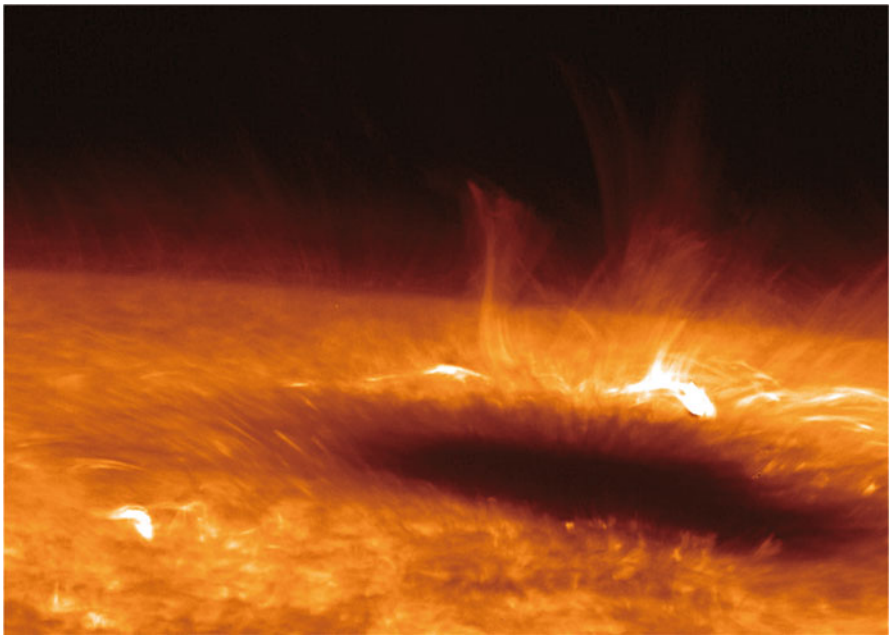

Fig. 18.1 Chromospheric jets around a sunspot observed with the Ca II H filter of the *Hinode* SOT

(Fig. 18.1). The speed of the plasma ejection is several tens of kilometers per second to over 100 km s^{-1}. Considering that the sound speed in a 10^4 K chromosphere is about 10 km s^{-1}, we can see how fast the plasma ejection is. Although visible light observations are possible with a ground-based telescope, studies of phenomena that change on a short time scale of several seconds to 10 s have been limited by the effect of atmospheric seeing. After *Hinode* attracted attention to active phenomena in the chromosphere, many studies have been done (Fig. 18.2) even with ground-based telescopes, thanks to advances in adaptive optics and seeing correction by image post-processing. Furthermore, the *Interface Region Imaging Spectrograph (IRIS)* satellite (described later), which specialized in high-resolution spectroscopic observations of the chromosphere, appeared in 2013. These developments were obviously triggered and accelerated by *Hinode*. The solar surface, i.e., the photosphere, has abundant thermal and kinetic energy driving turbulent convection, and magnetic fields receive energy from this convection. In the chromosphere, conversely, magnetic energy becomes dominant, and the ambient atmosphere can be accelerated and heated by the magnetic field. The ratio of the gas pressure to the magnetic pressure is called the plasma β, and β is high in the photosphere and low in the chromosphere. *Hinode* has provided data on the plasma dynamics in the low β atmosphere dominated by magnetic fields.

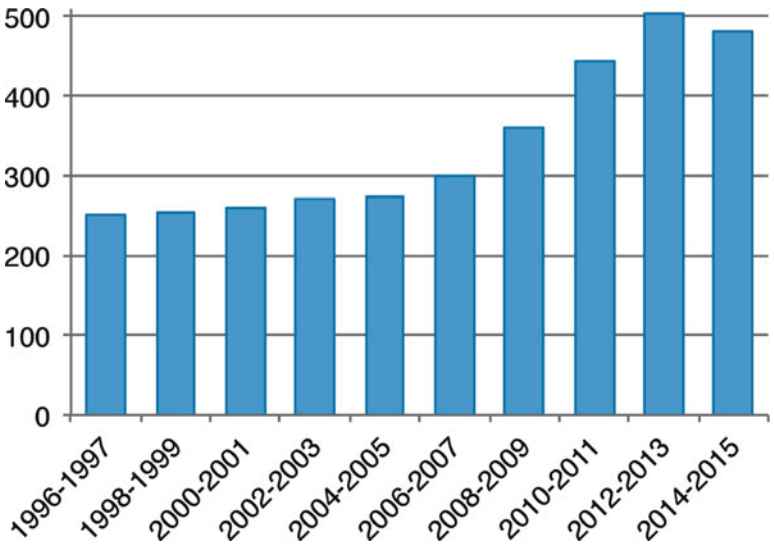

Fig. 18.2 Number of peer-reviewed papers including "solar chromosphere" in the abstract, retrieved by the Astrophysics Data System (ADS). Since 2007, when the first *Hinode* results appeared, the number of papers on the chromosphere has increased significantly (Reprinted from The Astronomical Herald by permission of ASJ)

There are various types of chromospheric jets. In quiet regions and the periphery of an active region, jet-like phenomena called spicules are ubiquitous (De Pontieu et al. 2007); they have a length of 2,000–10,000 km. Chromospheric jets around a sunspot in an active region are called chromospheric anemone jets that have a length of 2,000–5,000 km and often show an inverse Y-shaped structure around their roots (Shibata et al. 2007). Although these jet phenomena were already known even before *Hinode*, the mechanism driving them is being unveiled by studies of their temporal evolution and statistical properties based on data provided by *Hinode* observations. The penumbral microjets that I have been focusing on were newly discovered by *Hinode* (Katsukawa et al. 2007). Details on penumbral microjets are presented in the following sections.

18.2 Discovery of Penumbral Microjets

It was remarkably easy to notice fine-scale jet-like brightenings ubiquitously occurring in a sunspot penumbra when I watched a movie taken through the SOT Ca II H-band filter (Fig. 18.3). It was in November 2006, just after the top door of the telescope was opened. I was greatly impressed when I found the microjets and speculated that they could provide a major clue to solving the coronal heating

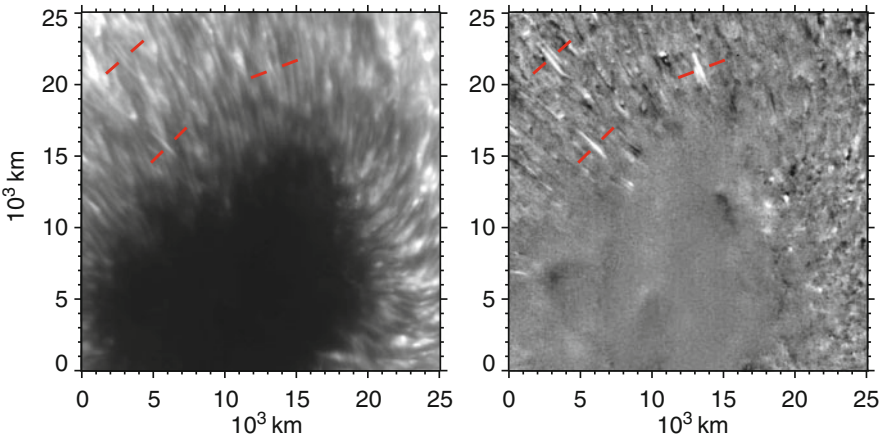

Fig. 18.3 *Hinode* observation of a sunspot chromosphere taken with the Ca II H-band filter of SOT (left) and a difference image from one taken 20 s earlier (right). The red dashed lines indicate penumbral microjets. We can easily see the microjets in the difference image (Reprinted from The Astronomical Herald by permission of ASJ)

problem. Because I studied the possibility that photospheric magnetic structures in a sunspot penumbra had influenced coronal heating in my PhD, I anticipated seeing an elemental process responsible for coronal heating. I then began to study the chromosphere, but the effect on coronal heating has not been clearly shown yet.

Penumbral microjets have a length of about 1,000–4,000 km, a width of 400 km or less, and a lifetime of 1 min or less, which makes them a short-lived and minute phenomenon compared with the known phenomena in the chromosphere. In a ground-based telescope, such a fine chromospheric phenomenon could not be detected, although it can be studied by a ground-based observation after *Hinode*, as described later. The apparent rising speed of the microjets is fast, exceeding $100\,\mathrm{km\,s^{-1}}$, and is much faster than the sound speed ($\sim 10\,\mathrm{km\,s^{-1}}$) in the chromosphere. Spectropolarimetric observations have revealed strong and interlaced magnetic structures inherent in a sunspot penumbra (Solanki 2003; Borrero and Ichimoto 2011; Katsukawa 2008). A relatively strong vertical magnetic component and a relatively weak horizontal component exist alternately to form an uncombed magnetic structure (Fig. 18.4). Penumbral microjets indicate decisively that chromospheric heating is caused by energy release due to magnetic reconnection at the boundary of these different magnetic components in a sunspot penumbra. Moreover, it is suggested that magnetic reconnection can occur and cause impulsive heating even if the magnetic fields are not completely antiparallel. The discovery of penumbral microjets revealed the importance of magnetic reconnection in chromospheric activity.

The plasma β is unity or lower even in the photosphere of a sunspot. This means that penumbral microjets occur in the environment where magnetic fields dominate.

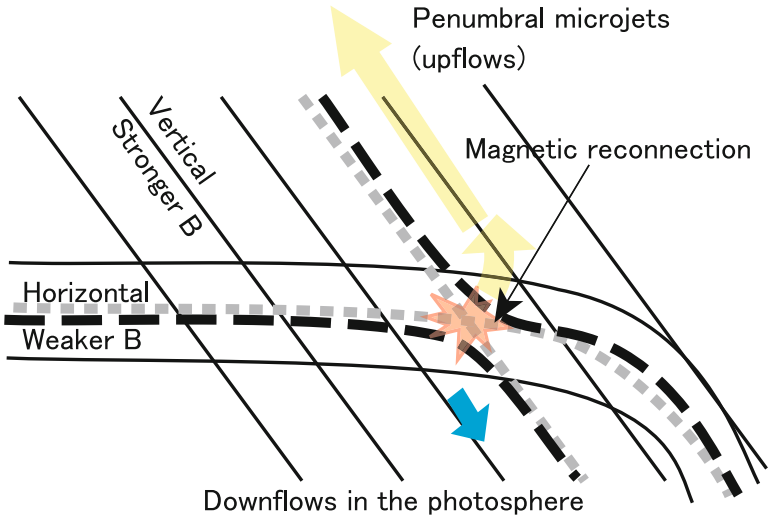

Fig. 18.4 Schematic diagram of a penumbral microjet. The black lines represent magnetic field lines in a penumbra. The dotted and broken lines show magnetic field lines before and after the magnetic reconnection causing the penumbral microjet. Yellow and blue arrows represent an upward flow causing chromospheric heating and a downward flow observed in the photosphere, respectively (Reprinted from The Astronomical Herald by permission of ASJ)

Furthermore, the interlaced magnetic structure is spontaneously and constantly generated by convection in the sunspot penumbra. Penumbral microjets are a natural consequence of heating and acceleration by magnetic reconnection in this region. No one had predicted them before *Hinode*, but the interpretation that magnetic reconnection plays an important role was convincing.

If a penumbral microjet is driven by magnetic reconnection, some questions arise naturally. For example, is it possible to see flows generated by magnetic reconnection? Or, can we see time variation in the magnetic fields? To investigate these questions, we investigated the relationship between penumbral microjets and the magnetic and velocity fields in the photosphere using a spectropolarimetric observation, which is another unique capability of the *Hinode* SOT. This was collaborative research with J. Jurcak, who visited Japan from the Czech Republic as a postdoctoral researcher. We revealed that jet-like brightenings are aligned with the relatively vertical magnetic field in a penumbra (Jurcak and Katsukawa 2008). Furthermore, we found that short-lived downflows are generated in the photosphere coincident with brightenings in the chromosphere (Katsukawa and Jurcak 2010; Jurcak and Katsukawa 2010). These studies suggested a scenario in which magnetic reconnection occurs in the upper photosphere or lower chromosphere, and intensity enhancements indicating a temperature rise occur along magnetic field lines in the atmospheric layer above the reconnection. A downward flow is generated in the photosphere beneath the reconnection, as shown in the schematic diagram in

Fig. 18.4. It is worth mentioning that we could obtain abundant knowledge from observations of the magnetic fields and velocities around the magnetic reconnection site, which is one of the unique features of penumbral microjets. On the other hand, time variation of the magnetic field structures has not yet been detected in association with penumbral microjets. The reason may be that magnetic reconnection site is located above the photosphere, where magnetic field measurements are less sensitive.

Another problem in studies of penumbral microjets is that we cannot distinguish apparent motion (e.g., propagation of waves and a temperature rise) and true mass motion using only the *Hinode* SOT's filter-based imaging observations. Therefore, an imaging spectroscopic observation of the near-infrared Ca II line at 854 nm was performed with a tunable Fabry-Pérot filter (IBIS) at the Dunn Solar Telescope of the National Solar Observatory (NSO), US. This work was done in collaboration with K. Reardon and A. Tritschler of the NSO. We succeeded in observing a large number of Ca II line spectral profiles associated with penumbral microjets (Reardon et al. 2013) (Fig. 18.5). Before the observation, we expected that the wavelength of the Ca II line center would shift owing to the Doppler effect of supersonic motion. However, the motion estimated from the Doppler shift of the line is at most $10\,\mathrm{km\,s^{-1}}$ and is considerably smaller than the apparent propagation speed seen in the filter imaging observation. After the discovery of penumbral microjets by *Hinode*, magnetohydrodynamic (MHD) numerical simulations have also been performed to reproduce the penumbral microjets; they succeeded in reproducing the jets along magnetic field lines (Magara 2010; Nakamura et al. 2012). In these numerical simulations, the upward speed of the jets is at most $10\,\mathrm{km\,s^{-1}}$, which is consistent with the observation. This is because it is impossible to create a high-speed flow when magnetic reconnection occurs in the relatively high-density photosphere or in the lower chromosphere. In this case, how can we explain the very fast apparent propagation seen in the Ca II filter imaging observation? There is a high possibility that part of the energy released by magnetic reconnection might propagate upward as an MHD wave along magnetic field lines, although there is little observational evidence to support wave propagation. It is important to reveal how the propagation speed changes along the height of penumbral microjets to capture a signature of the MHD waves. To clearly resolve a wave of $100\,\mathrm{km\,s^{-1}}$ passing through a length of 1,000 km, it is necessary to take an image sequence at a time interval sufficiently shorter than 5 s. We are making such observations with *Hinode* and ground-based telescopes, and we expect to catch a signature of MHD wave propagation in the near future.

18.3 Influence on Heating of the Transition Region and Corona

Since *Hinode* observations began, there was great interest in whether the chromospheric jets further influence heating in the upper atmosphere, that is, the transition region and corona. In observations of the photosphere and chromosphere,

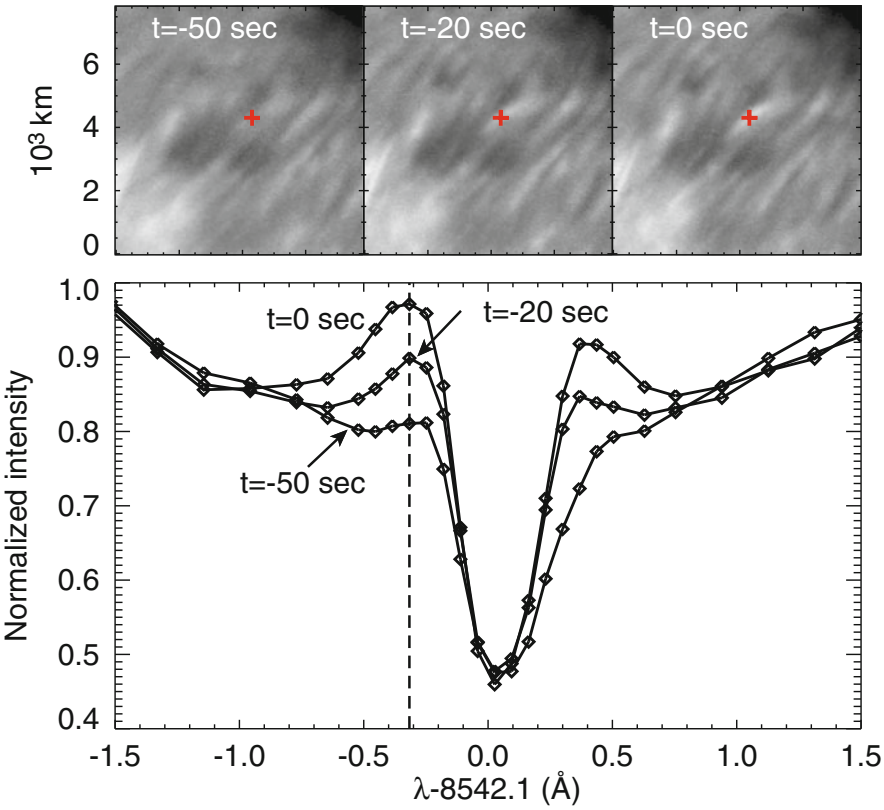

Fig. 18.5 Imaging spectroscopic observation of a penumbral microjet by IBIS at the NSO. The upper panel shows images of a penumbral microjet observed at the Ca II 854 nm spectral line (from left to right, 50 s before the peak, 20 s before, and at the peak time). The Ca II 854 nm spectral line profiles at the middle of the penumbral microjet (marked by the red cross) are shown in the bottom panel. Brightening is seen around ±0.3 Å. The blue side (shorter wavelength) of the Ca II 854 nm spectral line tends to be brighter, indicating that a heated portion of the atmosphere has a blue shift, that is, an upflow. However, the Doppler shift is at most 10 km s^{-1} and is much slower than the apparent velocity (Reprinted from The Astronomical Herald by permission of ASJ)

small-scale jets were captured with a resolution as high as 0.2 arcsec. The observations of the transition region and corona, however, had a spatial resolution of at most 1 to 2 arcsec. We actually tried to find a counterpart of penumbral microjets in the transition region and corona by comparing data taken with the Extreme Ultraviolet Imaging Spectrometer (EIS) aboard *Hinode* and Solar Ultraviolet Measurements of Emitted Radiation (SUMER) aboard the *Solar and Heliospheric Observatory (SoHO)* , but we could not find it. This situation is changing since NASA's *IRIS* started observations in 2013. The *IRIS* satellite is equipped with an ultraviolet (UV) spectrograph, and it can observe the UV spectral lines of the chromosphere, transition region, and corona. The unique capability of *IRIS* compared with past

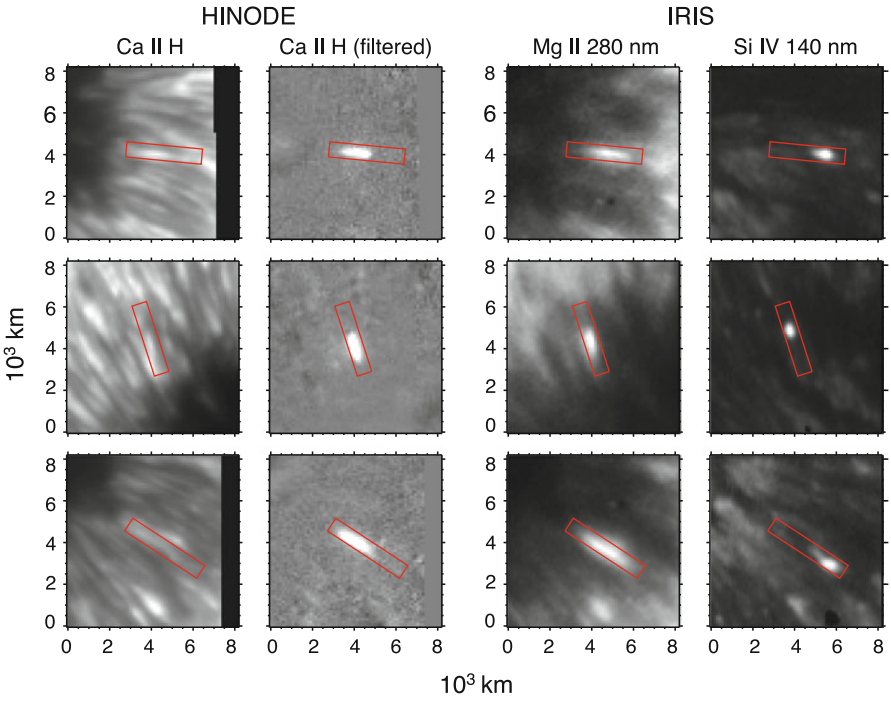

Fig. 18.6 Examples of penumbral microjets observed by *Hinode* and *IRIS*. Two images on the left show penumbral microjets seen in a *Hinode* Ca II H-band filter observation and images enhanced by image filtering. Two images on the right show *IRIS* observations of the penumbral microjets taken at the magnesium II line (wavelength of 280 nm) and the silicon IV line (wavelength of 140 nm). The penumbral microjets are clearly seen at the Mg II 280 nm line, which is sensitive to the 10^4 K chromospheric temperature, similar to the Ca II line. The Si IV 140 nm line is sensitive to the transition region temperature of about 10^5 K and shows point-like brightenings at the tip of the penumbral microjets (Reprinted from The Astronomical Herald by permission of ASJ)

instruments for observing the transition region and corona is a higher resolution of 0.4 arcsec. The *IRIS* observations have attracted attention to penumbral microjets again. In the transition region above a sunspot penumbra, countless point-like brightenings smaller than 1 arcsec have been observed (Tian et al. 2014). Furthermore, it was also found that the point-like brightenings were located at the tip of penumbral microjets in the chromosphere (Vissers et al. 2015; Samanta et al. 2017; Katsukawa et al. 2018) (Fig. 18.6). In other words, it was possible to confirm heating up to the transition region temperature ($\sim 10^5$ K) associated with penumbral microjets. In addition, the rocket experiment High-Resolution Coronal Imager (Hi-C) launched in 2012 revealed many point-like brightenings in the corona above a sunspot during its 5 min flight, thanks to its high resolution of 0.2 arcsec (Alpert

et al. 2016). It has not been well established yet whether penumbral microjets reach a coronal temperature of 1 million K. Detailed observations and analysis are necessary to combine multi-temperature observations.

18.4 Summary and Future Direction

In this article, I introduced research on chromospheric activity, especially on penumbral microjets. A variety of jet phenomena occurring in the chromosphere have a common origin in terms of magnetic reconnection as a driver of the jets. Because the magnetic field strength and configuration vary from place to place, chromospheric jets occur over various temporal and spatial scales. Regarding a jet phenomenon occurring in the light bridge of a sunspot, for example, it has been demonstrated that the jet is driven by magnetic reconnection between the vertical magnetic field and the horizontal one using *Hinode* and *IRIS* observations as well as a numerical simulation (Toriumi et al. 2015a,b). Although the light bridge jets have quite different spatial and temporal scales, the physical process can be easily interpreted as being the same as that of penumbral microjets. Because the magnetic field is weak on the average in areas other than a sunspot, it is expected that magnetic reconnection in the photosphere and chromosphere has a smaller effect on heating and acceleration of the ambient atmosphere because of the relatively high plasma β. However, there are certainly many places where strong magnetic fields are concentrated locally even outside of a sunspot. If magnetic reconnection occurs at such a place, it is possible that some of the released energy is transported upward by MHD waves and heats the corona. Observations of the chromosphere and corona with high spatial and temporal resolution are necessary to confirm the energy release and transfer processes associated with the jets. Another challenge is to catch temporal changes in the magnetic fields associated with the jets in the photosphere and chromosphere. It is necessary to observe the magnetic field and velocity evolution on a time scale shorter than 10 s. There are currently no instruments that have this capability. In the future, the next-generation solar observation satellite SOLAR-C will be able to attempt direct detection from space. The Daniel K. Inouye Solar Telescope (DKIST), a 4 m ground-based solar telescope under construction in Hawaii, will also have powerful spectropolarimetric capability to observe the magnetic fields in the chromosphere with high spatial resolution. Using these observations, I would like to obtain conclusive evidence for the chromospheric and coronal heating.

Acknowledgements I'd like to thank all the people who contributed to the development and operation of the *Hinode* SOT in Japan for 10 years, especially Drs. S. Tsuneta, T. Shimizu, Y. Suematsu, K. Ichimoto, T. J. Okamoto, and M. Kubo, and Mr. T. Bando. Members of the US-SOT team, especially Drs. T. Tarbell and R. Shine, are also acknowledged for their close cooperation. I'd also like to thank Drs. J. Jurcak and K. Reardon for their close cooperation in the studies of penumbral microjets.

References

Alpert, S.E., Tiwari, S.K., Moore, R.L.: Hi-C Observations of sunspot penumbral bright dots. ApJ **822**, 35 (2016)

Borrero, J.M., Ichimoto, K.: Magnetic structure of sunspots. Living Rev. Sol. Phys. **8**, 4 (2011)

De Pontieu, B., McIntosh, S.W., Hansteen, V.H., et al.: A tale of two spicules: the impact of spicules on the magnetic chromosphere. PASJ **59**, S655–S662 (2007)

Jurcak, J., Katsukawa, Y.: The properties of penumbral microjets inclination. A&A. **488**, L33–L36 (2008)

Jurcak, J., Katsukawa, Y.: Temporal downflows in a penumbra. A&A. **524**, A21 (2010)

Katsukawa, Y.: Fine structures in a Sunspot revealed by HINODE. Parity **23**, 39–43 (2008)

Katsukawa, Y., Jurcak, J.: A new type of small-scale downflow patches in sunspot penumbrae. A&A. **524**, A20 (2010)

Katsukawa, Y., Berger, T.E., Ichimoto, K., et al.: Small-scale jetlike features in penumbral chromospheres. Science **318**, 1594–1597 (2007)

Katsukawa, Y., Kimura, Y., Okamoto, T.J., Tarbell, T.D.: Rapid evolution of penumbral microjets and their impacts on heating of the outer solar atmosphere. ApJ (2018, submitted)

Magara, T.: A magnetohydrodynamic model focused on the configuration of magnetic field responsible for a solar penumbral microjet. ApJ **715**, L40–L43 (2010)

Nakamura, N., Shibata, K., Isobe, H.: Numerical simulation of three-dimensional asymmetric reconnection and application to a physical mechanism of penumbral microjets. ApJ **761**, 87 (2012)

Reardon, K., Tritschler, A., Katsukawa, Y.: Spectral signatures of penumbral transients. ApJ **779**, 143 (2013)

Samanta, T., Tian, H., Banerjee, D., Schanche, N.: Dynamics of subarcsecond bright dots in the transition tegion above sunspots and their relation to penumbral micro-jets. ApJ **835**, 19 (2017)

Shibata, K., Nakamura, T., Matsumoto, T., et al.: Chromospheric anemone jets as evidence of ubiquitous reconnection. Science **318**, 1591–1594 (2007)

Solanki, S.: Sunspots: an overview. A&ARv **11**, 153–286 (2003)

Tian, H., Kleint, L., Peter, H., et al.: Observations of subarcsecond bright dots in the transition region above sunspots with the interface region imaging spectrograph. ApJ **790**, L29 (2014)

Toriumi, S., Katsukawa, Y., Cheung, M.C.M.: Light bridge in a developing active region. I. Observation of light bridge and its dynamic activity phenomena. ApJ **811**, 137 (2015a)

Toriumi, S., Cheung, M.C.M., Katsukawa, Y.: Light bridge in a developing active region. II. Numerical simulation of flux emergence and light bridge formation. ApJ **811**, 138 (2015b)

Vissers, G.J.M., Rouppe van der Voort, L.H.M., Carlsson, M.: Evidence for a transition region response to penumbral microjets in Sunspots. ApJ **811**, L33 (2015)

Chapter 19
Physics of Partial Ionization in the Solar Chromosphere Revealed by the Solar Optical Telescope Onboard *Hinode*

Hiroaki Isobe

Abstract The Solar Optical Telescope (SOT) onboard *Hinode* revealed that small-scale explosions and jet phenomena are common occurrences in the chromosphere and the photosphere of the Sun. Their morphology, dynamics, and associated time scales normalized by the local Alfvén speed are similar to those in the coronal microflares and jets driven by magnetic reconnection. However, the lower atmosphere has very different plasma parameters from the corona: the former is partially ionized and fully collisional, while the latter is fully ionized and almost collisionless. Thus the findings of the SOT pose an important question in plasma physics about how such fast magnetic reconnection similar to that in the corona is accommodated in the photosphere and the chromosphere? In this paper we will review the chromospheric observations by the SOT and their implications for the physics of partially ionized plasmas.

Keywords Sun: photosphere · Sun: chromosphere · Partial ionization

19.1 Introduction

Contrary to the fully ionized and nearly collisionless corona, the lower atmosphere of the Sun, namely, the photosphere and chromosphere, is partially ionized and fully collisional. This is simply because the lower atmosphere is not hot enough. While the first ionization potential of hydrogen is $\sim$13.6 eV, corresponding $T \sim 10^5$ K, the temperature of the photosphere and the chromosphere is of the order of 10^4 K. Most of the particles present as well as the photons of the visible light from the photosphere do not have sufficient kinetic energy to the ionize hydrogen atoms

H. Isobe (✉)
Graduate School of Advanced Integrated Studies in Human Survivability, Kyoto University, Sakyo-ku, Kyoto, Japan
e-mail: isobe@kwasan.kyoto-u.ac.jp

T. Shimizu et al. (eds.), *First Ten Years of Hinode Solar On-Orbit Observatory*,
Astrophysics and Space Science Library 449,
https://doi.org/10.1007/978-981-10-7742-5_19

through collision. Thus, if the phenomena in the lower atmosphere are studied, the behavior of the partially ionized and gravitationally stratified plasma with magnetic fields is understood. However, except for some foresighted studies such as De Pontieu and Haerendel (2000), Goodman (2004), Leake and Arber (2006), the physics of partially ionized plasma was not a point of considerable interest in the solar context before the *Hinode* era. Perhaps one of the reasons is that the single fluid magnetohydrodynamics (MHD) is often an adequate approximation to describe the observable dynamics of interest in the solar atmosphere, because the neutral particles are well coupled to the plasma and hence with the magnetic field through collisions. The physics related to partial ionization becomes important at the small scales where differences in behaviors of neutral and plasma fluids become significant.

19.2 Plasma Parameters and Theoretical Treatments

Figure 19.1 shows the electron mean free path and the fraction of neutral hydrogen as a function of height in the solar atmosphere. Here we assumed the Vernazza, Avrett, and Loeser C (VALC) model (Vernazza et al. 1981) in the lower parts ($\leq$1500 km) and smoothly connected it to the conventional values in the corona. It should be noted that in time-dependent models with non-equilibrium hydrogen ionization the neutral fraction is smaller ($\sim 10^2$) on average (Leenaarts et al. 2007). The electron mean free path in the lower atmosphere is much smaller than the smallest scale ever resolved by observation ($\sim$0.1 arcsec $\sim$ 700 km).

In order to examine the coupling of the neutral fluid and the plasma, let us consider the equation of motion of ion fluid in a steady state where Lorentz force balances the drag force by collision with neutral fluid:

$$\nu_{ni}\rho_n(V_n - V_i) \approx \frac{JB}{c} \approx \frac{B^2}{4\pi L}\,, \tag{19.1}$$

where ν_{ni} is the neutral-ion collisional frequency, ρ_n is the mass density of neutral fluid, L is the characteristic scale of the system (width of the current sheet), and V, B, J, and c are the velocity, magnetic field current density, and speed of light, respectively. Subscripts n and i denote neutral and ion fluids, respectively. By substituting typical values in the chromosphere, the neutral-ion relative velocity $V_n - V_i$ can be estimated as

$$V_n - V_i \approx \frac{B^2}{4\pi L \nu_{ni}\rho_n} \approx 100\Big(\frac{V_A}{10\,\mathrm{km\,s^{-1}}}\Big)^2\Big(\frac{L}{100\,\mathrm{km}}\Big)^{-1}\Big(\frac{\nu_{ni}}{10^3\,\mathrm{Hz}}\Big)^{-1}\,\mathrm{cm\,s^{-1}}, \tag{19.2}$$

where V_A is the Alfvén velocity. This value is much smaller than the typical velocity of flows and waves in the chromosphere ($\sim$10 km s^{-1}). This is the reason why single fluid MHD is a good approximation to describe the observable dynamics.

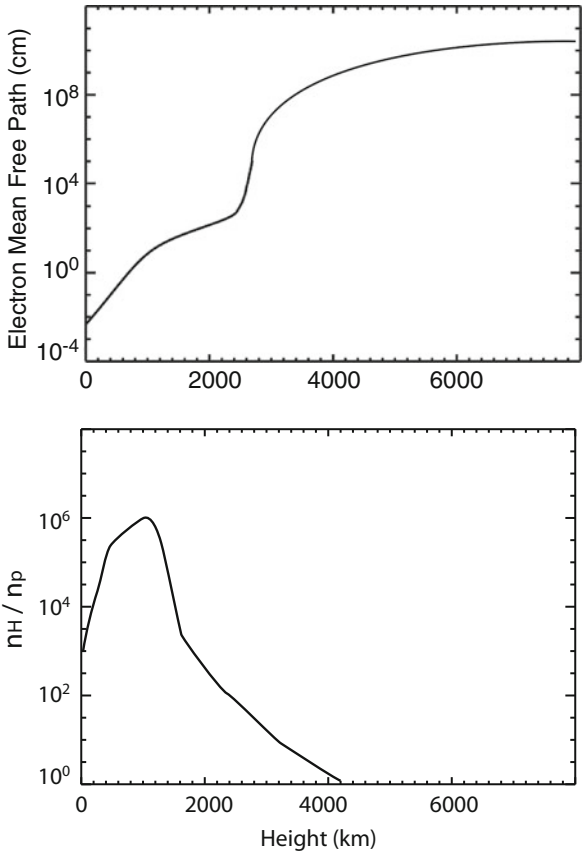

Fig. 19.1 Electron mean free path and the neutral fraction n_H/n_p as a function of the height in the solar atmosphere, where n_H and n_p is the number density of neutral hydrogen and proton, respectively

However, in the phenomena where small scale processes play important roles, such as magnetic reconnection and wave dissipation, the effects of neutrals become significant. In order to describe the effect of neutrals within the single fluid MHD approximation, generalized magnetic induction equation is often used (Leake and Arber 2006; Brandenburg and Zweibel 1994; Singh and Krishan 2010; Martinez-Sykora et al. 2012). It is given by

$$\frac{\partial \mathbf{B}}{\partial t} = \nabla \times \left[\mathbf{V} \times \mathbf{B} - \frac{\mathbf{J} \times \mathbf{B}}{e n_e} + \frac{(\mathbf{J} \times \mathbf{B}) \times \mathbf{B}}{c \nu_{ni} \rho_n} - \eta_O \mathbf{J} \right], \tag{19.3}$$

where n_e is the electron number density and η_O is the Ohmic resistivity. The second term on the right-hand side is the Hall term that stems from the relative motion of ion and electron fluids, i.e., the current density $\mathbf{J}$. The third term is called Pedersen term (also known as the ambipolar diffusion in the astrophysical context) that stems from ion-neutral friction. By comparison with the advection term $\mathbf{V} \times \mathbf{B}$, one can see that, phenomenologically, the Hall term and the Pedersen term advect the magnetic field in the direction of $\mathbf{J}$ and $\mathbf{J} \times \mathbf{B}$, respectively. Both Hall and

Pedersen terms are proportional to $\mathbf{J}$, and hence the coefficients can be regarded as "resistivities": $\eta_H = B/(en_e)$, $\eta_P = B^2/(c\nu_{ni}\rho_n)$. Hereafter we refer to the Hall, Pedersen, and Ohmic terms as to "resistive terms" just for convenience. It should be noted that the Hall term does not yield dissipation of the magnetic field, while the Pedersen term dissipates the electric current perpendicular to the magnetic field. A remarkable characteristics of the Pedersen term is that it sharpens the current sheet (Brandenburg and Zweibel 1994).

The Hall, Pedersen, and Ohmic resistivities are determined only by the local plasma parameters and do not depend on the spatial scale. Using typical plasma parameters, $\eta_H > \eta_O > \eta_P$ in the photosphere and $\eta_P > \eta_H > \eta_O$ in the chromosphere (Singh and Krishan 2010; Khomenko and Collados 2012). A detailed review of the plasma parameters in comparison with the Earth's ionosphere is given in Leake et al. (2014). It can be shown that the ratio of the Hall and Pedersen resistivities is given by the ratio of ion-neutral collision frequency and ion-cyclotron frequency; $\eta_H/\eta_P = \nu_{in}/\omega_{ci}$. From this relation one can see that the Hall effect becomes significant when ions are decoupled from the magnetic field due to the collision with the neutrals, while electrons are still coupled with the magnetic field.

It is also interesting to note that, in term of the relative strength of resistivities, the photosphere is similar to the inner part of protoplanetary disks, while the chromosphere is similar to the outer part of protoplanetary disks as well as the molecular clouds (Sano and Stone 2002). The lower atmosphere of the Sun can be regarded as a unique laboratory for the physics of partially ionized plasmas in other astrophysical systems.

Let us now compare the advection term and the other terms in the right-hand side of the induction equation. The ratio of the advection term and the other resistive terms depends on the scale; the resistive terms become more important in smaller scale. The condition for the Hall term to be larger than the advection term is given by

$$VB \leq \frac{JB}{en_e} \approx \frac{cB^2}{4\pi en_e L} \tag{19.4}$$

$$L \leq \frac{cB}{4\pi en_e V} \approx 10^5 \left(\frac{B}{20\,\mathrm{G}}\right)\left(\frac{n_e}{10^{10}\,\mathrm{cm}^{-3}}\right)^{-1}\left(\frac{V}{10^5\,\mathrm{cm\,s}^{-1}}\right)^{-1}\mathrm{cm}. \tag{19.5}$$

Similarly, the condition for the Pedersen term to be larger than the advection term is given by

$$VB \leq \frac{JB^2}{c\nu_{ni}\rho_n} \approx \frac{B^3}{4\pi\nu_{ni}\rho_n L} \tag{19.6}$$

$$L \leq \frac{B^2}{4\pi\nu_{ni}\rho_n V} \tag{19.7}$$

$$\approx 2\times 10^5 \left(\frac{B}{20\,\mathrm{G}}\right)^2\left(\frac{\nu_{ni}}{10^3\,\mathrm{Hz}}\right)^{-1}\left(\frac{\rho_n}{10^{-12}\,\mathrm{g\,cm}^{-3}}\right)^{-1}\left(\frac{V}{10^5\,\mathrm{cm\,s}^{-1}}\right)^{-1}\mathrm{cm}. \tag{19.8}$$

Thus, the Hall and Pedersen terms become significant only at such small (< a few km) scales that are far below the spatial resolution of the Solar Optical Telescope (SOT) (Cheung and Cameron 2012).

While the single-fluid MHD with the generalized Ohm's law (induction equation) is a convenient and still reasonable approximation to describe the global dynamics, it is obvious that it does not describe the plasma and neutral dynamics properly at the small scale. Multi-fluid treatment is necessary for this purpose (Zaqarashvili et al. 2011; Leake et al. 2012; Khomenko et al. 2014a).

19.3 Brief Overview of the SOT Results

The most outstanding achievement of *Yohkoh*, the Japanese solar mission prior to *Hinode*, is the establishment of magnetic reconnection model as the driver of magnetic energy release in the solar corona (Shibata 1996). The SOT onboard *Hinode* has revealed that the photosphere and the chromosphere are also full of explosive phenomena associated with magnetic reconnection (Katsukawa et al. 2007; Shibata et al. 2007).

Figure 19.2 shows an example of a chromospheric jet (Shibata et al. 2007; Singh et al. 2012) observed by *Hinode*/SOT with chromospheric Ca II H filter. It has an inverse-Y shape: the lower bright part corresponds to a magnetic loop, and the vertical structure is the jet. From the investigation of the morphology

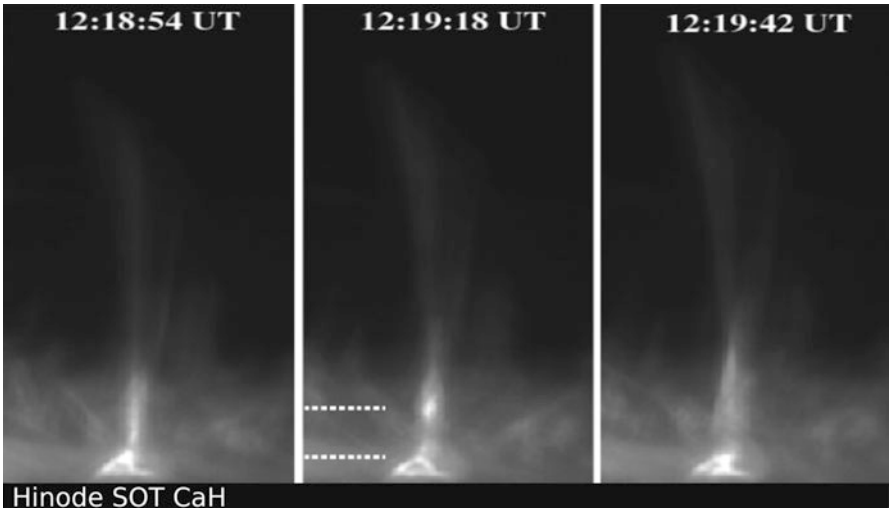

Fig. 19.2 Chromospheric jet on 2017 Jan 14 observed by *Hinode*/SOT with Ca II H filter. The horizontal lines in the middle panel indicate the loop structure and the ejected plasma blob. The length of the horizontal line is about 1000 km

and dynamics, it is interpreted that the small magnetic loop emerges from the photosphere, undergoes magnetic reconnection in the chromosphere with the nearly vertical and open magnetic field, and produces the collimated flow of chromospheric plasma and transverse (kink) waves (Isobe et al. 2008; Nishizuka et al. 2008). This scenario is essentially similar to that of coronal jets observed in X-ray (Shibata et al. 1992; Cirtain et al. 2007), though the mechanisms of plasma acceleration can be different (Shibata et al. 2007; Takasao et al. 2013).

The SOT's high-resolution images taken continuously without interruption from clouds, nights, and bad seeings allow us to study the dynamics in and around the reconnection region in detail. Singh et al. (2012) analyzed nine well-resolved chromospheric jets observed by the SOT and found that most of the jets showed intermittent brightening of the loop as well as the ejection of bright blobs. Such behavior is commonly observed in coronal reconnection (e.g., Takasao et al. 2012) as well as in the MHD simulations with high Lundquist number (e.g., Loureiro et al. 2007).

Transient brightenings in the lower chromosphere, known as Ellerman bombs (Ellerman 1917), had been associated with magnetic reconnection in the lower atmosphere (Pariat et al. 2004; Isobe et al. 2007). Observations of the *Hinode*/SOT coordinated with the spectroscopy from the ground-based telescopes have successfully located the height of magnetic reconnection to the upper photosphere or the lower chromosphere (Matsumoto et al. 2008; Morita et al. 2010; Nelson et al. 2013).

In sunspots, the SOT also found the jet phenomena associated with magnetic reconnection with strong guide fields (Katsukawa et al. 2007; Shimizu 2015). The presence of a strong guide field suppresses both the Hall and Pedersen terms. Detail comparison of the different behaviors of magnetic reconnection at different heights and with a different strength of the guide field will provide new insights into the effects of the Hall and Pedersen terms in magnetic reconnection (Hillier et al. 2016).

Another outstanding discovery by the SOT is the ubiquitous presence of transverse waves in the chromosphere and in the prominences (Alfvén wave or fast mode kink wave) (Okamoto et al. 2007; Okamoto and De Pontieu 2011). Transverse waves are of importance because they are the possible candidates for the energy transportation mechanism of coronal heating. It motivated the theoretical studies on the effect of partial ionization on the propagation and the damping of the transverse waves (e.g., Soler et al. 2009; Singh and Krishan 2010; Zaqarashvili et al. 2011). In short, the Pedersen term enhances the damping of the high-frequency waves, while the Hall term results in the dispersion and circular polarization of the Alfvén wave (Singh and Krishan 2010).

The SOT also found numerous "bubbles" and "plumes" in the quiescent prominence (Berger et al. 2008). A plausible mechanism for the formation of such plumes is magnetic Rayleigh-Taylor instability (Berger et al. 2011; Hillier et al. 2011). It has also been suggested that the magnetic Rayleigh-Taylor instability plays an role in the formation of filamentary structure in the emerging flux (Isobe et al. 2005, 2006). The partial ionization also affects the onset and the growth rate of the instability (Arber et al. 2007; Khomenko et al. 2014b).

19.4 Concluding Remark

The various dynamic phenomena in the solar lower atmosphere observed by the SOT have stirred the interests in the physics of partially ionized plasma. The effect of partial ionization is particularly important in the dissipation process of the magnetic field, whose spatial scale ($>$ a few km) is still far below the spatial resolution of the SOT ($\sim$0.2 arcsec $\sim$140 km). However, the associated time scale, given by a few km divided by the local Alfvén velocity ($\sim$ a few tens of km s^{-1}), is about 0.1 s, which is fast but not unachievable by the existing imaging instruments. Pursuit of higher temporal cadence as well as more accurate diagnostics of plasma parameters are the promising directions for the studies of partial ionization in the future.

Acknowledgements This work was partially supported by JSPS KAKENHI Grant Number 16H03955.

References

Arber, T.D., Haynes, M., Leake, J.E.: Emergence of a flux tube through a partially ionized solar atmosphere. Astrophys. J. **666**, 541–546 (2007)

Berger, T., Shine, R.A., Slater, G.L., Tarbell, T.D., Title, A.M., Okamoto, T.J., Ichimoto, K., Katsukawa, Y., Suematsu, Y., Tsuneta, S., Lites, B.W., Shimizu, T.: Hinode SOT observations of solar quiescent prominence dynamics. Astrophys. J. **676**, L89 (2008)

Berger, T., Testa, P., Hillier, A., Boerner, P., Low, B.C., Shibata, K., Schrijver, C., Tarbell, T., Title, A.: Magneto-thermal convection in solar prominences. Nature **472**, 197–200 (2011)

Brandenburg, A., Zweibel, E.G.: The formation of sharp structures by ambipolar diffusion. Astrophys. J. Lett. **427**, L91–L94 (1994)

Cheung, C.M.C., Cameron, R.H.: Magnetohydrodynamics of the weakly ionized solar photosphere. Astrophys. J. **750**, 6(9pp) (2012)

Cirtain, J.W., Golub, L., Lundquist, L., Van Ballegooijen, A., Savcheva, A., Shimojo, M., DeLuca, E., Tsuneta, S., Sakao, T., Reeves, K., Weber, M., Kano, R., Narukage, N., Shibasaki, K.: Evidence for Alfén waves in solar X-ray jets. Science **318**, 1580–1582 (2007)

De Pontieu, B., Haerendel, G.: Weakly damped Alfven waves as drivers for spicules. Astron. Astrophys. **338**, 729–736 (2000)

Ellerman, F.: Solar hydrogen "Bombs". Astrophys. J. **46**, 298–300 (1917)

Goodman, M.L.: On the efficiency of plasma heating by Pedersen current dissipation from the photosphere to the lower corona. Astron. Astrophys. **416**, 1159–1178 (2004)

Hillier, A., Isobe, H., Shibata, K., Berger, T.: Numerical simulations of the magnetic Rayleigh-Taylor instability in the Kippenhahn-Schlüter prominence model. Astrophys. J. **736**(L1), 1–6 (2011)

Hillier, A., Takasao, T., Nakamura, N.: The formation and evolution of reconnection-driven, slow-mode shocks in a partially ionized plasma. Astron. Astrophys. **591**, A112(16pp) (2016)

Isobe, H., Miyagoshi, T., Shibata, K., Yokoyama, T.: Filamentary structure on the Sun from the magnetic Rayleigh-Taylor instability. Nature **434**, 478–481 (2005)

Isobe, H., Miyagoshi, T., Shibata, K., Yokoyama, T.: Three-dimensional simulation of solar emerging flux using the Earth simulator I. Magnetic Rayleigh-Taylor instability at the top of the emerging flux as the origin of filamentary structure. Publ. Astron. Soc. Jpn. **58**, 423–438 (2006)

Isobe, H., Tripathi, D., Archontis, V.: Ellerman bombs and jets associated with resistive flux emergence. Astrophys. J. **657**, L53–L56 (2007)

Isobe, H., Proctor, M.R.E., Weiss, N.O.: Convection-driven emergence of small-scale magnetic fields and their role in coronal heating and solar wind acceleration. Astrophys. J. **679**, L57–L60 (2008)

Katsukawa, Y., Berger, T.E., Ichimoto, K., Lites, B.W., Nagata, S., Shimizu, T., Shine, R.A., Suematsu, Y., Tarbell, T.D., Title, A.M., Tsuneta, S.: Small-scale jetlike features in penumbral chromospheres. Science **318**, 1594–1597 (2007)

Khomenko, E., Collados, M.: Heating of the magnetized solar chromosphere by partial ionization effects. Astrophys. J. **747**, 87–97 (2012)

Khomenko, E., Collados, M., Díaz, A., VItas, N.: Fluid description of multi-component solar partially ionized plasma. Phys. Plasmas. **21**, 092901 (2014a)

Khomenko, E., Díaz, A., De Vidente, A., Collados, M., Luna, M.: Rayleigh-Taylor instability in prominences from numerical simulations including partial ionization effects. Astron. Astrophys. **565**, A45-1–A45-15 (2014b)

Leake, J.E., Arber, T.D.: The emergence of magnetic flux through a partially ionised solar atmosphere. Astron. Astrophys. **450**, 805–818 (2006)

Leake, J.E., Lukin, V.S., Linton, M.G., Meier, E.T., Multi-fluid simulations of chromospheric magnetic reconnection in a weakly ionized reacting plasma. Astrophys. J. **760**, 109(12pp) (2012)

Leake, J., DeVore, C.R., Thayer, J.P., Burns, A.G., Crowley, G., Gilbert, H.R., Huba, J.D., Krall, J., Linton, M.G., Lukin, V.S., Wang, W.: Ionized plasma and neutral gas coupling in the Sun's chromosphere and Earth's ionosphere/thermosphere. Space Sci. Rev. **184**, 107–172 (2014)

Leenaarts, J., Carlsson, M., Hansteen, V., Rutten, R.J.: Non-equilibrium hydrogen ionization in 2D simulations of the solar atmosphere. Astron. Astrophys. **473**, 625–632 (2007)

Loureiro, N.F., Schekochihin, A.A., Cowley, S.C.: Instability of current sheets and formation of plasmoid chains. Phys. Plasmas. **14**, 100703–100703-4 (2007)

Martinez-Sykora, J., De Pontieu, B., Hansteen, V., Carlsson, M.: The role of partial ionization effects in the chromosphere. Phys. Trans. R. Soc. A. https://doi.org/10.1098/rsta.2014.0268

Matsumoto, T., Kitai, R., Shibata, K., Nagata, S., Otsuji, K., Nakamura, T., Watanabe, H., Tsuneta, S., Suematsu, Y., Ichimoto, K., Shimizu, T., Katsukawa, Y., Tarbell, T.D., Lites, B.W., Shine, R.A., Title, A.M.: Cooperative observation of Ellerman bombs between the solar optical telescope aboard Hinode and Hida/Domeless solar telescope. Publ. Astron. Soc. Jpn. **60**, 577–584 (2008)

Morita, S., Shibata, K., Ueno, S., Ichimoto, K., Kitai, R., Otsuji, K.: Observations of chromospheric anemone jets with CaII broadband filtergraph and Hida CaII spectroheliograph. Publ. Astron. Soc. Jpn. **62**, 901–920 (2010)

Nelson, C.J., Shelyag, S., Mathioudakis, M., Doyle, J.G., Madjarska, M.S., Uitenbroek, H., Erdélyi, R.: Ellerman bombs – evidence for magnetic reconnection in the lower solar atmosphere. Astrophys. J. **779**, 125–134 (2013)

Nishizuka, N., Shimizu, M., Nakamura, T., Otsuji, K., Okamoto, J., Katsukawa, Y., Shibata, K.: Giant chromospheric anemone jet observed with Hinode and comparison with magnetohydrodynamic simulations: evidence of propagating Alfvén waves and magnetic reconnection. Astrophys. J. Lett. **683**, L83–L86 (2008)

Okamoto, T.J., De Pontieu, B.: Propagating waves along spicules. Astrophys. J. **736**, L24(6pp) (2011)

Okamoto, T.J., Tsuneta, S., Berger, T.E., Ichimoto, K., Katsukawa, Y., Lites, B.W., Nagata, S., Shibata, K., Shimizu, T., Shine, R.A., Suematsu, Y., Tarbell, T.D., Title, A.M.: Coronal transverse magnetohydrodynamic waves in a solar prominence. Science **318**, 1577–1580 (2007)

Pariat, E., Aulanier, G., Schmieder, B., Geogoulis, M.K., Rust, D.M., Bernasconi, P.N.: Resistive emergence of undulatory flux tubes. Astrophys. J. **614**, 1099–1112 (2004)

Sano, T., Stone, J.M.: The effect of the hall term on the nonlinear evolution of the magnetorotational instability. I. Local axisymmetric simulations. Astrophys. J. **570**, 314–328 (2002)

Shibata, K.: New observational facts about solar flares from YOHKOH studies – evidence of magnetic reconnection and a unified model of flares. Adv. Space Res. **17**, (4/5)9–(4/5)18 (1996)

Shibata, K., Ishido, Y., Acton, L.W., Strong, K.T., Hirayama, T., Uchida, Y., McAllister, A.H., Matsumoto, R., Tsuneta, S., Shimizu, T., Hara, H., Sakurai, T., Ichimoto, K., Nishio, Y., Ogawara, Y.: Observations of X-ray jets with the YOHKOH soft X-ray telescope. Publ. Astron. Soc. Jpn. **44**, L173–L179 (1992)

Shibata, K., Nakamra, T., Matsumoto, T., Otsuji, K., Okamoto, T.J., Nishizuka, N., Kawate, T., Watanabe, H., Nagata, S., UeNo, S., Kitai, R., Nozawa, S., Tsuneta, S., Suematsu, Y., Ichimoto, K., Shimizu, T., Katsukawa, Y., Tarbell, T.D., Berger, T.E., Lites, B.W., Shine, R.A., Title, A.M.: Chromospheric anemone jets as evidence of ubiquitous reconnection. Science **318**, 1591–1594 (2007)

Shimizu, T.: 3D magnetic field configuration of small-scale reconnection events in the solar plasma atmosphere. Phys. Plasmas. **22**, 101207 (2015)

Singh, K.A.P., Krishan, V.: Alfvén-like mode in partially ionized solar atmosphere. New Astron. **15**, 119–125 (2010)

Singh, K.A.P., Isobe, H., Nishizuka, N., Nishida, K., Shibata, K.: Multiple plasma ejections and intermittent nature of magnetic reconnection in solar chromospheric anemone jets. Astrophys. J. **759**, 33–42 (2012)

Soler, R., Oliver, R., Ballester, J.L.: Magnetohydrodynamic waves in a partially ionized filament thread. Astrophys. J. **699**, 1553–1562 (2009)

Takasao, S., Asai, A., Isobe, H., Shibata, K.: Simultaneous observation of reconnection inflow and outflow associated with the 2010 August 18 solar flare. Astrophys. J. Lett. **745**, L6–L12 (2012)

Takasao, S., Isobe, H., Shibata, K.: Numerical simulations of solar chromospheric jets associated with emerging flux. Publ. Astron. Soc. Jpn. **65**, 62 (2013)

Vernazza, J.E., Avrett, E.H., Loeser, R.: Structure of the solar chromosphere. III – models of the EUV brightness components of the quiet-sun. Astrophys. J. Supp. **45**, 635–725 (1981)

Zaqarashvili, T.V., Khodachenko, M.L., Rucker, H.O.: Magnetohydrodynamic waves in solar partially ionized plasmas: two-fluid approach. Astron. Astrophys. **529**, A82(9pp) (2011)

Chapter 20
Thermal Non-equilibrium Plasma Observed by *Hinode*

Shinsuke Imada

Abstract Plasma in the solar corona is believed to be in thermal equilibrium because of the occurrence of weak Coulomb collisions. To date, many studies have discussed the plasma dynamics in the solar corona assuming thermal equilibrium. Most phenomena observed in the solar corona can be explained under this assumption because the available temporal resolution is not sufficient to resolve non-equilibrium conditions. After *Hinode* was launched, a very high temporal resolution became available, especially for spectroscopic observation. Now, we can discuss plasma heating or acceleration in the solar corona using extreme-ultraviolet spectroscopic observations with high time resolution. Further, we can also observe the solar corona at multiple wavelengths with high spectral resolution. Owing to *Hinode* observations, we can now discuss plasma dynamics under thermal non-equilibrium conditions, such as non-equilibrium ionization. Recently, thermal non-equilibrium plasma has received attention not only in the field of solar physics but also in other fields such as X-ray astronomy.

Keywords Sun: UV radiation · Sun: flare · Sun: corona

20.1 Introduction

Because momentum exchange in plasma is very slow in the collisionless plasma regime, plasma is generally in the thermal non-equilibrium condition. In fact, plasma in the collisionless condition comes to equilibrium not by Coulomb collisions but by interaction through the electromagnetic field (Terasawa et al. 2000). For

S. Imada (✉)
Institute for Space-Earth Environmental Research (ISEE), Nagoya University, Nagoya, Aichi, Japan
e-mail: shinimada@isee.nagoya-u.ac.jp

T. Shimizu et al. (eds.), *First Ten Years of Hinode Solar On-Orbit Observatory*,
Astrophysics and Space Science Library 449,
https://doi.org/10.1007/978-981-10-7742-5_20

example, it is well known that ion and electron temperatures are not the same in the Earth's magnetosphere (Baumjohann et al. 1989), where plasma is certainly in the collisionless regime (collision scale: ∼1AU). On the other hand, in weak collisional plasmas such as the solar corona (collision scale: chromosphere $\sim 10^{-3}$ km, corona $\sim 10^{2}$ km), the spatial scale of certain phenomena can be on the same order as the collision scale. Therefore, plasma in the solar corona is sometimes in the non-equilibrium condition.

Non-equilibrium plasma can generally be categorized according to three frameworks: (1) the non-Maxwellian energy distribution function, (2) the different temperatures of different plasma species, and (3) non-equilibrium ionization. Non-Maxwellian energy distribution functions cannot survive long because they are generally relaxed by Coulomb collisions between the same species in the plasma, e.g., electron-electron collisions. For collisions between different plasma species, such as ion-electron collisions, the relaxation timescale is longer than that for collisions between the same plasma species. Thus, non-equilibrium conditions for different plasma species at different temperatures can survive for a longer time. Non-equilibrium ionization also relaxes owing to collisions between different plasma species. The relaxation time is further prolonged because ionization has several stages.

The non-Maxwellian energy distribution function has been discussed frequently in the field of high-energy (about 10–100 keV) particle acceleration physics in the *Yohkoh* era (Masuda et al. 1994). Currently, very few people discuss suprathermal particle acceleration in terms of extreme-ultraviolet spectroscopic observations (Jeffrey et al. 2016). Owing to the difficulty of observation, non-equilibrium conditions among the temperatures of different atomic species have not been discussed sufficiently (Seely et al. 1997). On the other hand, non-equilibrium ionization plasma has been actively discussed in recent years. For example, when we discuss micro-/nanoflare heating in the solar corona, it is suggested that ionization non-equilibrium occurs momentarily. Therefore, considering the ionization process, it is important to reveal the key region for the solar coronal heating problem (Bradshaw and Mason 2003). It is also known that the ionization state of the chromospheric plasma strongly affects the radiative transfer process, and the discussion of non-equilibrium ionization is important for interpreting observations of the chromosphere (Martinez-Sykora et al. 2106).

Thermal non-equilibrium plasma, which has rarely been discussed to date, has gradually gained attention since the launch of the *Hinode* satellite. In this paper, I introduce two examples of thermal non-equilibrium plasma observations by the *Hinode* satellite. One is non-equilibrium among the temperatures of different species in a solar active region. The other is a non-equilibrium ionization plasma in the chromospheric evaporation flow.

20.2 Ion Temperature in a Solar Active Region

One of the important topics in solar physics is corona heating. The problem is how to obtain a 10^6 K corona above the 6000 K solar surface (photosphere). Although several models such as wave heating and micro-/nanoflare heating have been proposed as the dominant heating mechanism, the answer is still not clear. Most discussions of the corona heating problem to date assume a thermal equilibrium plasma. For example, most studies assume that ions and electrons are always at the same temperature, and researchers do not distinguish whether primarily ions or electrons are heated in the solar corona. The fundamental processes of ion and electron heating are generally different, and it is very useful to distinguish them in terms of understanding the physical process.

To determine which ions and electrons are being heated in the solar corona, Imada et al. (2009) used the Extreme-Ultraviolet Imaging Spectrometer (EIS) onboard the *Hinode* satellite. They discussed the ion temperature and electron temperature in the limb active region using two different methods. Because ionization proceeds by collisions with electrons, it is generally possible to determine the electron temperature from the ionization degree. Figure 20.1 shows an example of the active region observed by EIS. The left panel shows the intensity of iron emission lines (a, Fe VIII, formation temperature 0.5×10^6 K; c, Fe XII, 1.5×10^6 K; e, Fe XVI, 2.5×10^6 K), and the right panel shows the intensity of silicon emission lines (b, Si VII, 0.5×10^6 K; d, Si X, 1.5×10^6 K) and a sulfur emission line (f, S XIII, 2.5×10^6 K). These formation temperatures can be determined from the ionization degree. We can clearly see that all of the images are very similar. This result indicates that the emission lines that are emitted from different atomic species but have almost the same formation temperature come from the same sources.

To discuss the ion temperature, Imada et al. (2009) used not only the information on the ionization degree but also the line widths of emission line pairs from different atomic species. Figure 20.1g, h shows examples of Fe XVI and S XIII emission lines, respectively, observed by EIS. The horizontal axis shows the wavelength, and the vertical axis shows the number of photons. The distribution of photons follows the Gaussian distribution. The difference in the line center position in the wavelength direction, that is, the Doppler shift, indicates the line-of-sight (LOS) velocity. The observed line width (W_{obs}) consists of three components: the instrumental width, ion thermal width, and nonthermal width (resulting from, for example, turbulence and waves). It is known that the observed line width can be described as

$$W_{obs} = \sqrt{W_I^2 + 4 \log 2 \left(\frac{2 k_B T_{ion}}{M} + \xi^2 \right)}, \tag{20.1}$$

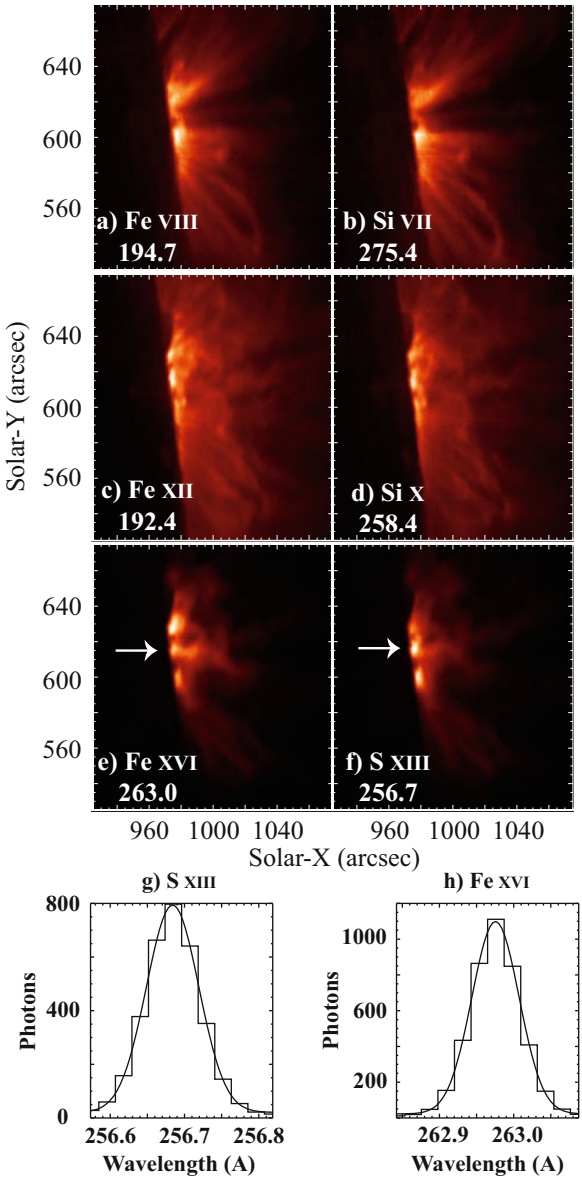

Fig. 20.1 (**a**)–(**f**): Intensity map of active region NOAA 10946. (**g**), (**h**): Example of Fe XVI and S XIII spectral lines, respectively (From Imada et al. 2009, reproduced by permission of the AAS)

where W_I is the instrumental width, k_B is the Boltzmann constant, T_{ion} is the ion temperature, M is the mass of the ion, and ξ is the nonthermal velocity (Imada et al. 2009). It is generally difficult to distinguish the nonthermal width from the ion thermal width without assuming that ions and electrons are at the same temperature (Brooks and Warren 2016). The ion thermal velocity can be distinguished from the observed line width by using two emission lines of different atomic species, because only the thermal width depends on the mass of the ion. By assuming that the two emission lines have the same ion thermal temperature and nonthermal velocity, the ion temperature can be derived directly as

$$T_{ion} = \frac{\widehat{W}_1^2 - \widehat{W}_2^2}{8k_B \log 2} \frac{M_1 M_2}{M_2 - M_1}, \tag{20.2}$$

where $\widehat{W}^2 \equiv W_{obs}^2 - W_I^2$ and where subscripts indicate ion species. In fact, using this method, Imada et al. (2009) confirmed that in most regions, the ion temperature in an active region is the same as the electron temperature which is estimated by the ionization degree. However, it was found that in the central part of the active region, the ion temperature was close to 4×10^6 K. This observation might indicate that severe ion heating occurs at the core of the active region and produces the non-equilibrium plasma. This is the first observational evidence of non-equilibrium plasmas ($T_i \neq T_e$) in a solar active region.

20.3 Non-equilibrium Ionization During a Solar Flare

Next, I introduce an example of non-equilibrium ionization plasma observed with a solar flare, which is the largest explosive phenomenon in the solar system. The observation of non-equilibrium ionization plasma in the magnetic reconnection region, which is the origin of the energy released in a solar flare, is extensively discussed in the paper Imada et al. (2011, 2013). In this paper, I focus mainly on non-equilibrium ionization plasma in the chromospheric evaporation flow during a solar flare.

Figure 20.2a, b shows images taken by the *Solar Dynamics Observatory* (*SDO*)/Atmospheric Imaging Assembly (AIA) in the 193 Å channel [Fe XII, 1.5 million Kelvin (MK)]. Because the bright points in Fig. 20.2a are spatially limited, the observation might represent the very early phase of the flare. The flare arcades are clearly formed at the peak time of the *GOES (Geostationary Operational Environmental Satellite)* light curve in Fig. 20.2b, which was obtained ∼4 min after the image in Fig. 20.2a. Clear bright points no longer appear in Fig. 20.2b.

The *Hinode*/EIS also successfully observed the evaporation flow during the flare with high temporal resolution (∼5 min cadence). Figure 20.2c shows the relationship between the chromospheric evaporation flow velocity and the electron

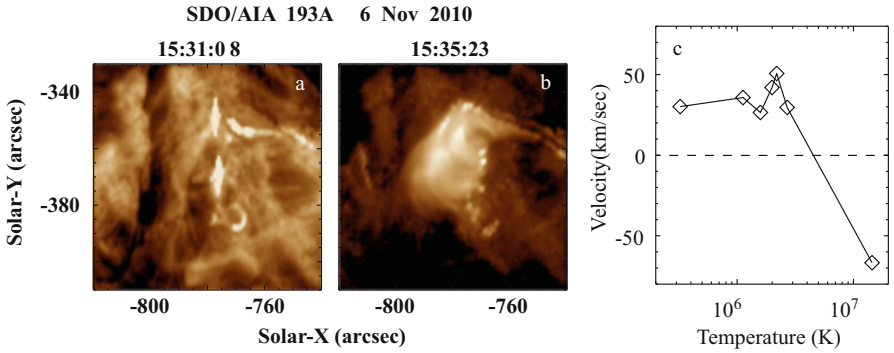

Fig. 20.2 Flare image of AIA 193 Å channel in the impulsive (**a**) and peak (**b**) phases. (**c**) Temperature dependence of the chromospheric evaporation upflow/condensation downflow during the impulsive phase of the flare. The LOS velocities are estimated from the Doppler shifts (From Imada et al. 2015, reproduced by permission of the AIP)

temperature at the bright kernel in Fig. 20.2a observed by EIS. The evaporation flow was well studied before the *Hinode* era. The temperature dependence of the evaporation flow was also well studied (Miligan et al. 2006). However, a new finding was made because of the high temporal resolution of EIS (∼5 min cadence). The solar corona, which is hotter than 10^6 K, is formed on top of the chromosphere (10^4 K) across a very thin transition region. Because of the atmospheric structure, it is generally believed that upward evaporation flows are observed in plasmas hotter than 10^6 K, and downward condensation flows are observed in plasmas cooler than 10^6 K. However, it was found that even high-temperature plasma ($>3 \times 10^6$ K) shows a downward flow of 50 km s^{-1} at the very beginning of the flare, as shown in Fig. 20.2c. Although many theoretical studies have been conducted to understand the temperature dependence of evaporation flows, it is difficult to reproduce the hot downflows during the early phase of a flare. Two new solutions to this problem have been suggested. One is to consider the time-dependent ionization effect, and the other is to modify the heat conduction coefficients. Figure 20.3 shows the result of a numerical simulation of chromospheric evaporation only 40 s after the flare began. From the top, (a) the density, (b) velocity, (c) temperature, (d) the normalized Fe XII intensities, (e) the normalized Fe XII flux (normalized intensity × velocity), (f) the normalized Fe XV intensities, (g) the normalized Fe XV flux, (h) the normalized Fe XXIII intensities, and (i) the normalized Fe XXIII flux are also shown. The horizontal axis shows the distance from the footpoint along the magnetic field lines. The dotted lines in Fig. 20.3f, g are the simulation results assuming ionization equilibrium, whereas the solid line is the result considering the time-dependent ionization effect. The downward flow of Fe XV is successfully reproduced by considering ionization non-equilibrium and the modification of the thermal conduction coefficient (Imada et al. 2015). Furthermore, it is found that the hot downward flow disappeared after 40 s (not shown here; see Imada et al. 2015). This result is also consistent with the observation of chromospheric

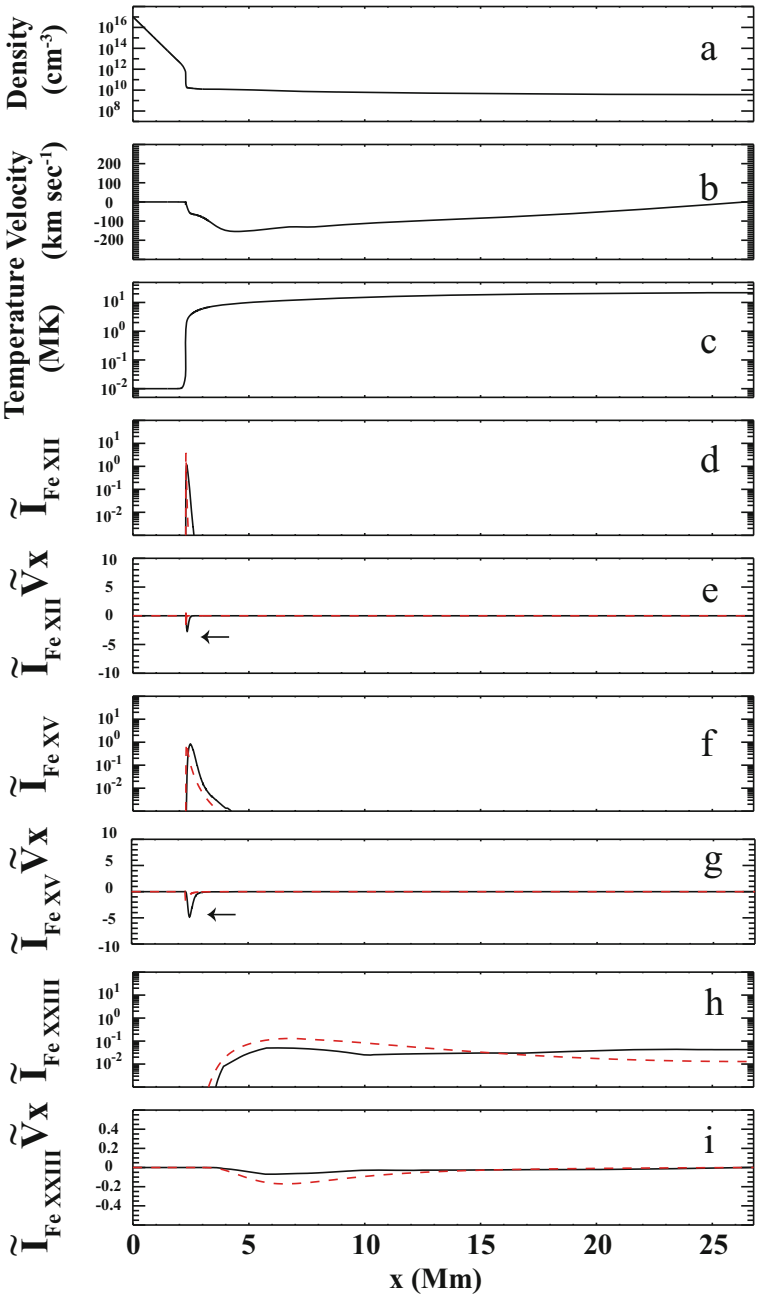

Fig. 20.3 Result of a numerical simulation of chromospheric evaporation 40 s after the beginning of a flare. From the top, (**a**) the density, (**b**) velocity, (**c**) temperature, (**d**) the normalized Fe XII intensities, (**e**) the normalized Fe XII flux, (**f**) the normalized Fe XV intensities, (**g**) the normalized Fe XV flux, (**h**) the normalized Fe XXIII intensities, and (**i**) the normalized Fe XXIII flux are also shown. The black solid line shows the result of a time-dependent ionization calculation, and the red dashed lines show the results assuming ionization equilibrium. The arrows show the redshift (downflows) at the flare footpoint in Fe XII and Fe XV (From Imada et al. 2015, reproduced by permission of the AIP)

evaporation. The plasma dynamics in the solar corona on a short timescale can now be discussed because of the high temporal resolution of *Hinode*/EIS. To interpret such a high-cadence observation, consideration of the ionization non-equilibrium plasma has become necessary. The field of solar physics has entered the thermal non-equilibrium plasma era.

20.4 Summary and Future Perspectives

Owing to *Hinode*, we can now discuss short-timescale phenomena in the solar corona. We can also observe the corona at multiple wavelengths simultaneously. These capabilities make it possible to start to discuss thermal non-equilibrium plasma in the solar corona. However, even with *Hinode*, the temporal resolution is not sufficient for discussing the thermal non-equilibrium plasma in detail. Unfortunately, we still cannot distinguish information regarding the physical process of coronal heating from information about the thermal non-equilibrium condition, for example. Recently, the next-generation solar observation satellite SOLAR-C has been discussed intensively. An ultraviolet imaging spectrometer with dramatically improved spatial and temporal resolution is planned for this satellite. In SOLAR-C, thermal non-equilibrium plasma will be extensively discussed. Active discussion of thermal non-equilibrium plasma is beginning in various fields. For example, by using the *Suzaku* X-ray observations of a supernova remnant, the activities of the parent star and surrounding environment were discussed in terms of ionization non-equilibrium (Yamaguchi et al. 2009). Observations and theoretical studies of thermal non-equilibrium plasma can be applied to not only solar physics but also various other fields, and it is expected that further developments will be made in cooperation with these fields in the future.

Acknowledgements I thank all members of the *Hinode* team. *Hinode* is a Japanese mission developed and launched by ISAS/JAXA, collaborating with NAOJ as a domestic partner and NASA and STFC (UK) as international partners. Scientific operation of the *Hinode* mission is conducted by the *Hinode* science team organized at ISAS/JAXA. This team mainly consists of scientists from institutes in the partner countries. Support for the postlaunch operation is provided by JAXA and NAOJ (Japan), STFC (UK), NASA (USA), ESA, and NSC (Norway). This work was partially supported by JSPS KAKENHI Grant Nos. JP26287143 and JP15H05816.

References

Baumjohann, W., et al.: Average plasma properties in the central plasma sheet. J. Geophys. Res. **94**, 6597 (1989)

Bradshaw, S.J., Mason, H.E.: The radiative response of solar loop plasma subject to transient heating. A&A **407**, 1127 (2003)

Brooks, D.H., Warren, H.P.: Measurements of non-thermal line widths in solar active regions. ApJ **820**, 63 (2016)

Imada, S., et al.: Ion temperature and non-thermal velocity in a solar active region: using emission lines of different atomic species. ApJ **705**, 208L (2009)
Imada, S., et al.: Magnetic reconnection in non-equilibrium ionization plasma. ApJ **742**, 70 (2011)
Imada, S., et al.: Evidence for hot fast flow above a solar flare arcade. ApJ **776**, L11 (2013)
Imada, S., et al.: Observation and numerical modeling of chromospheric evaporation during the impulsive phase of a solar flare. Phys. Plasmas **22**, 101206 (2015)
Jeffrey, N.L.S., et al.: First evidence of non-Gaussian solar flare EUV spectral line profiles and accelerated non-thermal ion motion. A&A **590**, 13 (2016)
Martinez-Sykora, J., et al.: Time dependent non-equilibrium ionization of transition region lines observed with IRIS. ApJ **817**, 46 (2106)
Masuda, S., et al.: A loop-top hard X-ray source in a compact solar flare as evidence for magnetic reconnection. Nature **371**, 495 (1994)
Miligan, R., et al.: RHESSI and SOHO CDS observations of explosive chromospheric evaporation. ApJ **638**, L117 (2006)
Seely, J.F., et al.: Turbulent velocities and ion temperatures in the solar corona obtained from SUMER line widths. ApJ **484**, L87 (1997)
Terasawa, T., et al.: Comparative study of flares and substorms. Adv. Space Res. **26**, 573 (2000)
Yamaguchi, H., et al.: Discriminating the progenitor type of supernova remnants with iron K-shell emission. ApJ **785**, L27 (2009)

Chapter 21
From *Hinode* to the Next-Generation Solar Observation Missions

Kiyoshi Ichimoto, Hirohisa Hara, Yukio Katsukawa, and Ryoko Ishikawa

Abstract Ten years of *Hinode* operation have indicated the direction of the new challenges in solar physics. The task of the next solar observation missions is to determine the three-dimensional (3D) structure of magnetic fields that connect the photosphere and the corona by resolving the elementary magnetic structures in the solar atmosphere. SOLAR-C is the long-awaited next-generation international solar physics satellite that will observe the magnetic field of the chromosphere and the plasma dynamics from the photosphere to the corona with much higher spatial and temporal resolutions than *Hinode*. To this end, the Japanese solar physics community is promoting a sounding rocket experiment, the Chromospheric Lyman-Alpha SpectroPolarimeter, and a balloon experiment, SUNRISE-3, to pave the way for measuring the chromospheric magnetic fields with spectropolarimetry in the ultraviolet and infrared, respectively. Additionally the algorithm for determining the 3D magnetic field from spectropolarimetric data is investigated using a newly developed multi-wavelength spectropolarimeter at the Hida observatory. Solar telescopes with 4 m aperture are expected to begin operating in Hawaii and the Canary islands in the 2020s and introduce a new approach to uncovering fine-scale structures with the highest-ever spatial resolution. The continuous and high-precision observation by SOLAR-C, which has large spatial and temporal coverage, will contribute indispensable information for understanding the fundamental plasma process occurring in the Sun and in the Universe and for establishing the foundation for the next-generation space weather prediction.

Keywords Solar observation · Space mission · Future plan

K. Ichimoto (✉) · H. Hara · R. Ishikawa
SOLAR-C Project Office, National Astronomical Observatory of Japan, Mitaka, Tokyo, Japan
e-mail: ichimoto@kwasan.kyoto-u.ac.jp; hirohisa.hara@nao.ac.jp; ryoko.ishikawa@nao.ac.jp

Y. Katsukawa
Solar Science Observatory, National Astronomical Observatory of Japan, Mitaka, Tokyo, Japan
e-mail: yukio.katsukawa@nao.ac.jp

T. Shimizu et al. (eds.), *First Ten Years of Hinode Solar On-Orbit Observatory*,
Astrophysics and Space Science Library 449,
https://doi.org/10.1007/978-981-10-7742-5_21

21.1 Introduction

As discussed in this volume, *Hinode* has achieved a significant progress in solar physics. It has been revealed that the solar atmosphere is governed by fundamental plasma processes such as magneto-convection, magnetic reconnection, magnetohydrodynamic waves, turbulence, and energy dissipation. The hot and dynamic solar atmosphere sustains occasional large-scale destabilizations and explosive energy releases, which are generated through a chain of such fundamental processes. Additionally, the high-quality images of *Hinode* have demonstrated that the chromosphere, an interface region between the photosphere and the corona, is extremely dynamic much more than previously thought and of crucial importance for understanding the origin of the active solar atmosphere. How the hot and dynamic solar atmosphere is formed; how flares, prominence explosions, and violent disturbances of solar wind are generated; and how the solar magnetic fields are maintained and modulated are still major questions in solar physics that must be answered. As a star that provides the magnetized plasma models that apply ubiquitously in the Universe, a huge-scale plasma laboratory that can never been realized on the ground, and the boundary condition that governs the space environment of the earth, the Sun is becoming recognized as an important research object in relation to research fields such as astronomy, plasma physics, and heliophysics. In this manuscript, we will discuss the future direction of solar research by focusing on future and ongoing projects undertaken by the Japanese solar physics community.

21.2 The SOLAR-C Project

Hinode has revealed the vigorous chromospheric activity (Okamoto 2016; Katsukawa 2016) and the plasma dynamics in the corona (Hara 2016) from space (see the other articles in this volume for details on the scientific achievements of *Hinode*). Although simultaneous observations from the photosphere to the corona have been achieved by *Hinode*, the physical processes producing these dynamic phenomena are still enigmas due to the lack of key observations that we have identified after *Hinode*. To further understand the physical processes that cause these activities, new observations with largely improved precision and spatial resolution are necessary. They are (1) the magnetic field observation in the chromosphere, which requires a higher precision polarimetry, for understanding the origin of the small-scale dynamics and (2) high-resolution observations of the corona that enable seamless coverage of the entire atmosphere for directly connecting the photospheric magnetic structure to the coronal structures. The SOLAR-C mission has been proposed to realize these key observations.

The following are the SOLAR-C science objectives, which include the major solar physics problems:

I. Investigate the formation mechanisms of the chromosphere, the corona, and the solar wind
II. Understand the physical origin of large-scale solar eruptions to build an algorithm for their prediction
III. Elucidate the origin of the solar activity cycle

Each science objective contains the following science topics: plasma heating and acceleration processes of plasmas (Topic I), destabilization of global magnetic structures and fast magnetic reconnection processes with the small-scale internal structure (Topic II), and regeneration of magnetic fields and magnetic flux transport in the Sun (Topic III). Through the study of these science topics, the scope of the mission includes a viewpoint that contributes to the understanding and prediction of the influence of the solar activity on the Earth and the human society.

The SOLAR-C spacecraft, shown in Fig. 21.1, consists of three major payloads: the Solar Ultraviolet(UV)-Visible-IR Telescope (SUVIT) for observing the velocity and magnetic fields in the photosphere and chromosphere in addition to the imaging observations; the High-Resolution Coronal Imager (HCI), with a spatial resolution improved by an order of magnitude compared to that of all instruments ever flown; and the Extreme UltraViolet Spectroscopic Telescope (EUVST) for spectroscopy of the chromosphere through the corona, with a similar spatial resolution to that of HCI. The candidate spacecraft orbit is the geosynchronous orbit to avoid the

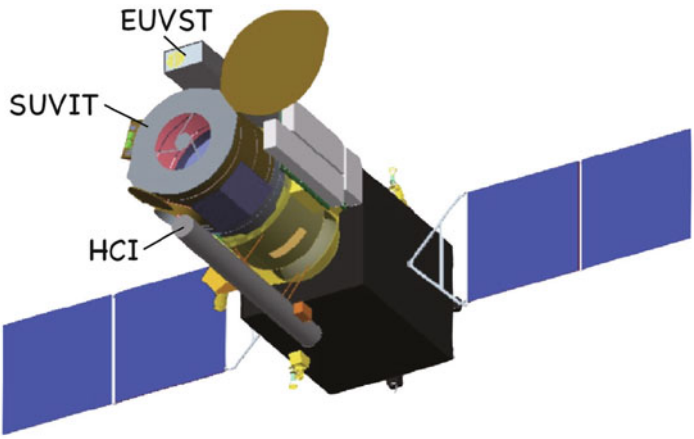

Fig. 21.1 Schematic view of the SOLAR-C spacecraft. The spacecraft is equipped with the 1 m-diameter optical telescope SUVIT at the center, the high-resolution spectrograph EUVST on one side, and the high-resolution imager HCI on the other side

eclipse due to the shadow of the Earth and to minimize the thermal distortion by the infrared (IR) radiation from the Earth. The SOLAR-C magnetic field observations are characterized by a spatial resolution of 0.1 arcsec to resolve the elemental magnetic field structure that we have inferred from the *Hinode* observations and a field of view of a few arcmin to cover entire sunspot regions, coronal loops, and flare structures. This superb targeted performance, which connects small-scale dynamics with the formation of large-scale structures and destabilization, makes SOLAR-C observations exceptionally unique.

SOLAR-C is a proposed Japanese-led mission that assumes international collaboration with the USA and European countries, and the mission proposal has been prepared for a target launch date in the 2020s. The task of aligning the step of the major space agencies for the first SOLAR-C proposal was not easy. A new approach, a working group activity whose committee members are selected by the major space agencies in the world, has started to realize the next-generation solar physics mission.

21.3 Small-Size Space Missions

The *Hinode* observations of the dynamic chromosphere were followed by spectroscopy of the chromospheric lines with the *Interface Region Imaging Spectrograph (IRIS)* which started measurements in 2013. *IRIS* is one of the small exploration (SMEX) NASA programs. Although the *IRIS* spacecraft is much smaller than *Hinode*, it has achieved significant progress in our understanding of chromospheric dynamics owing to its unique capability of performing high-resolution spectroscopic observation of UV emission lines. The success of *IRIS* suggests that new observations following *Hinode* strongly require the development of unique observational technologies. In parallel with a large-scale spacecraft mission like SOLAR-C, which requires a long realization period, it is important to acquire new technologies for the next mission through development of small-size space experiments, such as sounding rockets and balloon experiments.

21.3.1 Sounding Rocket Experiment, CLASP

As discussed in Sect. 21.2, the frontier of solar physics is the direct measurement of the magnetic fields in the upper atmosphere, where the magnetic forces dominate over the gas pressure. In the UV range that has to be observed from space, there are abundant spectral lines that are emitted from plasma of 10^4–10^5 K and allow us to access the chromosphere and the transition region. The magnetic field information in these upper atmospheric layers is embedded in these spectral lines, whose polarization signals have only been explored before in a few pioneering experiments

(Stenflo 1980; Henze and Stenflo 1987). One line of particular interests is the hydrogen Lyman-α line at 121.57 nm, which is the brightest in the vacuum-UV range and is expected to show a measurable scattering polarization sensitive to the Hanle effect (see next paragraph and Trujillo Bueno et al. 2011). To verify the utility of this spectral line, an international team consisting of Japan, the USA, Spain, France, and Norway started a sounding rocket project called the Chromospheric Lyman-Alpha SpectroPolarimeter (CLASP) in 2008 (2 years after the launch of *Hinode*).

One of the physical mechanism that produce the polarization in this spectral line is the Zeeman effect, which has been widely used for many years to characterize the magnetic field mainly in the photosphere. Indeed, *Hinode*/SOT reveals the new features of the photospheric magnetic fields by measuring the Zeeman effect with unprecedentedly high spatial resolution and high-precision spectropolarimetry. However, in many cases, the polarization signals induced by the Zeeman effect in spectral lines that originate from the upper atmospheric layers are too small to be detected because these spectral lines are broad and the magnetic field strength there is low.

The Hanle effect is expected to be an alternative diagnostic tool because it results in polarization signals that are not canceled out by Doppler broadening, and it is generally sensitive to weaker magnetic fields than the Zeeman effect. The Hanle effect is the physical mechanism with which the magnetic field modifies the polarization state that is induced by absorbing and scattering the anisotropic radiation. One application of the Hanle effect as a diagnostic tool of the chromospheric magnetic field is the spectropolarimetry of the He I triplet at 1083.0 nm with the ground-based telescopes. This spectral line is easily modeled, and the user-friendly inversion code HAZEL (HAnle and ZEeman Light) (Asensio Ramos et al. 2008), which assumes a constant-property slab located at a given height, is available to interpret the spectropolarimetric data. Thus, this spectral line is one of the candidate to be observed by SOLAR-C/SUVIT. However, the formation of this spectral line in the quiet region (especially in the internetwork region) is difficult, and there are limited quiet Sun observations in the He I triplet.

The Hanle effect in UV spectral lines could enable magnetic field measurements in the quiet Sun region, and it is anticipated to realize UV spectropolarimetry. However, precise spectropolarimetry in the UV range has never been successful, and the CLASP team must initiate the development of optical elements necessary for the UV spectropolarimetry. In addition, the core team members from Japan who led the design and integration of the instrument were Ph.D. students and young scientists who had never experienced the instrumentation. They were supervised by the senior scientists who developed the *Hinode* satellite, and started from the evaluation of the polarization elements at a synchrotron facility (Watanabe et al. 2011; Ishikawa et al. 2013, 2014, 2015; Narukage et al. 2015, 2017). Seven years later, the development of a flight model with diameter 27 cm and length 2.5 m was completed by the international collaboration (right panel of Fig. 21.2) (Giono et al. 2016a,b). CLASP was launched on September 3, 2015, from the White Sands Missile Range in the

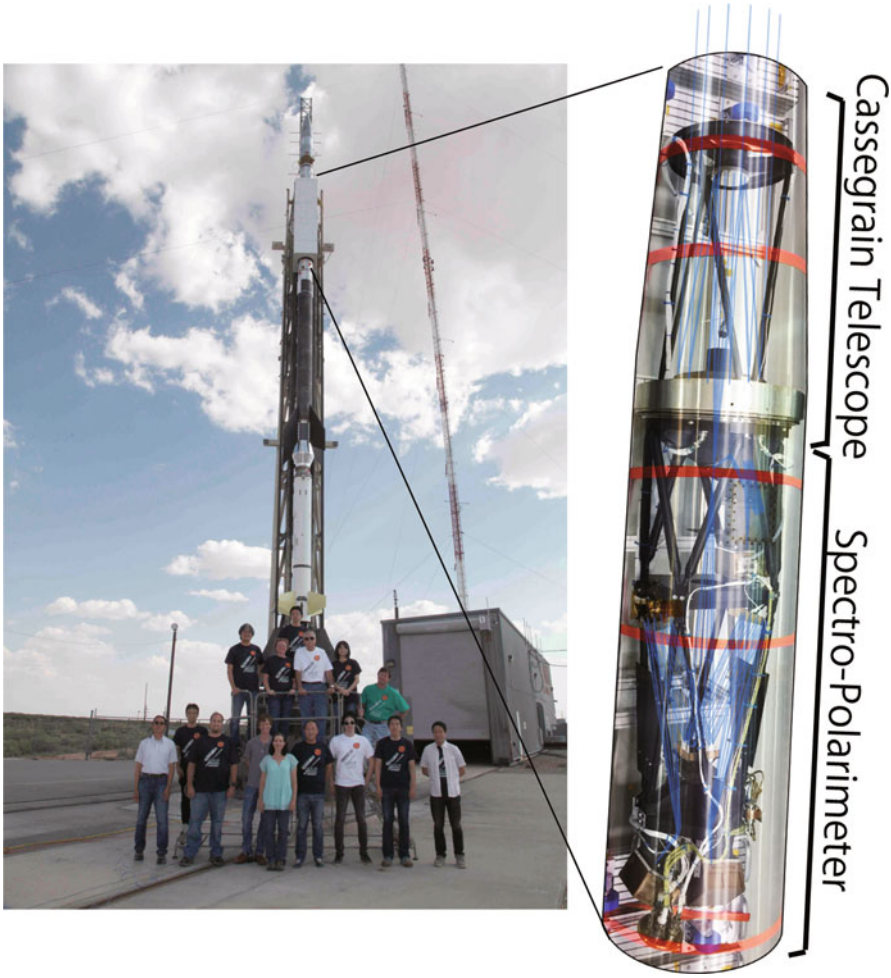

Fig. 21.2 Left: team photo in front of CLASP. Right: flight model of CLASP instrument developed at NAOJ (National Astronomical Observatory of Japan) (Courtesy of the CLASP team)

USA and achieved high-precision (<0.1%) UV spectropolarimetry for the first time (Giono et al. 2017; Kano et al. 2017). After the launch, the payload was recovered without any damage.

CLASP observations confirmed for the first time the presence of scattering polarization in the Lyman-α line (Kano et al. 2017). The Lyman-α wings, which are insensitive to the Hanle effect, show scattering polarization perpendicular to the solar limb with a clear center-to-limb variation (CLV) as predicted theoretically (Belluzzi et al. 2012). However, the Lyman-α core, where the Hanle effect acts,

does not show the CLV, in contrast to theoretical calculation with the currently available one-dimensional (1D) and three-dimensional (3D) solar atmospheric models (Trujillo Bueno et al. 2011; Štěpán et al. 2015). Although the interpretation of scattering polarization is not straightforward, the signature of the Hanle effect has been detected (Ishikawa et al. 2017) and new information on the magnetic field in the upper chromosphere and the transition region is being obtained.

The flight of CLASP2 (Chromospheric LAyer SpectroPolarimeter 2) has been approved by NASA and scheduled for 2019. By refitting the successfully recovered instrument, this second flight is aimed at performing spectropolarimetric observations of the Mg II h and k lines which are also candidates for exploring the magnetic field in the upper chromosphere (Belluzzi and Trujillo Bueno 2012; Alsina Ballester et al. 2016; del Pino Alemán et al. 2016). In the Mg II h and k lines, the circular polarization signals induced by the Zeeman effect can be measured in the strongly magnetized region, and this additional measurement will provide magnetic field information. Thus, in the second flight, circular and linear polarization will be examined. By completing these two CLASP missions (CLASP1 and 2), the effectiveness of UV spectropolarimetry in opening new avenues in solar physics will be investigated.

21.3.2 Balloon Experiment: SUNRISE

The balloon-borne solar telescope SUNRISE (Fig. 21.3) is a project aimed at obtaining high-quality solar data in terms of spatial resolution and polarimetric accuracy that are not affected by the Earth's atmosphere. SUNRISE is a stratospheric balloon mission that carries a 1 m aperture optical telescope. A flight altitude above 35 km allows it to perform (1) observations in the UV range that is inaccessible from a ground-based telescope and (2) high-precision polarimetric measurements without being affected by atmospheric seeing (Barthol et al. 2011; Solanki et al. 2010). The flight observations of SUNRISE were performed twice in 2009 and 2013 and provided many results on the dynamics on the solar surface, such as fine-scale magnetic structures resolved with an 0.1 arcsec (smaller than 100 km) resolution (Lagg et al. 2010) and the ubiquitous appearance of vortex motion on the surface (Steiner et al. 2010). More than 50 refereed papers based on data obtained from these two flights have been published. The SUNRISE mission was mainly led and developed by research groups in Germany and Spain. In the third flight that we are now proposing, our Japanese group will participate to develop the new infrared spectropolarimeter SCIP (Sunrise Chromospheric Infrared spectroPolarimeter) (Katsukawa et al. 2015, 2016). The 1 m aperture of the SUNRISE telescope can achieve 0.2 arcsec resolution (equal to the *Hinode* resolution) at near-infrared spectral lines such as Ca II

Fig. 21.3 SUNRISE balloon-borne stratospheric telescope. The 1 m aperture telescope is mounted on a gondola

854 nm and K I 769 nm, which have strong sensitivity to the Zeeman effect in the upper photosphere and the chromosphere. By having broad wavelength coverage to include many spectral lines originating from the photosphere to the chromosphere, we can obtain 3D magnetic field structures connecting the photosphere and the chromosphere. These magnetic structures and their temporal evolution are critical to determine the energy transfer and dissipation from the photosphere to the chromosphere under seeing-free conditions. A key engineering goal is to realize high polarimetric accuracy down to 0.03% by utilizing techniques developed for *Hinode*, CLASP, and SOLAR-C, including precise synchronization between the polarization modulator and cameras, efficient and precise polarization optics, and structural and thermal design of the spectrograph. The third flight, planned for 2020, will establish the scientific feasibility of chromospheric field measurements and develop the strong international collaboration required to realize SOLAR-C.

21.3.3 Wide Variety of Small-Size Experiments

Observations of solar coronae have revealed that unresolved fine-scale dynamics probably have a key role in coronal heating. It is thus strongly required to improve the spatial and spectral resolution as well as the wavelength coverage in UV and X-ray coronal observations. Here we introduce some rocket experiments that aim to

develop critical techniques required for future coronal observations and are critically important for planning future spacecraft missions. The Hi-C (High-Resolution Coronal Imager) rocket experiment conducted by NASA realized an innovative instrument that achieved a high resolution of 0.2 arcsec in an EUV (Extreme UltraViolet) imaging observation of the corona (Kobayashi et al. 2014). The Hi-C flight experiments were performed twice in 2012 and 2016. The High-Resolution Coronal Imager (HCI) proposed for SOLAR-C is an evolutionary successor of Hi-C. The FOXSI (Focusing Optics X-ray Solar Imager) is an instrument carried by a sounding rocket aimed at conducting imaging and spectroscopic observations in the X-ray region (below 15 keV) with focusing optics. The flight experiments of FOXSI were performed twice, in 2012 and 2014, to capture very hot plasma [hotter than 10 million Kelvin (MK)] in microflares and in active regions (Ishikawa 2016). The Japanese group is in charge of the development of the X-ray detectors aboard FOXSI. A new X-ray detector that uses a fast readout complementary MOS (CMOS) sensor and allows imaging spectroscopic measurements in the soft X-ray region is now under development for the third flight in 2018.

The advanced observational techniques developed by these small space projects are essential for future instruments planned for small-to-large spacecrafts, such as SOLAR-C. We are mapping a strategy to realize the next-generation solar physics mission in the next solar maximum around 2025 by international collaboration, considering various opportunities including small-size spacecrafts.

21.4 Ground-Based Observations

Space missions are required to focus on measurements that can never be realized from the ground and aim at obtaining maximum scientific outcome under considerable resource constraints. If a space instrument will observe the Sun in visible or near-infrared wavelengths, it is critically important for the planner to clarify the ultimate limitation of ground-based observations and to make extensive verification of the flight instrument and its products using ground facilities. In this regard, the role of the ground-based observations for developing and realizing fascinating space missions becomes more important. The advantages of ground-based observation against space missions are its abilities to employ a very large-size instrument, to use highly flexible observation setups in existing facilities, and to conduct century-long data acquisition using synoptic observation instruments. With these advantages, ground-based observations are expected to: (1) exhibit an extremely high spatial resolution with a big telescope, (2) develop new methods of plasma characterization by highly flexible spectropolarimetric observations, and (3) perform long-term monitoring observations to accumulate a historic record of the solar activity to study the mechanism of the solar cycle and solar forcing on the Earth's environment.

A 4 m-aperture solar telescope (DKIST, Daniel K. Inouye Solar Telescope) is now under construction in Maui island of Hawaii and planned for completion in 2019. A project for a large solar telescope (EST, European Solar Telescope, 4 m

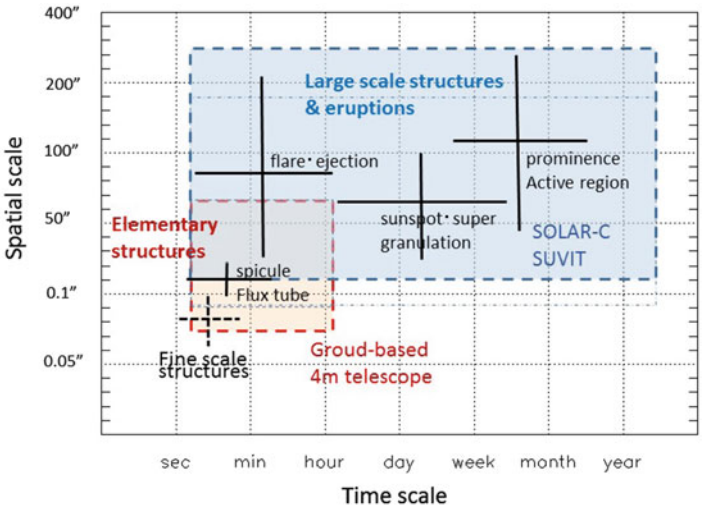

Fig. 21.4 Spatial and temporal scales covered by a 1 m space telescope and 4 m ground-based telescope

aperture) is also in progress in Europe. Both of these are expected to achieve an extremely high spatial resolution below 0.1 arcsec (approximately 70 km on the Sun) in imaging and spectroscopic observations and open a new window to the unexplored world of fundamental plasma processes in elementary magnetic structures on the Sun. Recently ALMA (Atacama Large Millimeter/submillimeter Array) has started observations of the Sun. It is strongly expected that ALMA will provide new methods to characterize thermal states of chromospheric fine-scale structures and high-energy electrons in flares with an unprecedented spatial resolution in submillimeter wavelengths, although its spatial and temporal coverage is rather limited. In contrast to large-size ground-based telescopes that observe the fine-scale elementary structures with the highest-ever spatial resolution like microscopes, the optical telescope aboard SOLAR-C covers large spatial and time scales at a high spatial resolution with the highest spectropolarimetric accuracy (see Fig. 21.4). The synergy of space and ground-based observations will ensure revolutionary progress in our understanding of the Sun.

Using the advantages of medium-size ground-based solar telescopes and their highly flexible usage, studies on the methodology for diagnosing 3D magnetic fields and experiments on the optical components that will be implemented in future space missions are conducted. For this purpose, a new multi-wavelength spectropolarimeter installed on the Domeless Solar Telescope (DST) at the Hida observatory of Kyoto University provides spectropolarimetric data of various photospheric and chromospheric lines in visible and near-infrared wavelengths simultaneously, which are used for developing an algorithm to reconstruct 3D magnetic fields from the

photosphere to the chromosphere and for evaluating the diagnostic capability of spectral lines that will be observed by SUNRISE and SOLAR-C.

Additionally, a network observation project aimed at promoting space weather forecast is ongoing with a participation of Japanese space- and ground-based facilities. The project (PSTEP, Project for Solar-Terrestrial Environment Prediction) aims to understand the occurrence of eruptions on the Sun and their propagation to the Earth as a whole. PSTEP involves the coordinated observation of magnetic field of dark filaments by the Solar Flare Telescope at NAOJ, the velocity field of filament eruption using Solar Magnetic Activity Research Telescope (SMART) at the Hida observatory, shock waves propagating in the corona using the radio spectrometer at NICT (National Institute of Information and Communications Technology), the disturbance in the solar wind with the IPS (interplanetary scintillation) system at Nagoya University, and the magnetic field in active regions using *Hinode*. PSTEP is expected to build a foundation for the next-generation space weather forecasting system.

21.5 Summary

Solar observation in Japan has a history of approximately 100 years beginning with the start of solar photography in Tokyo Astronomical Observatory in 1917. Since the 1950s, ground-based solar telescopes have been constructed at Norikura, Mitaka, Kwasan, Okayama, and Hida. Since the 1980s, the solar observation satellites, Hinotori, *Yohkoh*, and *Hinode* have been successfully launched, and they have played a leading role in solar physics worldwide. In the current era, the size and cost of the required future flagship instruments are considerable, and solar physicists worldwide share a common understanding that an extensive international collaboration is necessary to realize a large-size next-generation solar physics mission. In this manuscript, we have discussed the prospects of solar observation in the next 10 years by focusing on the ongoing and future projects in Japan. Our goal is to realize a revolutionary space mission (SOLAR-C) with a worldwide international collaboration and the support of ground-based observatories.

References

Alsina Ballester, E., Belluzzi, L., Trujillo Bueno, J.: The magnetic sensitivity of the Mg II k line to the joint action of Hanle, Zeeman, and magneto-optical effects. Astrophys. J. **831**, L15 (2016). https://doi.org/10.3847/2041-8205/831/2/L15

Asensio Ramos, A., Trujillo Bueno, J., Landi Degl'Innocenti, E.: Advanced forward modeling and inversion of stokes profiles resulting from the joint action of the Hanle and Zeeman effects. Astrophys. J. **683**, 542–565 (2008). https://doi.org/10.1086/589433

Barthol, P., et al.: The sunrise mission. Sol. Phys. **268**, 1 (2011). https://doi.org/10.1007/s11207-010-9662-9

Belluzzi, L., Trujillo Bueno, J.: The polarization of the solar Mg II h and k lines. Astrophys. J. **750**, L11 (2012). https://doi.org/10.1088/2041-8205/750/1/L11

Belluzzi, L., Trujillo Bueno, J., Štěpán, J.: The scattering polarization of the Lyα lines of H I and He II taking into account partial frequency redistribution and J-state interference effects. Astrophys. J. **755**, L2 (2012). https://doi.org/10.1088/2041-8205/755/1/L2

del Pino Alemán, T., Casini, R., Manso Sainz, R.: Magnetic diagnostics of the solar chromosphere with the Mg II h-k lines. Astrophys. J. **830**, L24 (2016). https://doi.org/10.3847/2041-8205/830/2/L24

Giono, G., Katsukawa, Y., Ishikawa, R., et al.: Optical alignment of the chromospheric Lyman-Alpha spectro-polarimeter using sophisticated methods to minimize activities under vacuum. In: Society of Photo-Optical Instrumentation Engineers (SPIE) Conference Series, vol. 9905, 99053D (2016a). https://doi.org/10.1117/12.2232312

Giono, G., Ishikawa, R., Narukage, N., et al.: Polarization calibration of the chromospheric Lyman-Alpha spectroPolarimeter for a 0.1% polarization sensitivity in the VUV range. Part I: pre-flight calibration. Sol. Phys. **291**, 3831–3867 (2016b). https://doi.org/10.1007/s11207-016-0950-x

Giono, G., Ishikawa, R., Narukage, N., et al.: Polarization calibration of the chromospheric Lyman-Alpha spectroPolarimeter for a 0.1% polarization sensitivity in the VUV range. Part II: in flight calibration. Sol. Phys. **292**, 57 (2017). https://doi.org/10.1007/s11207-017-1062-y

Hara, H.: Coronal heating: issues revealed from Hinode observations. Astron. Her. **109**, 533–539 (2016)

Henze, W., Stenflo, J.O.: Polarimetry in the MG II H and K lines. Sol. Phys. **111**, 243–254 (1987). https://doi.org/10.1007/BF00148517

Ishikawa, S.: Hinode investigations of microflares and nanoflares. Astron. Her. **109**, 544 (2016)

Ishikawa, R., Kano, R., Bando, T., et al.: Birefringence of magnesium fluoride in the vacuum ultraviolet and application to a half-waveplate. Appl. Opt. **52**, 8205 (2013). https://doi.org/10.1364/AO.52.008205

Ishikawa, R., Narukage, N., Kubo, M., et al.: Strategy for realizing high-precision VUV spectropolarimeter. Sol. Phys. **289**, 4727–4747 (2014). https://doi.org/10.1007/s11207-014-0583-x

Ishikawa, S., Shimizu, T., Kano, R., et al.: Development of a precise polarization modulator for UV spectropolarimetry. Sol. Phys. **290**, 3081–3088 (2015). https://doi.org/10.1007/s11207-015-0774-0

Ishikawa, R., Trujillo Bueno, J., Uitenbroek, H., et al.: Indication of the Hanle effect by comparing the scattering polarization observed by CLASP in the Lyman-α and Si III 120.65 nm lines. ApJ **841**, 31I (2017). https://doi.org/10.3847/1538-4357/aa6ca9

Kano, R., Trujillo Bueno, J., Winebarger, F., et al.: Discovery of scattering polarization in the hydrogen Lyman-α line of the solar disk radiation. ApJ **839**, L10 (2017). https://doi.org/10.3847/2041-8213/aa697f

Katsukawa, Y.: Penumbral microjets above a sunspot: evidence for magnetic reconnection in the solar chromosphere. Astron. Her. **109**, 548–553 (2016)

Katsukawa, Y., et al.: High resolution and high sensitivity spectropolarimetric observations of the solar chromosphere by the SUNRISE balloon-borne instrument. In: Balloon Symposium 2015, SA6000044039 (2015)

Katsukawa, Y., et al.: SUNRISE-3 balloon experiment: near-infrared spectropolarimeter SCIP. In: Balloon Symposium 2016, SA6000057028 (2016)

Kobayashi, K., et al.: The high-resolution coronal imager (Hi-C). Sol. Phys. **289**, 4393 (2014). https://doi.org/10.1007/s11207-014-0544-4

Lagg, A., Solanki, S.K., Riethmuller, Y., et al.: Fully resolved quiet-sun magnetic flux tube observed with the SUNRISE/IMAX instrument. ApJL **723**, L164 (2010). https://doi.org/10.1088/2041-8205/723/2/L164

Narukage, N., Auchère, F., Ishikawa, R., et al.: Vacuum ultraviolet spectropolarimeter design for precise polarization measurements. Appl. Opt. **54**, 2080 (2015). https://doi.org/10.1364/AO.54.002080

Narukage, N., Kubo, M., Ishikawa, R., et al.: High-reflectivity coatings for vacuum ultraviolet spectropolerimeter. Sol. Phys. **292**, 40 (2017). https://doi.org/10.1007/s11207-017-1061-z

Okamoto, J.: Waves in the solar corona. Astron. Her. **109**, 540–543 (2016)

Solanki, S., et al.: Sunrise: instrument, mission, data, and first results. Astrophys. J. **723**, L127 (2010). https://doi.org/10.1088/2041-8205/723/2/L127

Steiner, O., Franz, M., Bello Gonzalez, N., et al.: Detection of vortex tubes in solar granulation from observations with SUNRISE. ApJL **723**, L180 (2010). https://doi.org/10.1088/2041-8205/723/2/L180

Stenflo, J.O., Dravins, D., Wihlborg, N., et al.: Search for spectral line polarization in the solar vacuum ultraviolet. Sol. Phys. **66**, 13–19 (1980). https://doi.org/10.1007/BF00150514

Štěpán, J., Trujillo Bueno, J., Leenaarts, J., Carlsson, M.: Three-dimensional radiative transfer simulations of the scattering polarization of the hydrogen Lyα line in a magnetohydrodynamic model of the chromosphere-corona transition region. Astrophys. J. **803**, 65 (2015). https://doi.org/10.1088/0004-637X/803/2/65

Trujillo Bueno, J., Štěpán, J., Casini, R.: The Hanle effect of the hydrogen Lyα line for probing the magnetism of the solar transition region. Astrophys. J. **738**, L11 (2011). https://doi.org/10.1088/2041-8205/738/1/L11

Watanabe, H., Narukage, N., Kubo, M., et al.: Ly-alpha polarimeter design for CLASP rocket experiment. In: Solar Physics and Space Weather Instrumentation IV, 8148, 81480T (2011). https://doi.org/10.1088/0004-637X/736/1/71

Part V
Science Center and Public Outreach

Chapter 22
Hinode Science Center at NAOJ

Masumi Shimojo

Abstract The *Hinode* satellite project is the first solar satellite project in Japan that promotes the open use based on the systematical role sharing between the major Japanese institutes of solar physics. To maximize the scientific output from the *Hinode* project, *Hinode* Science Center (HSC) established in the National Astronomical Observatory of Japan (NAOJ) has promoted the scientific use of *Hinode*'s observation data, in cooperation with most of the Japanese institutes of solar physics. In this article, I describe our activities from before the organization of HSC to the present and outline the issues for the future.

Keywords Solar data · Science center · Data analysis environment

22.1 Particularity of Solar Observation Data in Astrophysical Studies

Observational astrophysics studies, especially those that use the data obtained with large telescopes [e.g., Atacama Large Millimeter/submillimeter Array (ALMA) and Subaru telescopes], usually start by preparing a proposal for an observation. This requires a great deal of attention in order to obtain observation time from such telescopes. Moreover, if a proposal is rejected, it is necessary to wait 1–2 years (proprietary period of principal investigator) for the observation data, even if your targets are observed based on the proposal submitted by the others. On the other hand, most of the solar observation data are provided to the public without delay after the observations; this is because the research communities related to solar

M. Shimojo (✉)
National Astronomical Observatory of Japan (NAOJ), National Institutes of Natural Sciences (NINS), Mitaka, Tokyo, 181-8588, Japan

Department of Astronomical Science, School of Physical Science, SOKENDAI (The Graduate University of Advanced Studies), Mitaka, Tokyo, 181-8588, Japan
e-mail: masumi.shimojo@nao.ac.jp

T. Shimizu et al. (eds.), *First Ten Years of Hinode Solar On-Orbit Observatory*,
Astrophysics and Space Science Library 449,
https://doi.org/10.1007/978-981-10-7742-5_22

phenomena understand the importance of exchanging the information about the Sun just after solar events have taken place, for furthering our understanding of various phenomena occurring in the solar atmosphere, heliosphere, geo-magnetosphere, and solar system objects. In particular, solar data obtained with satellites are made available just after downlinking without any limitations on their use for scientific studies. Recently, this trend toward openness may have been helped by the "open data policy" established by the Heliophysics Division of National Aeronautics and Space Administration (NASA) (NASA 2016). *Hinode*'s observation data are also made public just after downlinking and conversion of the file format. The *Hinode* satellite project accepts an observational proposal, which is called a *Hinode* Operation Plan (HOP), but the proposer is not permitted for exclusive use of the data. A similar data policy is adopted by other solar observing satellites. Therefore, a solar observing satellite project does not need to devote a great deal of effort to the call for proposal, reviewing of proposals, and control of the proprietary period of the data. To maximize scientific achievements resulting from the use of observation data, a project has to focus on promoting data usage to research communities. This is a significant difference between the use of data obtained from solar observing satellites and that obtained from the other large telescope projects.

22.2 Data Analysis System for Solar Observing Satellites

Before the era of the *Yohkoh* satellite that was launched in 1991 and operated scientifically until 2001, a development team for an instrument on aboard a satellite developed a data analysis system only for that instrument. In most cases, this development was carried out on a "mainframe" computer, and there is no de facto standard for the solar data analysis system's platform. Therefore, the data-analyzing programs of a particular instrument cannot be used for the data of another instrument. Moreover, it is very hard to use the programs when the platform is no longer use. For example, all downlinked data from the Hinotori satellite, which was the first solar observing satellite in Japan and was launched in 1981, are archived in the Scientific Information Retrieval Integrated Utilization System (SIRIUS) database of the Institute of Space and Astronautical Science at Japan Aerospace Exploration Agency (ISAS/JAXA). However, it is nearly impossible to analyze Hinotori's data using the Hinotori data analysis programs developed in the 1980s, because the platform does not exist in practically.

For the *Yohkoh* satellite project, the researchers at the Lockheed Martin Solar and Astrophysics Laboratory, who are the participants in the *Yohkoh* project from the USA, developed the data analysis platform using Interactive Data Language (IDL) on DEC workstations. Japanese/US/UK researchers in the *Yohkoh* team developed the programs for analyzing *Yohkoh*'s data on this platform and built the *Yohkoh* software package (Morrison et al. 1993). Since IDL can process image data interactively on several computer architectures (Unix, Linux, MacOS, and Microsoft Windows), it is a very powerful tool for solar data that consist mainly of images. The epoch-making *Yohkoh* data, and the use of IDL with the SolarSoftWare (SSW)

package (Freeland and Handy 1998), which was developed based on the *Yohkoh* software package, spread quickly through the global solar physics community. As a result, the IDL+SSW platform has become the de facto standard of the platform for solar data analysis, and all data analysis systems for new solar instruments developed after *Yohkoh* are, in effect, implemented on IDL+SSW basically.

The *Yohkoh* satellite produced not only marvelous scientific results but also a revolutionary data analysis platform for solar data. However, the price of a workstation and IDL in the *Yohkoh* era was too high and the combined cost of them being similar to the price of an imported luxury car. The Internet already existed in the early 1990s, but its bandwidth was not sufficient to use the servers at ISAS remotely, and so it was obviously impossible to transfer all of the *Yohkoh* data via the Internet. Therefore, the *Yohkoh* satellite project devoted much effort to building many workstations with IDL+SSW available to researchers, who visited the Sagamihara campus of ISAS, to promote scientific use of the *Yohkoh* data.

22.3 Preparation for Establishing the *Hinode* Science Center

The observation data obtained with the telescopes aboard the *Hinode* satellite are far more complex than the *Yohkoh* data. There are two reasons for this complexity. One is the increased of the dimensionality of the observation data. In *Yohkoh*'s case, the number of dimensions of the observation data is usually 2 or 3 (Time + Wavelength or Time + Coordinate on the Sun). Although the maximum number is 4 (Time + Coordinate on the Sun + Wavelength), there are only a few data points of the fourth dimension. On the other hand, the typical number of dimensions of the *Hinode* data is 4. Furthermore, the number of the dimensions of the data from Solar Optical Telescope (SOT)'s spectro-polarimeter (SP) is 5. The other reason for the data's increased complexity is that the typical field of view of *Hinode* is similar to the size of an active region. Hence, we cannot identify the region that is displayed only by looking at the image. Such properties of the data increase not only the complexity of data analysis but also the difficulty of searching for data. Moreover, the required computer resources also increase. It was clear that the scientific benefits resulting from *Hinode* data would be reduced, if we provided only the same data analysis environment for researchers as had been available in the *Yohkoh* era. Based on an awareness of these issues, we began planning for the *Hinode* Science Center (HSC) of National Astronomical Observatory of Japan (NAOJ) in 2003.

Figure 22.1 shows one of the presentation materials that were used to explain the plan of HSC to the Japanese parties concerned, in the early phase of the project. As shown in the figure, our plan was to maximize scientific results from *Hinode*, mainly by providing three items to researchers: (1) the data search/providing system, (2) the data analysis environment optimized for analyzing *Hinode* data, and (3) support for scientific workshops, like coordinated data analysis workshops.

One of the major issues for establishing HSC was role sharing between NAOJ and ISAS/JAXA. In the *Yohkoh* era, we did not need to consider the boundary

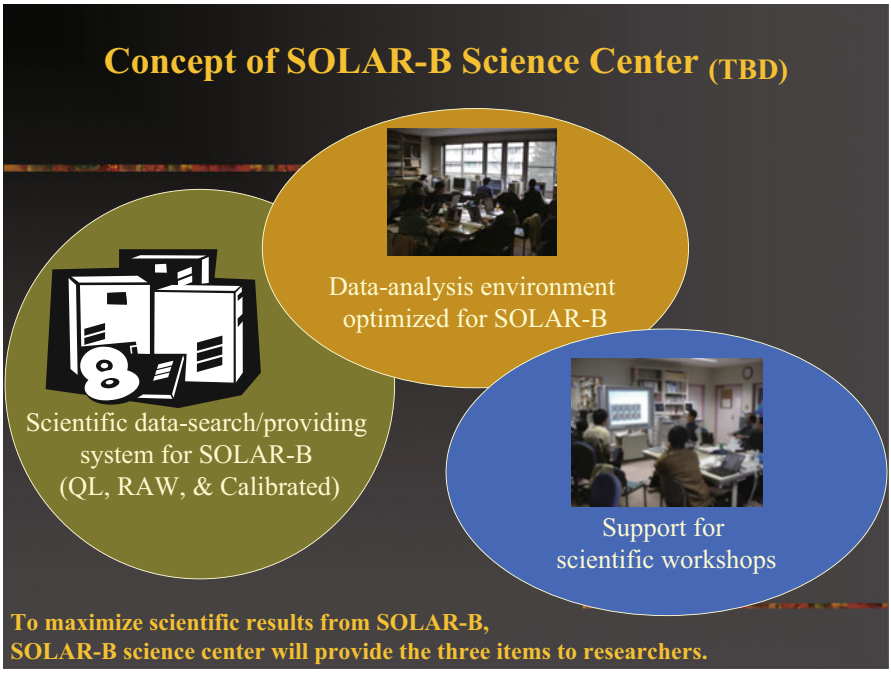

Fig. 22.1 The conceptual viewgraph of *Hinode* Science Center/NAOJ (Created in February 2004). Since it was created before the launch of *Hinode* satellite, the name of the center was "SOLAR-B Science Center"

between NAOJ and ISAS seriously, and it had been easy for a researcher at NAOJ to collaborate on a project of ISAS. The environment was dramatically changed in 2003–2004. During this period, JAXA was established through the merger of three institutions related to space and aeronautics research (ISAS, NAL, and NASDA), and national universities and national institutes (like NAOJ) in Japan were turned into independent administrative corporations. This changing in the administration of research institutes made it necessary to specify the tasks of each institute. The X-ray astronomy group in ISAS had already been involved in similar role sharing with other institutes. Referencing their role-sharing model, the *Hinode* project of ISAS/JAXA takes responsibility for satellite operation, data accumulation, and data provision (Matsuzaki et al. 2007). On the other hand, HSC of NAOJ takes charge of providing support to the researchers who use *Hinode* data and a part of the scientific operation of the telescopes (Shimojo and Tsuneta 2007). Based on the role sharing, the data search/providing system that is one of the main items of HSC was constructed as "Data ARchives and Transmission System (DARTS)/*Hinode*"[1] by ISAS/JAXA, in cooperation with NAOJ. Since ISAS/JAXA

[1] http://darts.isas.jaxa.jp/solar/*Hinode*/

already had experience of constructing such systems for other satellites, our choice was ideal for constructing the *Hinode* database system.

In the second half of 2004, we started constructing the data analysis environment for *Hinode* data at NAOJ. Just after starting the construction, we encountered a major issue – there was a budget problem. To create successively the maps of magnetic field vectors at the photosphere from the daily data, obtained with the SOT-SP, a PC cluster system was needed, even when the performance of the fastest CPU at the time was taken into consideration. HSC received financial support from the Grant-in-Aid for Creative Scientific Research "The Basic Study of Space Weather Prediction" (Head investigator: Prof. K. Shibata, Kyoto University) since 2006. However, our budget for HSC was too tight in 2004–2005 and lacked the budget for a PC cluster system. At first, we considered constructing the system based on homebuilt computers. Thanks to Prof. Mizumoto, who was the director of the Astronomy Data Center (ADC)/NAOJ, and Dr. Ukita, who is an associated professor at the Okayama Astrophysical Observatory/NAOJ, the required computing resources (x86 servers, OS, and middleware for a PC cluster system) were donated to us by Sun Microsystems K.K. (Currently: Oracle Corporation, Japan). Using the PC cluster system constructed from these donated resources, Dr. Yokoyama, who is an associated professor at the University of Tokyo, Dr. Katsukawa, who is an associated professor at NAOJ, and I wrote a Milne-Eddington inversion code for the SOT-SP data (named MEKSY). Thanks to the use of the PC cluster system and the MEKSY code, it was very easy to obtain a map of magnetic field vectors from the SOT-SP data, and this helped greatly in facilitating the scientific achievements that were made just after the scientific operation of *Hinode* began. Scientific results from the early phase of *Hinode*'s operation might have been significantly lesser, if there had been no support from Sun Microsystems K.K., the Grant-in-Aid for Creative Scientific Research, and collaborators.

22.4 10 Years of *Hinode* Science Center

HSC was established on September 4, 2005, which was 1 year before the launch of *Hinode*. To introduce the data analysis of the *Hinode* data, we held three "*Hinode* KOSYU-KAI" (workshops with the tutorials for *Hinode* data analysis) in 2005–2006. These were the first workshops supported by HSC. The number of the workshops supported by HSC during the decade since then is 42, and their subjects cover a broad range from "faint young Sun paradox" to "comparison between laboratory plasma and solar plasma." You can find details of the workshops on the home page of HSC.[2]

[2] http://hinode.nao.ac.jp/

HSC faced two turning points during this decade. One was the Great East Japan Earthquake on March 11, 2011. Due to the earthquake, the data backup of HSC was not functioning. The Sagamihara campus of ISAS/JAXA is located only 18 km away from the Mitaka campus of NAOJ. This distance is not sufficient to avoid the effects of such a natural disaster. Moreover, we needed to suspend our services for researchers in the next few months, because of the planned power outages in the Tokyo area to cope for with the nuclear plant disaster. To avert the effects of natural disasters, we established *Hinode* Science Center at Nagoya,[3] which is hosted by the Institute for Space-Earth Environment Research (ISEE), Nagoya University. This resulted in not only the establishment of a new backup site but also in a new foothold for *Hinode* data analysis. The other turning point for HSC was the union of the data analysis system of *Hinode* and the common-use data analysis system operated by ADC/NAOJ. It was implemented at the time of the ADC's computer system replacement in 2012–2013. Before the replacement, the computer system of HSC was operated by only a few solar researchers. Thanks to the union of the systems, the data analysis environment for solar data at NAOJ[4] is now operated by professional computing teams. At the current time, a data analysis environment is a basic infrastructure for all researches, and such an infrastructure must be operated based on a firm foothold. From this point of view, I think that the solar data analysis environment at NAOJ has finally achieved a real infrastructure.

22.5 Issues for the Future

For several years following the launch of *Hinode*, HSC could support researches in Japan very well. However, this supporting activity of HSC has been declining recently. Colleagues in the USA and Europe have built useful databases (e.g., the flare list for each instrument and database of the maps of magnetic field vectors) that are effective in encouraging *Hinode* data usage. On the other hand, HSC was not able to build such a database, apart from the mission-wide flare list leaded by Nagoya University, and it has been difficult to expand functions of user support. I think that user support is similar to a service industry, which means that we need to meet demands from users continuously. However, I have to say that maintaining such activities in Japan is too hard, because there is no scheme to evaluate user supports provided by researchers. Therefore, working in user support is not an effective way of building a career in Japan. If our long-term goal is for users to attain a continuous stream of scientific achievements, I think that we need to employ researchers whose main role is to provide scientific user support and then to evaluate these researchers

[3] http://hinode.stelab.nagoya-u.ac.jp/

[4] http://hinode.nao.ac.jp/SDAS/

Acknowledgements The author deeply thanks all persons who have collaborated with the *Hinode* Science Center. Especially, the author thanks to Mr. Hideaki Tonooka who is a former staff member of HSC (currently on the staff of C-SODA/JAXA). He took all responsibility for constructing and operating the computer system of HSC. Without his contribution, we could not analyze *Hinode* data at HSC.

This work is carried out at the NAOJ *Hinode* Science Center, which is supported by the Grant-in-Aid for Creative Scientific Research Basic Study of Space Weather Prediction from MEXT, Japan (Head investigator: K. Shibata), generous donations from Sun Microsystems, and NAOJ internal funding.

References

Freeland, S.L., Handy, B.N.: Data analysis with the SolarSoft system. Sol. Phys. **182**, 497–500 (1998). https://doi.org/10.1023/A:1005038224881

NASA Heliophysics Division: NASA Heliophysics Science Data Management Policy. https://hpde.gsfc.nasa.gov/Heliophysics_Data_Policy_v1.2_2016Oct04.html (2016). Accessed 7 Mar 2017

Matsuzaki, K., et al.: Data archive of the Hinode mission. Sol. Phys. **243**, 87–92 (2007). https://doi.org/10.1007/s11207-006-0303-2

Morrison, M.D., et al.: The Yohkoh software and database system. Bull. Am. Astron. Soc. **25**, 1188 (1993)

Shimojo, M., Tsuneta, S.: The solar-B science center in Japan. In: Shibata, K., Nagata, S., Sakurai, T. (eds.) New Solar Physics with SOLAR-B Mission, The 6th Solar-B Science Meeting. A.S.P. Conference Series, vol. 369, pp. 59-62. Astronomical Society of the Pacific, San Francisco (2007)

Chapter 23
Public Outreach and Education Activities of Solar Mission *Hinode* in Japan

Kentaro Yaji, Hideaki Tonooka, and Naoko Inoue

Abstract Solar mission *Hinode* has been promoting education and public outreach (EPO) in various ways since its launch in 2006. The EPO activities have included information release via their web page and the press, open house at the National Astronomical Observatory of Japan and Institute of Space and Astronautical Science at Japan Aerospace Exploration Agency, development of digital contents for education in collaboration with astronomy educators in public observatories and planetariums, lectures to the public, and release of teaching materials. This article reflects on the *Hinode* EPO activities in the last 10 years and introduces specific activities in Japan.

Keywords Hinode · Public outreach · Education · Collaboration · Communication

23.1 Introduction

The *Hinode* project team at the National Astronomical Observatory of Japan (NAOJ) and Institute of Space and Astronautical Science at Japan Aerospace Exploration Agency (ISAS/JAXA) recognizes the importance of continuing public outreach activities for communicating the scientific results of solar mission *Hinode* to the public. At the time when *Hinode* had its tenth anniversary in orbit, we looked back on our public outreach activities in Japan. A couple of distinguishing characteristics can be found in our activities. One is that the *Hinode* team has

K. Yaji (✉) · N. Inoue
National Astronomical Observatory of Japan, Mitaka, Tokyo, Japan
e-mail: kentaro.yaji@nao.ac.jp; naoko.inoue@nao.ac.jp

H. Tonooka
Institute of Space and Astronautical Science, Japan Aerospace Exploration Agency, Sagamigara, Kanagawa, Japan
e-mail: tonooka.hideaki@jaxa.jp

T. Shimizu et al. (eds.), *First Ten Years of Hinode Solar On-Orbit Observatory*,
Astrophysics and Space Science Library 449,
https://doi.org/10.1007/978-981-10-7742-5_23

recognized the importance of public outreach activities much earlier than at the time of the *Hinode* launch. We actively released the latest status of the spacecraft development, such as satellite functional checking and launch preparation at the launch site, to the public on the website, and made leaflets that shed light on *Hinode*'s framework and goals. The second is that the *Hinode* team has encouraged the use of *Hinode* data to astronomy educators. Japan has many lifelong learning facilities, such as public observatories, planetariums, and science museums, and we have had positive collaborations with such facilities. We observed astronomical phenomena, such as solar eclipses and the transit of Mercury and Venus, which are easily interesting to the public, and have actively released observation images.

In this article, we introduce three specific topics and reflect on the last 10 years of *Hinode*'s public outreach activities.

23.2 Working Group for Public Use of *Hinode* Data

Public relations hold a crucial role and not only in scientific satellite projects. However, allocating a sufficient budget for public relations is challenging because the entire project budget is limited. The budget for public relations is lower in Japanese scientific projects compared with the case of National Aeronautics and Space Administration (NASA), which has poured funding into the distribution of educational movies, DVDs, and merchandise. In focusing on the public relations of scientific results, researchers want to spread widely scientific results obtained from research projects to the public, with consideration for the fact that the public may not be perceptive of difficult or overly technical reports. As such, researchers must convey scientific results plainly; however, few researchers are good at such a task. Scientific projects should thus employ those who can understand both research and public relations; however, they hardly have the required budget as described above.

Social educational facilities, such as public observatories, planetariums, and science museums, and their staffs are tasked with relaying scientific research to the public. In the Japanese astronomy community, the Public Astronomical Observatory NETwork (PAONET) has been organized for sharing astronomy information, such as images, resources, and teaching materials, among the related educational facilities. The *Hinode* team organized a PAONET Working Group for Public Use of *Hinode* Data, so-called PAO-Hinode, composed of PAONET members to promote public outreach activities through the social educational facilities (Yaji et al. 2008). Researchers and educators exchange ideas and information, which enables the researchers to engage in outreach with the educators' know-how and in turn enables the educators to obtain cutting-edge research results from researchers and use them for education and outreach (Shimojo 2009; Tokimasa 2009). Thus, these two groups share a mutually beneficial relationship.

One good point in solar research is to capture solar phenomena with images or movies. Solar researchers arrange solar images in a time series and make movies, to promote understanding of solar phenomena. Such movies tend to be impressive

Fig. 23.1 DVDs produced by PAO-Hinode WG, *The Sun Captured by Hinode* (2008) in Japanese (left) and English (middle) and *Approaching the Solar Mystery* (2009) (right) (Reprinted from Yaji et al. (2016) (Fig.1) by permission of ASJ)

to amateur eyes, and they clearly express solar dynamic phenomena. Explanations are then added to the movies for the educators. DVDs, including the movies for showing at the facilities, are produced and distributed. At present, PAO-Hinode's focus activity is the production of educational DVDs.

PAO-Hinode has produced two types of DVDs containing combined movies and HTML sources (Fig. 23.1). The two are available at social educational facilities. Given the budget limit, the DVDs were produced in house. *Hinode* has imagers with many pixels for managing both wide field of view and high spatial resolutions. For the best use of these high-resolution images, the movies were produced in full HD, which was rare in the late 2000s, when the DVDs were made.

The Sun Captured by Hinode (named DVD1), released in March 2008, contains two kinds of short films (2 and 17 min each) that introduce *Hinode*'s goals and initial observation results. The HTML materials contain useful data for education and outreach, such as teaching materials on the Sun, exhibition samples, and instruction for using the DVD1. This DVD1 was distributed to PAONET-affiliated social educational facilities in Japan and at *Hinode*'s exhibition booth in international conferences. An English version of the DVD1, in which the movies are translated to English, was released in September 2008. More than 10,000 copies have been released of the Japanese and English versions.

The second production *Approaching the Solar Mystery* (named DVD2) was released in April 2009. This DVD2 was planned to drum interest in the Sun in anticipation of the total solar eclipse to be observed in Japan in July 2009. The movies in the DVD2 were composed of four themes. As regards their target age, the movies were deemed appropriate for the all age groups and also for those who have knowledge on the Sun. The HTML contents included instructions for observing the total eclipse safely. The DVD2 was bundled with Science Window, a bimonthly magazine published by the Japan Science and Technology Agency (JST), and distributed to elementary, junior high, and high schools all over Japan. Therefore, the number of distributed DVDs exceeded 50,000 copies. In addition, a picture book was derived from one of the movies included in the DVD2.

One peculiarity of this DVD production activity is the in-house production. Its disadvantage is the strain on labor. Meanwhile, an advantage is that it enabled the working group discretion to produce necessary items and collect content that are free to use and show. As scientific accuracy was the priority of the production, the content of DVDs tended to be difficult for the public to absorb. This was an inevitable trade-off.

Certainly, we were limited in producing easy-to-understand content for the public, compared with professionals in producing science programs. The conclusion was that the inclusion of contents that we can freely use is more necessary in the educational fields (Hideaki Tonooka).

23.3 Let's Look at the Sun with *Hinode*!

"Let's look at the Sun with *Hinode*!" is one of the education and outreach activities that uses *Hinode* observation data (Yaji 2013). Called "With *Hinode*!" for short, it is highly evaluated as a unique activity. This activity is a simultaneous observation campaign for high and junior high school students that started in 2010. It encouraged the use of *Hinode* data for education. PAO-Hinode aimed to provide opportunities for students to be more actively involved with *Hinode* data. Thus, we developed the idea of an observation program for simultaneous solar observation by *Hinode* and students, later defined as one of *Hinode* Operation Plans (HOP). In Japan, many students engage in solar observation, with sketching and photography as related club activities, in high and junior high schools. Recently, the students observe the Sun not only with white light but also with Hα line, Ca-K line, and radio. The students compare their own observational data with *Hinode*, which is the most important goal of "With *Hinode*!".

The *Hinode* team has widely accepted observation proposals from any researchers over the world, and a HOP number has been given to each approved proposal. One of the authors (Yaji) submitted a proposal entitled "EPO Campaign observation mainly for high school students," which was approved as HOP173. Although only a few schools participated in "With *Hinode*!" initially, 25 schools and astronomy facilities eventually participated for 6 years. Participants included high/junior high schools and public observatories and the education department and astronomical clubs of universities. Further, six more schools participated in 2014, coinciding with the solar maximum passing. As "With *Hinode*!" was carried out, the students received the observation targets through a mailing list and occasionally suggested the observation targets themselves. A number of schools studied the simultaneous observation data and compared these with their own data. They held presentations at their schools' festivals, prefectural science contests, and junior sessions in the astronomical society's annual meeting. Notable examples of recent presentations include "Following the Relations between Prominences and X-ray"

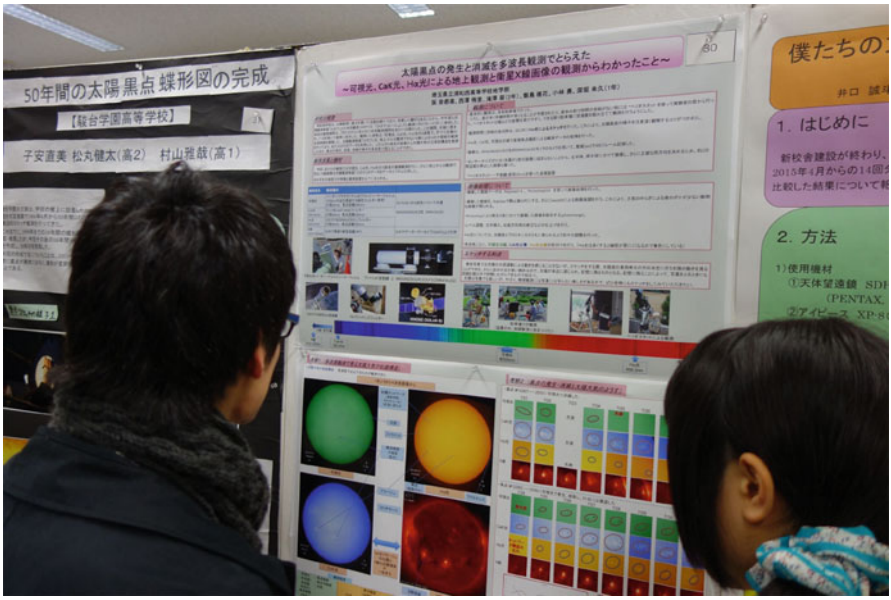

Fig. 23.2 An example of a presentation in the junior session of an annual meeting of Astronomical Society of Japan (Courtesy of Mr. Sakae, Urawa Nishi High School) (Reprinted from Yaji et al. (2016) (Fig.2) by permission of ASJ)

by Tsuno High School in Miyazaki Prefecture and "Sunspots Appearance and Disappearance with Multiwave Observations" by Urawa-Nishi High School in Saitama Prefecture (Fig. 23.2). Many students compared their own solar images observed in white light and Hα line with X-ray images from *Hinode*. Results of the questionnaire surveys that were carried out after the joint observations showed that the students had enhanced understanding of the Sun through *Hinode* and were motivated to learn by the joint observations. Recently, inquiries were received from countries such as Sri Lanka and Thailand.

"Let's look at the Sun with *Hinode*!" is the first observation proposal for the purpose of education, which *Hinode* carried out, and has not been seen even in other satellite projects of Europe and the USA. As such, foreign solar researchers are highly interested in the joint observations. At *Hinode* science meetings, participants have praised the proposal and inquired on the observation results of high school students. "With *Hinode*!" has been implemented smoothly because *Hinode* observation data is more accessible to the students compared with other satellite data. "With *Hinode* !" has spread to other schools and facilities and has piqued interest in the public. According to the recent solar condition, the solar activity is getting lower and lower, but we will continue "With *Hinode*!" in the coming years (Kentaro Yaji).

23.4 A Lot of Thought into Our Outreach Activities

Researchers want to communicate the basis of the science even if this is difficult for the public, who tend to ignore difficult reports. Table 23.1 shows the hits of some articles posted on the Japanese version of the NAOJ *Hinode* website for 1 week from the release date. The article with beautiful images and movies of the Venus transit sets the best record by a large margin. Other than this, articles on solar eclipses, the Mercury transit, huge sunspots, and those with beautiful images and movies on the Sun released in the early stage of *Hinode*'s operation rank high.

Table 23.1 Access to principal articles placed on the Japanese version of the NAOJ *Hinode* website

Article title	Posted dates (YYYY. MM.DD)	Access numbers for one week from the posted date
Transit of Venus captured by Hinode	2012. 6. 6	114,879
Initial results of Hinode Solar Optical Telescope (SOT)	2006.11.27	62,001
Start of all Hinode observational data release	2007.5.27	40,553
Rotation of the Sun and dynamic corona seen by Hinode X-ray telescope (XRT)	2007.5.27	40,227
Polar field reversal as observed with Hinode	2012.4.19	32,047
Annular eclipse captured by Hinode	2011.1.6	31,973
Opening of the Hinode latest images page	2007.5.27	31,650
Observation of the partial eclipse – the shadows of craters of the Moon were found	2007.2.26	22,954
Release of the images of the Sun taken by three telescopes	2006.10.31	21,553
Partial eclipse on March 19 – total eclipse in orbit – total eclipse observed by Hinode	2007.3.21	18,803
Transit of Mercury captured by Hinode	2006.11.9	18,221
Huge sunspots and their magnetic structure observed by Hinode	2014.11.19	14,771
Hinode featured in American scientific journal "Science"	2007.12.7	11,956
Hinode discovered strong magnetic field patches in the Sun's polar region	2010.3.9	10,514
Massive flare observed by Hinode	2007.3.22	9,825
A new solar dynamo mechanism discovered by the Hinode satellite	2009.4.8	5,244
Hinode captured the precursor structure of the sunspots penumbra formation for the first time	2012.3.8	3,344
CLASP was launched	2015.9.4	1,082
Hinode, IRIS, and ATERUI cooperate on 70 year old solar mystery – Magnetically driven resonance helps heat the Sun's atmosphere! –	2015.8.24	982
Mechanism of explosions and plasma jets associated with sunspot formation revealed	2015.9.30	838

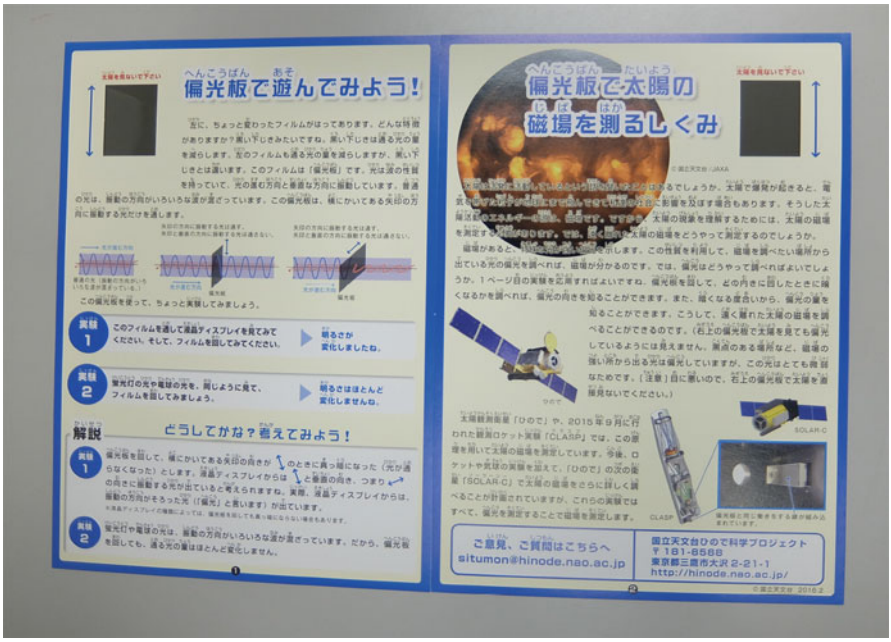

Fig. 23.3 A leaflet with a polarizer (Reprinted from Yaji et al. (2016) (Fig.3) by permission of ASJ)

In this way, the articles carrying astronomical events are deemed useful for increasing *Hinode*'s presence. Therefore, we have been releasing reports on such kinds of topics in a timely manner. Meanwhile, the hits of articles carrying *Hinode*'s scientific results are much smaller. These data show how difficult it is to communicate scientific sources, which may be difficult for the public to grasp. However, we have no intention of giving up on such communication. The key to achieve this is a "hook," i.e., a way to catch people's interest and imagination. As an example, we introduce a leaflet with a polarizer (Fig. 23.3). To communicate the significance of magnetic fields in understanding solar activities and means for measuring magnetic fields, the working group adopted a simple experiment with a polarizer as a "hook" and then made a leaflet. The A4 size leaflet has a 4×3 cm hole in a corner, through which a polarizer is placed.

The front page (Fig. 23.3, left) explains the nature of the polarizer, as well as a simple experiment of looking at a liquid crystal display through the polarizer and rotating the polarizer. When it looks dark, the direction perpendicular to the polarization axis of the polarizer is the polarized direction of the light emitted from the display. Through this experiment, people see how it is possible to determine the direction of light polarization by rotating a polarizer. The back page (Fig. 23.3, right) describes the significance of the magnetic fields in understanding solar activities, as well as explains the use of the polarizer to measure the magnetic fields of the Sun.

The leaflets were distributed at the exhibition booth of Japan Geoscience Union (JpGU) meetings and exhibition on the open house day of NAOJ. The number of leaflets distributed was much larger than that of conventional *Hinode* pamphlets, in which only the outline and scientific results of *Hinode* are presented. With this leaflet as a start, we could expand the dialogue with visitors and communicate not only how to measure the magnetic fields of the Sun but also that *Hinode* successfully measured the photospheric magnetic fields. The significance of measuring the chromospheric magnetic fields has also been highlighted for determining the heating mechanism of the corona and the mechanism of flare occurrence.

Finally, in commemoration of the tenth anniversary of the *Hinode* launch, we revamped the NAOJ *Hinode* website (http://hinode.nao.ac.jp/en/). The design has been renewed to make the site more attractive. On the main page, there is a "hook" in the form of a series of beautiful movies of the Sun taken by *Hinode*. Moreover, new pages for the public have been created. These pages explain in easy terms the results of the 10-year observation of *Hinode*. In addition, the tenth anniversary movie introduces typical observational results (Naoko Inoue)

23.5 Conclusion

As mentioned above, we have performed unique public outreach activities not restricted to conventional ways. At the time of *Hinode*'s tenth anniversary and with the aim of realizing the next solar mission, SOLAR-C, we recognize the great significance of the public's recognition of *Hinode*'s achievements and what remains to be achieved, as well as future aims for the succeeding solar missions. Thus, public outreach will become more important. In the educational field, the boost in students' motivation brought by "Let's look at the Sun with *Hinode*!" as regards observing the Sun is highly appreciated, and further contribution to the field of education is expected. By taking advantage of the accumulated know-how and with flexible ideas, we will connect society to the state-of-the-art research of *Hinode* and succeeding solar missions.

References

Shimojo, S.: Astronomical Public Relations Activity promoted by Hinode. Sokendai Journal. **16**, 23–27 (2009)

Tokimasa, N.: What role do public observatories play? Sokendai Journal. **16**, 26–27 (2009)

PAONET.: Working Group for Public Use of Hinode Data: The Sun Captured by Hinode (2008)

PAONET.: Working Group for Public Use of Hinode Data: Approaching the Solar Mystery (2009)

Yaji, K.: PAONET working group for public use of Hinode data: Activities of PAONET. Astronon. Her. **101**, 565–575 (2008)

Yaji, K.: Let's Look at the Sun with Hinode together! Astronon. Her. **106**, 503–511 (2013)

Yaji, K., Tonooka, H., Inoue, N.: Public Outreach and Education Activity of Hinode. Astronon. Her. **109**, 642–646 (2016)

Appendix A
Hinode Image Gallery

A large number of images were acquired with the three telescopes onboard *Hinode* in its first 10 years. Remarkable images, which are impressive to not only researchers but also the general public, have been released via various forms of media. This image gallery is a collection of some of the released images. The copyright of the images in the gallery is JAXA/NAOJ/Hinode,[1] if not mentioned.

A.1 Quiet Sun

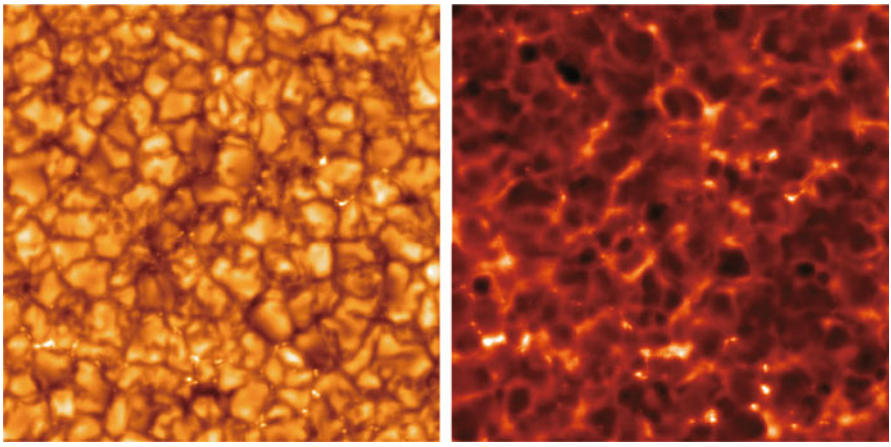

Fig. A.1 Solar granulation, visible everywhere on the solar surface. The photospheric (left, G-band) and chromospheric (right, Ca II H) images, captured by the Solar Optical Telescope (SOT) broadband filter imager with a spatial resolution of 0.2 arcsec (equivalent to 150 km on the solar surface)

[1] Japan Aerospace Exploration Agency/National Astronomical Observatory of Japan/Hinode.

T. Shimizu et al. (eds.), *First Ten Years of Hinode Solar On-Orbit Observatory*,
Astrophysics and Space Science Library 449,
https://doi.org/10.1007/978-981-10-7742-5

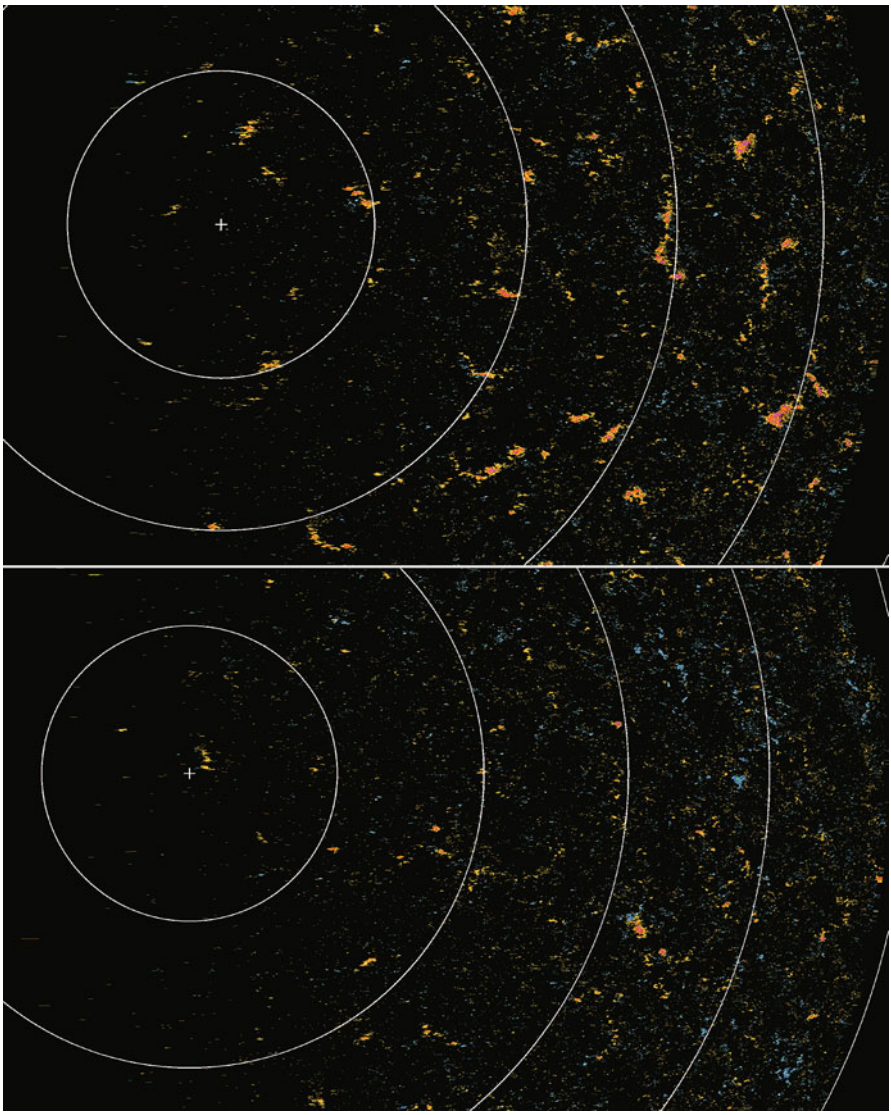

Fig. A.2 Magnetic flux patches distributed in the northern polar region. Owing to its high spatial resolution, the SOT observations provide accurate measurements of the spatial distribution of magnetic flux in the polar regions of the Sun in monthly intervals. These regions are difficult to view from the Earth due to foreshortening. The high spatial resolution observations allowed us to resolve magnetic flux patches with a magnetic flux density higher than 1000 Gauss (0.1 Tesla). This magnetic field map was measured on 20 September 2008 (top) and 9 October 2011 (bottom). The cross mark is the location of the North Pole, and each white line shows 85, 80, 75, 70, and 65° in heliographic latitude from the polar side. Red and blue colors represent positive and negative magnetic polarity, respectively

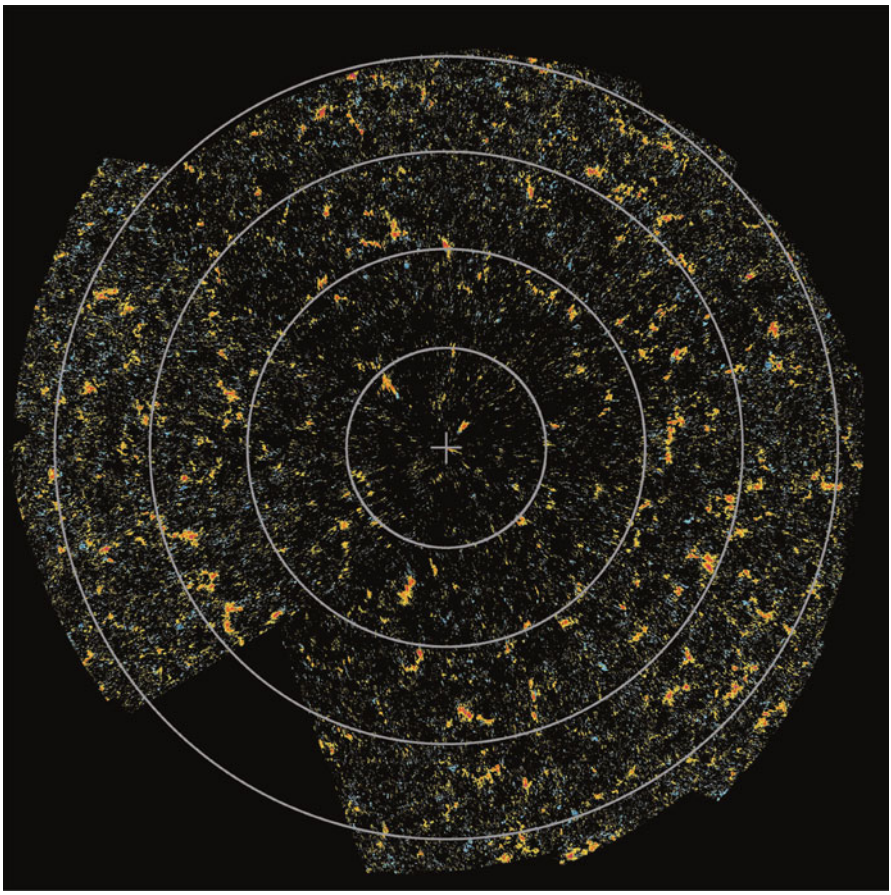

Fig. A.3 A panorama map of magnetic flux at the northern polar region on September 2007. The 360° coverage in the heliographic longitude is achieved via magnetic field measurements carried out every few days in a month. The cross mark is the location of the North Pole, and each white circle shows 85, 80, 75, and 70° in heliographic latitude from the polar side. Red and blue colors represent positive and negative magnetic polarity, respectively

A.2 Sunspots

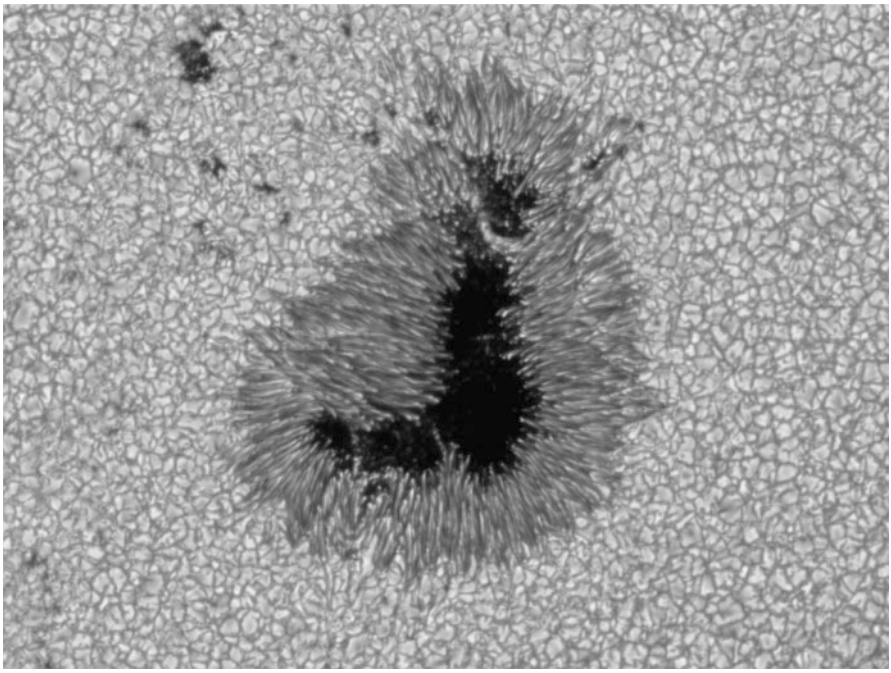

Fig. A.4 "Japan" sunspot, which was the main sunspot in active region NOAA (National Oceanic and Atmospheric Administration) 10953 on 3 May 2007. The name comes from the fact that the overall shape of the umbrae is similar to the islands of Japan. This image was taken with the blue continuum filter by the SOT

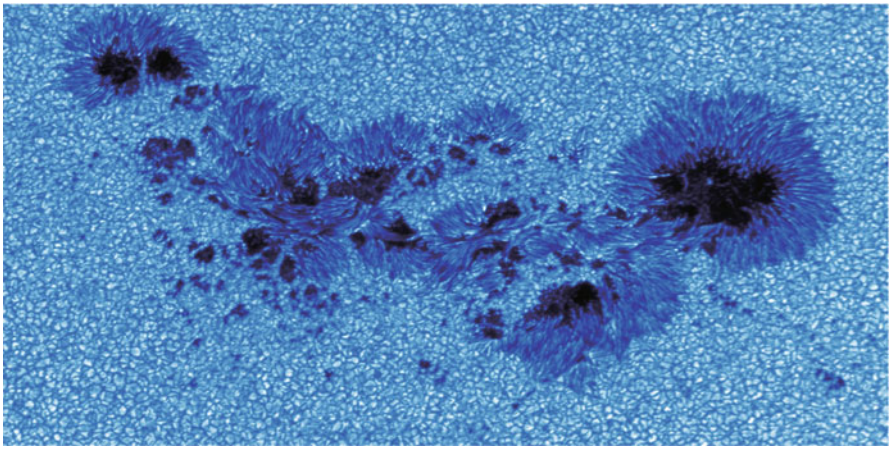

Fig. A.5 Active region NOAA 11429 on 8 March 2012, which produced X-class flares on 7 March 2012. This image was taken with the blue continuum filter by the SOT

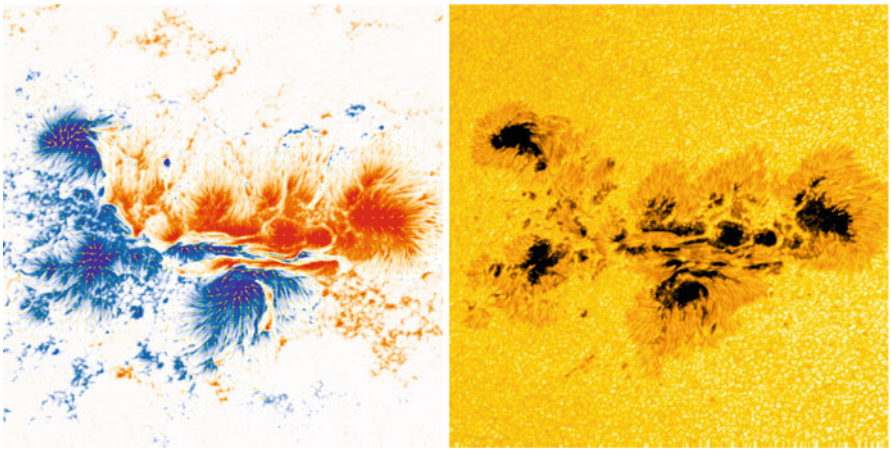

Fig. A.6 Active region NOAA 11429 on 6 March 2012, recorded a few hours before the start of an X-class flare. Vector magnetic field (left) map and sunspot continuum image (right), derived from the spectropolarimeter data. The SOT's spectropolarimeter records the full-polarization states (Stokes I, Q, U, and V) of line profiles of two magnetically sensitive Fe I lines at 630.15 and 630.25 nm, allowing us to determine the magnetic flux vectors accurately with a spatial resolution of 0.3 arcsec. Red and blue are the positive and negative polarities of magnetic flux, respectively, and arrows represent the direction of magnetic field at the solar surface

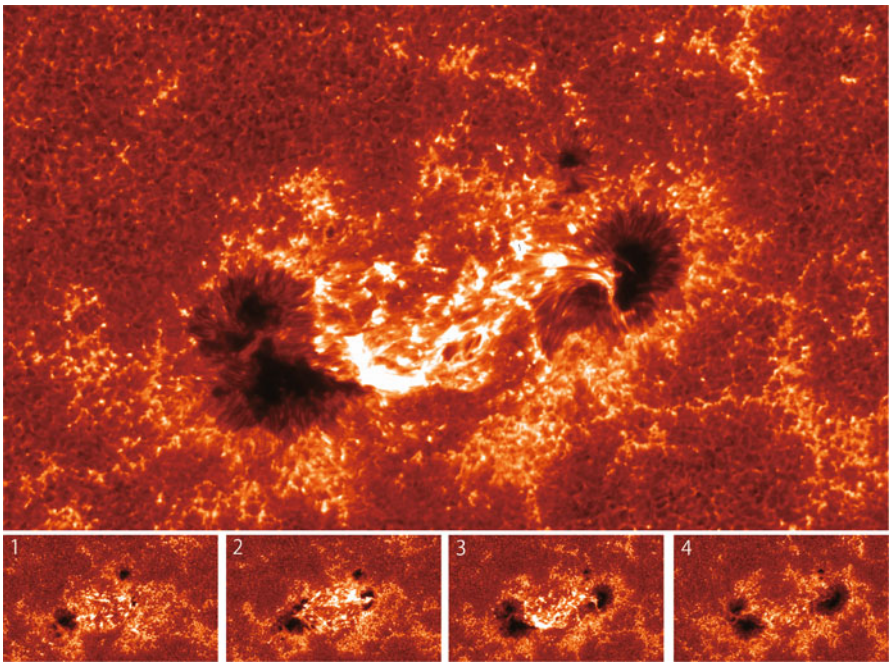

Fig. A.7 A large emerging flux region appeared from 30 to 31 December 2009 in active region NOAA 11039. The SOT captured the totality of the evolution, from the birth of the pores to the development of the bipolar pair of sunspots with Ca II H filter

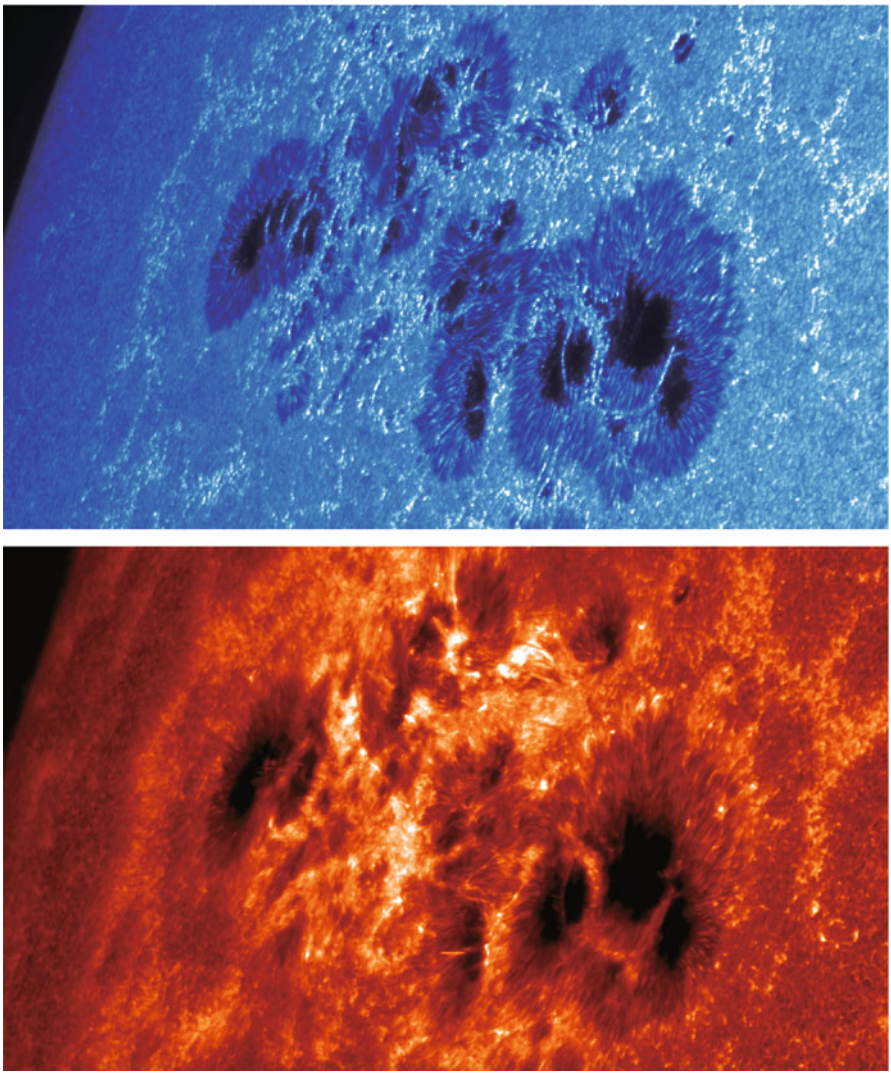

Fig. A.8 Active region NOAA 11339, rotated from behind the east limb in early November 2011. An X-class flare was produced about 10 h after these images were taken. Taken by the SOT with Ca II H (top) and G-band filters (bottom)

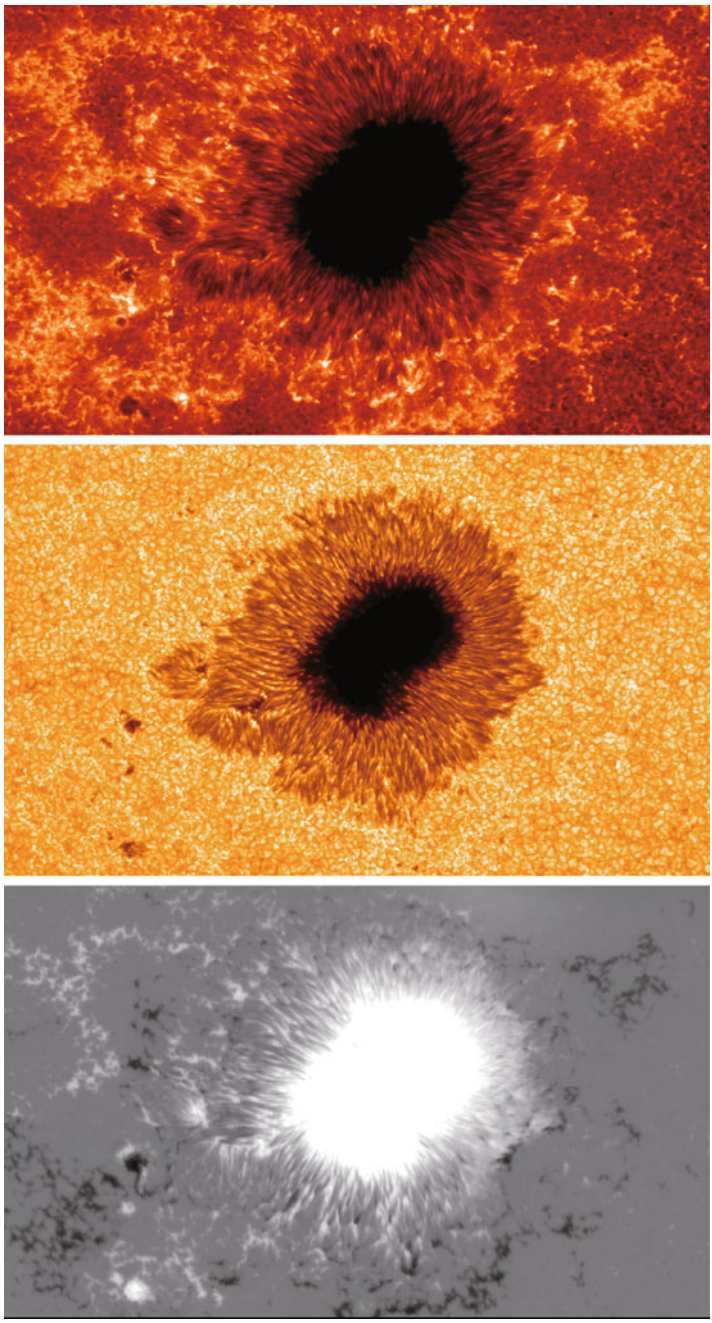

Fig. A.9 A moderate-sized sunspot observed by the SOT. Filtergrams with chromospheric Ca II H filter (top) and G-band filter (middle) and magnetogram (bottom)

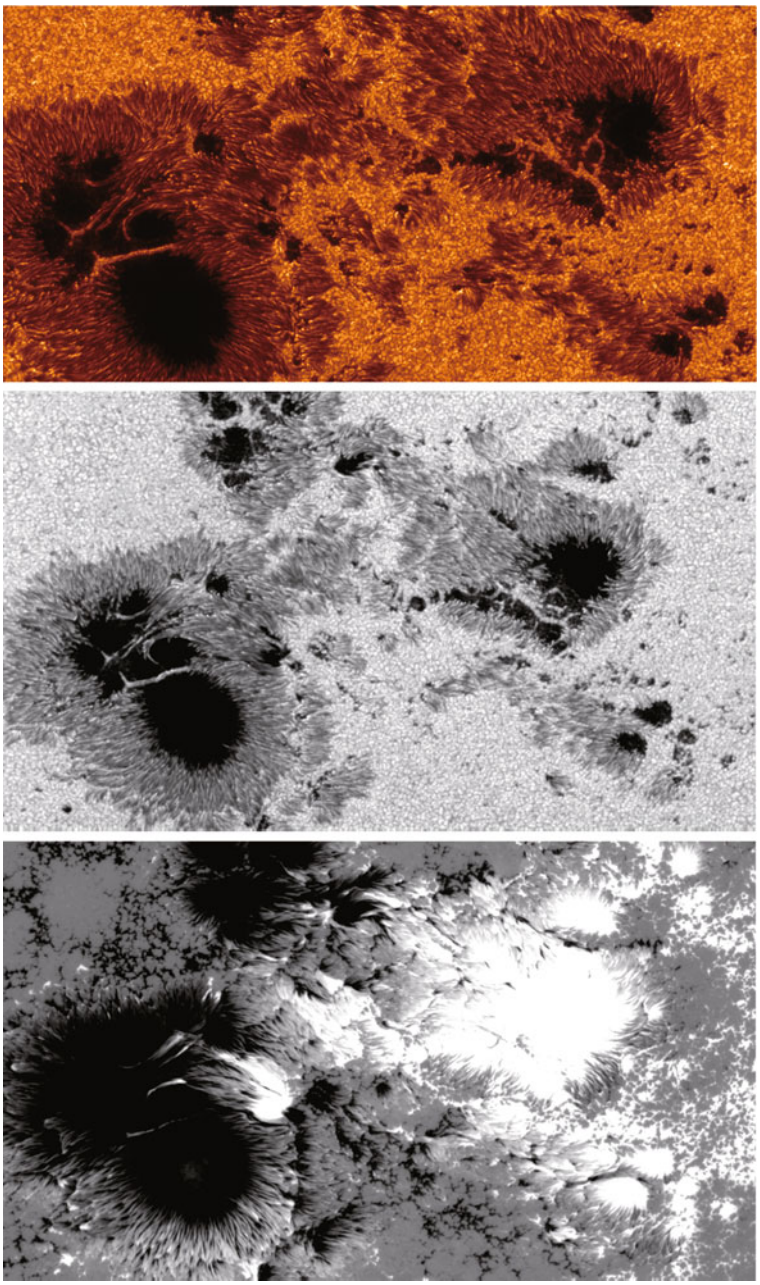

Fig. A.10 Active region NOAA 12192 on 24 October 2014, recorded by the SOT: highest resolution G-band image (top), continuum image (middle), and line-of-sight magnetogram (bottom). The G-band's field of view (108 × 84 arcsec, check) could capture only a limited area of this sunspot group. The size of the sunspot group is about 66 times larger than the size of the Earth, which has been considered to be the largest since 18 November 1990. In the magnetogram, white and black correspond to positive and negative magnetic polarity, respectively

A.3 Chromosphere

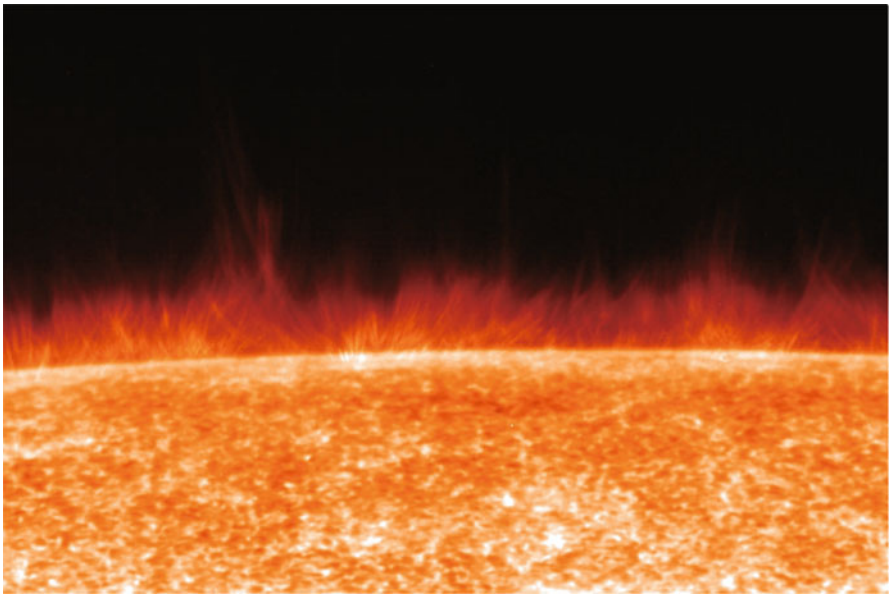

Fig. A.11 The solar limb, observed by the SOT with a Ca II H filter, showing dynamical behaviors of chromospheric spicules. The chromosphere, the interface layer between the photosphere and the corona, consists of large number of dynamic straw-like features known as spicules

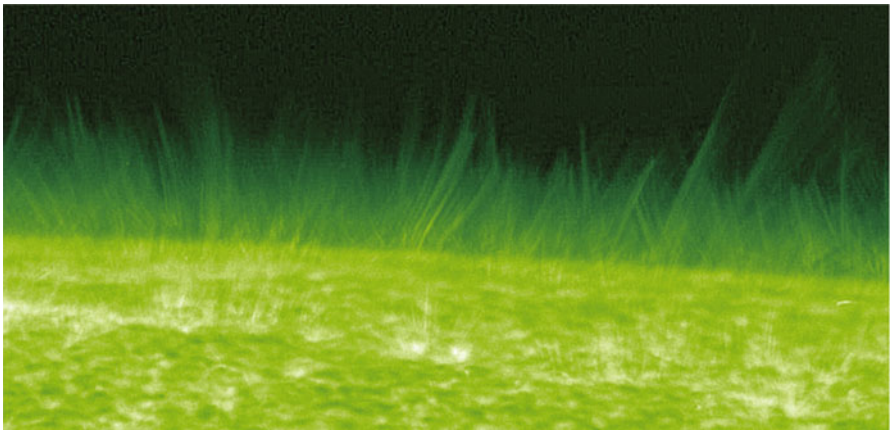

Fig. A.12 High-resolution image of the solar limb showing fine structures of spicules, obtained by the SOT with a Ca II H filter on 22 November 2006

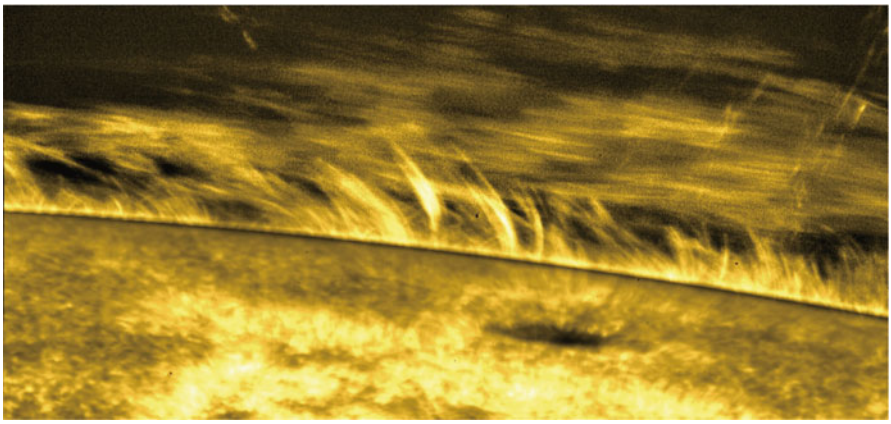

Fig. A.13 Discovery of Alfvén waves. The time series of high-resolution Ca II H images taken by the SOT has revealed transversal oscillations of minuscule magnetic structures, such as prominence threads and spicules, with small amplitude. These oscillations are thought to be a signature of magnetohydrodynamic waves along the magnetic structures. Horizontally oriented threads at the upper portion of this photograph show oscillations in the up-and-down direction

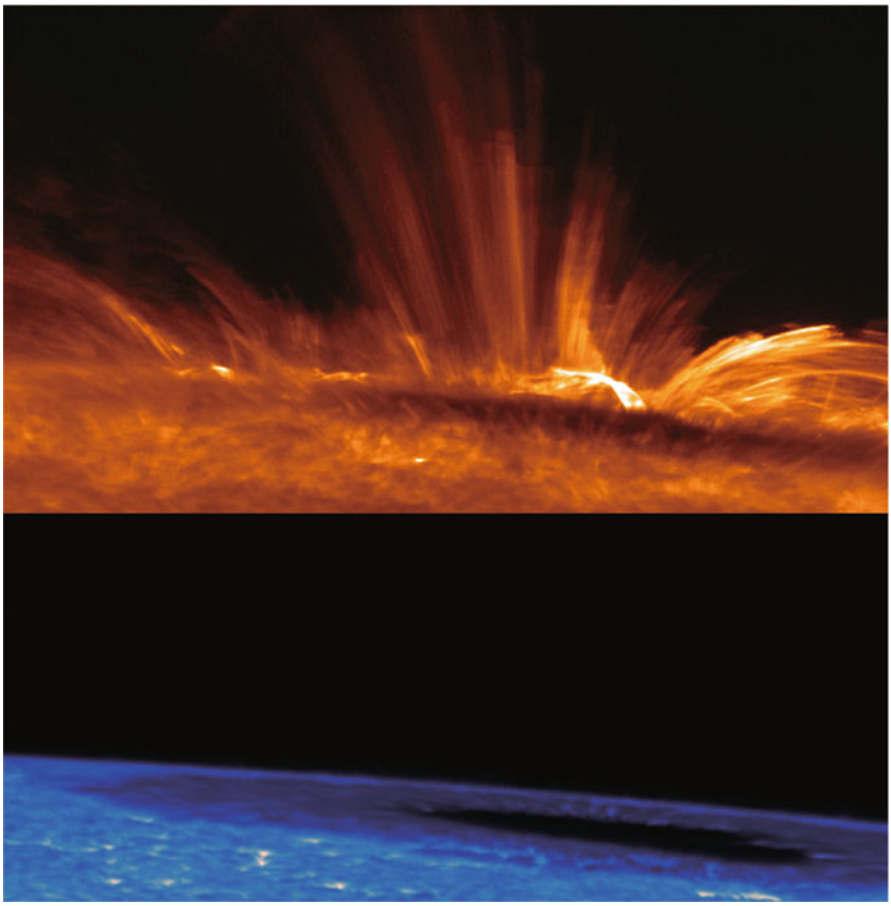

Fig. A.14 A comparison of the chromospheric and photospheric images of the solar limb where a large sunspot is located. The chromospheric image was taken with Ca II H filter, whereas the photospheric image was taken with G-band filter. The region in and around the large sunspot showed dynamical behaviors of the chromosphere including transient heating and plasma ejections

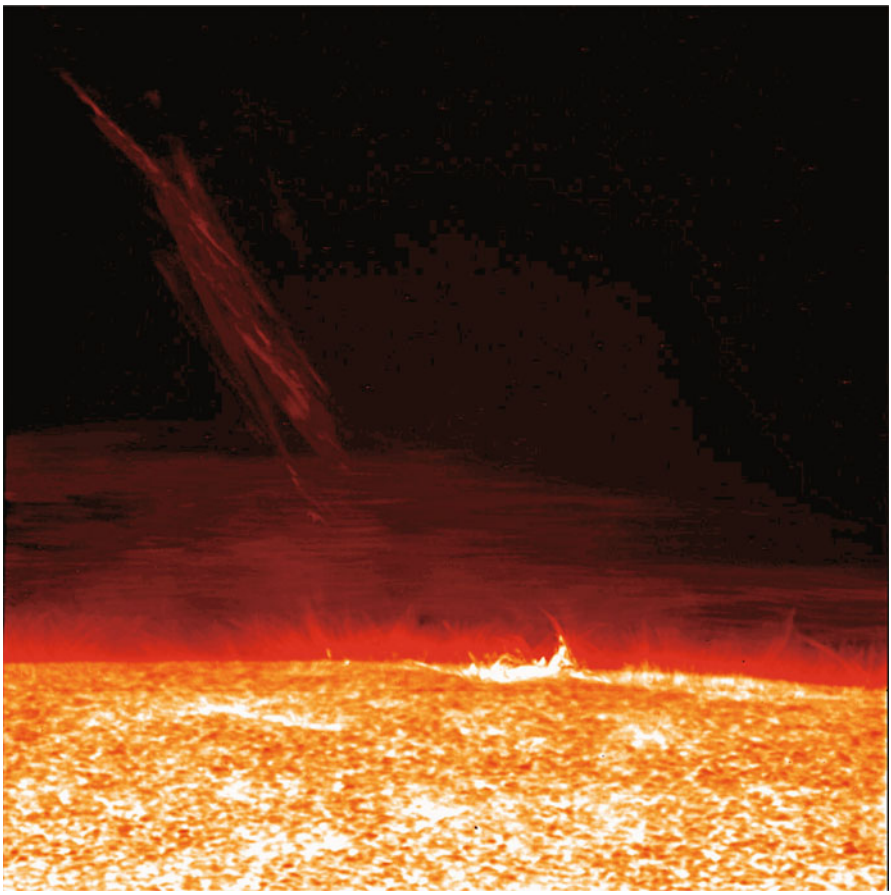

Fig. A.15 A giant chromospheric jet, captured by the SOT with Ca II H filter. Chromospheric materials were ejected obliquely upward with a transient heating of the chromospheric material at the base. The ejections may reach beyond a few 10,000 km

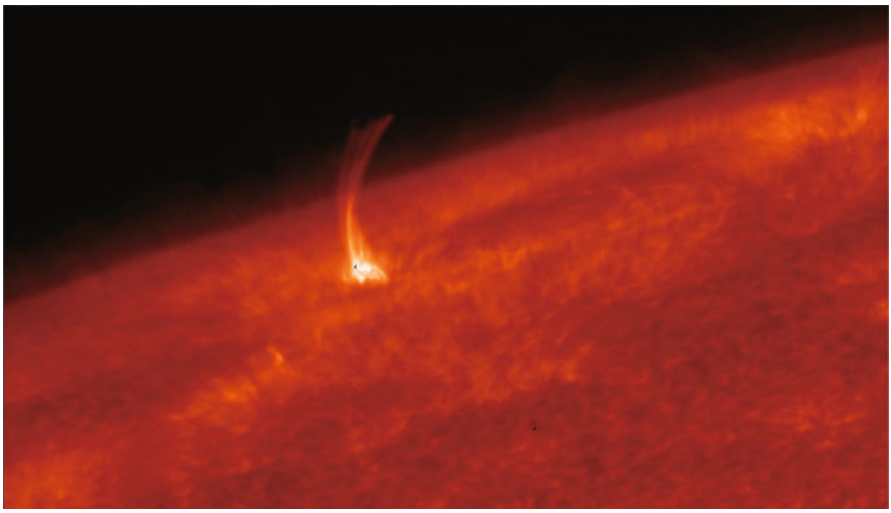

Fig. A.16 A chromospheric jet observed by the SOT with Ca II H filter. The footpoint region of the jet is the brightest under the Ca II H filter, indicating that chromospheric plasma is transiently heated

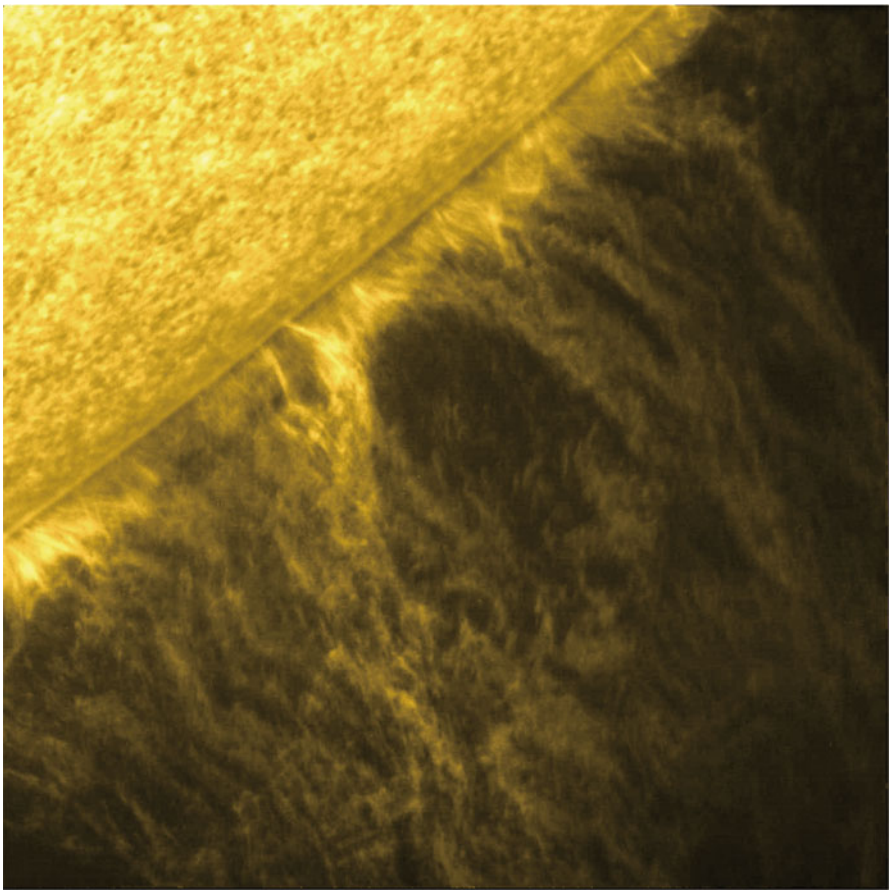

Fig. A.17 Dynamical fine structure in chromospheric prominence. The Ca II H images from the SOT are used to investigate dynamical behaviors of chromospheric materials in the prominence, including Kelvin-Helmholtz instability

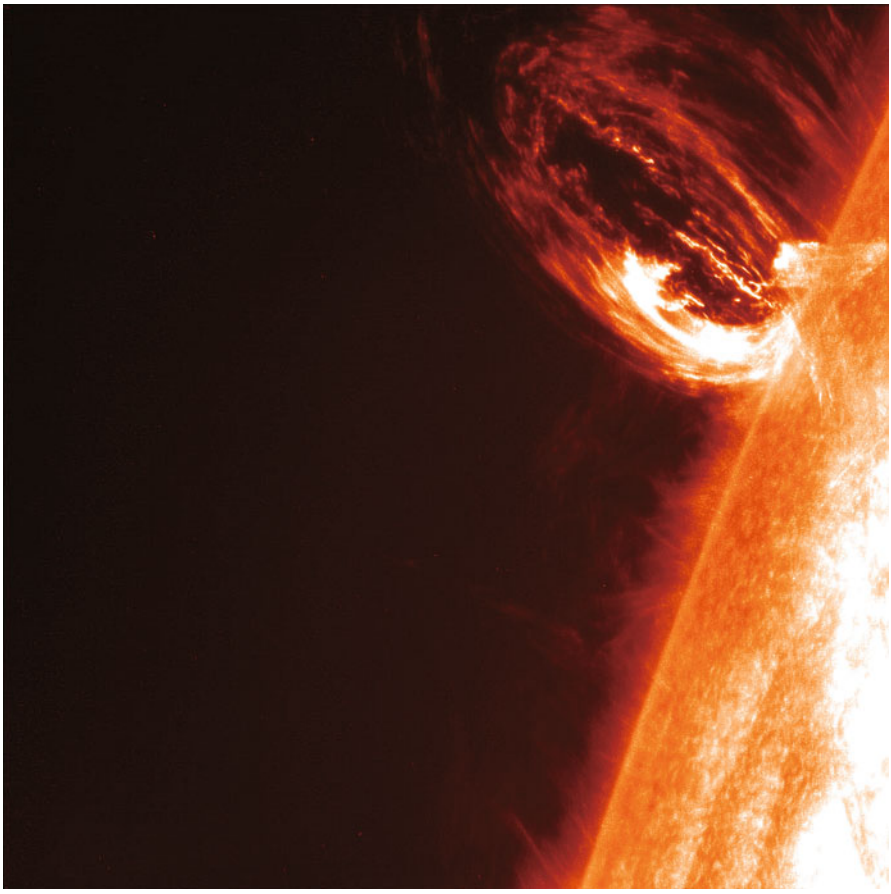

Fig. A.18 Chromospheric materials erupting above the east limb, captured by the SOT with Ca II H filter

A.4 Corona

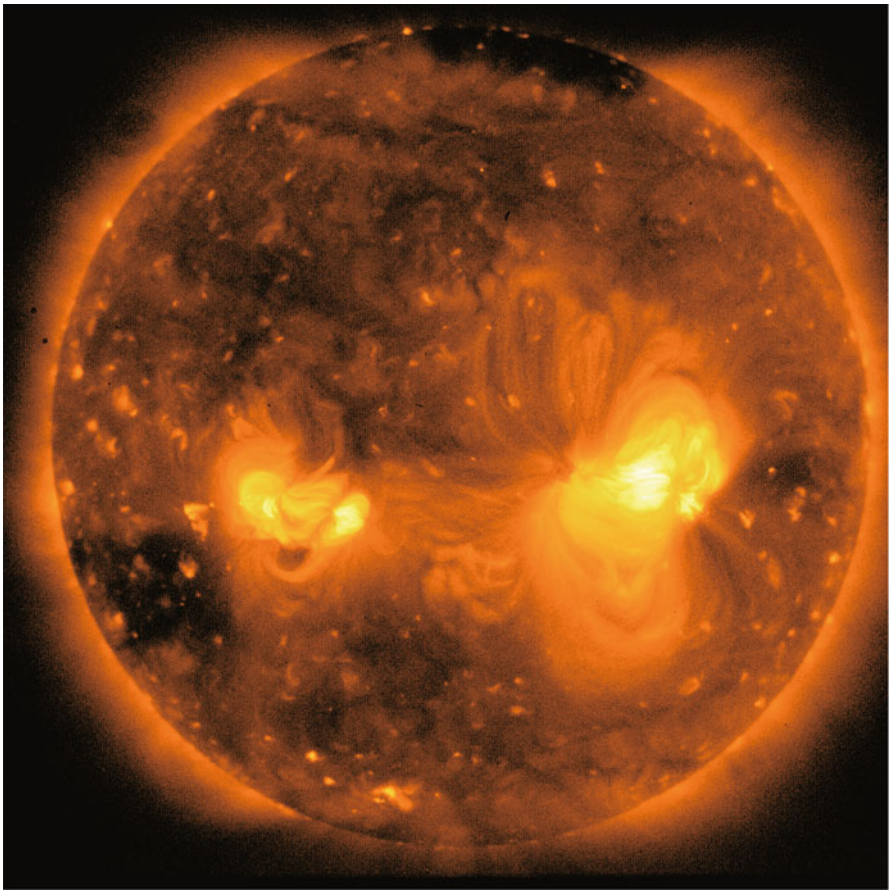

Fig. A.19 Soft X-ray corona, captured by *Hinode*'s X-Ray Telescope (XRT). The XRT has a spatial resolution of about 1 arcsec, covering the entire solar disk when the spacecraft is pointing directly at the disk center

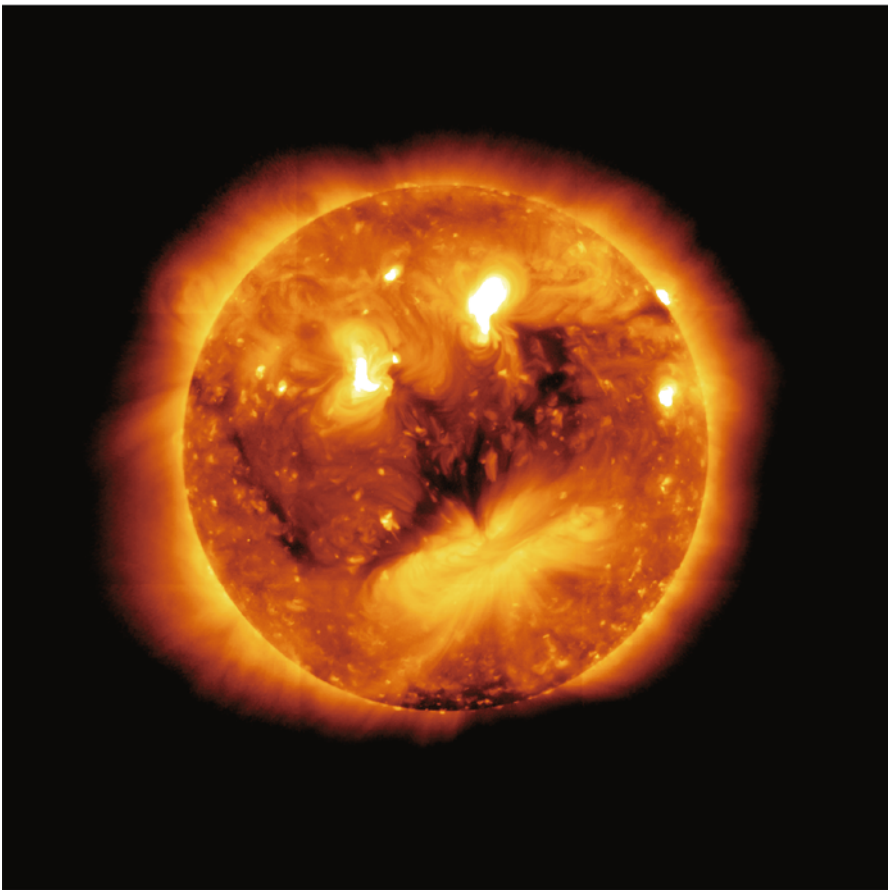

Fig. A.20 Soft X-ray corona on 9 December 2010. The coronal features look like the face of a man. The image was taken by the XRT

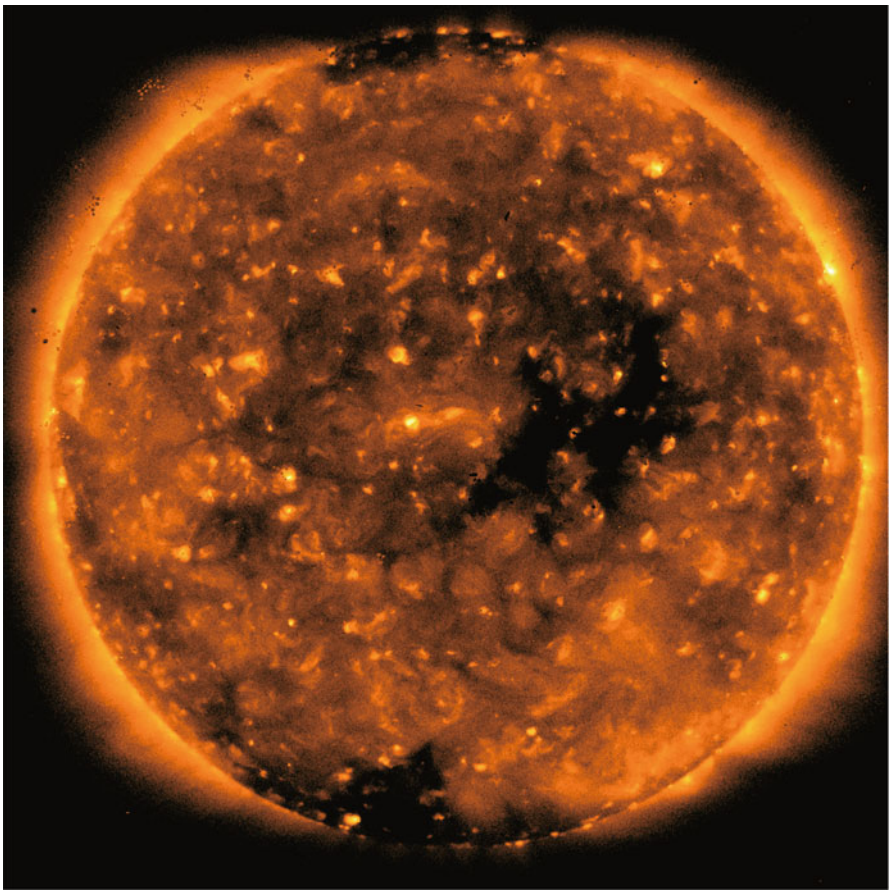

Fig. A.21 Soft X-ray corona in the solar minimum. The image was taken by the XRT on 11 March 2008. A lot of small bright points, called X-ray bright points (XBPs), are distributed over the entire disk in the solar minimum

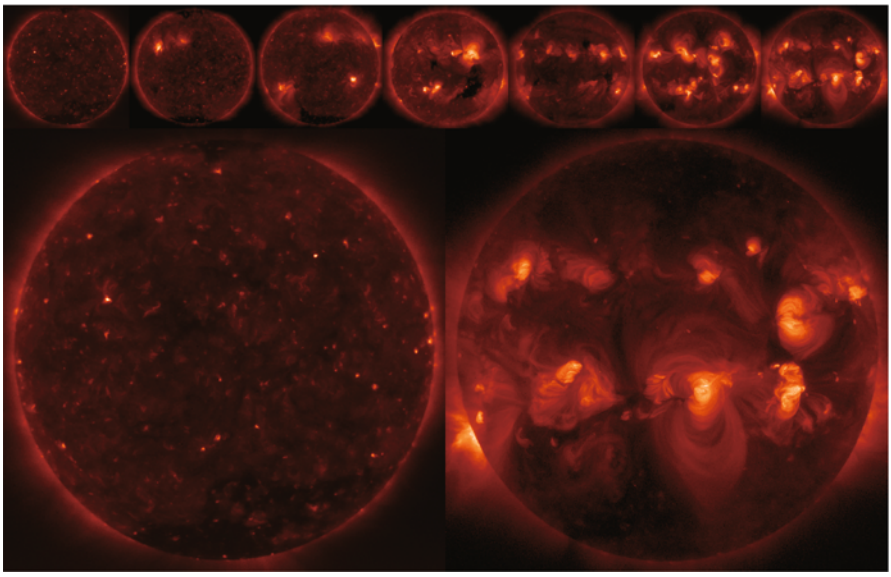

Fig. A.22 The solar cycle seen in soft X-ray corona. The XRT has taken a unique set of XRT synoptic data, which are the full-disk images only taken twice per day when the spacecraft is directed to the disk center. The series of X-ray images at the upper portion show the yearly evolution of the X-ray corona from 2008 to 2014. The image at the lower left is taken in 2008, when it is in the solar minimum, whereas that in the lower right is in 2014, when it is in the solar maximum

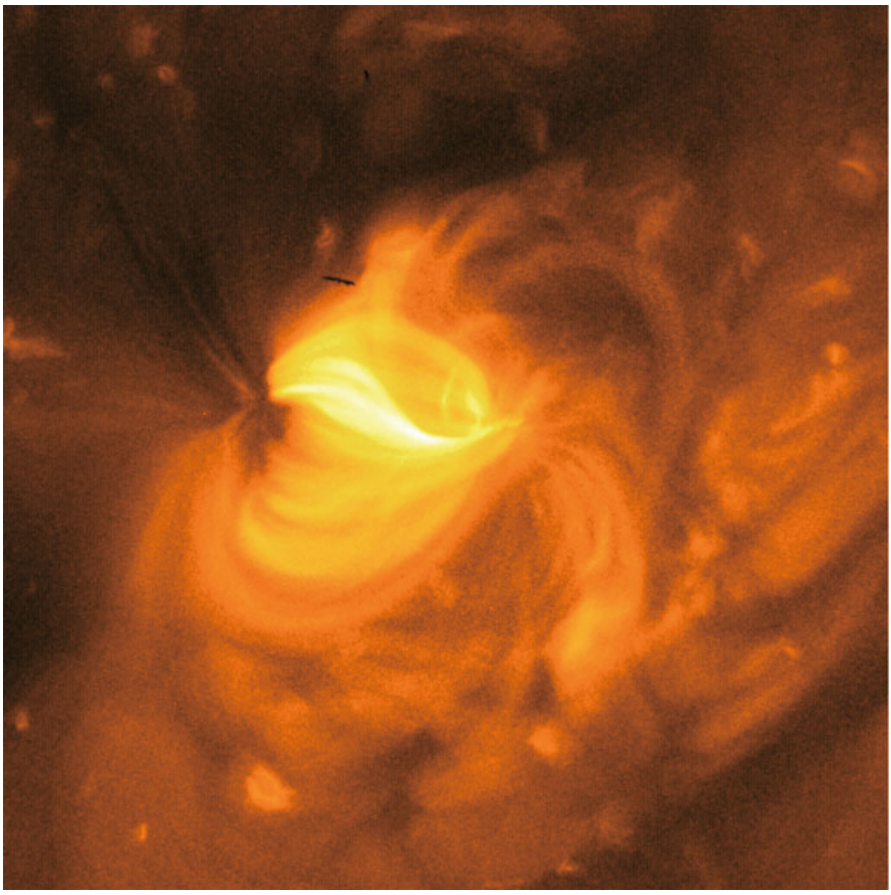

Fig. A.23 Soft X-ray image of an active region, taken by the XRT. At the low-intensity region located at the left side of the bright active region, it was found that the coronal plasma is continuously outflowing along the magnetic field lines upwardly at about 140 km s^{-1}. This outflow is considered to be a source of slow solar winds

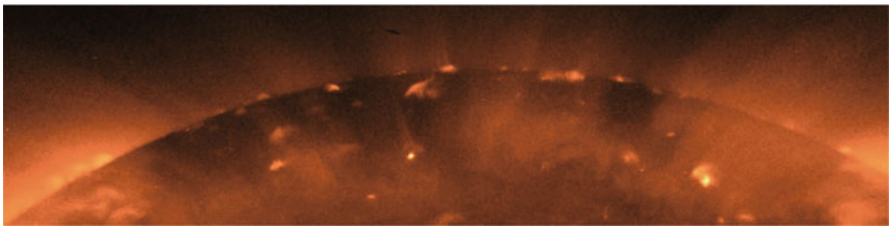

Fig. A.24 Soft X-ray image of a polar region, taken by the XRT. The coronal hole located at polar regions is considered to be the source of fast solar winds with their speed being higher than 700 km s^{-1}. High cadence observations of XRT have revealed frequent occurrence of X-ray jets

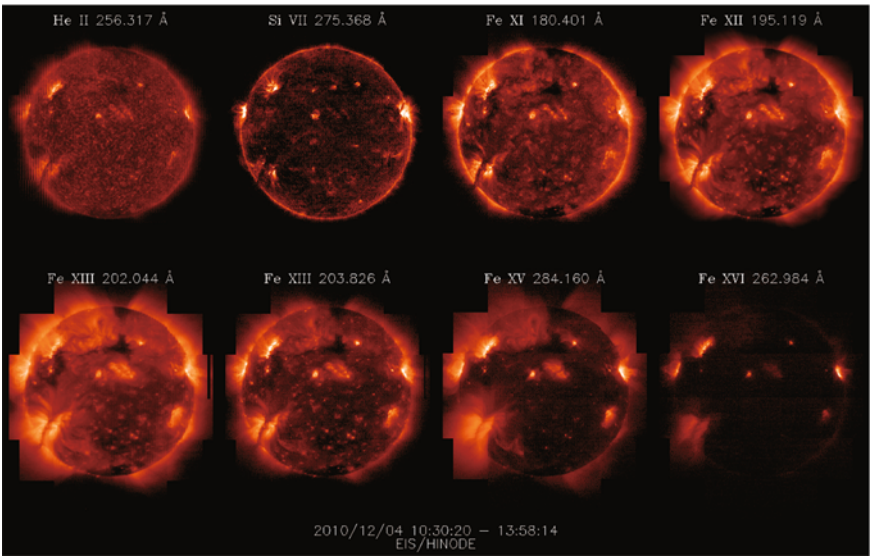

Fig. A.25 The solar corona observed by the Extreme ultraviolet Imaging Spectrometer (EIS) on 4 December 2010. Many spectral emission lines in EUV wavelength originate in the corona and transition region. The excitation of each spectral line depends on the temperature of plasma, determining the amount of plasma at the excitation temperature of each spectral line. From the upper left to the lower right, the temperature of the plasma is increased from the chromospheric temperature (He II) to the coronal temperatures (Fe XI to Fe XVI). Because of the narrow EIS field of view, the full images of the Sun were created from the data acquired at 13 different spacecraft pointing coordinates

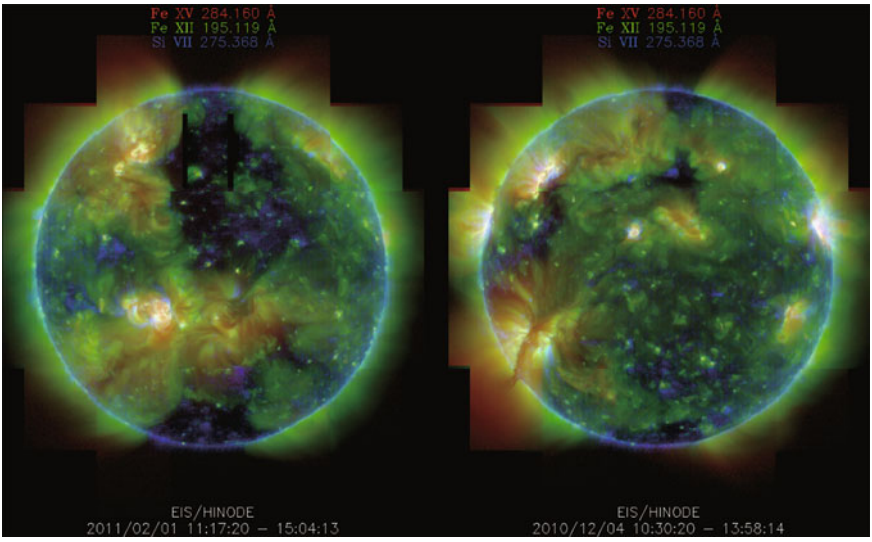

Fig. A.26 The composite images of the solar corona on 1 February 2011 (left) and 4 December 2010 (right). Images of Si VII, Fe XII, and Fe XV lines measured with EIS are used to create these composite images. Blue indicates the lower temperature corona, whereas red shows a higher temperature, indicating that the solar corona consists of plasma at a range of temperatures

A.5 Flares and Eruptions

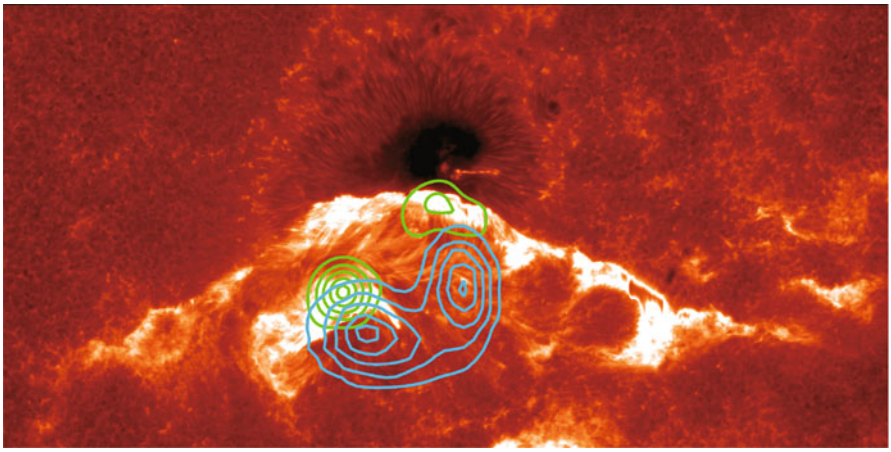

Fig. A.27 An X-class solar flare successfully observed by three independent instruments on 13 December 2006. The *Hinode* SOT acquired a time series of the chromospheric features with a Ca II H filter, revealing dynamic development of bright flare ribbons, which corresponds to the footpoints of extremely hot plasma created by the energy release in the corona. An arcade-like flare structure, which is an assembly of many flare loops, is formed in the corona. Green contours show the location of hard X-ray emission measured by National Aeronautics and Space Administration (NASA)'s *Reuven Ramaty High Energy Solar Spectroscopic Imager (RHESSI)* satellite, and blue contours are the location of microwave (17 GHz) emission measured by the Nobeyama Radioheliograph at the impulsive phase of the flare. The hard X-ray emission and microwave emission show the location of electrons accelerated to high energies by the flare. (c) NAOJ/JAXA/Hinode/RHESSI

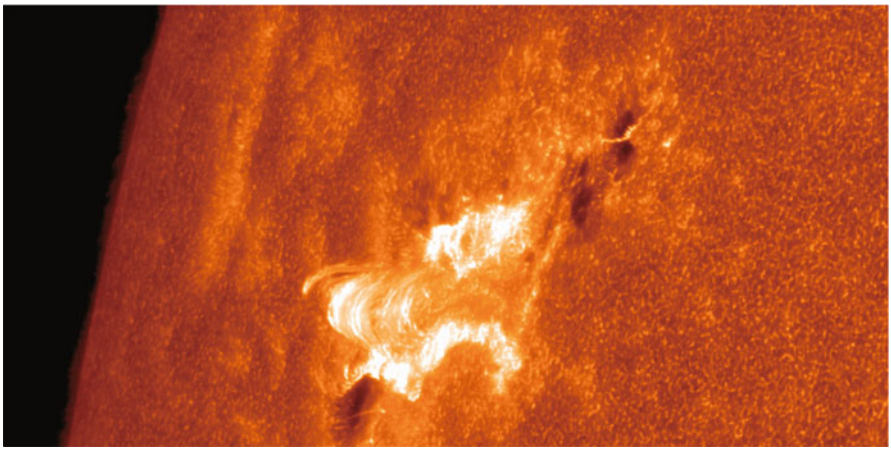

Fig. A.28 Post-flare arcade appeared after the occurrence of an X-class flare on 15 May 2013, captured by the SOT with a Ca II H filter. The post-flare arcade represents an arched magnetic field structure connecting flare ribbons and appears due to the cooling of flare loops in the corona. The size of the arcade is approximately twice that of the diameter of the Earth

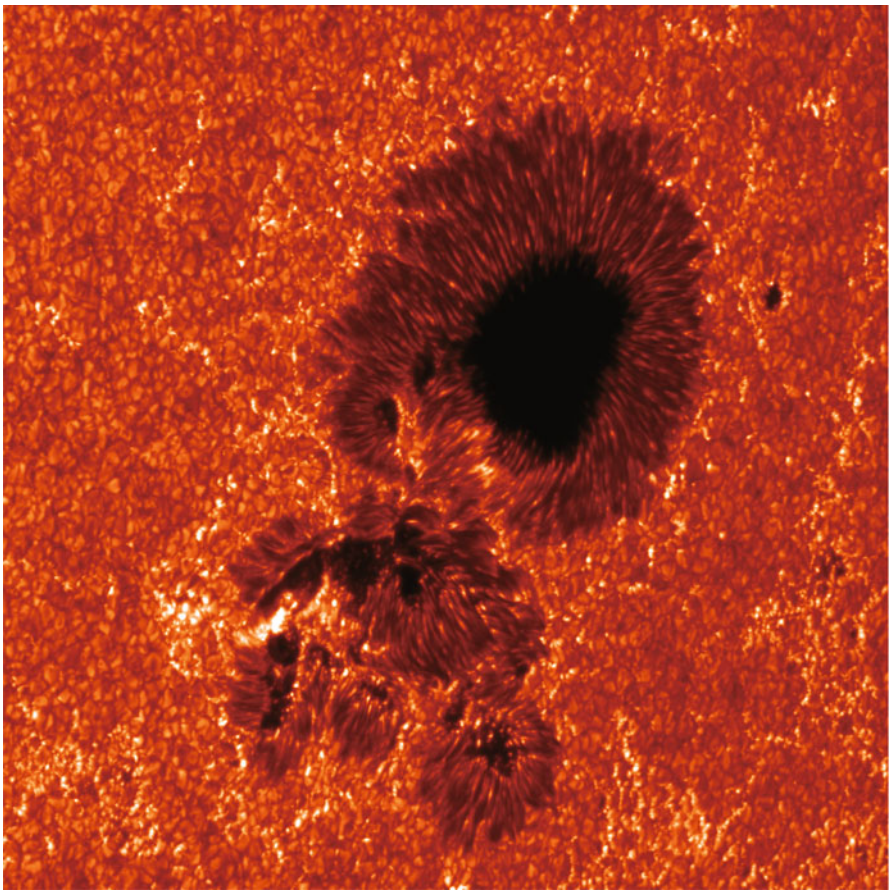

Fig. A.29 SOT observation of a white light flare on 14 December 2006. White light emissions may appear along with the occurrence of solar flares. In this G-band image, bright emissions are seen in the lower left portion of the sunspot group. Comparing the intensity of the emission with that of the hard X-ray flux measured with *RHESSI*, highly accelerated electrons contribute significantly to the appearance of white light emissions, which have been one of the mysteries since the discovery of white light flares about 150 years ago

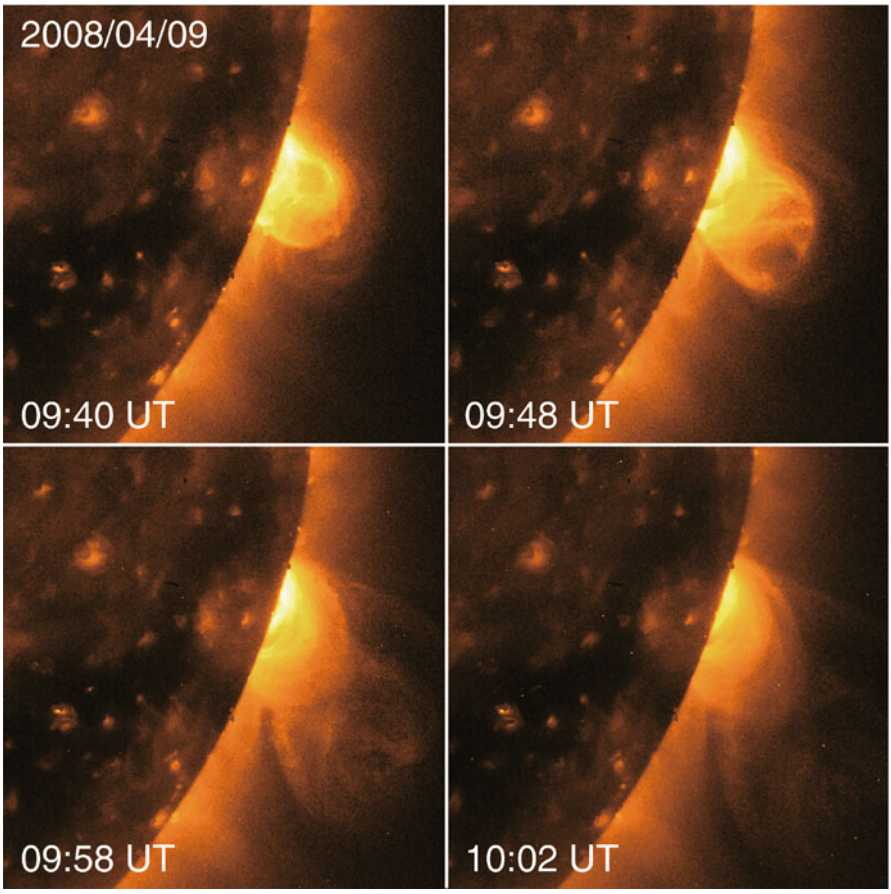

Fig. A.30 Time series of soft X-ray images by XRT on 9 April 2008, showing the temporal evolution of coronal magnetic structures when the coronal materials are suddenly ejected. Such ejections are called coronal mass ejections (CME), which are one of main sources of magnetic storms on Earth

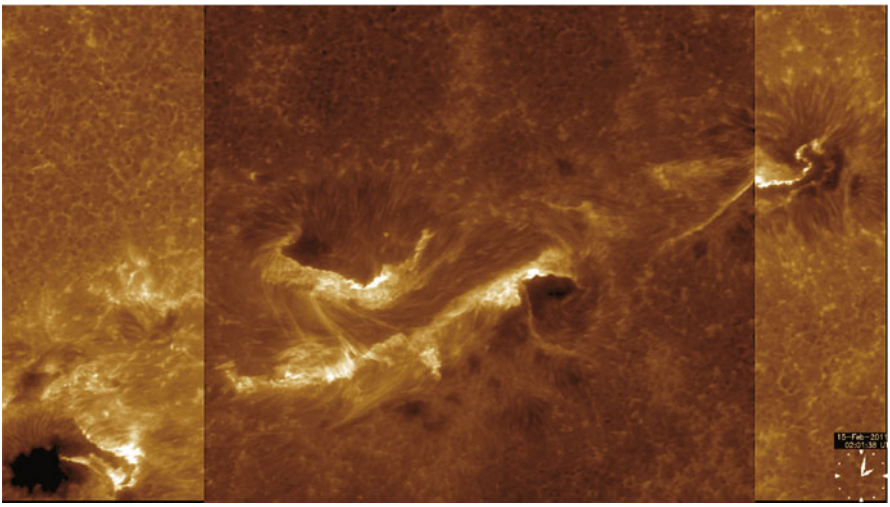

Fig. A.31 The first large flare in the solar cycle 24 successfully captured by the SOT. A composite image of two Ca II H images with different exposure times. This X-class flare occurred on 15 February 2011, which is more than 4 years after the previous X-class flare

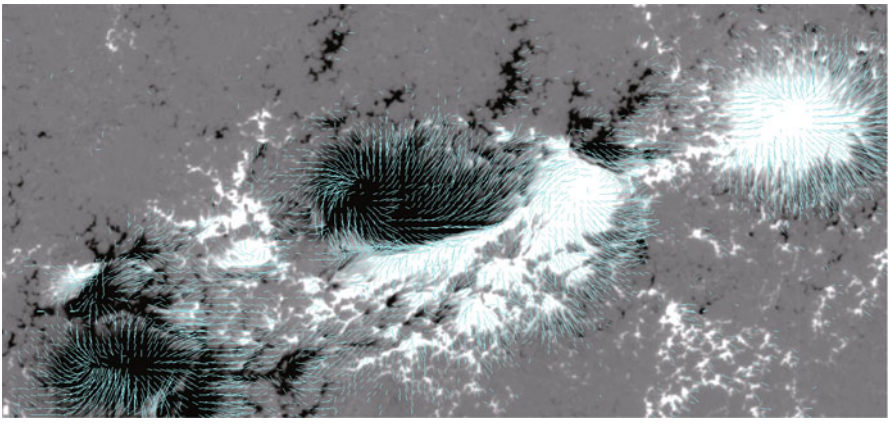

Fig. A.32 A map of vector magnetic fields at the photosphere, derived from the SOT, for the X-class flare on 15 February 2011. White and black are positive and negative magnetic polarity, respectively. Blue arrows show the direction of horizontal magnetic fields

A.6 Astronomical Events

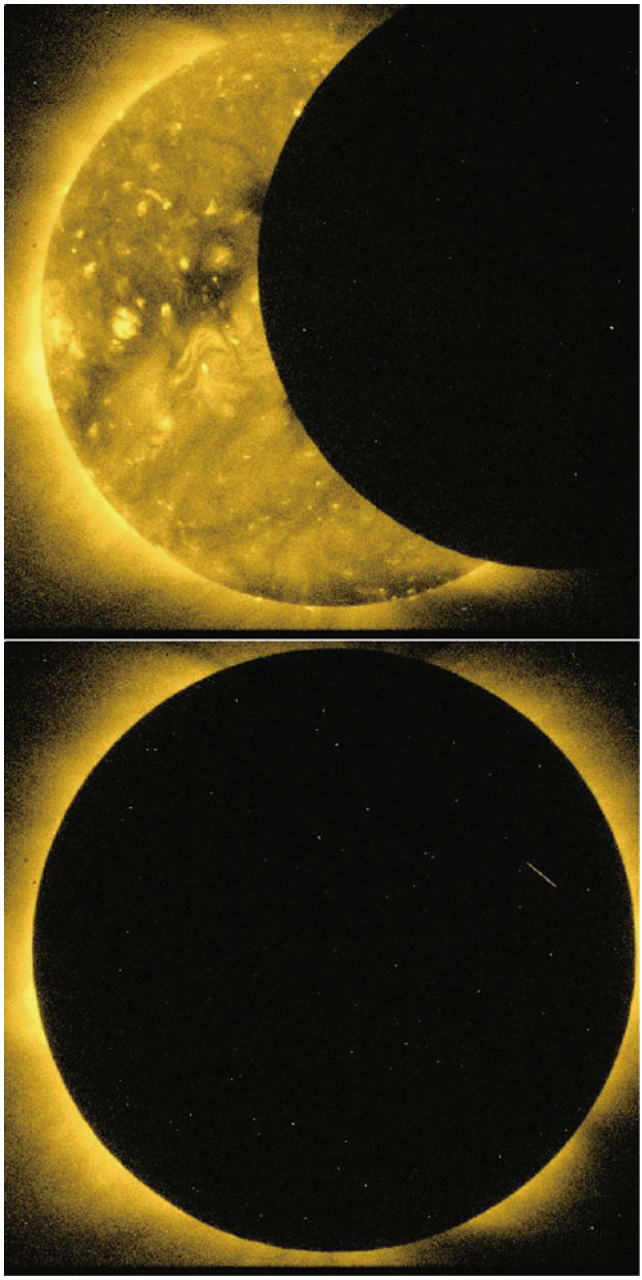

Fig. A.33 A total eclipse encountered in orbit on 19 March 2007. This eclipse was visible from eastern Asia and parts of northern Alaska with the eclipse magnitude reaching 0.8754 on the ground. *Hinode* was the only witness of the episode for the totality, which was visible from the orbit. This is the soft X-ray images from the XRT

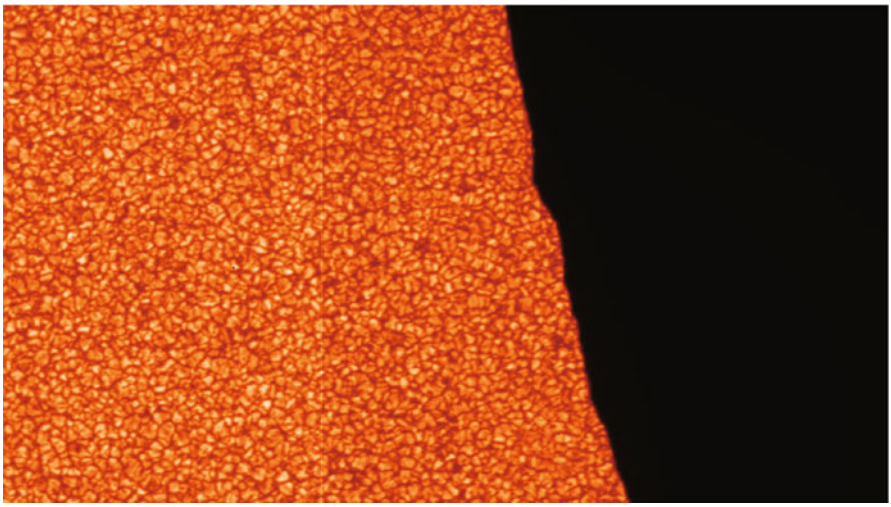

Fig. A.34 A blue continuum image acquired by the SOT during an eclipse on 19 March 2007. The dark shadow is the partial limb of the moon, showing high mountains and valleys located at the limb. The highest spatial resolution of the SOT is 0.2 arcsec, corresponding to 0.4 km on the surface of the moon

Fig. A.35 An annular eclipse from space, only viewed from *Hinode* on 4 January 2011. This is the soft X-ray image acquired by the XRT at the time of the annular eclipse. The dark shadow is the silhouette of the moon

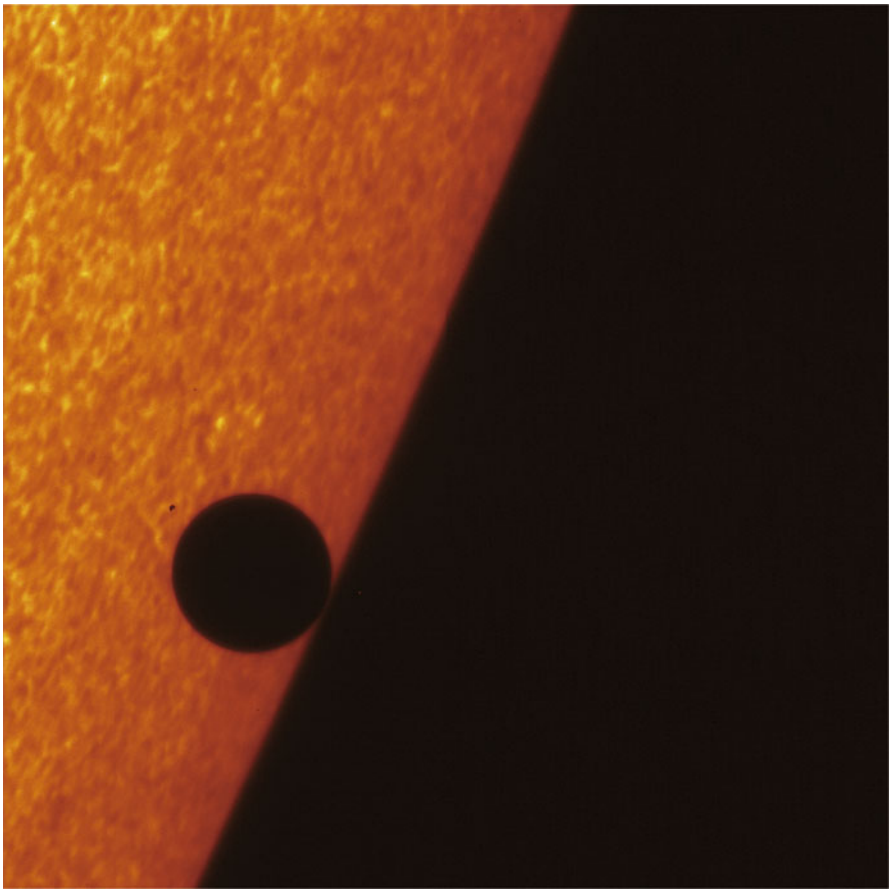

Fig. A.36 Transit of Mercury across the Sun on 9 November 2006, which occurred about one month after *Hinode*'s telescopes had begun observations. This image is G-band image recorded by the SOT at the third contact (interior egress). The diameter of Mercury is approximately 10 arcsec

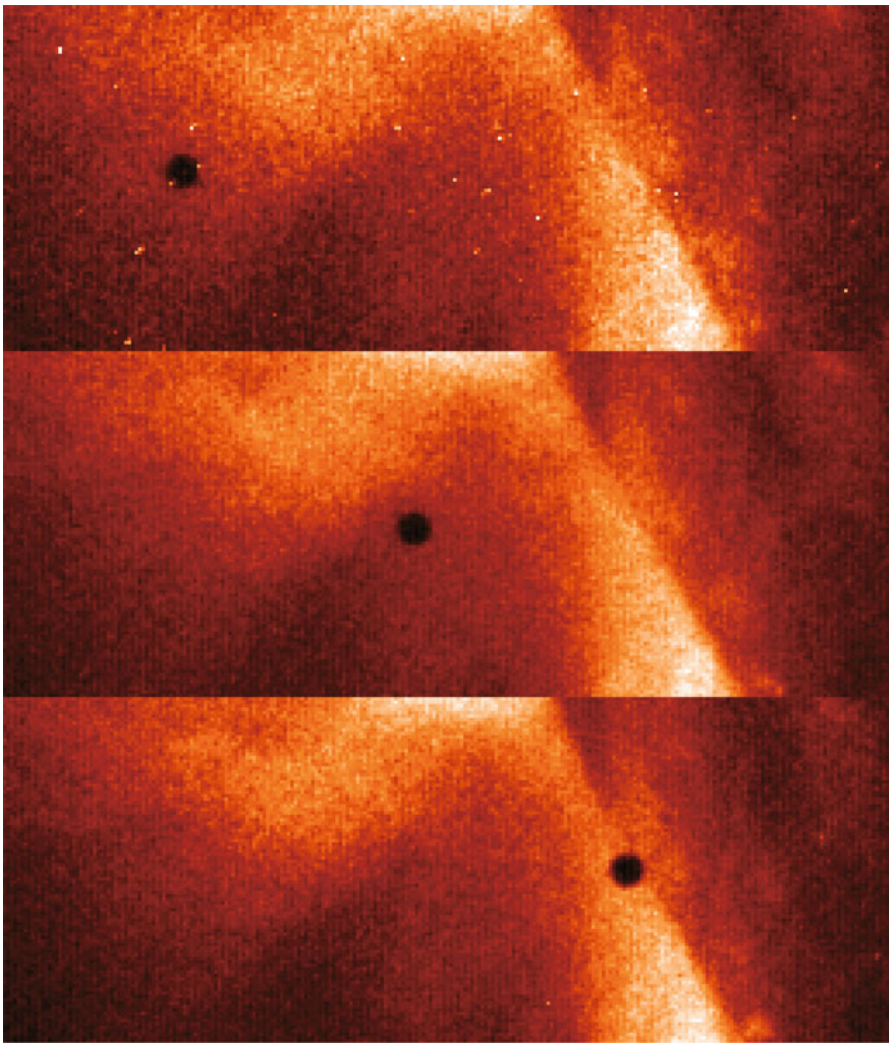

Fig. A.37 Mercury captured in soft X-ray images on 9 November 2006. The Mercury is observed as a small dark disk in front of soft X-rays from the coronal plasma. These images were taken by the XRT when the Mercury was approaching the southeast portion of the solar limb

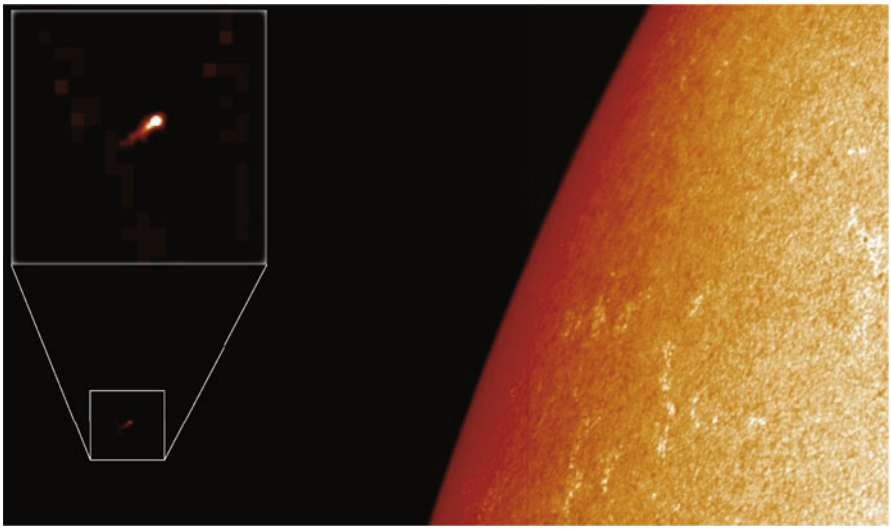

Fig. A.38 Comet Lovejoy, formally designated C/2011 W3 (Lovejoy), successfully captured by the SOT. This comet was discovered by an amateur astronomer in November 2011. It passed through the Sun's corona on 16 December 2011. The closest distance to the solar surface was about 140,000 km (0.2 solar radius). The SOT captured the comet core with a short tail in visible light, along with the very bright visible solar disk

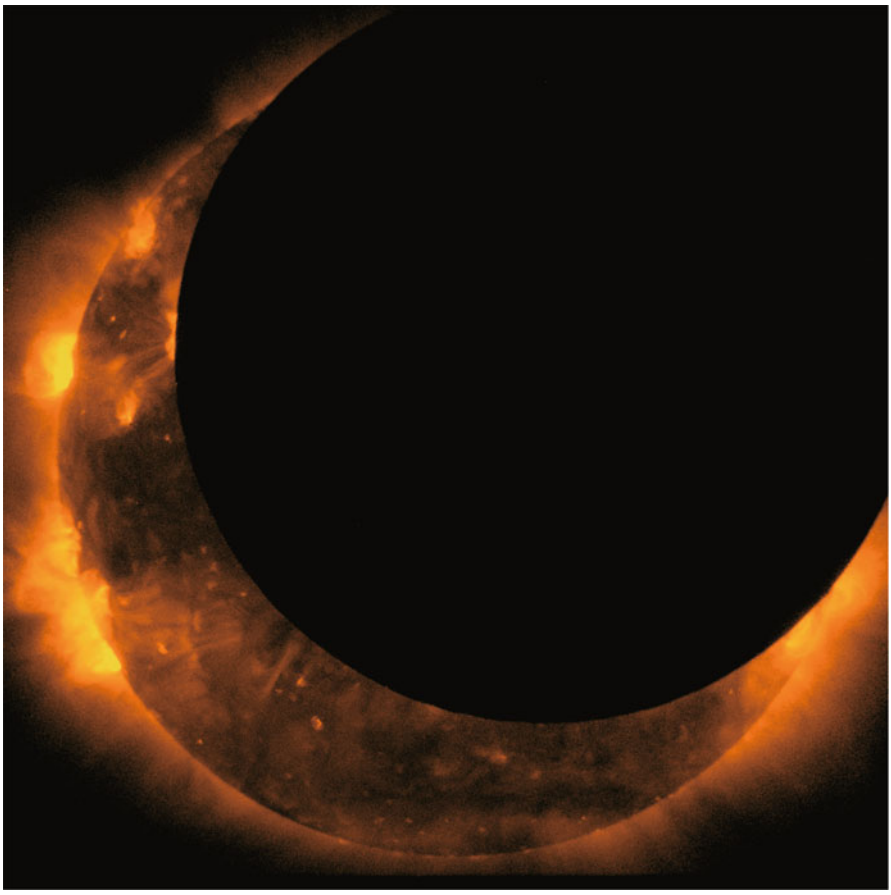

Fig. A.39 On 20 May 2012, an annular eclipse was visible from a 240 to 300 km wide track that traversed eastern Asia, the northern Pacific Ocean, and the western United States. From the orbit, *Hinode* observed this as a partial eclipse

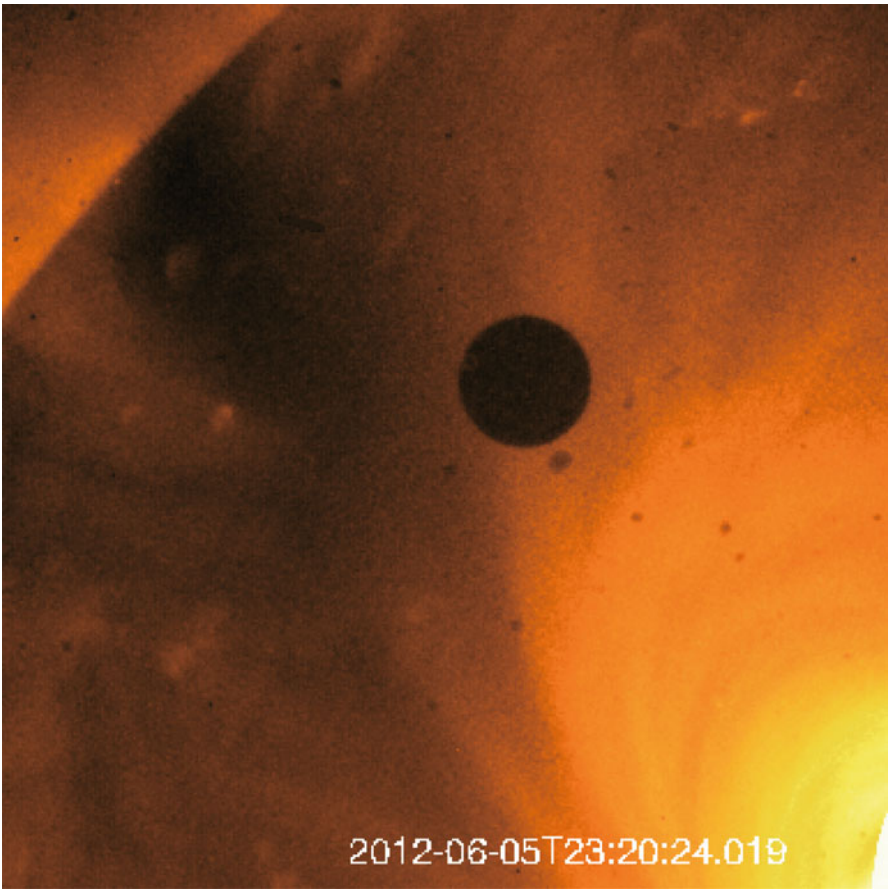

Fig. A.40 Transit of Venus on 5 June 2012, observed by the XRT. The shadow disk is Venus

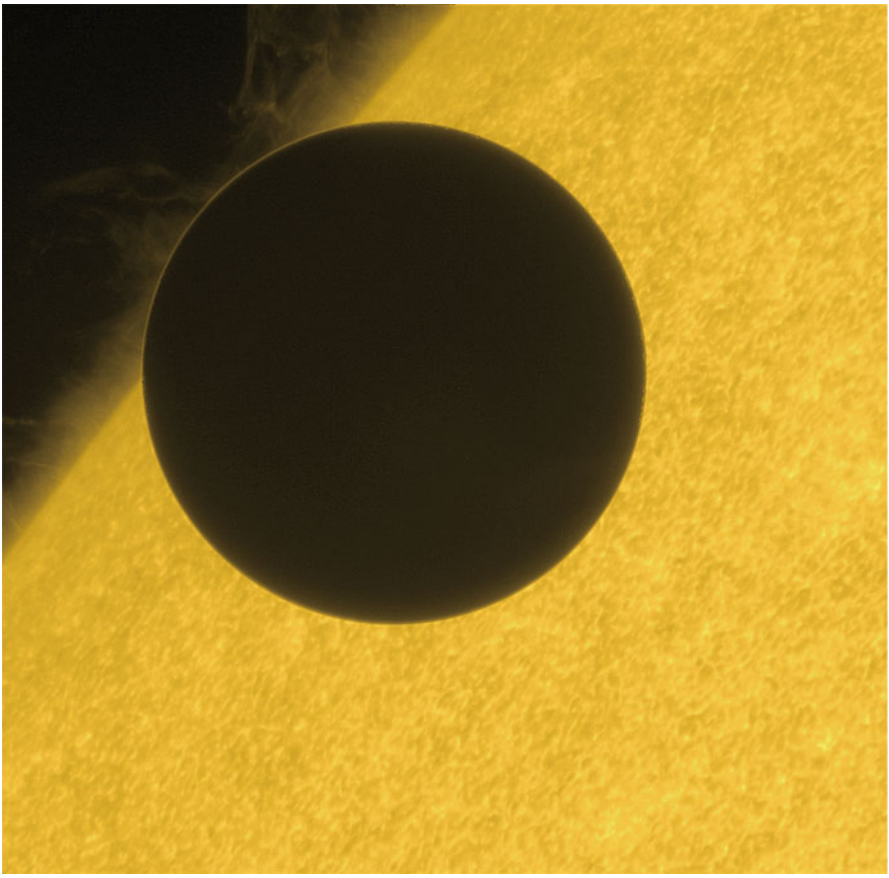

Fig. A.41 Transit of Venus on 5/6 June 2012, observed by the SOT with a Ca II H filter. The shadow disk is Venus and its diameter is 57.8 arcsec. The limb of Venus in front of the chromospheric atmosphere above the solar limb shows a bright arc, which is caused by scattering of the solar radiation in the Venusian atmosphere

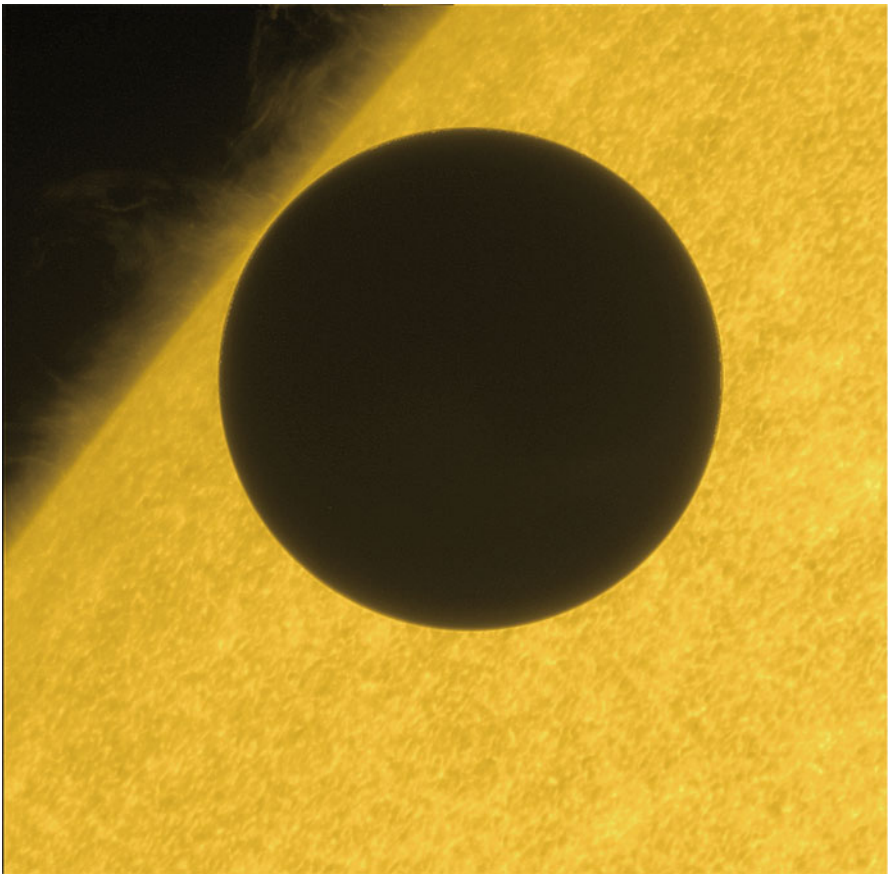

Fig. A.42 Another Ca II H image taken by the SOT during the transit of Venus on 5/6 June 2012. This image was taken shortly after the second contact (interior ingress)

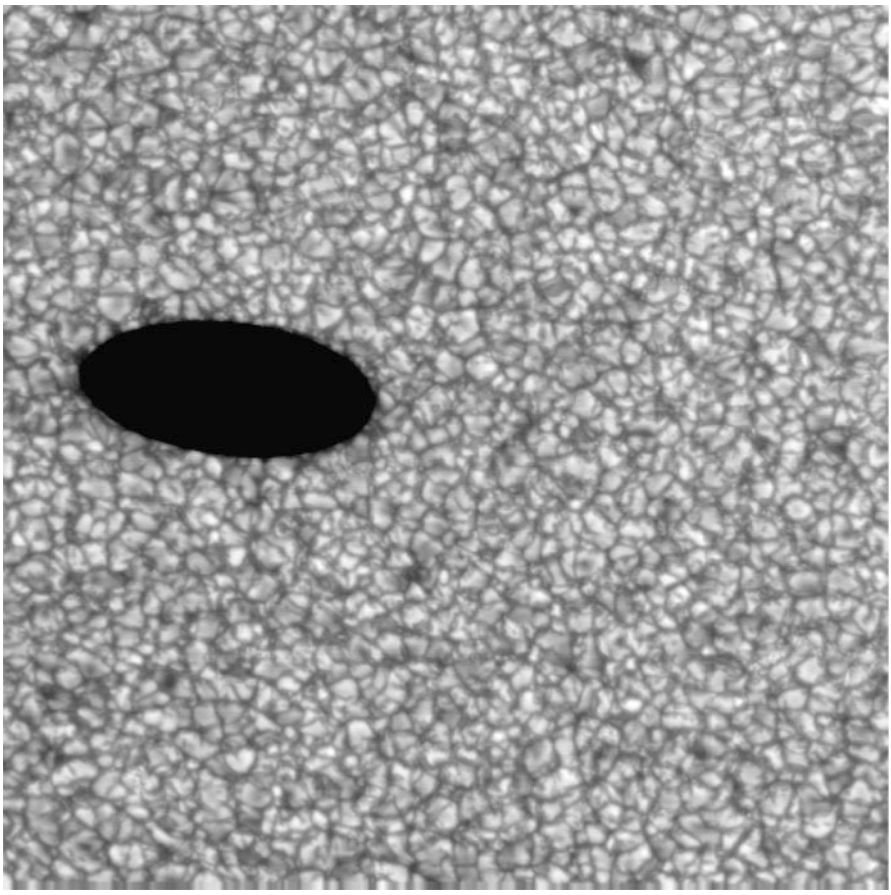

Fig. A.43 Transit of Mercury on 9/10 May 2016. This image was recorded with the spectropolarimeter of the SOT. The spectropolarimeter is a slit spectrograph used for measuring the full state of polarization at a 630 nm range. One exposure provides a one-dimensional data in the vertical (north-south) direction, and the scanning of the slit in the horizontal (east-west) direction makes the two-dimensional map. The shadow of Mercury is what is seen as an elongated shape due to the movement of the planet during the scanning process

Index

T. Shimizu et al. (eds.), *First Ten Years of Hinode Solar On-Orbit Observatory*,
Astrophysics and Space Science Library 449,
https://doi.org/10.1007/978-981-10-7742-5